

EARLY AND LATE TRANSITION METAL COMPLEXES FEATURING 1,3-*N,O*-  
CHELATES: DEVELOPMENT OF HOMOGENOUS CATALYSTS FOR THE  $\alpha$ -  
ALKYLATION OF AMINES VIA HYDROAMINOALKYLATION

by

Jason W. Brandt

B.Sc. Honors, University of Alberta, 2012

A THESIS SUBMITTED IN PARTIAL FULFILLMENT OF  
THE REQUIREMENTS FOR THE DEGREE OF

DOCTOR OF PHILOSOPHY

in

THE FACULTY OF GRADUATE AND POSTDOCTORAL STUDIES  
(Chemistry)

THE UNIVERSITY OF BRITISH COLUMBIA  
(Vancouver)

April 2018

© Jason W. Brandt, 2018

The following individuals certify that they have read, and recommend to the Faculty of Graduate and Postdoctoral Studies for acceptance, the dissertation entitled:

Early and Late Transition Metal Complexes Featuring 1,3-*N,O*-Chelates: Development of Homogenous Catalysts for the  $\alpha$ -Alkylation of Amines via Hydroaminoalkylation

submitted by Jason W. Brandt in partial fulfillment of the requirements

the degree of Doctor of Philosophy

in Chemistry

**Examining Committee:**

Prof. Laurel Schafer (Chemistry)

Supervisor

Prof. Glenn Sammis (Chemistry)

Supervisory Committee Member

Prof. Parisa Mehrkhodavandi (Chemistry)

University Examiner

Prof. Mark Martinez (Chemical and Biological Engineering)

University Examiner

Prof. Roland Roesler (Chemistry, University of Calgary)

External Examiner

**Additional Supervisory Committee Members:**

Prof. Mike Fryzuk (Chemistry)

Supervisory Committee Member

Prof. Alex Wang (Chemistry)

Supervisory Committee Member

## Abstract

This thesis details the development of transition-metal complexes that are utilized as precatalysts for catalytic hydroaminoalkylation chemistry. Hydroaminoalkylation is the activation of an  $\alpha$ -C(sp<sup>3</sup>)-H of an amine, and subsequent addition across a C=C unsaturation. This results in  $\alpha$ -alkylated amines in a 100% atom-economical reaction, while avoiding amine protection/deprotection strategies.

A series of 2-pyridonate chloro tris(dimethylamido) tantalum complexes have been synthesized and tested for the hydroaminoalkylation of alkenes with secondary amines. These complexes were found to exhibit high reactivity for a broad range of internal alkene substrates and represent the first, general hydroaminoalkylation of cyclic and linear internal alkenes that occurs without isomerization of the C=C double bond. Further study supports the assertion that minimized steric parameters of the 2-pyridonate and chloro ligands allow for reactivity with sterically demanding internal alkenes. Kinetic studies and deuterium labeling experiments reveal a complex kinetic profile and provide evidence for off-cycle equilibria that dominate catalytic activity.

Complementary to this work, an alternative 1,3-*N,O*-chelating phosphoramidate ligand framework was explored to synthesize Nb complexes for hydroaminoalkylation. A variety of monophosphoramidate tetrakis(dimethylamido) Nb complexes were synthesized, as well as bis(phosphoramidate) niobaziridines, which are proposed as intermediates for the hydroaminoalkylation mechanism. The optimal precatalyst system was found to be an *in situ* preparation of 2:1 phosphoramidate:Nb(NMe<sub>2</sub>)<sub>5</sub>. This offers comparable results to analogous phosphoramidate Ta complexes, but with a significantly different phosphoramidate ligand set.

New cationic complexes of Ru, Rh, and Ir were synthesized featuring a bidentate  $\kappa^2$ -*P,N*-phosphino-2-pyridonate ligand. These complexes were not viable precatalysts for hydroaminoalkylation, but were found to promote the stoichiometric dehydrogenation of amines to generate cationic metal hydrides. Analogous cationic complexes of 1,3-*N,O*-chelating 2-pyridonate complexes were prepared *in situ* and were found to catalyzed the reaction of dibenzylamine to tribenzylamine. A 2-pyridonate Ru complex was found to catalyze the dehydrogenation of benzylamine to the corresponding imine in the presence of isoprene, which acted as the hydrogen acceptor. Attempted hydroaminoalkylation reactions with non-arene supported 2-pyridonate complexes did not result in catalysis. These results provide insight into the use of late-transition metal complexes in amine activation and reactivity.

## **Lay Summary**

Amines are compounds that contain a nitrogen atom, and play a crucial role in biological systems. The development of new reactions that can efficiently synthesize amines are therefore of academic, pharmaceutical, agrochemical, and other industrial importance. These developments can improve our general understanding of how amine containing molecules chemically react, which can spur further developments in chemistry, biology, etc. A transition-metal complex can be defined as a metal ion chemically bound to molecules termed ligands. This thesis describes the development of new transition-metal complexes that function as catalysts in the efficient chemical transformation of simple amines into more complex amines that may be useful in synthesis of biologically active molecules or materials.

## Preface

In collaboration and consultation with my supervisor Prof. Dr. Laurel Schafer, I designed and conducted all of the experiments described herein, except for specific instances described below. I have written the text of this document entirely with input and suggestions from my supervisor Prof. Dr. Laurel Schafer, except for specific instances described below.

A version of the data contained in Chapter 2.2.1 has been published: Chong, E.; **Brandt, J. W.**; Schafer, L. L. *J. Am. Chem. Soc.* **2014**, *136*, 10898-10901. This work (experimental and otherwise) was done in collaboration with former Schafer group colleague Dr. Eugene Chong. Dr. Chong was responsible for the discovery and synthesis of complexes **2.12** and **2.13**, and the initial reactivity as presented in Scheme 2.10. Catalyst optimization, and evaluation of substrate scope was performed collaboratively. Dr. Chong performed the final isolation and characterization of substrates presented in Scheme 2.12 and Scheme 2.13 after optimization.

A version of Chapters 2.2.2, 2.2.3, and 2.2.4 have been published: **Brandt, J. W.**; Chong, E.; Schafer, L. L. *ACS Catal.* **2017**, *7*, 6323-6330. This work was inspired by the work discussed above. Dr. Chong contributed the reaction found in Scheme 2.20. I wrote the text of this publication entirely, with input and suggestions from Prof. Schafer.

## Table of Contents

<b>Abstract.....</b>	<b>iii</b>
<b>Lay Summary .....</b>	<b>v</b>
<b>Preface.....</b>	<b>vi</b>
<b>Table of Contents .....</b>	<b>vii</b>
<b>List of Schemes.....</b>	<b>xi</b>
<b>List of Tables .....</b>	<b>xvi</b>
<b>List of Figures.....</b>	<b>xvii</b>
<b>List of Abbreviations .....</b>	<b>xix</b>
<b>List of Symbols .....</b>	<b>xxv</b>
<b>Acknowledgements .....</b>	<b>xxvi</b>
<b>Dedication .....</b>	<b>xxvii</b>
<b>Chapter 1: Introduction .....</b>	<b>1</b>
1.1    Scope of Thesis .....	2
1.2    2-Pyridones as Ligands for Transition-Metal-Catalyzed Reactions .....	3
1.2.1    Group 4 – 7 Transition-Metal Precatalysts with 2-Pyridone Ligands .....	4
1.2.2    Group 8 Transition-Metal Precatalysts with 2-Pyridone Ligands .....	6
1.2.2.1    Transfer Hydrogenation and Hydrogenation of Ketones.....	6
1.2.2.2    Additional Reactions with Group 8 Complexes .....	11
1.2.2.3    Bio-Inspired Complexes .....	17
1.2.3    Group 9 Transition-Metal Precatalysts with 2-Pyridone Ligands .....	18
1.2.3.1    Reactions Involving Acceptorless Dehydrogenation.....	18
1.2.3.2    Hydrogenation of Carbon Dioxide and Dehydrogenation of Formic Acid .....	26

1.2.3.3	Additional Catalytic Reactions .....	34
1.2.4	Group 10 – 12 Transition-Metal Precatalysts with 2-Pyridone Ligands .....	37
1.2.5	Conclusion .....	40
<b>Chapter 2: 2-Pyridonate Tantalum Complexes for the Hydroaminoalkylation of Unactivated Internal Alkenes with Unprotected Secondary Amines – Synthetic Development and Mechanistic Insights .....</b>		<b>42</b>
2.1	Introduction.....	42
2.1.1	Early-Transition-Metal Hydroaminoalkylation .....	45
2.1.2	Late-Transition-Metal Hydroaminoalkylation.....	51
2.1.3	Scope of Chapter.....	53
2.2	Results and Discussion .....	54
2.2.1	Development of a Novel 2-Pyridonate Precatalyst for the Hydroaminoalkylation of Internal Alkenes.....	54
2.2.2	Exploration of 2-Pyridonate Ligand Effects on Hydroaminoalkylation Catalysis	59
2.2.3	Mechanistic Interpretation .....	65
2.2.4	Investigations into Precatalyst Activation and Off-Cycle Equilibria .....	67
2.3	Conclusions.....	76
2.4	Experimental Details.....	77
2.4.1	General Considerations.....	77
2.4.2	Instrumentation .....	78
2.4.3	Materials .....	78
2.4.4	Synthesis and Characterization of Compounds .....	79
2.4.5	Reaction and Experimental Details:.....	85



**Chapter 3: Phosphoramidate Niobium Complexes for the Hydroaminoalkylation of Alkenes with Secondary Amines – Synthesis of Novel Niobium Complexes and Catalytic Reactivity .....91**

3.1	Introduction.....	91
3.1.1	Niobium Catalyzed Hydroaminoalkylation .....	91
3.1.2	Phosphoramidate Ancillary Ligands for Early-Transition-Metal-Catalyzed Hydroaminoalkylation .....	93
3.2	Scope of Chapter.....	94
3.3	Results and Discussion .....	95
3.3.1	Synthesis of Phosphoramidate Nb Complexes .....	95
3.3.2	Catalytic Hydroaminoalkylation Reactivity of Phosphoramidate Nb Complexes	
	101	
3.4	Conclusions.....	108
3.5	Experimental Details.....	109
3.5.1	Materials .....	110
3.5.2	Synthetic and Experimental Details.....	110

**Chapter 4: 6-Substituted-2-Pyridonate and 2-Pyridonate Ligated Ru, Rh, and Ir Complexes for the Activation of Unprotected Amines – Efforts Towards Hydroaminoalkylation Catalysis for the  $\alpha$ -Functionalization of Amines.....118**

4.1	Introduction.....	118
4.1.1	Alkylation of Amines through Hydrogen-Borrowing Catalysis.....	118
4.1.2	Acceptorless Dehydrogenation of Amines .....	121
4.2	Scope of Chapter.....	123

4.3	Results and Discussion .....	126
4.3.1	Arene Supported Ru, Rh, and Ir Complexes and Reactivity .....	126
4.3.2	Initial Investigations into Non-Arene Ligated Late-Transition-Metal Complexes for Hydroaminoalkylation.....	138
4.4	Conclusions.....	142
4.5	Experimental Details.....	143
4.5.1	Materials .....	143
4.5.2	Synthetic and Experimental Details.....	144
<b>Chapter 5: Conclusion.....</b>		<b>159</b>
5.1	Summary .....	159
5.2	Future Directions .....	161
5.2.1	Early-Transition Metal Catalyzed Hydroaminoalkylation.....	161
5.2.2	Late-Transition Metal Catalyzed Hydroaminoalkylation .....	163
5.3	Concluding Remarks.....	165
<b>References.....</b>		<b>166</b>
<b>Appendices.....</b>		<b>176</b>
Appendix A NMR Spectra.....		176
Appendix B Solid State Molecular Structures and X-ray Data: .....		227

## List of Schemes

Scheme 1.1 2-Pyridonate Ti complexes for polymerization reactions .....	4
Scheme 1.2 Hydroamination and hydroaminoalkylation reactions .....	5
Scheme 1.3 Mn complexes for hydrogenative chemistry .....	6
Scheme 1.4 Ru complexes 1.17 – 1.30 for transfer hydrogenations and hydrogenations .....	7
Scheme 1.5 Comparative study of Ru complexes 1.22, 1.31-1.38 for transfer hydrogenation .....	9
Scheme 1.6 Ru complexes 1.38-1.44 for transfer hydrogenation.....	10
Scheme 1.7 Os Complex 1.45 (right) and Ru catalyzed hydroesterification of ethylene (left) ....	11
Scheme 1.8 2-Pyridonate Ru paddlewheel complexes .....	13
Scheme 1.9 Ru catalyzed terpenylation of piperidines .....	14
Scheme 1.10 Ru catalyzed hydroboration of nitriles .....	14
Scheme 1.11 Ru catalyzed hydrogen borrowing catalysis.....	15
Scheme 1.12 Ru complexes 1.72-1.75 uses in catalytic reactions.....	16
Scheme 1.13 [Fe]-hydrogenase active site Fe-GP cofactor and synthetic derivatives .....	16
Scheme 1.14 [Fe]-hydrogenase inspired Fe and Co complexes .....	17
Scheme 1.15 Dehydrogenative formation of aldehydes with complexes 1.87-1.91.....	22
Scheme 1.16 Dehydrogenative formation of carboxylic acids with 1.96 .....	22
Scheme 1.17 Formation of aldehydes from alcohols using a hydrogen acceptor.....	22
Scheme 1.18 Use of complex 1.88 in dehydrogenative catalysis .....	23
Scheme 1.19 2,2'-Bipyridine derived ligands on Ir precatalysts for dehydrogenative reactions..	24
Scheme 1.20 Ir catalyzed acetal formation with bi- and tri-dentate phosphine-2-pyridone ligands .....	24
Scheme 1.21 Ir catalyzed dehydrogenation/hydrogenation of <i>N</i> -heterocycles.....	25

Scheme 1.22 Ir complex 1.88 used in the catalytic synthesis of unsaturated <i>N</i> -heterocycles .....	26
Scheme 1.23 Square planar Rh(I) complexes 1.139-1.140 ligated with 2,2'-bipyridine derivatives .....	34
Scheme 1.24 Ir complexes for hydrogen borrowing catalysis .....	35
Scheme 1.25 Transfer hydrogenation of ketones with Ir complexes .....	35
Scheme 1.26 Ir complexes for the transfer hydrogenation/hydrogenation of 5-hydroxymethylfurfural and catalytic formation of pyrrolidinones .....	36
Scheme 1.27 Ni 2-pyridonate complex 1.158 and bimetallic Pd/Cu 2-pyridonate complex used in catalysis .....	37
Scheme 1.28 Pd complexes 1.160-1.165 and their activity in catalytic reactions .....	38
Scheme 1.29 Cu 2-pyridonate systems for catalytic reactivity .....	39
Scheme 2.1 Catalytic synthesis of amines by hydroaminomethylation, hydroamination, and Buchwald-Hartwig amination. ....	43
Scheme 2.2 Examples of metal-catalyzed $\alpha$ -C–H functionalization of amines .....	44
Scheme 2.3 Use of steric control for selective C–H functionalization .....	45
Scheme 2.4 Inter- and intra-molecular variants of hydroaminoalkylation .....	46
Scheme 2.5 Intramolecular hydroaminoalkylation reactions .....	47
Scheme 2.6 Sc catalyzed hydroaminoalkylation of trialkyl amines .....	49
Scheme 2.7 Ru and Ir catalyzed hydroaminoalkylation utilizing <i>N</i> -pyridyl directing groups .....	51
Scheme 2.8 Late-transition-metal catalyzed hydroaminoalkylation without a directing group ...	53
Scheme 2.9 Synthesis of 2-pyridonate Ta complexes .....	54
Scheme 2.10 Complementary catalytic reactivity of 2.12 and 2.13 with cyclohexene and 1-octene .....	55

Scheme 2.11 Hydroaminoalkylation of cyclohexene with known precatalyst under our conditions .....	56
Scheme 2.12 Alkene substrate scope for the hydroaminoalkylation catalyzed by 2.12 .....	57
Scheme 2.13 Amine substrate scope for hydroaminoalkylation catalyzed by 2.12.....	58
Scheme 2.14 Substrate scope limitations for hydroaminoalkylation catalyzed by 2.12.....	59
Scheme 2.15 Synthesis of new Ta complexes 2.14-2.20 .....	60
Scheme 2.16 Hydroaminoalkylation activity of new precatalyst complexes with cyclohexene substrate .....	62
Scheme 2.17 Hydroaminoalkylation activity of new precatalyst complexes with 1-octene substrate .....	63
Scheme 2.18 Comparative hydroaminoalkylation reactivity of 2.15 and 2.17.....	65
Scheme 2.19 Deuterium Scrambling Experiment.....	68
Scheme 2.20 Isolation of dialkylated byproduct.....	69
Scheme 2.21 Stoichiometric experiments with variable equivalents of alkene to determine relative amounts of product and byproduct formation.....	70
Scheme 2.22 Ortho-deuteration off-pathway equilibrium .....	73
Scheme 2.23 Analysis of Deuterium Incorporation into Product and Byproduct Aniline after Partial Catalytic Conversion with Variably Deuterated Aniline Substrates .....	75
Scheme 3.1 Comparative hydroaminoalkylation reactivity of Nb and Ta precatalysts.....	92
Scheme 3.2 Deuterium scrambling experiments with complexes 3.7 and 3.8 .....	93
Scheme 3.3 Hydroaminoalkylation reactivity of phosphoramidate ligated Ta complexes .....	93
Scheme 3.4 Synthesis of phosphoramidate Nb complexes 3.13 – 3.17.....	96
Scheme 3.5 Synthesis of niobaziridine complex 3.18 .....	97

Scheme 3.6 Reaction of Nb(NMe <sub>2</sub> ) <sub>5</sub> with two equivalents of phosphoramidate.....	99
Scheme 3.7 Synthesis of niobaziridine 3.20 .....	100
Scheme 3.8 Synthesis of phosphoramidate imido Nb complex 3.21 .....	101
Scheme 3.9 Substrate combinations that are not reactive for hydroaminoalkylation with a phosphoramidate Nb catalytic system .....	108
Scheme 4.1 <i>N</i> -alkylation of amines with alkylamines <i>via</i> hydrogen-borrowing catalysis .....	119
Scheme 4.2 <i>N</i> -alkylation of amines with alcohols <i>via</i> hydrogen borrowing catalysis .....	119
Scheme 4.3 $\alpha$ -Alkylation of cyclic amines with alkenes .....	121
Scheme 4.4 Ru-catalyzed synthesis of $\alpha$ -alkylated amines .....	121
Scheme 4.5 Acceptorless dehydrogenation of <i>N</i> -heterocycles by 2-pyridonate Ir complexes...	122
Scheme 4.6 Mechanism for the acceptorless dehydrogenation of 1,2,3,4-tetrahydroquinoline proposed by DFT calculations .....	123
Scheme 4.7 Stoichiometric dehydrogenation of pyrrolidine by a 1,3- <i>N,O</i> -chelated phosphoramidate Ir complex.....	124
Scheme 4.8 Proposed catalytic cycle for the late-transition metal catalyzed hydroaminoalkylation of amines .....	125
Scheme 4.9 Synthesis of bidentate phosphine-2-pyridone ligands.....	127
Scheme 4.10 Synthesis of Rh, Ir and Ru complexes 4.25, 4.26, and 4.27.....	128
Scheme 4.11 Synthesis of small-bite-angle complexes 4.28 and 4.29 .....	129
Scheme 4.12 Attempted hydroaminoalkylation of isoprene with pyrrolidine .....	130
Scheme 4.13 Reaction of 4.25, 4.26, and 4.27 with 5 equivalents of pyrrolidine .....	131
Scheme 4.14 Reaction of 4.28 and 4.29 with 5 equivalents of pyrrolidine .....	132
Scheme 4.15 Synthesis and isolation of 4.31 and 4.31•pyrrolidine.....	133

Scheme 4.16 Attempted hydroaminoalkylation of isoprene with dibenzylamine .....	135
Scheme 4.17 Generation of tribenzylamine from dibenzylamine .....	135
Scheme 4.18 Attempted catalytic acceptorless dehydrogenation of dibenzylamine .....	137
Scheme 4.19 Attempted catalytic reactions between dibenzylamine and C–C unsaturations....	138
Scheme 4.20 Synthesis and reactivity of 4.41 .....	139
Scheme 4.21 (a) Synthesis of Rh(I) and Ir(I) complexes 4.45 and 4.46; (b) attempted use of M(I) as precatalysts for hydroaminoalkylation .....	140
Scheme 4.22 Attempted synthesis of phosphino-2-pyridonate ligated Ru–H complexes .....	141
Scheme 4.23 Attempted hydroaminoalkylation of 2,3-dimethyl-1,3-butadiene with piperidine <i>in situ</i> generated Ru catalysts.....	142
Scheme 4.24 Attempted hydroaminoalkylation of isoprene with pyrrolidine using Ru complexes 4.43 and 4.44.....	142
Scheme 5.1 Synthesis of Ta alkyl complexes analogous to 2.12.....	162
Scheme 5.2 Potential tethered diphosphoramidate protio-ligands for use in Nb catalyzed hydroaminoalkylation .....	163

## List of Tables

Table 1.1 Dehydrogenation of 1-phenylethanol to acetophenone .....	20
Table 1.2 Compiled results of catalytic hydrogenation of CO <sub>2</sub> .....	30
Table 1.3 Compiled results of catalytic dehydrogenation of formic acid .....	31
Table 2.1 Comparison of key bond lengths and angles of the solid state molecular structures of 2.12, 2.15, 2.16, and 2.18.....	61
Table 3.1 Evaluation of monophosphoramidate Nb complexes as precatalysts for hydroaminoalkylation .....	103
Table 3.2 Evaluation of diphosphoramidate and imido Nb complexes as precatalyst for hydroaminoalkylation .....	105
Table 3.3 Evaluation of substrate scope of Nb catalyzed hydroaminoalkylation.....	107
Table B.1 Single crystal X-ray diffraction data for complexes 2.15, 2.16, and 2.18 .....	229
Table B.2 Single crystal X-ray diffraction data for complexes 3.13, 3.18, 3.20, 3.21 .....	230
Table B.3 Single crystal X-ray diffraction data for complexes 4.25, 4.26, and 4.41 .....	232



## List of Figures

Figure 1.1 Nomenclature and binding modes of 2-pyridone derived ligands.....	3
Figure 1.2 Complexes 1.81-1.100 used for catalysis discussed in this section .....	20
Figure 1.3 Complexes 1.117-1.138 utilized in catalytic hydrogenation/dehydrogenation of CO <sub>2</sub> /HCOOH.....	27
Figure 1.4 Ir complexes studied for catalytic water oxidation.....	36
Figure 1.5 Cu complexes 1.167-1.175 tested as catalyst in electrochemical water oxidation.....	39
Figure 2.1 Early-transition-metal catalysts used for the intermolecular hydroaminoalkylation of secondary amines .....	48
Figure 2.2 Proposed mechanism for early-transition-metal catalyzed hydroaminoalkylation .....	50
Figure 2.3 Proposed mechanism for directed, late-transition-metal catalyzed hydroaminoalkylation .....	52
Figure 2.4 ORTEP representations of 2.15 (top-left), 2.16 (top-right), and 2.18 (bottom) .....	62
Figure 2.5 Hydroaminoalkylation Reaction Monitoring with 5, 8, and 12 mol % of [Ta] Precatalyst 2.15 .....	71
Figure 2.6 Graphical representation of resting state equilibria.....	73
Figure 2.7 Plot of reaction monitoring experiments with 5, 8, and 12 mol% 2.15 as precatalyst for the hydroaminoalkylation reaction between N-methylaniline and 1-octene. Overlay of both experiments .....	89
Figure 2.8 Plot of reaction monitoring experiments with 12 mol% 2.15 as precatalyst for the hydroaminoalkylation reaction between <i>N</i> -methylaniline (variably deuterated) and 1-octene. Overlay of both experiments.....	90
Figure 3.1 Nb complexes reported for hydroaminoalkylation and their direct Ta analogues .....	91

Figure 3.2 ORTEP representation of 3.13 with select bond lengths and angles.....	96
Figure 3.3 ORTEP representation of 3.18 and select bond lengths and angles .....	98
Figure 3.4 ORTEP representations of 3.20 (left) and 3.21 (right) with select bond lengths and angles .....	100
Figure 4.1 Transition-metal complexes reported to catalyze the acceptorless dehydrogenation of amines .....	124
Figure 4.2 ORTEP representations of the solid-state molecular structures of 4.25 and 4.26 .....	128
Figure 4.3 ORTEP representation of the solid-state molecular structure of 4.41 .....	139
Figure 5.1 Examples of alternative ligand sets for future work toward late-transition-metal catalyzed hydroaminoalkylation chemistry .....	165

## List of Abbreviations

Abbreviation	Description
1D	1-dimensional
2D	2-dimensional
Ac	acetyl
Ad	adamantyl
Anal.	analysis
aq	aqueous
$[\text{B}(\text{ArF})_4]^-$	tetrakis(3,5-trifluoromethylphenyl)borate
BINAP	(1,1'-binaphthalene-2,2'-diyl)bis(diphenylphosphine)
BINOL	1,1'-bi-2-naphthol
bipy	2,2'-bipyridine
br	broad (spectral)
Bn	benzyl
Bu	butyl
$^{13}\text{C}\{^1\text{H}\}$	$^{13}\text{C}$ with $^1\text{H}$ broadband decoupling NMR experiment
Calc'd	calculated
cat.	catalyst
CL	caprolactone
Cp	cyclopentadienyl
Cp*	$\eta^5$ -1,2,3,4,5-pentamethylcyclopentadienyl

<b>Abbreviation</b>	<b>Description</b>
COD	1,5-cyclooctadiene
COSY	correlation spectroscopy
Cy	cyclohexyl
d	doublet (spectral)
dap	2,9-disubstituted-1,10-phenanthroline
DCM	dichloromethane
dCypm	bis(dicyclohexylphosphino)methane
dCypp	bis(dicyclohexylphosphino)propane
dd	doublet of doublets (spectral)
Dipp	2,6-diisopropylphenyl
DFT	density functional theory
DMAP	4-dimethylaminopyridine
DMF	dimethylformamide
DMSO	dimethylsulfoxide
dppe	bis(diphenylphosphino)ethane
dppp	bis(diphenylphosphino)propane
dtbbpy	4,4'-bis( <i>tert</i> -butyl)-2,2'-bipyridine
E/Z	entgegen (“opposite”) / zusammen (“together”) (isomers)
EA	elemental analysis
EI	electron impact
ESI	electrospray ionization

<b>Abbreviation</b>	<b>Description</b>
equiv.	equivalents
Et	ethyl
Fc	ferrocene
Fe-GP	Fe-guanylylpyridinol
g	gram
G	Gibb's free energy
GC	gas chromatography
GMP	guanosine monophosphate
H	enthalpy
HA	hydroamination
HAA	hydroaminoalkylation
HMDS	bis(trimethylsilyl)amide
H <sub>4</sub> MPT <sup>+</sup>	tetrahydromethyanopterin
h	hour(s)
hex	hexyl
Hz	Hertz
iPr	isopropyl
Ind	indenyl
K	kelvin
kJ	kilojoule

<b>Abbreviation</b>	<b>Description</b>
kcal	kilocalorie
L	liter
LA	lactide
LAH	lithium aluminum hydride
LED	light emitting diode
M	molarity
m	multiplet (spectral)
m	meta
Me	methyl
mg	milligram
mL	milliliter
mmol	millimole
MS	mass spectrometry
MOF	metal-organic framework
mol	mole
m/z	mass-to-charge ratio
n	normal
ND	not determined
NHC	<i>N</i> -heterocycliccarbene
nM	nanomolar

<b>Abbreviation</b>	<b>Description</b>
NMR	nuclear magnetic resonance
o	ortho
OAc	acetate
OPiv	trimethylacetate, 2,2-dimethylpropionate
ORTEP	Oakridge thermal ellipsoid plot
p	para
p-cymene	1-isopropyl-4-methylbenzene, 4-isopropyltoluene
PE	petroleum ether
Ph	phenyl
pH	potential of hydrogen
ppm	parts per million
PMP	para-methoxyphenyl
pyr	pyridine
q	quartet (spectral)
quint	quintet (spectral)
R	ideal gas constant
RT	room temperature
rac	racemic
red	reduction
ROMP	ring-opening metathesis polymerization
s	singlet (spectral)

Abbreviation	Description
S	entropy
sec	second
sept	septet (spectral)
t	triplet (spectral)
t-	tertiary
tert-	tertiary
temp	temperature
t-amyl	1,1-dimethyl propyl, $-\text{C}(\text{CH}_3)_2\text{CH}_2\text{CH}_3$
TBA	tetrabutyl ammonium
TBDMS	tert-butyldimethylsilyl
Tf	trifluoromethylsulfonyl
THF	tetrahydrofuran
TMS	tetramethylsilane (molecule)
TMS-	trimethylsilyl (group)
Tol	toluene (molecule)
Tol-	tolyl (group)
tol-BINAP	2,2'-bis(di- <i>p</i> -tolylphosphino)-1,1'-binaphthyl
VT	variable temperature



## List of Symbols

Symbol	Description
°	degree
°C	degrees Celsius
Å	angstrom
δ	chemical shift in ppm
Δ	thermal heat; change
Đ	polydispersity (polymers)
η <sup>x</sup>	eta, denotes hapticity of x atoms
<sup>n</sup> J <sub>AB</sub>	n-bond coupling constant between atoms A and B (spectral)
k <sub>obs</sub>	observed rate constant
κ <sup>x</sup>	kappa, denotes denticity of x atoms
K <sub>eq</sub>	equilibrium constant
μ <sup>x</sup>	mu, denotes bridging of ligand to x metal centers

## Acknowledgements

I would like to sincerely express my thanks and gratitude to the many people and organizations that made this thesis possible. First and foremost, I would like to thank my supervisor Prof. Laurel Schafer. The time, patience, and effort required to teach, develop, and encourage a student through completion of a Ph.D. is immense.

Many thanks go to my current and former colleagues of the Schafer group, who have been continually insightful and supportive. Thank you to Erica Lui, whose editing has made this document appear to be written in English.

Thank you to Prof. Glenn Sammis and Prof. Jen Love for offering their time and insight towards the assembly of this document. Their comments and suggestions have greatly improved the quality of this thesis.

I would also like to thank the many members of the UBC Chemistry department who maintain and make our lab equipment and instruments. Without them, this research would not be possible. Thank you to UBC (4YF) and NSERC (CGS-M, PGS-D) for financial support throughout my graduate studies.

Finally, I would not be where I am today without the support of my parents, Bill and Jane, my sister, Rebecca, and my girlfriend, Erica. I will be forever indebted to them for their love, support, encouragement, and for putting up with my nonsense for all these years.

## **Dedication**

I dedicate this thesis to my parents and my sister,  
and to Erica.

## Chapter 1: Introduction

Organic molecules containing amine functional groups are ubiquitous throughout the chemical industries and often play significant roles in the function of many useful products.<sup>1-3</sup> Specific examples of amine utilization include pharmaceuticals,<sup>4-5</sup> the development of novel polymers, electronic and other advanced materials,<sup>6-10</sup> and industrially used chemicals, such as compounds for the sequestration of CO<sub>2</sub>.<sup>11</sup> Fundamental research into the general reactivity and synthesis of amines provides the foundational concepts and chemical space for this class of molecules. In turn, this allows for advances in biochemistry, chemical biology, pharmacology, and industry.

Catalytic syntheses can offer multiple advantages over their stoichiometric counterparts. Catalysis offers the ability to alter the reaction pathway for a given set of starting materials and products.<sup>12</sup> This can allow for novel reactivity of traditionally unreactive bonds, and provide alternative and/or improved chemo-, regio-, and stereo-selectivity of the product. Ultimately, catalysis allows for alternate disconnection strategies in the synthesis of molecules, significantly broadening the available chemical space, in turn leading to new developments. Catalysis can also significantly reduce the associated synthetic cost by reducing the number steps in a synthetic pathway, gaining step- and atom-efficiencies, and by reducing, or eliminating, the byproducts associated with a stoichiometric synthesis.<sup>13</sup> A general theme of research into catalysis is to develop novel reactions while undertaking studies to understand the general reactivity properties of a catalyst, thereby leading to improved catalyst development.

One way to catalytically synthesize amine containing molecules is through the use of homogenous transition-metal complexes as catalysts. Amines can serve many chemical functions, such as acting as an acid or base, a hydrogen bond donor or acceptor, or as a

nucleophile. While this diverse reactivity can be exploited for a variety of applications, this reactivity often makes the synthesis of amine-containing molecules difficult as unintended side-reactions often occur. With specific reference to transition-metal based catalysis, the high Lewis basicity of amines causes them to often be good ligands themselves. As a base and/or nucleophile, amines can also react with the ligand of the transition-metal catalyst. Additionally, the oxidation potential of amines often overlaps with the reduction potential of the transition-metal complex, causing reduction of the metal center. Together, these effects lead to catalyst deactivation. Often, conversion of the free amine into a deactivated or protected form (e.g. amide, carbamate, sulfonamide, etc.) is required to avoid catalyst deactivation. However, requiring stoichiometric protection/deprotection strategies adds complexity and inefficiency to a synthetic pathway. A desirable catalytic transformation would be able to avoid the use of protection/deprotection steps.

To promote the desired reactivity of a transition-metal catalyst, significant effort must be made toward ligand and complex design. Choice of ligands will affect the electron density at the metal center and the steric environment about the metal center. Choice of the transition-metal ion and oxidation state will also bring about drastic changes in reactivity of the complex towards organic molecules, and, in the case of this thesis, amines.

## **1.1 Scope of Thesis**

The focus of this thesis will be on the use of transition-metal complexes containing 1,3-*N,O*-chelating ligands as precatalysts towards the transformation of simple amine substrates into complex amine products. A central goal of this thesis is to present novel conclusions on how the design of specific 1,3-*N,O*-chelating ligands can affect the reactivity of transition-metal complexes with amines and catalytic transformation of amines.

Significant research has been devoted to the use of 2-pyridonate and 2-pyridone ligated transition-metal complexes in catalytic reactions. The remainder of Chapter 1 will review this topic and highlight the significance of ligand design in the reactivity of transition metal complexes. Chapter 2 will present the development of a novel 2-pyridonate tantalum precatalyst for the hydroaminoalkylation of alkenes with amines. Chapter 2 will also provide an introduction to the hydroaminoalkylation reaction and other catalytic  $\alpha$ -C(sp<sup>3</sup>)-H functionalization of amines. Chapter 3 will present the development of alternative 1,3-*N,O*-chelating systems, phosphoramidate niobium precatalysts, for the hydroaminoalkylation reaction. In addition, it will introduce Nb precatalysts and phosphoramidates as ancillary ligands for the hydroaminoalkylation reaction. Chapter 4 will present efforts to develop phosphine-tethered 2-pyridonate Ru, Rh, and Ir precatalysts towards the hydroaminoalkylation reaction and the acceptorless dehydrogenation of amines. Further, Chapter 4 introduces the concept of alkylation of amines *via* a dehydrogenative/hydrogen-borrowing approach. Chapter 5 will offer concluding remarks and future outlooks on the chemistry presented in the thesis.

## 1.2 2-Pyridones as Ligands for Transition-Metal-Catalyzed Reactions

2-Pyridones (or 2-hydroxypyridines) are found in equilibrium between the two tautomeric forms, where the equilibrium can depend on substitution and the solvent (Figure 1.1).<sup>14-16</sup> As will be discussed in the following sections, ligation of the 2-pyridone can result in multiple binding modes, with various naming conventions, as detailed in Figure 1.1 for reference.

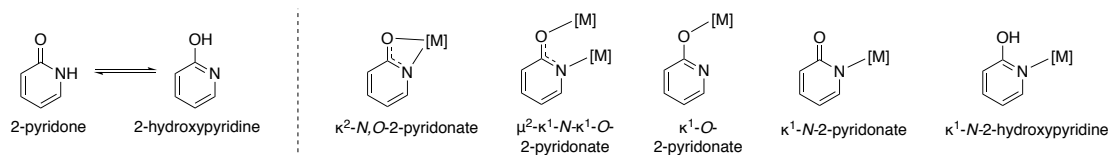
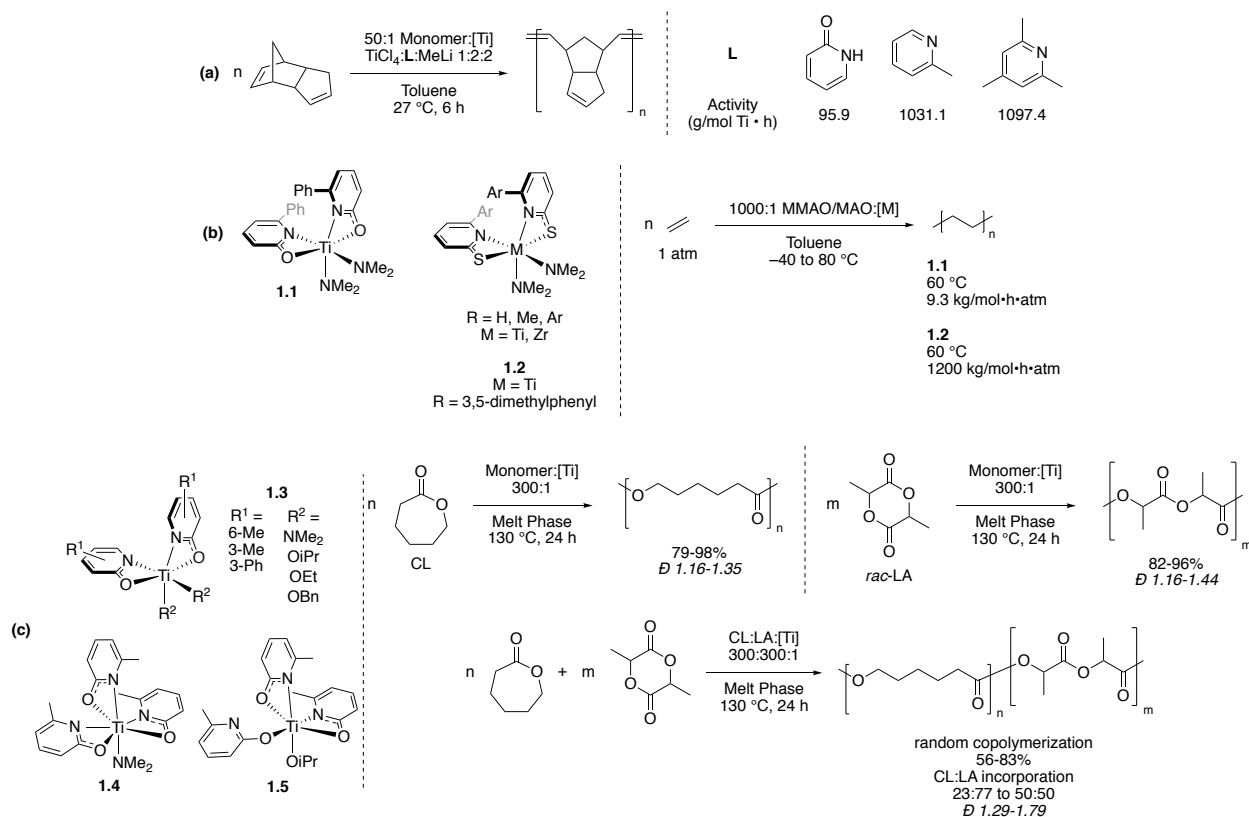


**Figure 1.1 Nomenclature and binding modes of 2-pyridone derived ligands**

### 1.2.1 Group 4 – 7 Transition-Metal Precatalysts with 2-Pyridone Ligands

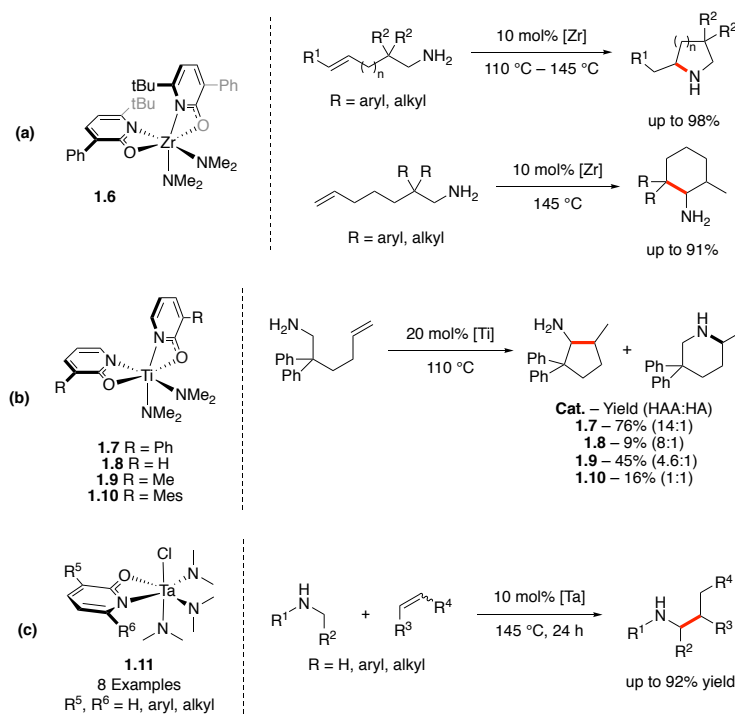
Examples of 2-pyridonate complexes of early-transition metals (groups 4-6) utilized for catalysis are limited to Ti,<sup>17-21</sup> Zr,<sup>22-23</sup> and Ta.<sup>24-26</sup> 2-Pyridonate Ti complexes have been utilized in multiple polymerization reactions (Scheme 1.1). In ring opening polymerization (Scheme 1.1a), the 2-pyridonate ligand is found to have significantly lower activity than other pyridine derivatives.<sup>17</sup> Isolated Ti complex **1.1** is active for ethylene polymerization but has significantly worse reactivity compared to thiopyridinate complex **1.2** (Scheme 1.1b).<sup>18</sup> Complexes **1.3**, **1.4**, and **1.5** demonstrate structural variety that is possible with 2-pyridonate ligands and are active pre-catalysts for the ring opening polymerization of  $\epsilon$ -caprolactone and lactide (Scheme 1.1c).<sup>20-21</sup> While multiple derivatives of the 2-pyridonate motif were utilized in polymerization, Schafer



Scheme 1.1 2-Pyridonate Ti complexes for polymerization reactions

and co-workers did not determine a direct structure-activity relationship with respect to the 2-pyridonate ligand.

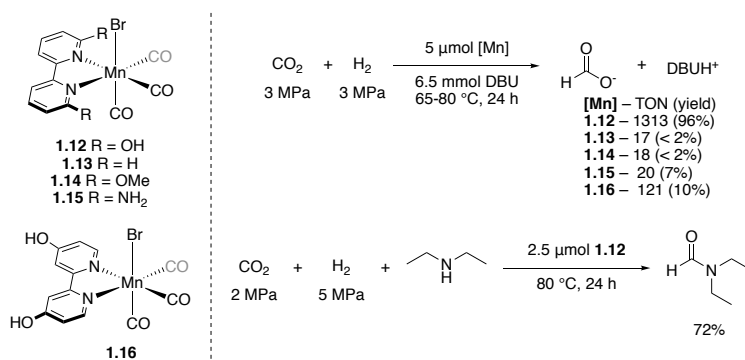
Zr complex **1.6** (Scheme 1.2a) has been demonstrated to show substrate dependent intramolecular hydroamination (HA) and hydroaminoalkylation (HAA) reactivity.<sup>22-23</sup> A series of structurally varied 2-pyridonate Ti complexes **1.7** – **1.10** were evaluated for selective hydroaminoalkylation over hydroamination (Scheme 1.2b).<sup>19</sup> Interestingly, it was shown that 3-phenyl-2-pyridonate **1.7** provided superior yield and selectivity for hydroaminoalkylation with only minor structural change to the 2-pyridonate ligand. This suggests that modification of the pyridonate can have a significant effect on activity and selectivity. This is also shown in Ta catalyzed hydroaminoalkylation (Scheme 1.2c).<sup>24-26</sup> Complexes of the type **1.11** are the first reported complexes active for hydroaminoalkylation of internal alkenes without isomerization (see Chapter 2).



**Scheme 1.2 Hydroamination and hydroaminoalkylation reactions**



A single report on Mn bipyridine complexes highlights the high reactivity of complex **1.12** in the hydrogenation of CO<sub>2</sub> (Scheme 1.3).<sup>27</sup> Compared to analogues **1.13** – **1.16**, the presence of the 2-hydroxypyridine motif is required for the high activity observed. Khusnutdinova and co-workers here propose the ability of the 2-hydroxypyridine motif to act as an intramolecular proton shuttle that is positioned in close proximity to the reactive site as key to the reactivity. This concept reappears significantly in the following late-transition metal discussions (Chapter 1.2.2, 1.2.3, and 1.2.4). Complex **1.12** highlights the  $\kappa^1$ -*N*-2-hydroxypyridine binding mode (with respect to a single pyridyl ring).

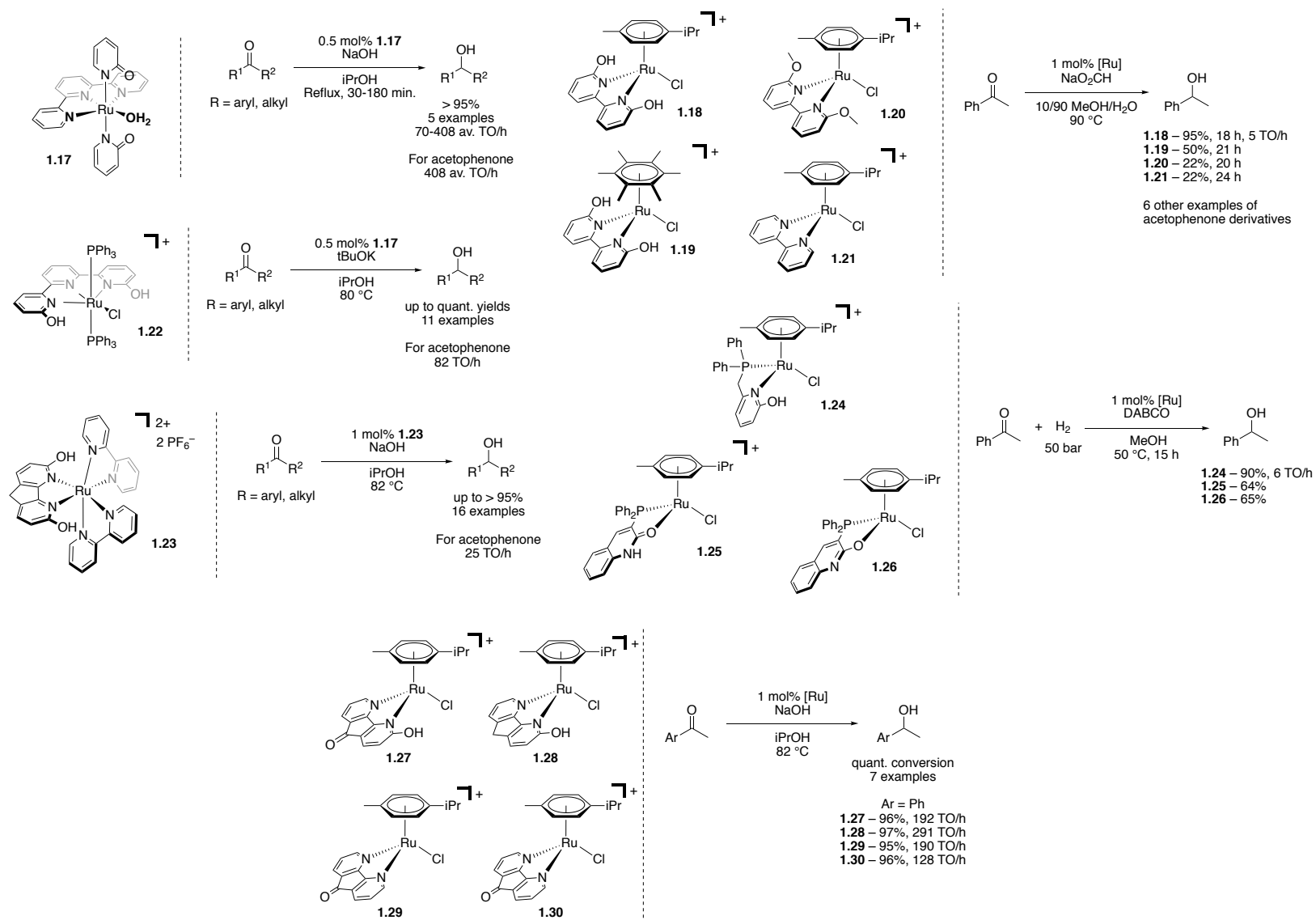


Scheme 1.3 Mn complexes for hydrogenative chemistry

## 1.2.2 Group 8 Transition-Metal Precatalysts with 2-Pyridone Ligands

### 1.2.2.1 Transfer Hydrogenation and Hydrogenation of Ketones

Many examples of group 8 metals featuring 2-hydroxypyridine ligands have been synthesized and tested for hydrogenation and dehydrogenation reactions. Additionally, many have also been compared against analogues that have the 2-hydroxy functionality removed, blocked, or transferred to another position of the pyridine ring. This effectively isolates the hydroxyl functionality from the reactive site to determine if cooperative action of the hydroxyl group is required for the reported activity.



Scheme 1.4 Ru complexes 1.17 – 1.30 for transfer hydrogenations and hydrogenations

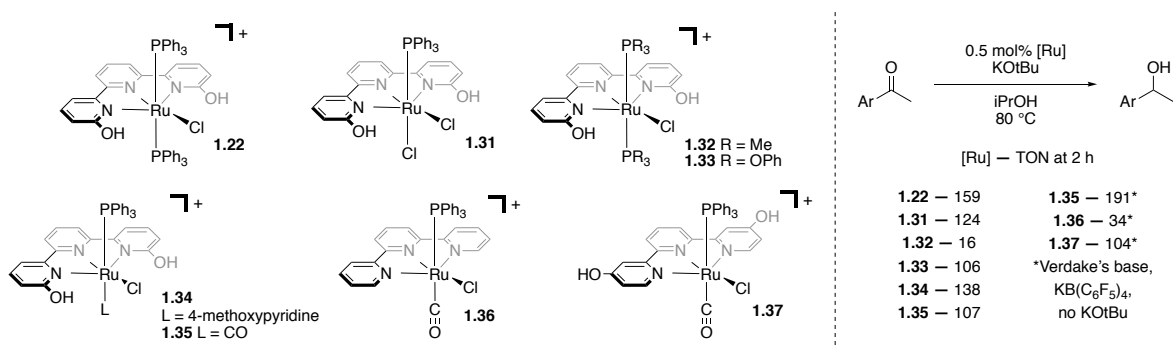
An early report, in 2000, detailed the transfer hydrogenation of ketones by **1.17** achieving promising turnovers per hour (TO/h) (Scheme 1.4).<sup>28</sup> This catalyst has recently been stabilized on colloidal Fe nanoparticles as a reusable transfer hydrogenation catalyst.<sup>29</sup> Not until 2011 was interest renewed in 2-hydroxypyridine complexes of Ru for these reaction types. This coincides with interest in similar Ir complexes for hydrogenation/dehydrogenation reactions (See Chapter 1.2.3).

A comparative study of complexes **1.18** – **1.21** demonstrates the ability of this type of complex to perform transfer hydrogenations in water (Scheme 1.4).<sup>30</sup> The 6,6'-dihydroxy-2,2'-bipyridine complex **1.18** significantly outperformed 6,6'-dimethoxy-2,2'-bipyridine complex **1.20** and 2,2'-bipyridine complex **1.21**, highlighting the importance of the 2-hydroxypyridine motif. Complex **1.22** is effective for the transfer hydrogenation of ketones.<sup>31</sup> For ketone substrates that incorporate alkenes ( $\alpha,\beta$ -unsaturated ketones not reported), **1.22** was found to be selective for the reduction of ketones. The dicationic complex **1.23** was also active for this reaction and includes high yields with 16 ketone examples and comparable turnover rates.<sup>32</sup>

Complexes **1.24** – **1.26** incorporate a phosphine tether to create a *P,N* (**1.24**) or *P,O* (**1.25**, **1.26**) type chelate. These were found to be active for the hydrogenation of acetophenone with 50 bar H<sub>2(g)</sub>. Notably, a base additive was required to achieve high reactivity, as the anionic 2-pyridonate was proposed to be involved in the splitting of H<sub>2</sub> to form the active [Ru–H] species.<sup>33</sup> The 4,5-diazafluorene motif has also been utilized on arene supported complexes and tested for the transfer hydrogenation of acetophenone derivatives. Of the seven new complexes reported, **1.27** – **1.30** directly compare the effect of including a 3-hydroxy group (forming the 2-hydroxypyridine sub-motif) to those precatalysts without this functionality (Scheme 1.4).<sup>34</sup> While **1.28** provided the highest turnover per hour (TO/h), the other complexes were also highly

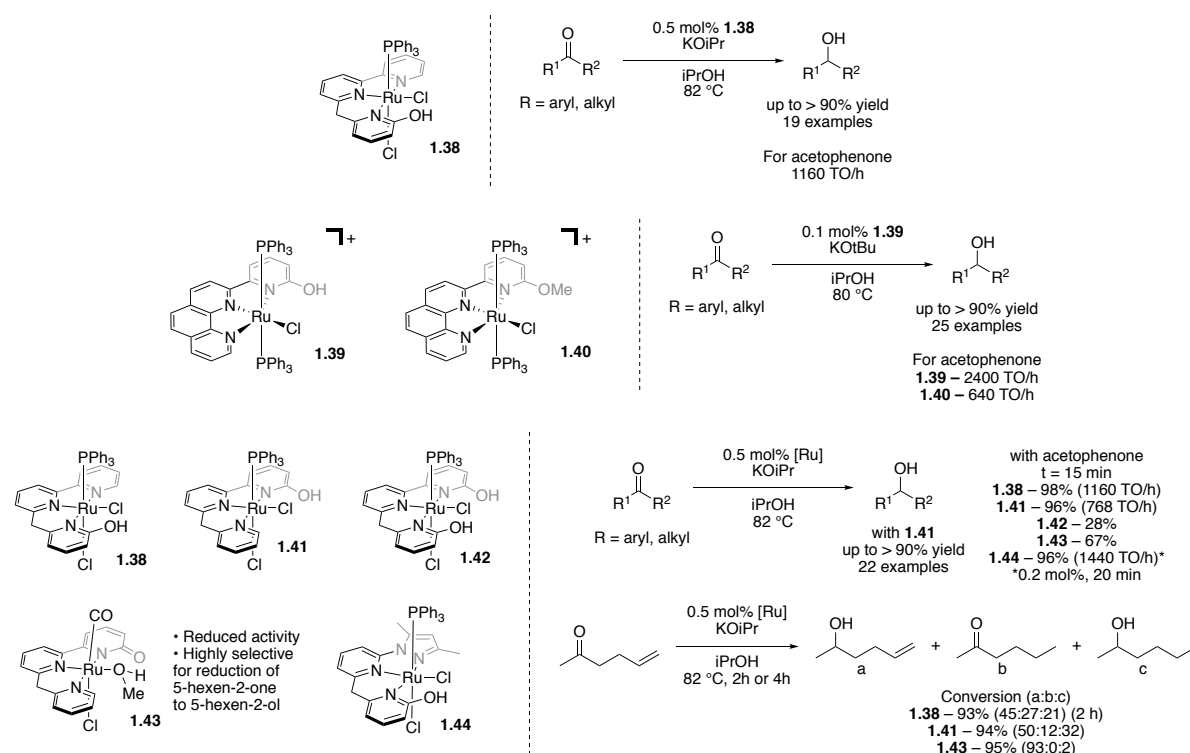
effective for this reaction. The comparative hydrogenation activities leave ambiguity as to the significance of the 2-hydroxypyridine motif in transfer hydrogenation with Ru complexes chelated with bidentate 4,5-diazafluorene derived ligands.

A recent report by Szymczak and co-workers has built upon the success of complex **1.22**, and has investigated the analogous complexes **1.31** – **1.37**.<sup>35</sup> Scheme 1.5 illustrates the complexes and their reported turnover numbers (TON) at 2 h. Complex **1.35** proves to be most active. However, **1.37** is also comparable to most of the other complexes. In basic reaction conditions, the deprotonated hydroxyl functionality may serve to create a more electron rich metal center enhancing the reactivity in both **1.35** and **1.37** over **1.36**. Additionally, this report details reaction kinetics, as well as identified a strong cation effect that significantly affected the rate of the reaction. Transfer hydrogenation of 5-hexen-2-one to 5-hexen-2-ol with complex **1.35** results in 96% conversion in 3 h with complete selectivity for reduction of the ketone. Complexes **1.36** and **1.37** produce only 13% and 12% conversion with a mixture of alkene and double reduction products. The authors suggest a concerted hydrogenation mechanism that involves the 2-hydroxypyridine motif acting as a proton source during the hydrogenation.



**Scheme 1.5 Comparative study of Ru complexes 1.22, 1.31-1.38 for transfer hydrogenation**

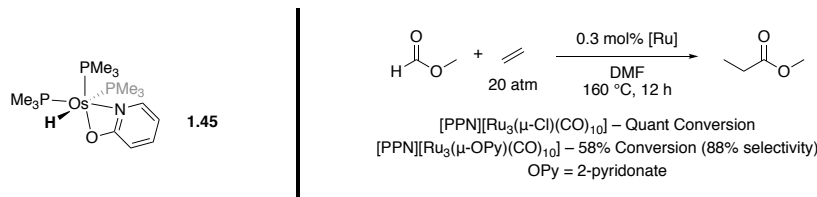
The addition of a single methylene linker in **1.38**, as a modification to the terpyridine derivatives, resulted in an order of magnitude increase in turnover rate at 1160 turnover per hour for acetophenone reduction (Scheme 1.6).<sup>36</sup> Complex **1.39** also offered significant improvements with turnover frequency of 2400/h for acetophenone reduction (Scheme 1.6).<sup>37</sup> The methoxy-derivative, complex **1.40**, is also active for this transfer hydrogenation. However, the significantly reduced 640 turnovers per hour for acetophenone reduction demonstrates the role of the 2-hydroxy group for improved rate. A more complete follow up examination of derivatives of **1.38** has also been reported (Scheme 1.6).<sup>38</sup> Among the 11 complexes reported, the most relevant to this discussion are the illustrated **1.42** and **1.43**. Ru complex **1.43** demonstrates high activity, although reduced compared to **1.38**. Complex **1.39**, featuring two 2-hydroxypyridine motifs, resulted in a significant decrease in reaction rate. Optimization found that an axial carbon



Scheme 1.6 Ru complexes **1.38**-**1.44** for transfer hydrogenation

monoxide ligand (**1.43**) significantly improves selectivity over phosphine ligated complexes **1.38** and **1.39**, while reducing activity.<sup>36,38</sup> Additional *N,N,N*-chelates have been reported with **1.44** exhibiting the highest activity.<sup>39</sup> This increased activity decreases selectivity for the reduction of 5-hexen-one consistent with the reports on these tridentate derivatives.

A 2-pyridonate Os complex **1.45** has been tested for the hydrogenation of 1-hexene. While the reactivity was middling, further study demonstrates the strained chelate improves reactivity relative to other, derivative Os catalysts, but did not comment on the role of the 2-pyridonate ligand (Scheme 1.7).<sup>40</sup>

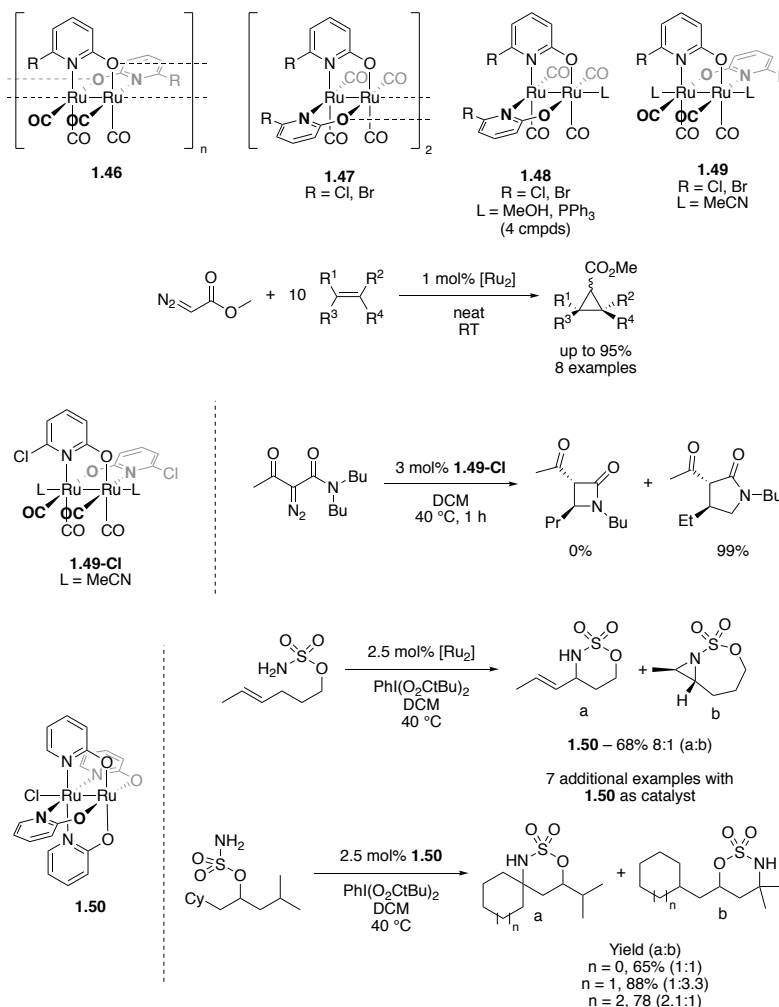


Scheme 1.7 Os Complex **1.45** (right) and Ru catalyzed hydroesterification of ethylene (left)

### 1.2.2.2 Additional Reactions with Group 8 Complexes

One of the earliest reports utilizing 2-pyridonate ligands was of a tri-ruthenium system (Scheme 1.7).<sup>41</sup> However, reactivity for hydroesterification of ethylene was poor compared to a chloro tri-ruthenium complex. Multiple examples of di-ruthenium paddlewheel-type complexes bearing 2-pyridonate ligands have been reported for multiple reactions. Complexes of the types **1.46** – **1.49** have been demonstrated to be active catalysts for cyclopropanation reactions with diazo compounds (Scheme 1.8). However, pyridonate derivatives exhibit poor reactivity and selectivity compared to their acetate analogues.<sup>42</sup> Complex **1.49-Cl** has been utilized in the synthesis of  $\gamma$ -lactams along with a large variety of Ru complexes (Scheme 1.8).<sup>43-44</sup> Ru complex **1.49-Cl** is a competent precatalysts with some of the best reactivity and selectivity for the synthesis of  $\gamma$ -lactams. Related complex **1.50** was found to be highly successful for

intramolecular allylic C–H amination (Scheme 1.8).<sup>45</sup> Complex **1.50** provided significant enhancement to both reactivity and selectivity compared to acetate derivatives in screening, and provided high selectivity with eight substrates. Compound **1.50** was also utilized in a similar C–H amination of aliphatic substrates (Scheme 1.8).<sup>46</sup> Reactivity and selectivity both suffered in comparison to a variety of Ag catalysts also screened for this reaction. It should be noted that the paddlewheel complexes demonstrate varied binding modes for 2-pyridonate ligands such as  $\mu^3$ - $\kappa^2$ -*N,O*- $\kappa^1$ -*O* binding (**1.46**, **1.47**) and  $\mu^2$ - $\kappa^2$ -*N,O* binding in others (**1.48**, **1.49**).

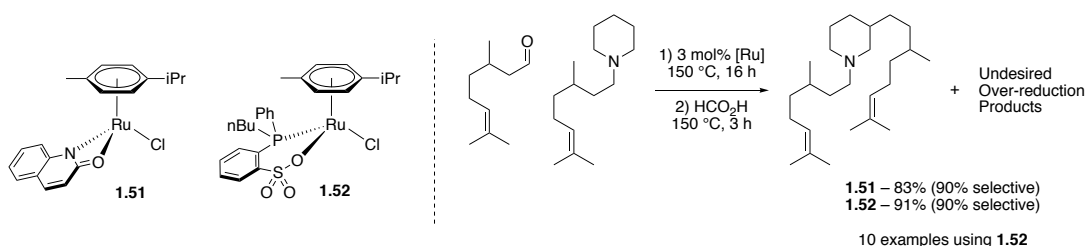


**Scheme 1.8 2-Pyridonate Ru paddlewheel complexes**

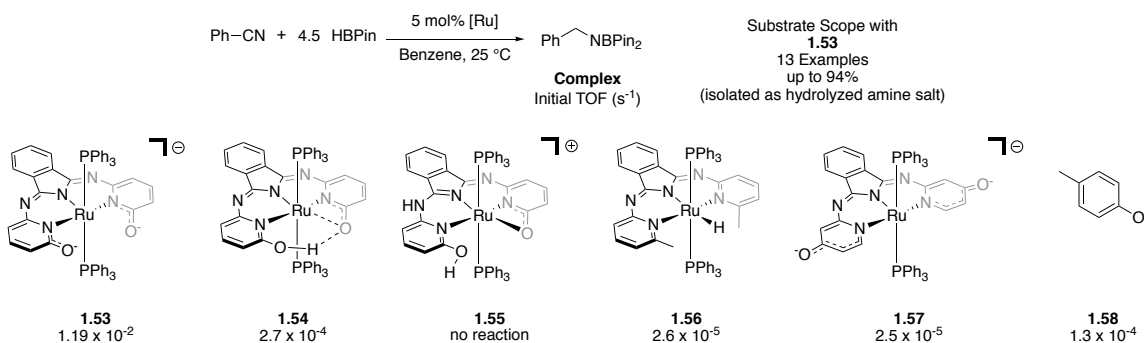
Complex **1.51** was examined for an interesting C–C bond forming terpenylation of *N*-heterocycles (Scheme 1.9).<sup>47</sup> While **1.51** demonstrated similar reactivity and selectivity to the optimal precatalyst candidate **1.52**, substrate scope was examined only with **1.52**. While the mechanism is not discussed, a transfer hydrogenation utilizing formic acid as the hydrogen source was also exploited in the reaction.



Tridentate complexes **1.53** – **1.57** (and **1.58** as a control) were examined for the hydroboration of arylcyanides to benzylamines (after acidic workup) (Scheme 1.10).<sup>48</sup> The anionic complex **1.53** is highly successful for this reaction and 13 examples are provided. These complexes highlight interesting aspects of coordination for the 2-pyridonate fragments. The addition of one equivalent of an acid to **1.53** resulted in protonation of one 2-pyridonate fragments to form **1.54**. A second equivalent of acid, interestingly, did not protonate the second 2-pyridonate fragment, and rather protonated a backbone nitrogen atom to generate **1.55**.



**Scheme 1.9 Ru catalyzed terpenylation of piperidines**

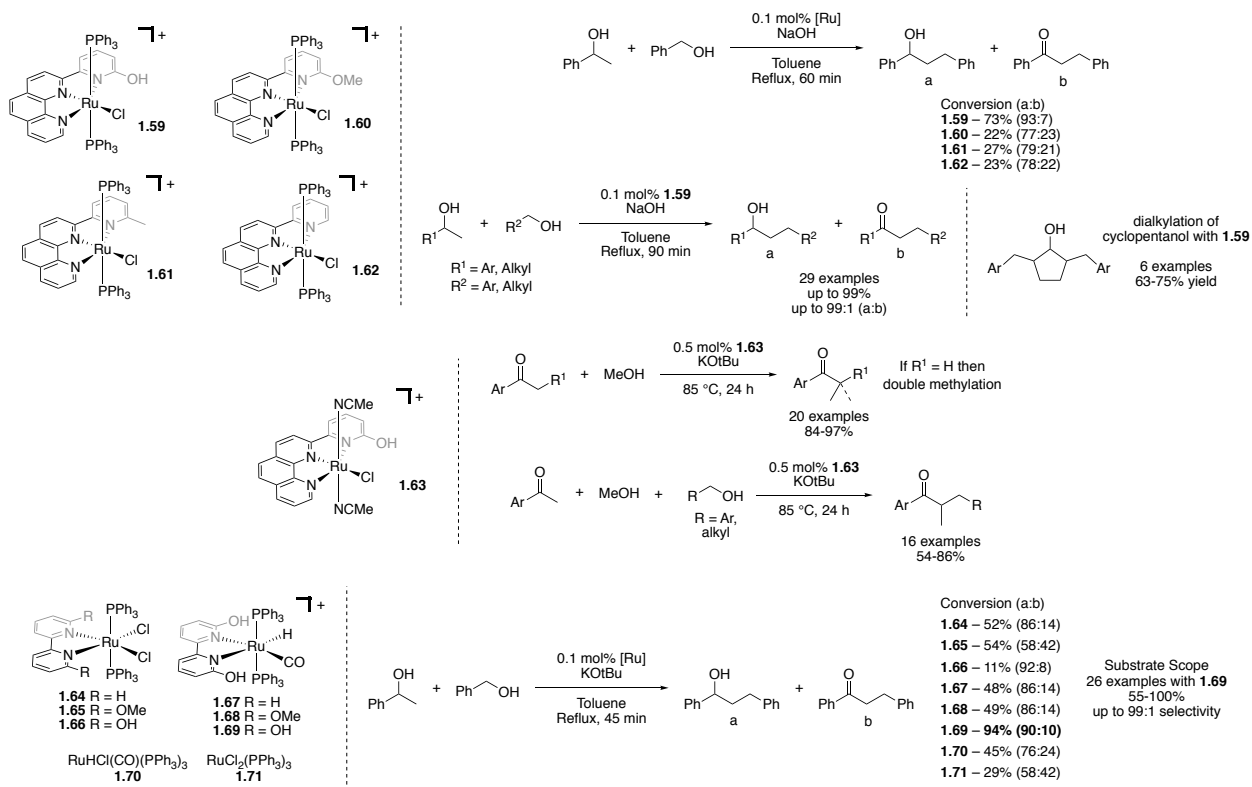


**Scheme 1.10 Ru catalyzed hydroboration of nitriles**

Many Ru complexes are reported for hydrogen-borrowing catalysis. Ru complexes **1.59** – **1.62** are compared for their reactivity in the Geurbet reaction, the coupling of two alcohols resulting in the  $\alpha$ -alkylated alcohol product (Scheme 1.11).<sup>49</sup> These derivatives demonstrate that the 2-hydroxypyridine fragment in **1.59** plays a crucial role to improving the reactivity and the selectivity of the reaction. Related complex **1.63** was found to be an active precatalyst for the mono- and di-methylation of ketones utilizing methanol as the C1-source. Additionally, **1.63** was

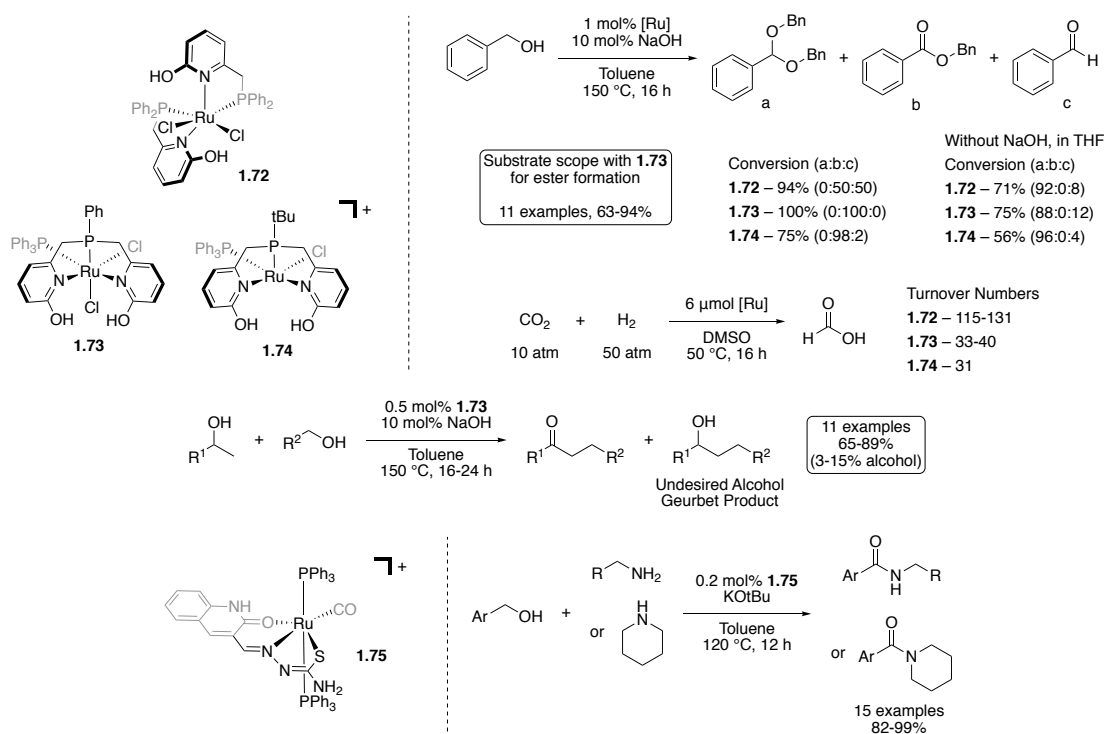
exploited for a multicomponent alkylation-methylation of ketones (Scheme 1.11).<sup>50</sup> A study of the Geurbet reaction involving a variety of bipyridine Ru complexes included the use of the 6,6'-dihydroxy-2,2'-bipyridine complexes **1.66** and **1.69** (Scheme 1.11).<sup>51</sup> As illustrated, their findings demonstrated the 2-hydroxypyridine fragment was important to selectivity and reactivity in this reaction.

A series of 2-hydroxy-6-phosphinomethyl-pyridine Ru complexes **1.72** – **1.74** were reported for the dehydrogenation reactions of alcohols to form acetals or esters, and the hydrogenation of CO<sub>2</sub> with H<sub>2</sub> to form formic acid (Scheme 1.12).<sup>52</sup> Interestingly, the addition of base significantly altered reactivity. With base, ester formation was favoured, with **1.73** providing the highest activity and complete selectivity. In the absence of base, the acetal product was formed, with **1.73** as the best performing precatalyst. Complex **1.73** was also reported for

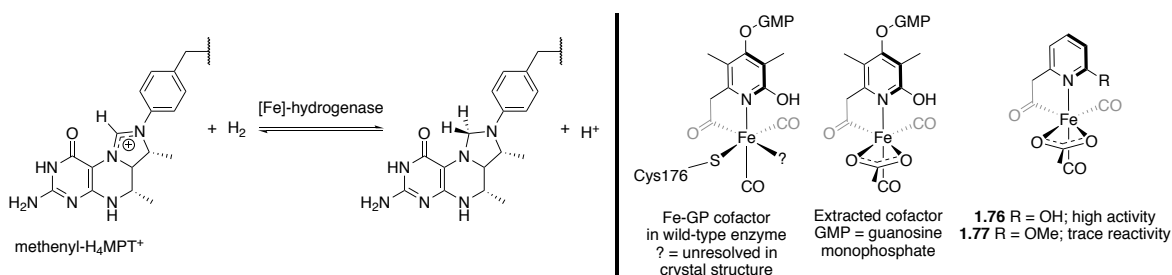


**Scheme 1.11 Ru catalyzed hydrogen borrowing catalysis**

the cross coupling of secondary alcohols with primary alcohols to generate  $\alpha$ -alkylated ketones.<sup>53</sup> This is similar to the Geurbet reaction, however, H<sub>2</sub> loss occurs instead of hydrogenation of the ketone to generate an alcohol. A one-pot two step procedure was also explored to synthesize the  $\alpha,\alpha'$ -dialkylated ketone product. A similar reaction generated amides from the cross coupling of primary alcohols and amines. Ru complex **1.75**, featuring by *O,N,S*-tridentate ligand, catalyzed this reaction in high yields with 15 examples (Scheme 1.12).<sup>54</sup>



Scheme 1.12 Ru complexes **1.72-1.75** uses in catalytic reactions

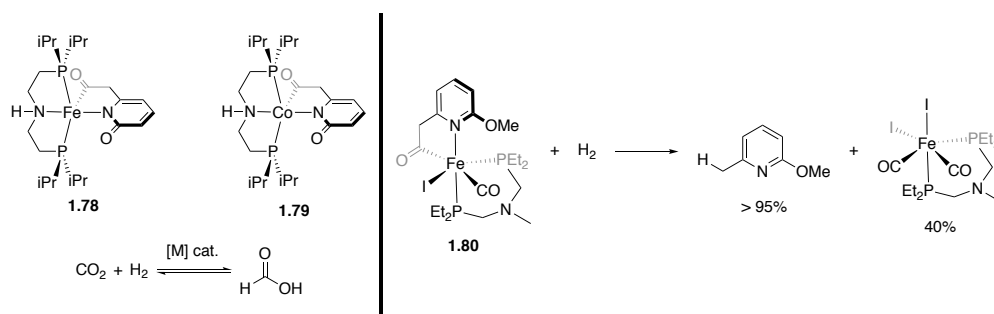


Scheme 1.13 [Fe]-hydrogenase active site Fe-GP cofactor and synthetic derivatives

### 1.2.2.3 Bio-Inspired Complexes

[Fe]-hydrogenase containing an Fe cofactor has been demonstrated to reversibly hydrogenate methenyl- $\text{H}_4\text{MPT}^+$  (methenyl tetrahydromethyanopterin) (Scheme 1.13).<sup>55-57</sup> The crystal structure of the enzyme reveals an Fe-guanylylpyridinol (Fe-GP) cofactor (Scheme 1.13).<sup>57-58</sup> Recently, a series of synthetic cofactors, **1.76** and **1.77**, have been reconstituted into enzymes to form semisynthetic [Fe]-hydrogenases (Scheme 1.13).<sup>59</sup> Interestingly, enzymes reconstituted with **1.76** showed high activity while those with **1.77** showed low activity for both the forward and reverse hydrogenation reaction. This demonstrated a critical importance of the 2-hydroxypyridine in the [Fe]-hydrogenase to modulate proton transfer. DFT calculations suggest the deprotonated hydroxyl group functions as a base to promote  $\text{H}_2$  heterolysis.<sup>59</sup>

Additional DFT calculations have been made on both Fe and Co synthetic models **1.78** and **1.79** towards the proposed hydrogenation of  $\text{CO}_2$  with  $\text{H}_2$  (Scheme 1.14).<sup>60-61</sup> These calculations suggest  $\text{H}_2$  heterolysis is facile and this reaction theoretically attainable. The 2-methoxy pyridine derivative **1.80** has been synthesized. However, without the surrounding enzyme, exposure to  $\text{H}_2$  leads to decomposition of the complex (Scheme 1.14).<sup>62</sup>



Scheme 1.14 [Fe]-hydrogenase inspired Fe and Co complexes

### 1.2.3 Group 9 Transition-Metal Precatalysts with 2-Pyridone Ligands

#### 1.2.3.1 Reactions Involving Acceptorless Dehydrogenation

A significant amount of research has been undertaken on the group 9 catalyzed acceptorless dehydrogenation of alcohols by pentamethylcyclopentadienyl (Cp\*) Ir(III) complexes ligated with the 2-hydroxypyridine (or anionic 2-pyridonate) ligands and ligand derivatives. Additionally, Cp\*Co(III) and Cp\*Rh(III) analogues have also been explored. These reactions are of particular interest as they provide the synthetically useful transformation of readily obtained alcohols into the corresponding ketone or aldehyde with the benign, or even desired, byproduct of H<sub>2</sub> gas.

Figure 1.2 represents the many precatalysts that have been tested, including many of which that do not incorporate the 2-hydroxypyridine/2-pyridonate motif. These direct comparisons help to elucidate the significance (or lack thereof) of incorporating this ligand design feature, and help discover additional ligand properties that enhance reactivity. Table 1.1 presents the data for the dehydrogenation of 1-phenylethanol to acetophenone that serves as a standard benchmark reaction. Substrate scope is highlighted for a given precatalyst.

An initial report compared complexes **1.81** – **1.83** (entries 1-4) and highlights a significant improvement in rate at for complex **1.82** featuring the 2-hydroxypyridine ligand.<sup>63</sup> Inspired by the [Fe]-hydrogenase cofactor (*vide supra*), **1.85** (entry 5) mimics the bidentate ligand found there with a bidentate *O,N*-bidentate ligand. Complex **1.85** (entry 6) removed the 2-hydroxy group and resulted in approximately a three-fold decrease in activity.

$\text{Ph}-\text{CH}(\text{OH})-\text{CH}_3 \longrightarrow \text{Ph}-\text{C}(=\text{O})-\text{CH}_3 + \text{H}_2$						
Entry	Precatalyst	Conditions	Yield%	Turnovers/h (TO/h) (calculated if not reported)	Substrate Scope	Ref
1	<b>1.81</b>	0.1 mol%, Toluene, Reflux, 20 h	9	4.5		63
2	<b>1.82</b>	0.1 mol%, Toluene, Reflux, 20 h	70	35	15 ketone products, up to 95% yield	63
3	<b>1.83</b>	0.1 mol%, Toluene, Reflux, 20 h	10	5		63
4	<b>1.84</b>	0.1 mol%, Toluene, Reflux, 20 h	13	6.5		63
5	<b>1.85</b>	0.1 mol%, neat, 130 °C, 24 h	19.2	8		64
6	<b>1.86</b>	0.1 mol%, neat, 130 °C, 24 h	6.5	2.7		64
7	<b>1.87</b>	0.1 mol%, <i>p</i> -Xylene, Reflux, 20 h	96	48	9 ketone and 23 aldehyde products, up to 100% yield	65
8	<b>1.89</b>	1.0 mol%, H <sub>2</sub> O, 20 h	92	4.6	11 ketone and 9 aldehyde products, up to 98% yield	66
9	<b>1.92</b>	0.5 mol%, Pentane, Reflux, 5 h	100	40		67
10	<b>1.92</b>	0.0002 mol%, <i>p</i> -Xylene, Reflux, 48 h	55	5729 (exhaustive)	12 ketone (up to 275,000 TON) and 7 aldehyde (up to 47,500 TON) products, up to 95% yield,	67
11	<b>1.93</b>	0.5 mol%, Pentane, Reflux, 5 h	36	14.4		67
12	<b>1.92</b>	0.5 mol%, Benzene, Reflux, 20 h	100	10		68
13	<b>1.94</b>	0.5 mol%, Benzene, Reflux, 20 h	95	9.5		68
14	<b>1.95</b>	0.5 mol%, Benzene, Reflux, 20 h	97	9.7		68
15	<b>1.92</b>	0.5 mol%, H <sub>2</sub> O, Reflux, 1h	15	30		69
16	<b>1.96</b>	0.5 mol%, H <sub>2</sub> O, Reflux, 1h	46	92	15 ketone and 7 carboxylic acid products, up to 95% yield	69

<div><div><div><div><div></div><div>OH</div></div><div>Ph</div><div></div></div><div></div><div><div><div>O</div><div></div></div><div>Ph</div><div></div></div><div>+ H<sub>2</sub></div></div></div>						
Entry	Precatalyst	Conditions	Yield%	Turnovers/h (TO/h) (calculated if not reported)	Substrate Scope	Ref
17	<b>1.97</b>	0.5 mol%, H <sub>2</sub> O, Reflux, 1h	4	8		69
18	<b>1.98</b>	0.5 mol%, H <sub>2</sub> O, Reflux, 1h	4	8		69
19	<b>1.99</b>	0.5 mol%, H <sub>2</sub> O, Reflux, 1h	8	16		69

**Table 1.1 Dehydrogenation of 1-phenylethanol to acetophenone**

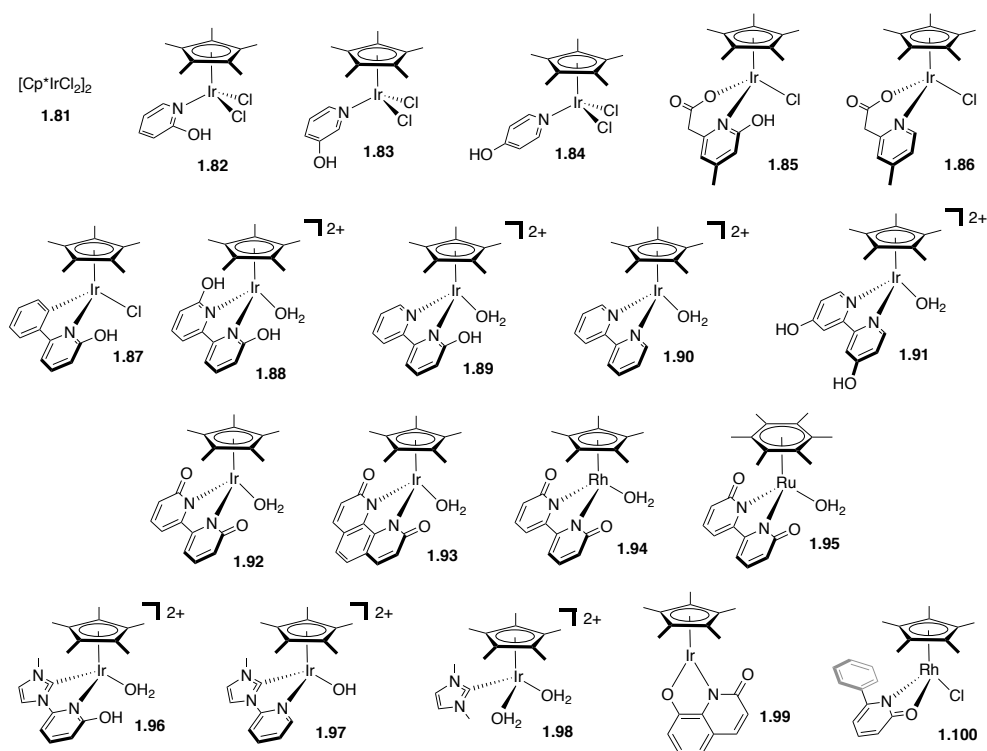
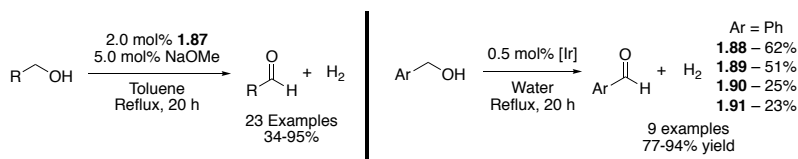


**Figure 1.2 Complexes 1.81-1.100 used for catalysis discussed in this section**

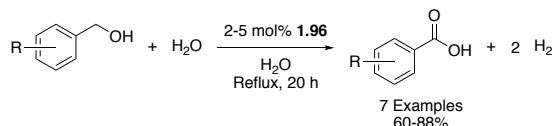
The use of an *ortho*-metallated tethered phenyl group in **1.87** (entry 7) not only allowed for the formation of ketones but allowed for the efficient synthesis of aldehydes while avoiding the common alcohol coupling reaction resulting in ester formation (Scheme 1.15).<sup>65</sup> Complexes **1.89** – **1.91** were also competent for the formation of aldehydes (Scheme 1.15) and ketones (entry 8).<sup>66</sup> Interestingly, these complexes allowed for water to be used as the reaction solvent, and for significant reusability, with a drop in yield from 98% to 94% by the eighth consecutive reaction. Ligand design accounts for the effects of the 2-hydroxypyridine moiety, and was consistent with the increased rates associated with the 2-hydroxy group being present. Complex **1.92** (entries 9 and 10) was demonstrated to significantly outperform **1.93** (entry 11).<sup>67</sup> It was also found that **1.92** offered extremely high turnover numbers of 275,000 (formation of acetophenone) and 47,500 (formation of benzaldehyde). The derivative Rh (**1.94**) and Ru (**1.95**) complexes were predicted by DFT computation and have been demonstrated experimentally to be effective for the acceptorless dehydrogenation reaction (entries 13 and 14).<sup>68</sup>

Complex **1.96** tethers the 2-hydroxypyridine fragment to an *N*-heterocycliccarbene (NHC) to form a *N,C*-bidentate ligand. Complex **1.96** was active for this reaction in water (entry 16) and performed better than **1.92** under the same conditions (entry 15).<sup>69</sup> Ir complexes **1.97** and **1.98** both functioned as control reactions, and were consistent with demonstrating the requirement of the 2-hydroxypyridine functionality for increased activity (compare entries 16-18). The use of benzylalcohol (and 6 derivatives) in water resulted in the formation of the corresponding carboxylic acids in good yields (Scheme 1.16). While competent for the dehydrogenation of 1-phenylethanol, and the hydrogenation of acetophenone, Rh complex **1.100** was demonstrated to undergo formation of nanoparticles and behave as a heterogeneous catalyst for both reactions.<sup>70</sup>



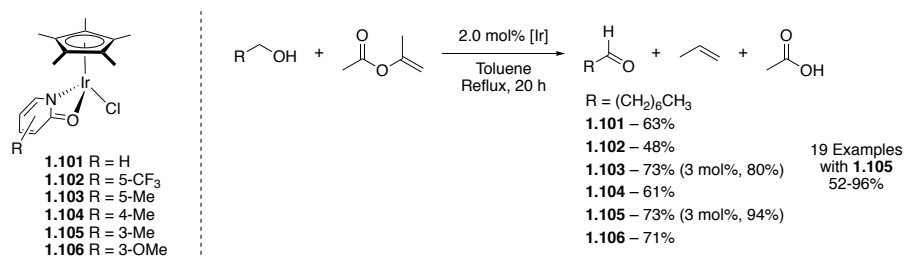


**Scheme 1.15 Dehydrogenative formation of aldehydes with complexes 1.87-1.91**



**Scheme 1.16 Dehydrogenative formation of carboxylic acids with 1.96**

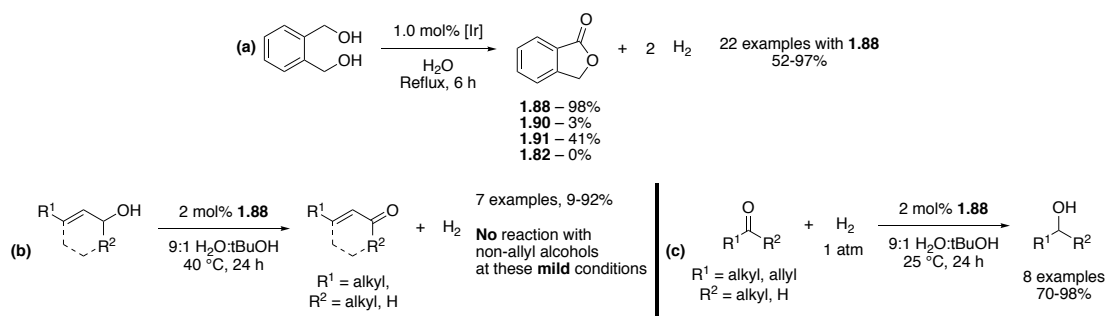
A series of 2-pyridonate Ir complexes, **1.101** – **1.106**, were explored for the dehydrogenation of alcohols to aldehydes using a hydrogen acceptor (Scheme 1.17).<sup>71</sup> Interestingly, this report also demonstrated that the substitution pattern of the 2-pyridonate ring can affect the activity of this reaction.



**Scheme 1.17 Formation of aldehydes from alcohols using a hydrogen acceptor**

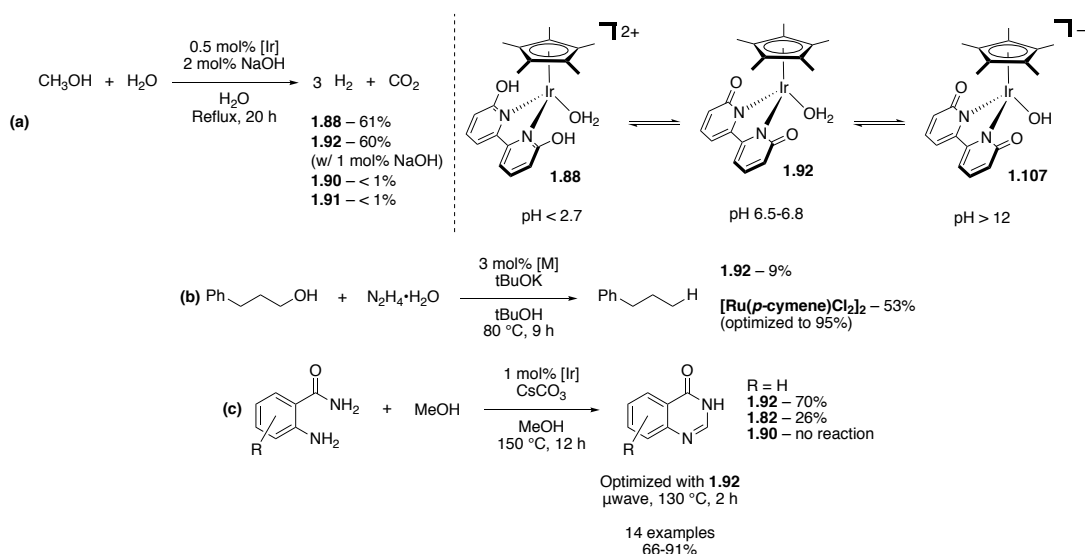
Cp\*Ir 2-pyridonate complexes have been exploited as precatalysts for other dehydrogenative reactions (Scheme 1.18). Complex **1.88** was found to be superior to derivatives with the 2-hydroxy functionality removed as a precatalyst for the dehydrogenative lactonization of diols (Scheme 1.18a).<sup>72</sup> This same Ir complex was found to be effective for the acceptorless dehydrogenation of allyl alcohols under mild conditions (Scheme 1.18b).<sup>73</sup> Additionally, **1.88** was also used for the hydrogenation of variety of ketones and aldehydes with only 1 atm of H<sub>2</sub> at 40 °C (Scheme 1.18c). Complexes **1.88** and **1.92** catalyzed the reaction of methanol and water to

produce H<sub>2</sub> and CO<sub>2</sub> (Scheme 1.19a).<sup>74</sup> The 2-hydroxy functionality was crucial to reactivity, with only trace gas production with **1.90** and **1.91**. This report also detailed the reversible protonation and deprotonation of **1.88** to **1.92** to **1.107**, dependent on pH of the solution. Complex **1.92** was attempted for a tandem, one-pot dehydrogenation–deoxygenation reaction, but served as a poor catalyst (Scheme 1.19b).<sup>75</sup> Scheme 1.19c demonstrates the use of **1.92** for the dehydrogenative coupling of *ortho*-aminobenzamides and methanol to form quinazolinones in high yields.<sup>76</sup> Complex **1.82** was found to show some catalytic activity, but the absence of the 2-hydroxy functionality in **1.90** results in no product formation.

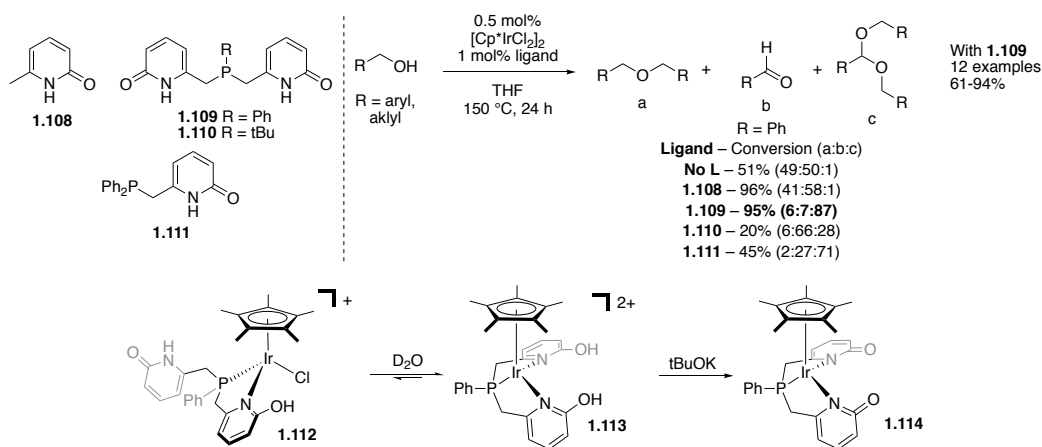


**Scheme 1.18 Use of complex 1.88 in dehydrogenative catalysis**

Recently, phosphino-2-hydroxypyridine ligands were utilized as ligands for the Ir-catalyzed dehydrogenative homo-coupling of alcohols to generate acetals.<sup>77</sup> Here, *in situ* preparation of the catalyst system was employed utilizing  $[\text{Cp}^*\text{IrCl}_2]_2$  and ligands **1.108** – **1.111** (Scheme 1.20). A Ir complex incorporating ligand **1.109** was found to be highly active and highly selective for acetal formation. Ligand **1.108** would likely form a similar complex to **1.82**, and while exhibiting high activity is non-selective, producing only trace acetal. Complexation of



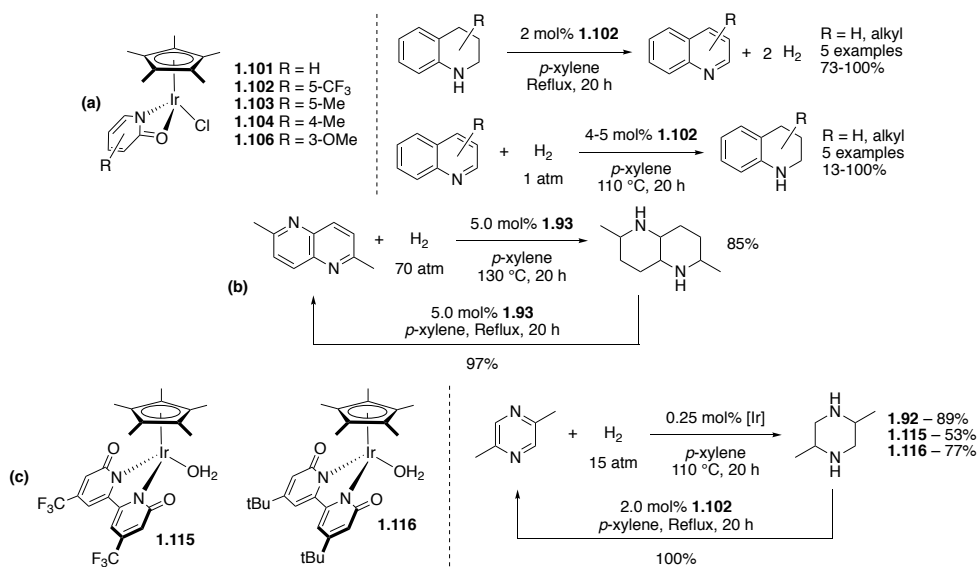
Scheme 1.19 2,2'-Bipyridine derived ligands on Ir precatalysts for dehydrogenative reactions



Scheme 1.20 Ir catalyzed acetal formation with bi- and tri-dentate phosphine-2-pyridone ligands

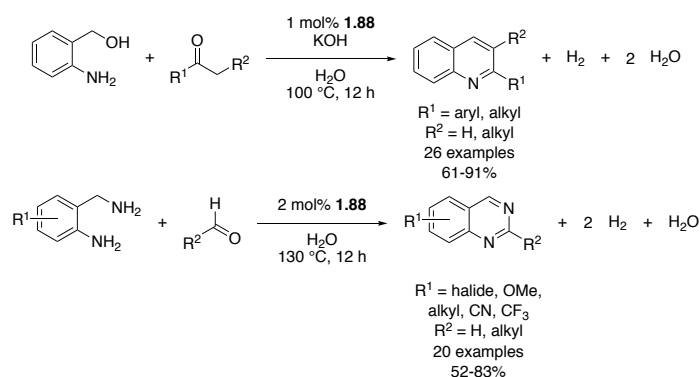
**1.109** reveals an equilibrium between Ir complexes **1.112** and **1.113**, with the addition of base leading to **1.114**.

Complexes of this type have also been reported for the acceptorless dehydrogenation of cyclic amines. Scheme 1.19 illustrates that **1.101** – **1.104** and **1.106** were all found to catalyze the dehydrogenation of 1,2,3,4-tetraquinoline with **1.102** bearing an electron withdrawing CF<sub>3</sub> group providing the highest activity (Scheme 1.21a).<sup>78</sup> Complex **1.102** was also found to catalyze the reverse reaction, and through 5 dehydrogenation/hydrogenation cycles conversion only dropped from 100% to 98%. Ir complex **1.92**, its electronically varied derivatives **1.115** and **1.116**, and **1.93** have been explored for the dehydrogenation and hydrogenation of *N*-heterocycles (Scheme 1.21b,c).<sup>79-80</sup> Contrasting with **1.102** above, the electron withdrawing character of **1.115** significantly reduced activity, and the electron donating character of **1.116** also reduced activity compared to **1.102**. Importantly, no decrease in reactivity with **1.102** was found over 4 dehydrogenation/hydrogenation cycles.



**Scheme 1.21** Ir catalyzed dehydrogenation/hydrogenation of *N*-heterocycles

Two reports have combined these dehydrogenation reactions to form unsaturated *N*-heterocycles (Scheme 1.22). While numerous Ir complexes and one Rh complex were screened, **1.88** was found to significantly outperform all others for the cyclization of *ortho*-aminobenzylalcohol with ketones.<sup>81</sup> Similarly, **1.88** also results in significantly higher yields than other reported complexes for the cyclization of *ortho*-aminobenzylamines with aldehydes.<sup>82</sup>



Scheme 1.22 Ir complex **1.88** used in the catalytic synthesis of unsaturated *N*-heterocycles

### 1.2.3.2 Hydrogenation of Carbon Dioxide and Dehydrogenation of Formic Acid

A compilation of complexes utilized for this reaction, in addition to those already presented, can be found in Figure 1.3. Compiled results for the hydrogenation reaction can be seen in Table 1.2, and for dehydrogenation in Table 1.3. The initial reports for 2-hydroxypyridine derivatives and their use in the hydrogenation of carbon dioxide to formate (under basic conditions) and the reverse dehydrogenation reaction involve complexes **1.117** and **1.118** and are compared to reported results for 4-hydroxypyridine containing derivative **1.91**.<sup>83-84</sup> Complex **1.117** provided a significant improvement over **1.118** and **1.91** based on turnover number (Table 1.2, entries 1-4).<sup>84</sup> This is again born out in the dehydrogenation of formic acid (Table 1.3, entries 1-4).

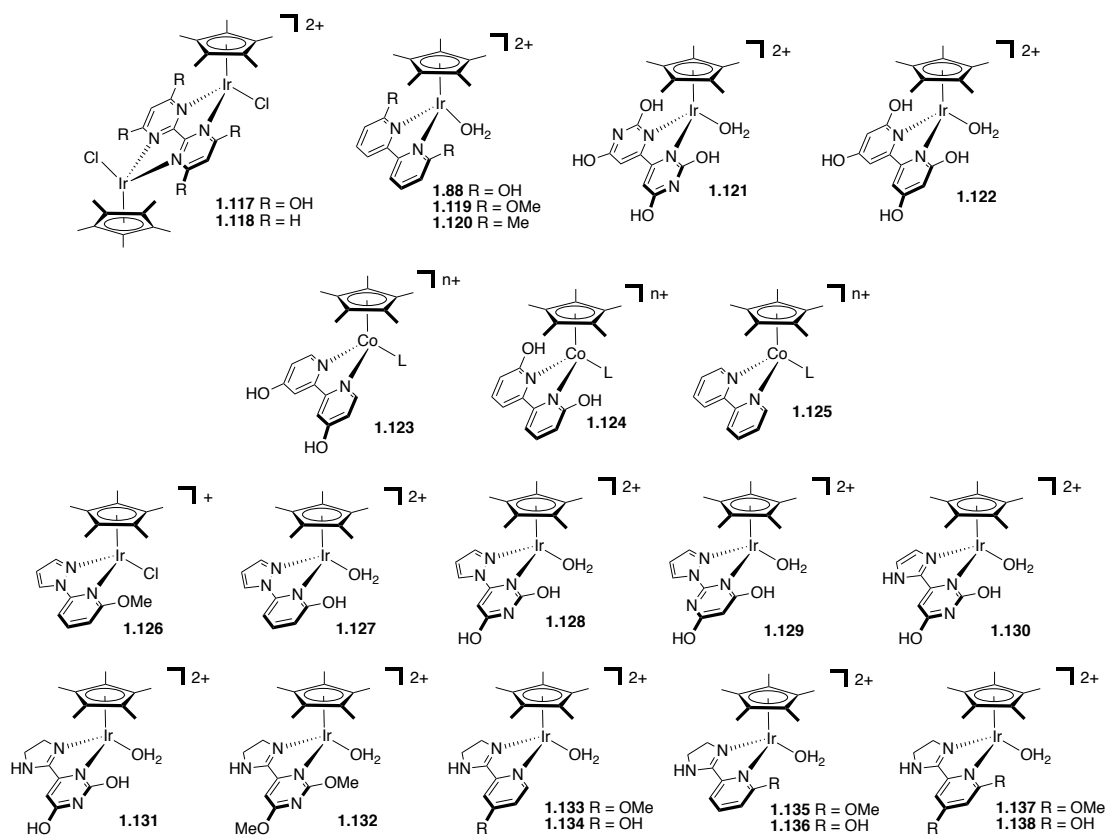


**Figure 1.3** Complexes 1.117-1.138 utilized in catalytic hydrogenation/dehydrogenation of CO<sub>2</sub>/HCOOH

Entry	Precatalyst	Conditions	Precatalyst Concentration ( $\mu\text{M}$ )	Initial Turnover Frequency ( $\text{h}^{-1}$ )	Turnover Number	Ref
1	<b>1.117</b>	1:1 $\text{H}_2$ : $\text{CO}_2$ at 0.1 MPa, 1 M $\text{NaHCO}_3$ , 25 °C, 336 h	50	64	7,200	84
2	<b>1.118</b>	1:1 $\text{H}_2$ : $\text{CO}_2$ at 0.1 MPa, 1 M $\text{NaHCO}_3$ , 25 °C, 25 h	50	0	0	84
3	<b>1.91</b>	1:1 $\text{H}_2$ : $\text{CO}_2$ at 0.1 MPa, 1 M $\text{NaHCO}_3$ , 25 °C, 24 h	50	7	92	83- 84
4	<b>1.117</b>	1:1 $\text{H}_2$ : $\text{CO}_2$ at 4 MPa, 1 M $\text{NaHCO}_3$ , 80 °C, 2 h	10	53,800	79,000 (up to 153,000 other cond.)	84
5	<b>1.91</b>	1:1 $\text{H}_2$ : $\text{CO}_2$ at 1 MPa, 1 M $\text{NaHCO}_3$ , 50 °C, 30 h	20	790	7,700	85
6	<b>1.117</b>	1:1 $\text{H}_2$ : $\text{CO}_2$ at 1 MPa, 1 M $\text{NaHCO}_3$ , 50 °C, 8 h	20	4,200	24,000	85
7	<b>1.88</b>	1:1 $\text{H}_2$ : $\text{CO}_2$ at 1 MPa, 1 M $\text{NaHCO}_3$ , 50 °C, 9 h	20	1,650	5,150	85
8	<b>1.119</b>	1:1 $\text{H}_2$ : $\text{CO}_2$ at 1 MPa, 1 M $\text{NaHCO}_3$ , 80 °C, 8 h	20	565	410	85
9	<b>1.12</b>	1:1 $\text{H}_2$ : $\text{CO}_2$ at 1 MPa, 1 M $\text{NaHCO}_3$ , 80 °C, 8 h	200	30	50	85

Entry	Precatalyst	Conditions	Precatalyst Concentration ( $\mu\text{M}$ )	Initial Turnover Frequency ( $\text{h}^{-1}$ )	Turnover Number	Ref
10	<b>1.88</b>	1:1 $\text{H}_2$ : $\text{CO}_2$ at 1 MPa, 1 M $\text{NaHCO}_3$ , 120 $^\circ\text{C}$ , 8 h	10	25,200	12,500	85
11	<b>1.121</b>	1:1 $\text{H}_2$ : $\text{CO}_2$ at 1 MPa, 1 M $\text{NaHCO}_3$ , 50 $^\circ\text{C}$ , 24 h	20	3,060	28,000	86
12	<b>1.123</b>	1:1 $\text{H}_2$ : $\text{CO}_2$ at 4 MPa, 1 M $\text{NaHCO}_3$ , 100 $^\circ\text{C}$ , 1 h	400	39 (total)	39	87
13	<b>1.124</b>	1:1 $\text{H}_2$ : $\text{CO}_2$ at 4 MPa, 1 M $\text{NaHCO}_3$ , 50 $^\circ\text{C}$ , 1 h	400	1.3 (total)	1.3	87
14	<b>1.125</b>	1:1 $\text{H}_2$ : $\text{CO}_2$ at 4 MPa, 1 M $\text{NaHCO}_3$ , 60 $^\circ\text{C}$ , 3 h	1000	0.22	0.66	87
15	<b>1.132</b>	1:1 $\text{H}_2$ : $\text{CO}_2$ at 1 MPa, 2 M $\text{KHCO}_3$ , 50 $^\circ\text{C}$	20	532	—	88
16	<b>1.131</b>	1:1 $\text{H}_2$ : $\text{CO}_2$ at 1 MPa, 2 M $\text{KHCO}_3$ , 50 $^\circ\text{C}$	20	1,500	—	88
17	<b>1.133</b>	1:1 $\text{H}_2$ : $\text{CO}_2$ at 1 MPa, 2 M $\text{KHCO}_3$ , 50 $^\circ\text{C}$	20	402	—	88
18	<b>1.134</b>	1:1 $\text{H}_2$ : $\text{CO}_2$ at 1 MPa, 2 M $\text{KHCO}_3$ , 50 $^\circ\text{C}$	20	1,090	—	88
19	<b>1.135</b>	1:1 $\text{H}_2$ : $\text{CO}_2$ at 1 MPa, 2 M $\text{KHCO}_3$ , 50 $^\circ\text{C}$	20	441	—	88
20	<b>1.136</b>	1:1 $\text{H}_2$ : $\text{CO}_2$ at 1 MPa, 2 M $\text{KHCO}_3$ , 50 $^\circ\text{C}$	20	1,600	—	88
21	<b>1.137</b>	1:1 $\text{H}_2$ : $\text{CO}_2$ at 1 MPa, 2 M $\text{KHCO}_3$ , 50 $^\circ\text{C}$	20	550	—	88



Entry	Precatalyst	Conditions	Precatalyst Concentration ( $\mu\text{M}$ )	Initial Turnover Frequency ( $\text{h}^{-1}$ )	Turnover Number	Ref
22	<b>1.138</b>	1:1 $\text{H}_2$ : $\text{CO}_2$ at 1 MPa, 2 M $\text{KHCO}_3$ , 50 °C	20	2,600	–	88
23	<b>1.138</b>	1:1 $\text{H}_2$ : $\text{CO}_2$ at 0.1 MPa, 1 M $\text{NaHCO}_3$ , 25 °C, 336 h	25	98	7,280	88

**Table 1.2 Compiled results of catalytic hydrogenation of  $\text{CO}_2$**

Entry	Precatalyst	Conditions	Precatalyst Concentration ( $\mu\text{M}$ )	Initial Turnover Frequency	Turnover Number	Ref
1	<b>1.117</b>	1 M $\text{HCO}_2\text{H}/\text{HCO}_2\text{Na}$ (1:1), 60 °C, 18 h	50	31,600	16,800	84
2	<b>1.118</b>	2 M $\text{HCO}_2\text{H}/\text{HCO}_2\text{Na}$ (1:1), 60 °C, 1.5 h	50	32,000	10,000	84
3	<b>1.91</b>	3 M $\text{HCO}_2\text{H}/\text{HCO}_2\text{Na}$ (1:1), 60 °C, 4 h	200	2,400	5,000	83-84
4	<b>1.117</b>	1 M $\text{HCO}_2\text{H}/\text{HCO}_2\text{Na}$ (1:1), 90 °C, 7 h	3.1	228,000	165,000 (up to 308,000 other cond.)	84
5	<b>1.88</b>	1 M $\text{HCO}_2\text{H}/\text{HCO}_2\text{Na}$ (1:1), 60 °C, 4.5 h	100	5,440	5,300	89
6	<b>1.88</b>	1 M $\text{HCO}_2\text{H}/\text{HCO}_2\text{Na}$ (1:1), 90 °C, 4.5 h	33.3	19,800	30,000	89
7	<b>1.119</b>	1 M $\text{HCO}_2\text{H}/\text{HCO}_2\text{Na}$ (1:1), 60 °C, 8 h	200	910	2,500	89
8	<b>1.120</b>	1 M $\text{HCO}_2\text{H}/\text{HCO}_2\text{Na}$ (1:1), 60 °C, 9 h	4000	6	25	89

Entry	Precatalyst	Conditions	Precatalyst Concentration ( $\mu\text{M}$ )	Initial Turnover Frequency	Turnover Number	Ref
9	<b>1.121</b>	1 M $\text{HCO}_2\text{H}/\text{HCO}_2\text{Na}$ (1:1), 60 °C, 6 h	100	12,200	6,340	89
10	<b>1.122</b>	1 M $\text{HCO}_2\text{H}/\text{HCO}_2\text{Na}$ (1:1), 60 °C, 6 h	100	3,300	4,800	89
11	<b>1.126</b>	1 M $\text{HCO}_2\text{H}/\text{HCO}_2\text{Na}$ (1:1), 60 °C, 5 h	100	160	430	90
12	<b>1.127</b>	1 M $\text{HCO}_2\text{H}/\text{HCO}_2\text{Na}$ (1:1), 60 °C, 7 h	100	3,620	5,000	90
13	<b>1.128</b>	1 M $\text{HCO}_2\text{H}/\text{HCO}_2\text{Na}$ (1:1), 60 °C, 1 h	100	11,400	5,500	90
14	<b>1.1.29</b>	1 M $\text{HCO}_2\text{H}/\text{HCO}_2\text{Na}$ (1:1), 60 °C, 1.5 h	100	10,800	7,640	90
15	<b>1.130</b>	1 M $\text{HCO}_2\text{H}/\text{HCO}_2\text{Na}$ (1:1), 60 °C, 1 h	100	5,520	10,000	90
16	<b>1.131</b>	1 M $\text{HCO}_2\text{H}/\text{HCO}_2\text{Na}$ (1:1), 60 °C, 0.5 h	100	32,500	7,850	90
17	<b>1.128</b>	4 M $\text{HCO}_2\text{H}/\text{HCO}_2\text{Na}$ (49:1), 100 °C, 6 h	20	269,000	196,000	90
18	<b>1.131</b>	4 M $\text{HCO}_2\text{H}/\text{HCO}_2\text{Na}$ (2:1), 100 °C, 0.5 h	40	322,000	68,000	90
19	<b>1.134</b>	1 M $\text{HCO}_2\text{H}/\text{HCO}_2\text{Na}$ (1:1), 60 °C, 6 h	25	14,500	28,000	88
20	<b>1.136</b>	1 M $\text{HCO}_2\text{H}/\text{HCO}_2\text{Na}$ (1:1), 60 °C, 5.5 h	25	16,000	27,900	88
21	<b>1.137</b>	1 M $\text{HCO}_2\text{H}/\text{HCO}_2\text{Na}$ (1:1), 60 °C, 5 h	25	16,500	28,900	88
22	<b>1.138</b>	1 M $\text{HCO}_2\text{H}/\text{HCO}_2\text{Na}$ (1:1), 60 °C, 1 h	25	56,900	29,000	88

**Table 1.3 Compiled results of catalytic dehydrogenation of formic acid**

Catalysis with complex **1.117** resulted in some of the highest activity and turnover numbers reported for both of hydrogenation and dehydrogenation reactions using mild conditions (25 °C, atmospheric pressures). Further investigations have explored the catalytic activity of **1.88** and closely related derivatives **1.119** and **1.120** in an effort to examine the role of the 2-hydroxy functional group for the hydrogenation of carbon dioxide.<sup>85</sup> A comparison of **1.117**, **1.88**, **1.119**, and **1.120** demonstrated that **1.117** was multiple times more active than **1.88** (Table 1.2, entries 5-10). Importantly, **1.88** demonstrated the necessity for the 2-hydroxy functional group with **1.119** and **1.120** performing poorly for the hydrogenation of carbon dioxide. An additional report Himeda and co-workers adds complex **1.121** to the list of competent precatalysts for hydrogenation of carbon dioxide.<sup>86</sup> Complex **1.121** was found to be comparable to the high performing complex **1.117** (Table 1.2, entry 11). Additional kinetic details including kinetic isotope effects of both H<sub>2</sub>/D<sub>2</sub> and KHCO<sub>3</sub>(H<sub>2</sub>O)/KDCO<sub>3</sub>(D<sub>2</sub>O) have been reported along with DFT computational details. In a separate report, these complexes along with **1.122** were evaluated for their reactivity for the dehydrogenation of formic acid, (Table 1.3, entries 5-10) and a series of kinetic investigations were carried out.<sup>89</sup> Compared to **1.88**, complex **1.91** performed poorly, while **1.121** and **1.122** offer comparable results. This study offers additional confirmation of the significant importance of the 2-hydroxypyridine motif as **1.119** and **1.120** showed poor reactivity comparatively.

A series of related bipyridine Co complexes, **1.123** – **1.125**, were synthesized and tested for the hydrogenation of carbon dioxide (Table 1.2, entries 12-14).<sup>87</sup> These system required significantly higher catalyst loading, temperature, and pressures to achieve limited activity. Interestingly, unlike the Ir complexes studied, the Co complex ligated by the 6,6'-

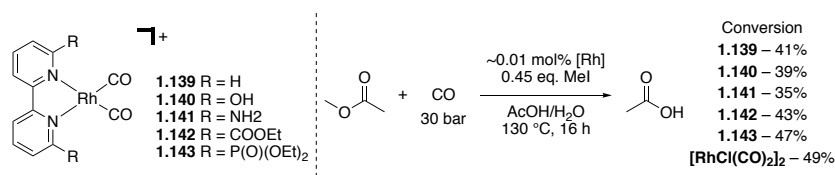
dihydroxybipyridine ligand (**1.124**) was significantly less effective than the 4,4'-dihydroxybipyridine complex (**1.123**) suggesting a departure in this trend with Co catalysts.

A series of Ir compounds feature modified *N,N*-chelating ligands (**1.126** – **1.131**) have also been tested for the dehydrogenation of formic acid reactions (Table 1.3, entries 11-16).<sup>90</sup> While all proved to be quite active, **1.128** (Table 1.3, entry 17) was found to have turnover numbers of up to 196,000 and **1.131** (Table 1.3, entry 18) was found to have initial turnover frequency of up to 320,000, with high reaction temperatures at 100°C. These results are comparable to that of the high perform Ir complex **1.117** (Table 1.3, entries 1, 4). Due to the promising reactivity of **1.131**, derivatives **1.132** – **1.138** were explored for both hydrogenation of carbon dioxide (Table 1.2, entries 15-23) and dehydrogenation of formic acid (Table 1.3, entries 19-22) in an effort to further understand the ligand requirements for these reactions.<sup>88</sup> For hydrogenation of carbon dioxide, the methoxy substituted pyridine or pyrimidine ligands all performed poorly, highlighting the requirement of the deprotonated hydroxyl group for high reactivity, under basic conditions. Of these, complex **1.138** had the highest initial turnover frequency (Table 1.2, entry 22), and outperformed the benchmark complex **1.117** under ambient conditions (Table 1.2, compare entry 1 and 23). Given this success, the hydroxyl variants (**1.131**, **1.134**, **1.136**, **1.138**) and a single methoxy substituted variant (**1.137**) were tested for the dehydrogenation of formic acid (Table 1.3, entries 19-22). Again, complex **1.138** has the highest initial turnover frequency (Table 1.3, entry 22) and, under similar conditions, outperformed previously reported complexes **1.131** (Table 1.3, entry 16) and **1.117** (Table 1.3, entry 1). Interestingly, unlike the poor performance for hydrogenation, methoxy substituted **1.137** (Table 1.3, entry 21) performed comparably to **1.131** (Table 1.3, entry 16), **1.134** (Table 1.3, entry 19),

and **1.136** (Table 1.3, entry 20). This makes it unclear as to the effect of the 2-hydroxyl substituent under the acidic conditions used for formic acid dehydrogenation.

### 1.2.3.3 Additional Catalytic Reactions

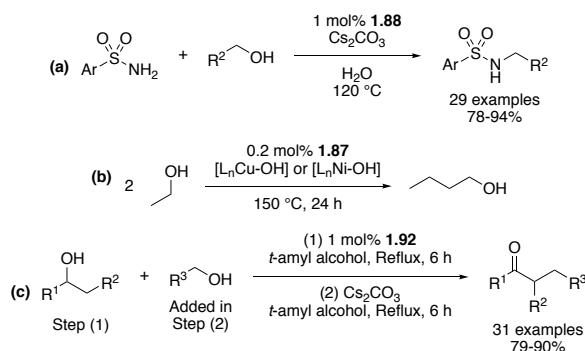
Rh(I) complexes with 6,6'-functionalized bipyridine derivatives (**1.139** – **1.143**), including 6,6'-dihydroxy-2,2'-bipyridine (**1.140**) were evaluated for the carbonylation of methylacetate (Scheme 1.23).<sup>91-92</sup> Only small differences in reactivity were observed and these complexes were slightly less active than  $[\text{RhCl}(\text{CO})_2]_2$ . Additionally, 2,2'-bipyridine derivatives, including **1.88** and **1.90**, were tested for an aldehyde water shift (AWS) reaction. Complex **1.88**, and the  $\text{Cp}^*\text{Rh}$  and  $\text{ArRu}$  analogues, provided trace activity for the AWS reaction with mainly aldehyde disproportionation observed.  $[(p\text{-Cymene})\text{Ru}(\text{bipy})(\text{OH}_2)][\text{OTf}]$  provided the highest selectivity with only trace disproportionation observed.<sup>93</sup>



Scheme 1.23 Square planar Rh(I) complexes **1.139**-**1.140** ligated with 2,2'-bipyridine derivatives

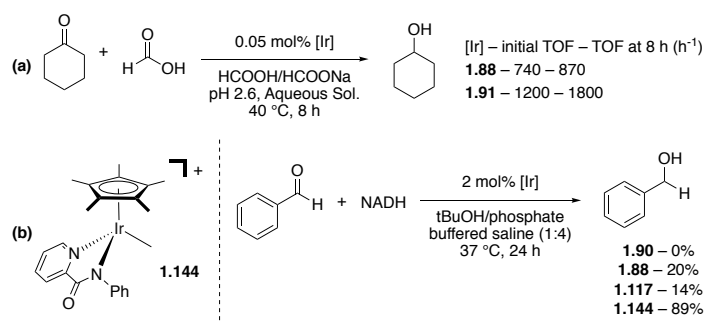
Many  $\text{Cp}^*\text{Ir}$  complexes bearing the 2-hydroxypyridine ligand motif have been utilized in various hydrogen borrowing catalysis. Complex **1.88** allowed for the alkylation of sulfonamides with alcohols, where complex **1.90** gave no yield (Scheme 1.24a).<sup>94</sup> Recently, 2,2'-bibenzimidazole  $\text{Cp}^*\text{Ir}$  complexes have been shown to be active for the same reaction with comparable reactivity to **1.88**.<sup>95</sup> Complex **1.87** was found to be highly active for the Guerbet reaction of ethanol into *n*-butanol when combined with specific sterically demanding  $[\text{L}_n\text{Cu}-\text{OH}]$  or  $[\text{L}_n\text{Ni}-\text{OH}]$  bases (Scheme 1.24b). Importantly, **1.87** was found to be highly selective for this reaction with minimal oligomer or ketone formation. Complex **1.92** was found to be highly

active for the coupling of alcohols to form  $\alpha$ -alkylated ketones in a two-step procedure: 1) oxidation of alcohol to the ketone, then 2) addition of second alcohol and base (Scheme 1.24c).<sup>96</sup>



**Scheme 1.24 Ir complexes for hydrogen borrowing catalysis**

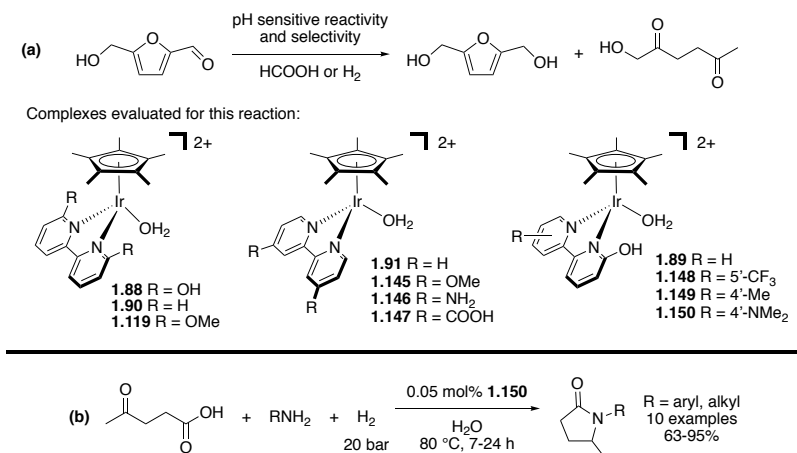
The transfer hydrogenation of ketones with formic acid (Scheme 1.25a),<sup>97</sup> and the transfer hydrogenation of aldehydes by NADH (under biological conditions, Scheme 1.25b) were used to compare complexes containing the 2-hydroxypyridine motif to many other complexes.<sup>98</sup> Interestingly, it was found that the 2-hydroxypyridine containing complexes did not achieve the best performance, highlighting the complexity involved with evaluating trends in ligand design to design an optimal organometallic catalyst.



**Scheme 1.25 Transfer hydrogenation of ketones with Ir complexes**

Many Cp\*Ir complexes containing 2-hydroxypyridine ligand derivative have been tested for the transfer hydrogenation (and hydrogenation) of 5-hydroxymethylfurfural, a renewable feedstock chemical that is known to be transformed into a wide range of chemicals.<sup>99-101</sup> Activity and selectivity of these reactions were shown to be both precatalyst and pH dependent. However,

the 2-hydroxypyridine fragment appeared to be beneficial, especially with complex **1.150** (Scheme 1.26a).<sup>100</sup> Complex **1.150** has additionally been exploited for the reductive amination of levulinic acid with hydrogen to pyrrolidinones (Scheme 1.26b).<sup>102</sup>



**Scheme 1.26 Ir complexes for the transfer hydrogenation/hydrogenation of 5-hydroxymethylfurfural and catalytic formation of pyrrolidinones**

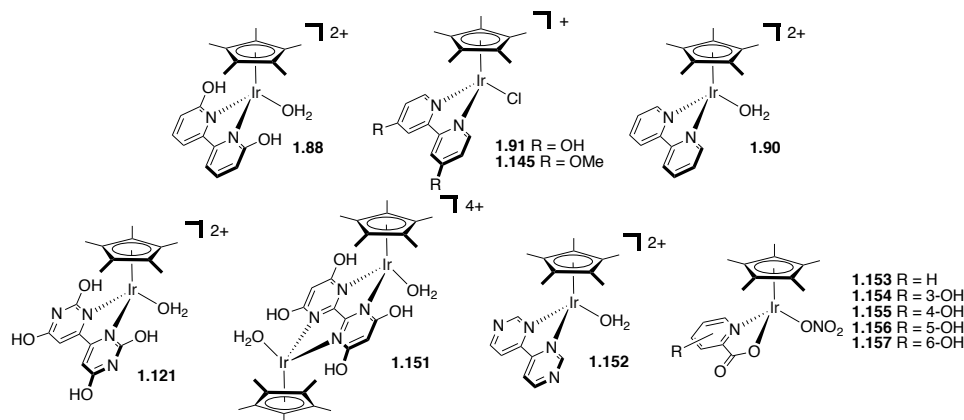
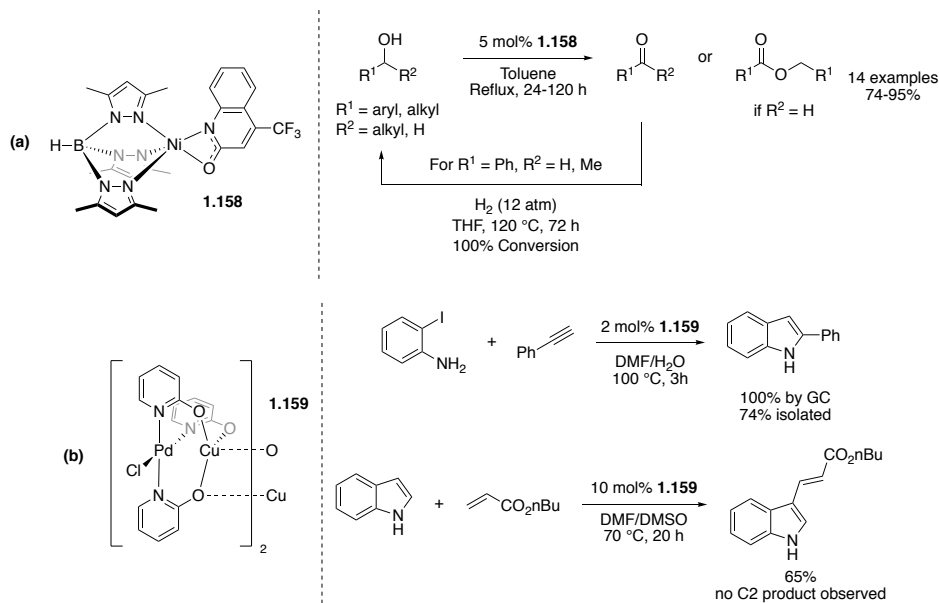


**Figure 1.4 Ir complexes studied for catalytic water oxidation**

Multiple Cp\*Ir(III) complexes of this type have also been compared for catalytic water oxidation (Figure 1.4).<sup>103-105</sup> Interestingly, complexes containing a hydroxypyridine fragment were found to have excellent activity that was demonstrated to be significantly affected by pH, creating pH-switchable catalysts. However, the position of the hydroxy group on the pyridine ring did not play a significant role in altering activity.

### 1.2.4 Group 10 – 12 Transition-Metal Precatalysts with 2-Pyridone Ligands

To date, only a few complexes of groups 10 – 12 have been reported for their activity in catalytic reactions. However, despite the small number of complexes, group 10 – 12 complexes demonstrate a wide variety of coordination modes for the 2-pyridone ligand motif. A Ni complex **1.158** exploits a 2-hydroxyquinoline ligand for the acceptorless dehydrogenation of alcohols and the hydrogenation of ketones with H<sub>2</sub> (Scheme 1.27a).<sup>106</sup> The bimetallic Pd/Cu complex **1.159** has been shown to be a competent catalyst for the one-pot synthesis of 2-phenylindole,<sup>107</sup> and provided complete selectivity for C3-alkenylation of indole (Scheme 1.27b).<sup>108</sup>

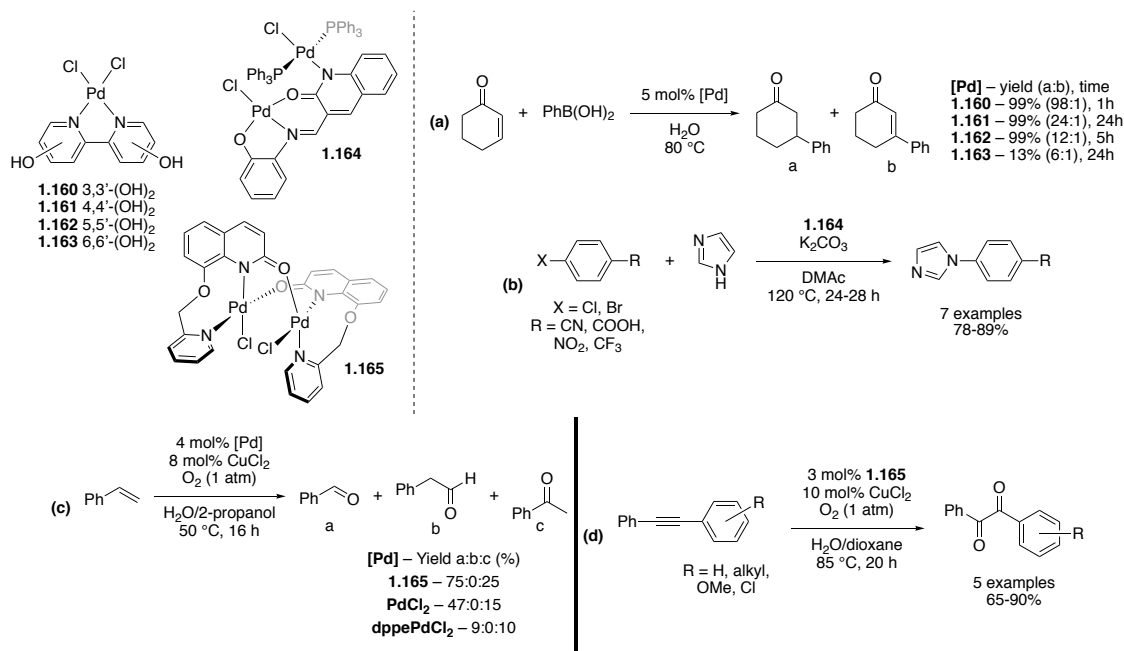


Scheme 1.27 Ni 2-pyridonate complex **1.158** and bimetallic Pd/Cu 2-pyridonate complex used in catalysis

Multiple other Pd complexes feature a 2-hydroxypyridine or 2-pyridonate motif have been synthesized, and evaluated for their catalytic reactivity in a number of organic transformations (Scheme 1.28).<sup>109-111</sup> Interestingly, in the study of conjugate addition chemistry with **1.160** – **1.163**, complex **1.163**, featuring the 2-hydroxypyridine motif, severely diminished reactivity for this reaction (Scheme 1.28a).<sup>109</sup>

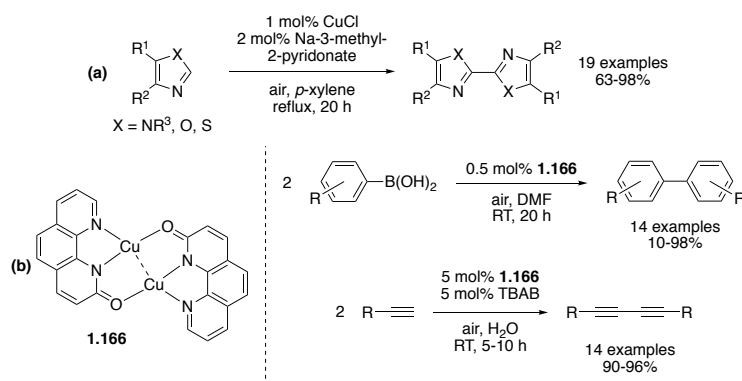


A Cu(I)/Na-2-pyridonate system was found to be highly efficient for the synthesis of biazoles by aerobic oxidative homocoupling (Scheme 1.29a).<sup>112</sup> While many bipyridine derivatives were tested, the 2-pyridonate functionality proved crucial for reactivity. A prepared bimetallic Cu complex **1.166** served as a competent precatalyst for the homocoupling of boronic acids and alkynes (Scheme 1.29b).<sup>113-114</sup>



Scheme 1.28 Pd complexes 1.160-1.165 and their activity in catalytic reactions

Multiple Cu species with 6,6'-dihydroxy-2,2'-bipyridine ligands and their derivatives have been reported for their use in electrocatalytic catalytic water oxidation (Figure 1.5).<sup>115-116</sup> These studies have demonstrated high activity at low over potential is due to the 6,6'-dihydroxy groups. Altering these group or moving the placement of the hydroxy functionality was shown to significantly decreases activity.



**Scheme 1.29 Cu 2-pyridonate systems for catalytic reactivity**

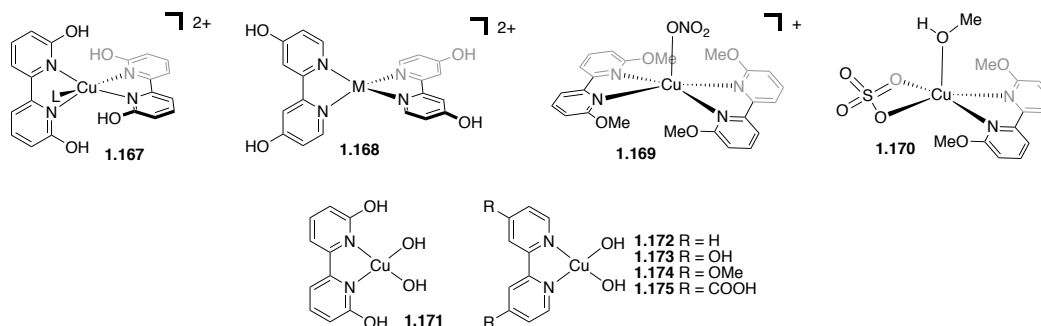


**Figure 1.5 Cu complexes 1.167-1.175 tested as catalyst in electrochemical water oxidation**

There are also examples where the 2-hydroxypyridine motif has been exploited in supramolecular chemistry. These have been tested as catalyst for a variety of common organic transformations as proof-of-concept that these structures are catalytically active and with significant focus on their catalytic reusability. A 2,4,6-trioxotetrahydropyrimidinylidene was used to form Zn and Cd coordination polymers that were tested as precatalysts for the Knoevenagel condensation of benzaldehyde with malononitrile.<sup>117</sup> 2-Pyrimidonate is used as a ligand to form a Pd(II) metal-organic-framework (MOF) that has been shown to be effective in Suzuki cross coupling,<sup>118</sup> oxidation of allyl alcohols with  $\text{O}_2$  at the terminal oxidant,<sup>118</sup> and the hydrogenation of alkenes with  $\text{H}_2$ .<sup>118-121</sup> The 2-pyrimidonate ligand also forms a Cu(II) MOF.<sup>122</sup> It has been shown as an effective precatalyst for benzylic C–H oxidation with  $\text{O}_2$ ,<sup>123-124</sup> azide-

alkyne “click” coupling,<sup>125</sup> alkynylation of imines,<sup>126</sup> hydroxylation and nitration of aryl halides,<sup>127</sup> and the oxidative C–O coupling of alcohols with formamides, aldehydes, and ethers by direct C–H activation.<sup>128</sup>

### 1.2.5 Conclusion

The 2-pyridone/2-pyridonate ligand motif has been shown to be a highly versatile ligand framework for complexes across the transition metals. This review has highlighted the use of complexes featuring this motif in a wide range of catalysis, and highlighted the diverse range of coordination modes these ligands can support.

In early-transition metal complexes, 2-pyridonate ligands have been utilized as ancillary ligands. Substitution of the 2-pyridonate has been utilized to optimize catalytic performance for polymerization, hydroamination, and hydroaminoalkylation reactions.

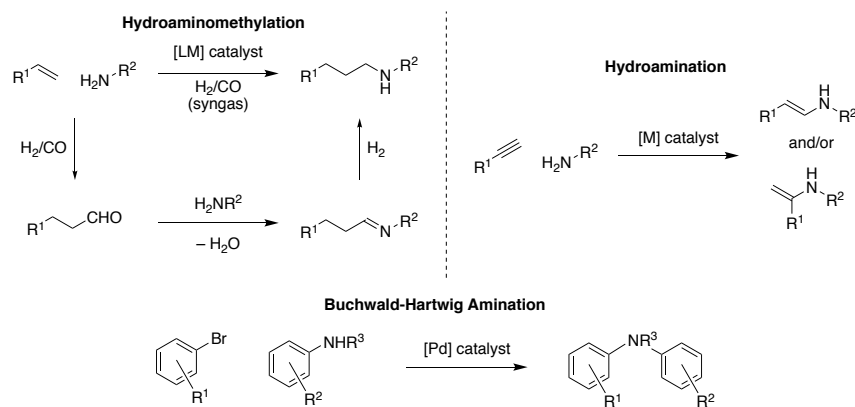
As ligands in late-transition metal complexes, the 2-pyridonate motif has been invoked as an internal base, in effect, storing a proton equivalent from a substrate in the 2-hydroxypyridine form. Significant research has demonstrated this effect in Ru and Ir complexes for simple hydrogenation and dehydrogenation reactions of ketones/alcohols and CO<sub>2</sub>/HCOOH. Additionally, more complex synthetic reactions have been developed exploiting the ability of Cp\*M 2-pyridonate complexes to readily promote hydrogen transfer reactions. While many reactions are demonstrated to require the 2-hydroxypyridine substitution, placing the hydroxyl group in close proximity to the metal center, some late-transition metal complexes remain highly active for a variety of reactions with 6-hydroxypyridine substitution. In these situations, the low pK<sub>a</sub> of coordinated pyridine is exploited under mild, basic conditions to create a more electron rich metal center through donation of anionic 2-pyridonate or 6-pyridonate donor. The 2-

pyridonate ligand motif has also been incorporated as an ancillary ligand in late-transition metal complexes, such as in paddlewheel complexes or in MOFs.

## **Chapter 2: 2-Pyridonate Tantalum Complexes for the Hydroaminoalkylation of Unactivated Internal Alkenes with Unprotected Secondary Amines – Synthetic Development and Mechanistic Insights**

### **2.1 Introduction**

As discussed in Chapter 1, amines are broadly important across multiple industries. While there is a significant volume of work on the use of stoichiometric reagents to achieve amine containing products,<sup>1-3</sup> the development of novel catalytic syntheses of amines is a significant challenge. Multiple catalytic reactions for the synthesis of amines are known, and have become reliable and highly used in laboratory settings. Some examples include Buchwald-Hartwig amination,<sup>129-130</sup> hydroamination,<sup>131</sup> and hydroaminomethylation reactions (Scheme 2.1).<sup>132</sup> While these three examples offer unique disconnection strategies, hydroamination and hydroaminomethylation reactions are both 100% atom-economic reactions – where each atom in the reactants are found in the products – and utilize readily available substrates – avoiding additional steps that may be needed to functionalize or activate the substrate to achieve the desired reactivity in other catalytic methods. From an end-user/industrial context, methodologies that employ these strategies are economically efficient by avoiding waste products and reducing the number required steps.

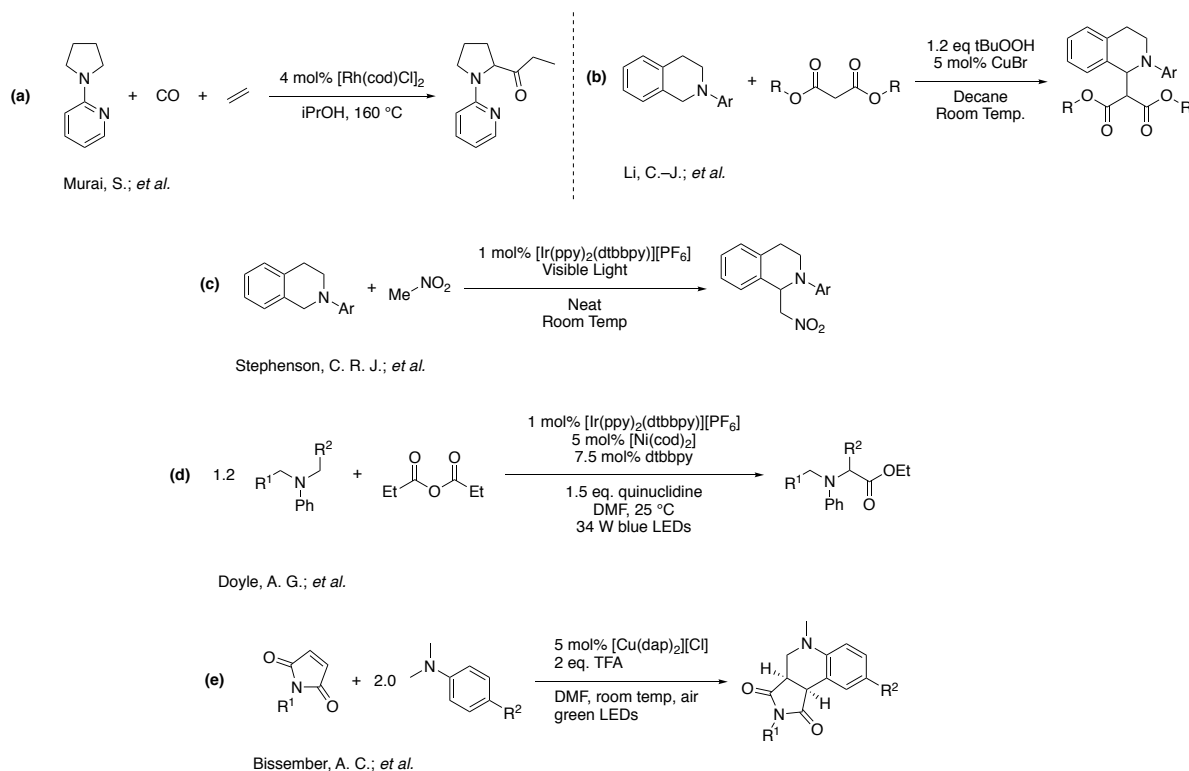


**Scheme 2.1** Catalytic synthesis of amines by hydroaminomethylation, hydroamination, and Buchwald-Hartwig amination.

One strategy that has garnered significant recent interest, is the transition-metal-catalyzed C(sp<sup>3</sup>)-H activation of amine substrates and subsequent functionalization to create new C-C or C-heteroatom bonds. These synthetic methodologies are of interest as they are able to generate complex amine products from simple amine starting materials. Importantly, these methodologies provide new disconnection strategies, where the starting amine substrate is not required to be pre-activated or pre-functionalized at the to-be-functionalized carbon. Of these examples, a simple way to categorize these examples is by the position of C-H functionalization relative to the amine.

The majority of examples focus on the α-C(sp<sup>3</sup>)-H functionalization of amines. Pioneering examples include amine alkyl group exchange via C-H activation,<sup>133</sup> carbonylation of tertiary *N*-pyridyl amines (Scheme 2.2a),<sup>134</sup> and oxidative functionalization of tertiary amines with cyanide,<sup>135</sup> alkenes,<sup>136-137</sup> alkynes,<sup>138-139</sup> and acidic carbon nucleophiles in a cross-dehydrogenative-coupling (Scheme 2.2b).<sup>140-142</sup> Other examples include Fe-catalyzed oxidative coupling of tertiary methyl amines with heteroarenes,<sup>143</sup> and Ru-catalyzed arylation of tertiary *N*-pyridyl amines.<sup>144</sup> An important contribution of a Rh-catalyzed carbenoid insertion into an α-C-H bond of a tertiary amine has been reported as a late stage functionalization of brucine (a

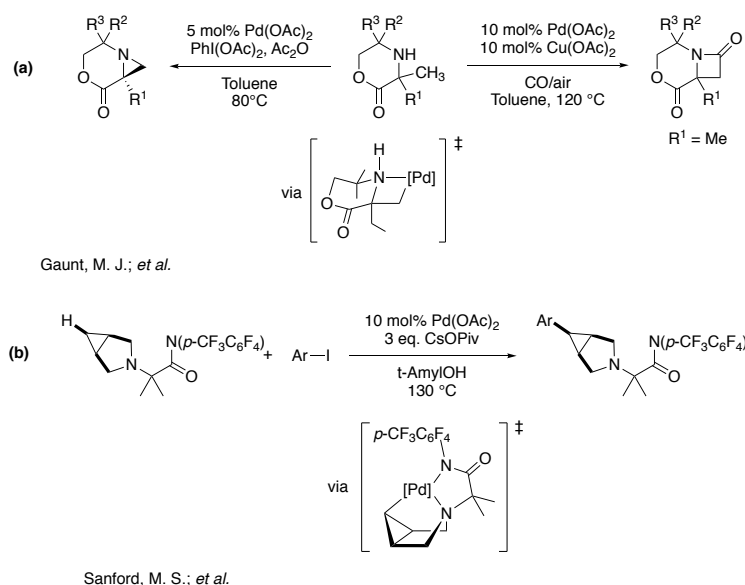
cytotoxic alkaloid).<sup>145</sup> Recently, significant advances have been made in this chemistry by utilizing photo-redox catalysis and photo-redox dual-catalysis.<sup>146</sup> This strategy has allowed for diverse  $\alpha$ -functionalization of tertiary amines allowing for functionalization with nitromethanes (Scheme 2.2c),<sup>147</sup> cyanoaromatics,<sup>148</sup> aryl halides,<sup>149-150</sup> anhydrides (Scheme 2.2d),<sup>151</sup> and an oxidative cyclization via combined  $\alpha$ -C(sp<sup>3</sup>)-H and  $\beta$ -C(sp<sup>2</sup>)-H activations of *N,N*-dialkyl anilines (Scheme 2.2e).<sup>152</sup>



**Scheme 2.2 Examples of metal-catalyzed  $\alpha$ -C-H functionalization of amines**

Others have developed intriguing examples that functionalize amine C-H bonds at positions further away from the amine. Reactions that functionalize the  $\beta$ -C-H bond of amines include Pt-catalyzed cyclization of amino acids,<sup>153</sup> and Pd-catalyzed aziridination,  $\beta$ -lactonization, and arylation of sterically constrained aliphatic amines lacking  $\alpha$ -C-H bonds (Scheme 2.3a).<sup>154-156</sup> Others have developed late-transition-metal catalyzed reactions that

perform terminal selective activation such as the Ir-catalyzed  $\alpha$ -,  $\beta$ -, or  $\gamma$ -C–H borylation of tertiary amines,<sup>157</sup> and Pd-catalyzed  $\beta$ -,  $\gamma$ -, and  $\delta$ -hydroxylation of aliphatic amines.<sup>158</sup> Additional examples of selective functionalization include the  $\gamma$ -acetylation of 4-ethyloxazolidines,<sup>159</sup> and  $\gamma$ -arylation of tertiary piperidines and 3-methyl-3-azabicyclo[3.1.0]hexanes (Scheme 2.3b).<sup>160</sup> A different approach involves the conversion of a free amine into an intermediate product containing a directing group in the reaction mixture, using a catalytic amount of the directing group precursor. Both examples are Pd-catalyzed and generate an imine in situ allowing for the  $\delta$ -arylation of primary aliphatic amines from aryl iodides,<sup>161</sup> or diaryliodonium salts.<sup>162</sup> Notably many of these selective examples utilize designed steric constraints to effectively direct the selectivity of the metal-mediated C–H activation event.



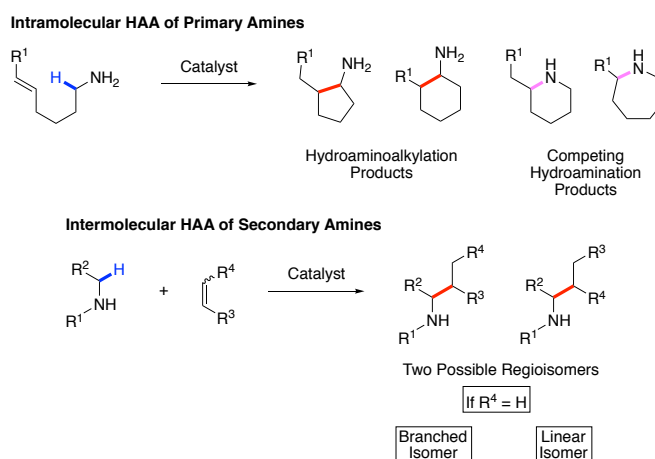
**Scheme 2.3 Use of steric control for selective C–H functionalization**

### 2.1.1 Early-Transition-Metal Hydroaminoalkylation

Absent from the above discussions are  $C(sp^3)$ –H activation and functionalization with alkenes to form alkylation products. As this reaction is the focus of this chapter and the next, a detailed discussion is necessary.



The catalytic  $\alpha$ -C(sp<sup>3</sup>)-H activation of amines and subsequent  $\alpha$ -alkylation with an alkene is commonly referred to as hydroaminoalkylation. This atom-economical approach involves the direct activation of an  $\alpha$ -C(sp<sup>3</sup>)-H bond and its subsequent addition across an alkene unsaturation in an intra- or intermolecular fashion (Scheme 2.4). This method of C-H activation produces complementary products to the examples previously discussed. Importantly, this reaction is 100% atom-economical, and therefore does not produce stoichiometric waste byproducts.



**Scheme 2.4 Inter- and intra-molecular variants of hydroaminoalkylation**

First noted in the early 1980's using homoleptic early-transition-metal amido complexes of the type Zr(NMe<sub>2</sub>)<sub>4</sub>, Nb(NMe<sub>2</sub>)<sub>5</sub>, Ta(NMe<sub>2</sub>)<sub>5</sub>, and W<sub>2</sub>(NMe<sub>2</sub>)<sub>6</sub>/W(NMe<sub>2</sub>)<sub>6</sub>, these reactions produced only single digit turnovers for the alkylation of dimethylamine with 1-pentene or 1-hexene.<sup>163-164</sup> Since then significant developments have occurred, with the majority of research focused on early-transition-metal catalysts for both the inter- and intra-molecular variants of this reaction.

Reaction scheme showing the synthesis of HAA and HA from a substituted allylamine derivative (2.1) in Toluene at 110 °C, yielding a 14:1 ratio of HAA:HA.

2.1

$\text{R-NH}_2 + \text{Cyclohexene} \xrightarrow[\text{n-hexane, } 140^\circ\text{C}]{5 \text{ mol\% } \mathbf{2.2}}$ 
  
 $\text{R-NH-Cyclohexane}$ 
  
 $\text{R} = \text{Ar}, \text{CH}_2\text{CH}_2\text{Ph}$

47

The intermolecular variant of this reaction with secondary amines has seen significantly more development. Practical turn-over numbers (15-20) were originally achieved with the realization that *N*-methyl anilines were effective hydroaminoalkylation substrates with a variety of terminal alkenes and norbornene.<sup>170</sup> Numerous Ti, Nb, and Ta metal complexes have since been developed for this reaction utilizing a variety of ligand substitutions and motifs (Figure 2.1).<sup>170-176</sup> The use of  $\text{Ti}(\text{NMe}_2)_4$  and  $\text{TiBn}_4$  initially focused on the use of *N*-methylaniline derivatives and terminal alkenes. However, these Ti catalysts suffered from poor selectivity between the branched and linear regioisomers (Figure 2.1).<sup>167-168</sup> Significant improvement in regioselectivity for the branched hydroaminoalkylation product was found by using  $\text{Ti}(\text{Ind})_2\text{Me}_2$  and **2.3** as catalysts.<sup>177-178</sup> The use of ligands with increased steric bulk is proposed to be the reason for the improved selectivity toward the branched product. By comparison, *in situ* generation of **2.1** results in large substrate scope but poor selectivity, generally favouring the linear isomer.

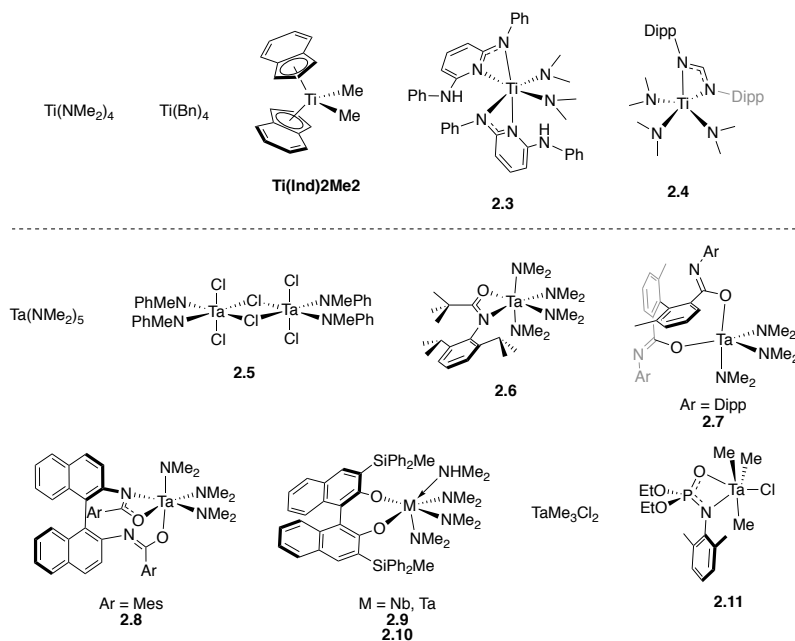
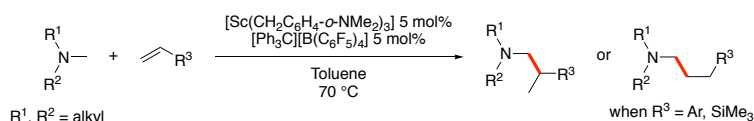


**Figure 2.1** Early-transition-metal catalysts used for the intermolecular hydroaminoalkylation of secondary amines

Group 5, in particular Ta, has seen significant advances from the first synthetically useful report utilizing  $\text{Ta}(\text{NMe}_2)_5$ .<sup>170</sup> Generally, group 5 catalysts provide almost exclusively the branched regioisomer, with some exceptions for styrenes and vinyltrimethylsilane as the alkene substrates.<sup>175</sup> The use of **2.5** expands the substrate scope to include dialkylamines; to date, utilizing **2.5** provides broadest scope for dialkylamines.<sup>171</sup> Notably, 1,3-*N,O*-chelating ligands (as either amidates or phosphoramidates) provide highly active hydroaminoalkylation catalysts. Of note, **2.6** exhibits remarkable stability, allowing for increased reaction temperatures and extended reaction time for challenging substrates. Complex **2.6** is the only catalyst reported for the hydroaminoalkylation of cyclic secondary amines such as piperidine, piperazine, morpholine, etc.<sup>172,179</sup> While **2.6**, **2.7**, and other chiral biaryl-bisamidate Ta complexes provide good enantioselectivities,<sup>173,180-181</sup> the BINOLate complexes **2.9** and **2.10** provide good to excellent enantioselectivities (up to 98 %ee for certain substrates) for hydroaminoalkylation of *N*-methylaniline derivatives with a broad scope of alkene coupling partners.<sup>174,182</sup> Notably, **2.10** is the only reported catalyst that exhibits room temperature hydroaminoalkylation reactivity.



**Scheme 2.6** Sc catalyzed hydroaminoalkylation of trialkyl amines

Additionally, a cationic Sc complex has recently been reported for the hydroaminoalkylation of trialkyl tertiary amines with a variety of terminal alkenes. This system exclusively provides for the branched regioisomer with all alkene substrates except styrene derivatives and allyltrimethylsilane, which give the linear regioisomer selectively (Scheme 2.6).<sup>183-184</sup>

The proposed mechanism for early-transition-metal catalyzed hydroaminoalkylation has been adopted for all group 4 and 5 catalyst systems. Figure 2.2 shows a simplified proposed mechanism for intermolecular hydroaminoalkylation with secondary amines (relevant to the results presented within this thesis).<sup>164,174,185</sup> Entry into the active catalytic cycle occurs *via* ligand exchange to ligate the substrate amine to the metal center, followed by C–H activation *via* hydrogen abstraction by an adjacent amido ligand to give tantalaziridine **A**. Insertion of the alkene into the reactive Ta–C bond forms metallacycle **B**. Subsequent protonolysis of the Ta–C bond with incoming amine substrate generates **C**. Another C–H activation event allows for release of the significantly larger product amine, releasing steric strain around the metal center, and regenerating the reactive tantalaziridine moiety. In this proposed mechanism, there is no change in oxidation state of the metal center. This contrasts with the proposed mechanism for the many late-transition-metal-catalyzed hydroaminoalkylation reactions (Figure 2.3).

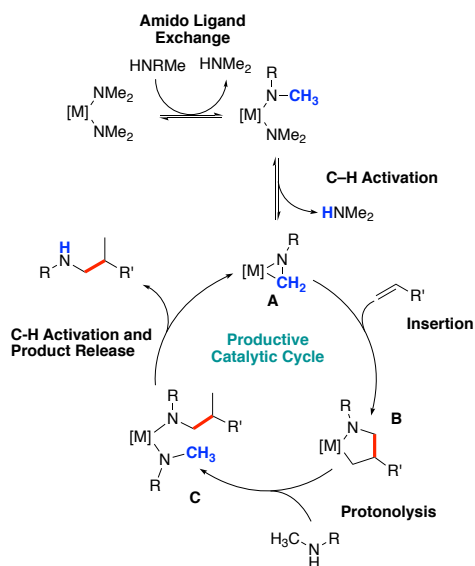
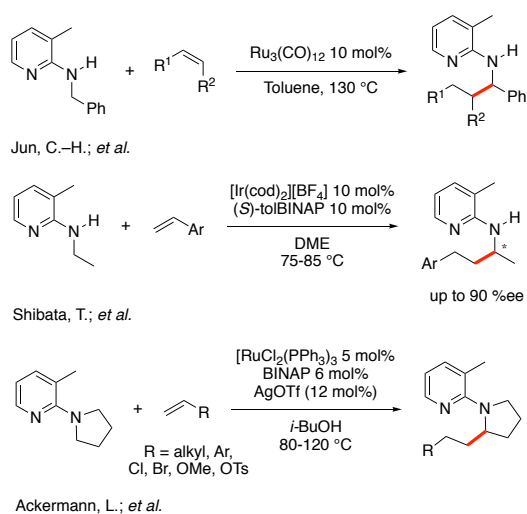


**Figure 2.2 Proposed mechanism for early-transition-metal catalyzed hydroaminoalkylation**

### 2.1.2 Late-Transition-Metal Hydroaminoalkylation

Significant advances in hydroaminoalkylation chemistry have also been made with late-transition metal catalysts.<sup>137,186-197</sup> With few exceptions, development of this methodology has occurred utilizing Ru and Ir catalyst systems, with the majority of examples requiring the use of *N*-pyridyl secondary and tertiary amines (Scheme 2.7).<sup>137,186-190,193-194</sup> The pyridyl group in these examples acts as a directing group, and encourages coordination and activation of the substrate by placing the  $\alpha$ -C(sp<sup>3</sup>)-H bond in the proper orientation for the C-H activation event.



**Scheme 2.7** Ru and Ir catalyzed hydroaminoalkylation utilizing *N*-pyridyl directing groups

These examples are proposed to proceed through a mechanism involving 2e<sup>-</sup> oxidative and reductive processes at the metal center (Figure 2.3).<sup>186-188</sup> In this mechanism, coordination of the substrate via the pyridyl moiety occurs. C-H activation via oxidative addition occurs to generate the 5-membered metallaacycle (**A** to **B**). The alkene then inserts into the M-H bond. Importantly, if internal, alkyl functionalized alkenes are utilized, chain walking will occur until the M-C bond is at the terminal carbon. This is followed by a reductive elimination (**C** to **D**), product de-coordination, and regeneration of the metal catalyst. Due to the chain-walking

mechanism, this mechanism is consistent with the observed linear products. This is in direct contrast to the early-transition-metal catalyst that can selectively result in the branched regioisomer.

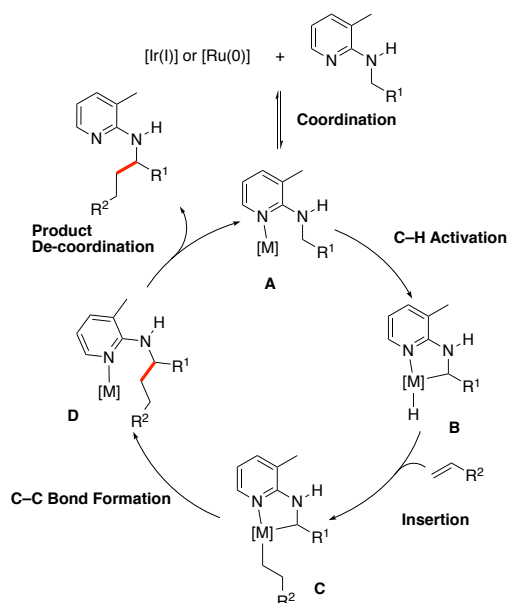
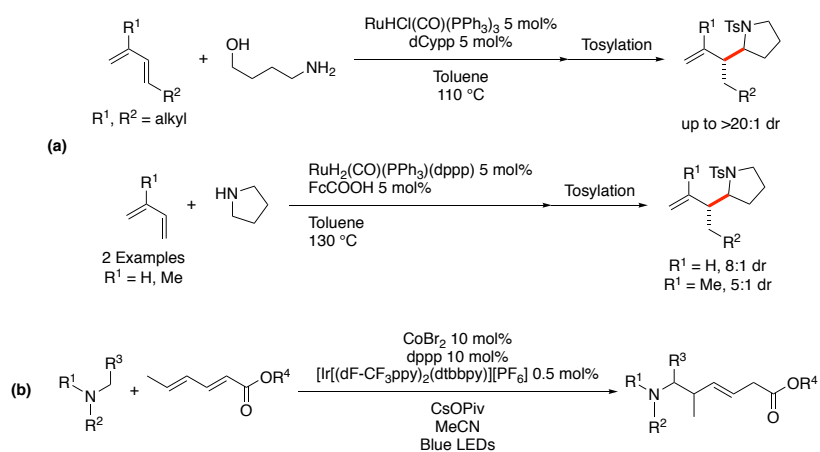


**Figure 2.3 Proposed mechanism for directed, late-transition-metal catalyzed hydroaminoalkylation**

Interestingly, a Ru-catalyzed reaction of 4-aminobutanol with dienes results in 2-allyl pyrrolidine hydroaminoalkylation products (Scheme 2.8a). This communication also provides one example where pyrrolidine undergoes direct C(sp<sup>3</sup>)-H functionalization with dienes. Another recent report utilizes dienes as the unsaturated coupling partner.<sup>195</sup> Alternatively, photo-redox dual-catalysis (Ir photo-catalyst, Co-catalyst system), allows for the hydroaminoalkylation of dienes with tertiary amines with broad substrate scope (Scheme 2.8b).<sup>197</sup> It should be noted that these examples follow a different mechanism than presented in Figure 2.3.

While the focus of this thesis is the catalytic transformation of amines, it is also important to mention other late-transition-metal-catalyzed reactions of other nitrogen functional groups (e.g. amides, ureas, sulfonamides, etc.), upon stoichiometric deprotection, can result in alkylated

amine products. Of direct relevance to this discussion is the Ru-catalyzed hydroalkylation of hydantoin with dienes,<sup>192</sup> Pd-catalyzed  $\beta$ -alkylation of protected amino-amides (from unnatural amino acids) with alkenes,<sup>198</sup> Ir-catalyzed  $\alpha$ -alkylation of *N*-alkoxythiocarbonyl functionalized aza-heterocycles,<sup>199</sup> and the  $\beta$ -alkylation ( $\alpha$  to N) of ureas with alkenes.<sup>200</sup> These reactions avoid the inherent basicity and reducing potential of free amines that can negatively impact transition-metal-catalyzed reactions.



**Scheme 2.8** Late-transition-metal catalyzed hydroaminoalkylation without a directing group

### 2.1.3 Scope of Chapter

Complex **2.5**, and the related  $[\text{Ta}(\text{NEt}_2)_2\text{Cl}_3]$ , are both reported to exhibit similar reactivity.<sup>171</sup> These complexes are interesting as they exhibit high reactivity for dialkyl amine substrates. Most catalyst systems reported to date struggle with these non-aniline derivatives. Additionally, **2.5** exhibits good reactivity at lower temperatures with *N*-methylaniline as a substrate, which is only equaled by the exceptional  $25^\circ\text{C}$  reactivity of **2.11**.<sup>175</sup> Notably, **2.11** also utilizes a chloro ligand. While the role of the chloro ligand is not fully understood, its inclusion appears to be important for broad substrate scope and high activity.

2-Pyridonate ligands have been utilized as ligands on Ti and Zr precatalysts,<sup>19,166</sup> but have not been explored on Ta precatalysts for hydroaminoalkylation. We desired to explore the

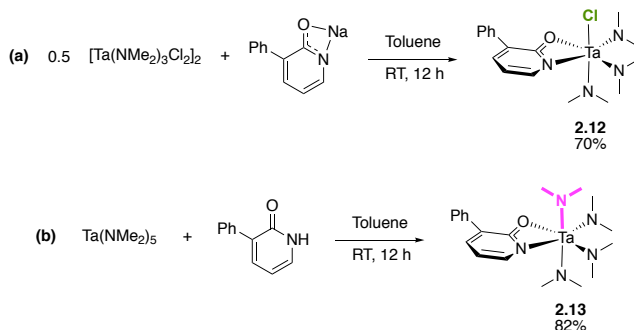


use of 2-pyridonate as ancillary ligands on Ta complexes for hydroaminoalkylation. Additionally, we wished to create complexes that did and did not contain chloro ligand(s) in an attempt to determine the role of the chloro ligand in hydroaminoalkylation precatalysts. Thermal robustness also appears to be important for broad substrate scope, so complexes with amido ligands are targeted.

This chapter reports the synthesis and catalytic studies of a variety of 2-pyridonate Ta complexes that are the only reported complexes that exhibit broad substrate scope for the hydroaminoalkylation of internal alkenes that occurs without isomerization of the alkenes. These complexes revealed a substrate/precatalyst dependence for optimal activity. Kinetic and deuterium labelling investigations reveal that off-cycle equilibria limit the activity of the discovered precatalysts.

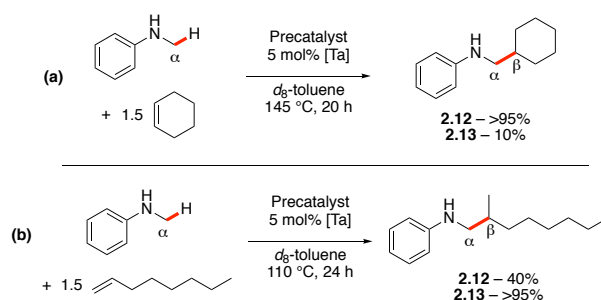
## 2.2 Results and Discussion

### 2.2.1 Development of a Novel 2-Pyridonate Precatalyst for the Hydroaminoalkylation of Internal Alkenes



Dr. Eugene Chong developed the synthesis of **2.12** and **2.13**

**Scheme 2.9 Synthesis of 2-pyridonate Ta complexes**



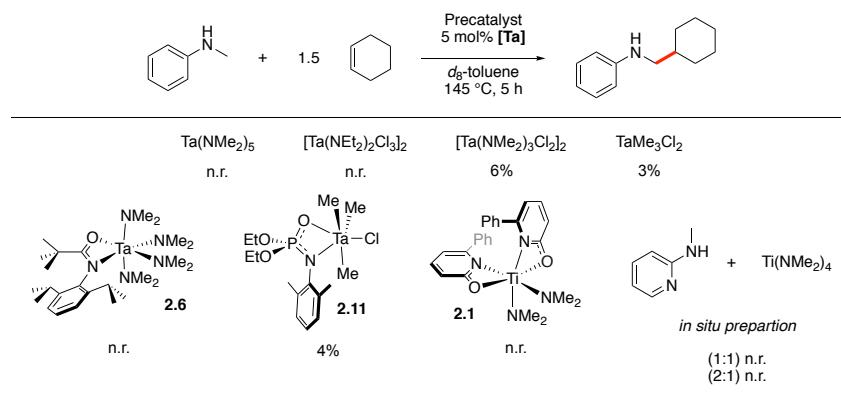
Dr. Eugene Chong performed the catalysis in this scheme

**Scheme 2.10 Complementary catalytic reactivity of **2.12** and **2.13** with cyclohexene and 1-octene**

Dr. Eugene Chong discovered a route for the selective synthesis of 3-phenyl-2-pyridonate complexes of Ta (Scheme 2.9). Intriguingly, complexes **2.12** and **2.13** show complementary reactivity toward terminal and internal alkenes (Scheme 2.10). Complex **2.12** shows high reactivity with cyclohexene, while complex **2.13** shows better reactivity with 1-octene.

To date, few complexes have been demonstrated to be active catalysts for the hydroaminoalkylation of secondary amines with unactivated internal alkenes (multiple complexes have been reported to catalyzed the hydroaminoalkylation with highly strained norbornene as a substrate). Complex **2.6** is reported to undergo hydroaminoalkylation of *N*-methylaniline with 1,5-cyclooctadiene (83%, 96 h, 165 °C).<sup>172</sup> TaMe<sub>3</sub>Cl<sub>2</sub> is reported to undergo the hydroaminoalkylation of *N*-methylaniline with cyclooctene (73%, 102 h, 110 °C), cycloheptene (83%, 30 h, 110 °C), cyclohexene (88%, 47 h, 145 °C), and *Z*-3-hexene (65%, 36 h, 145 °C).<sup>176</sup> As reported in an initial communication, Ti complex **2.4** is reported to undergo hydroaminoalkylation of cyclopentene with *N*-methylaniline (75%, 96 h, 180 °C), cyclohexene (72%, 96 h, 180 °C), 1,4-cyclohexadiene (93%, 96 h, 180 °C), and *E*-2-octene (16% mixture of isomers, 96 h, 180 °C). Notably, **2.12** demonstrates significantly increased the turnover frequency compared to known examples.

To ensure our results were a product of **2.12** and not due to reaction conditions, we attempted the reaction of *N*-methylaniline and cyclohexene with known for hydroaminoalkylation precatalysts (Scheme 2.11). To our surprise, only a few complexes produced any conversion at our catalyst loading (5 mol%) under our reaction conditions (sealed vessel, 20 h, 145 °C) highlighting the efficacy of **2.12**.

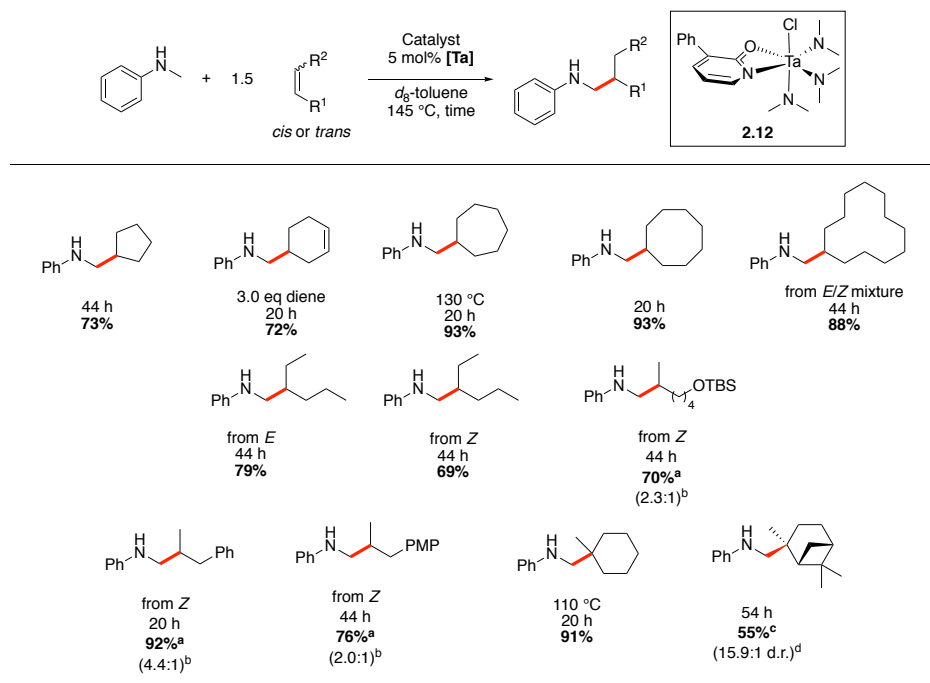


Reaction conditions: *N*-methylaniline (0.5 mmol), cyclohexene (0.75 mmol), [Ta] precatalyst (0.025 mmol), *d*<sub>8</sub>-toluene (0.5 mL). Conversion was determined by <sup>1</sup>H NMR spectroscopy.  
I synthesized the above complexes and performed the catalysis in this scheme.

**Scheme 2.11 Hydroaminoalkylation of cyclohexene with known precatalyst under our conditions**

We next turned to elucidating the substrate scope of **2.12** as a precatalyst. To explore the alkene scope, we utilized *N*-methylaniline as the amine substrate (Scheme 2.12). Gratifyingly, **2.12** is able to catalyze the hydroaminoalkylation of a wide variety of internal alkenes. Cyclopentene, -hexadiene, -heptene, -octene, and -dodecene are all tolerated in good to excellent yields. Both *E*- and *Z*-3-hexene react giving the desired products in 79% and 69% yields, respectively, while requiring longer reaction times of 44 h than their cyclic counterparts. Here *Z*-3-hexene is less reactive, producing a lower yield. These linear alkenes, represent the first examples of hydroaminoalkylation of these substrates that produce the β-branched products, and avoid chain-walking to produce the linear coupled products. Unsymmetrical alkenes 2-silylether-*Z*-4-hexene, *cis*-β-methylstyrene, and *trans*-anethole react in good to excellent yields albeit with

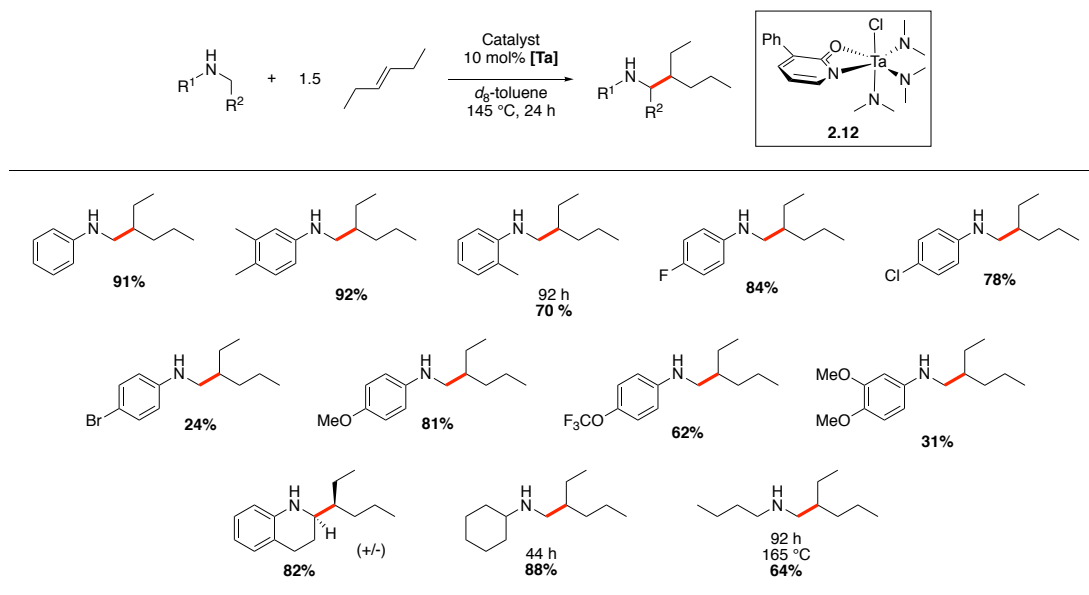
limited regioselectivity. Here, silyl ether functionality is tolerated, and the first examples of  $\beta$ -styrenes to undergo hydroaminoalkylation are presented. 1,1-Disubstituted alkenes are also tolerated with complete regioselectivity. In particular, (1S)- $\beta$ -pinene undergoes hydroaminoalkylation with high diastereoselectivity.



**Scheme 2.12 Alkene substrate scope for the hydroaminoalkylation catalyzed by 2.12**

Scope in amine substrate was explored using *E*-3-hexene (Scheme 2.13). Increasing the precatalyst loading to 10 mol% allows for 91% yield in 24 h reaction time with *N*-methylaniline. Multiple *N*-methylaniline derivatives are tolerated in excellent yields. Notably, sterically encumbering 2-methyl substituents are tolerated in good yields. 4-Fluoro, -chloro, -methoxy, and -trifluoromethoxy result in high yields. 4-Bromo-, and 3,4-dimethoxy-*N*-methylanilines are tolerated but in low yields. Tetrahydroquinoline results in an excellent yield and produces a

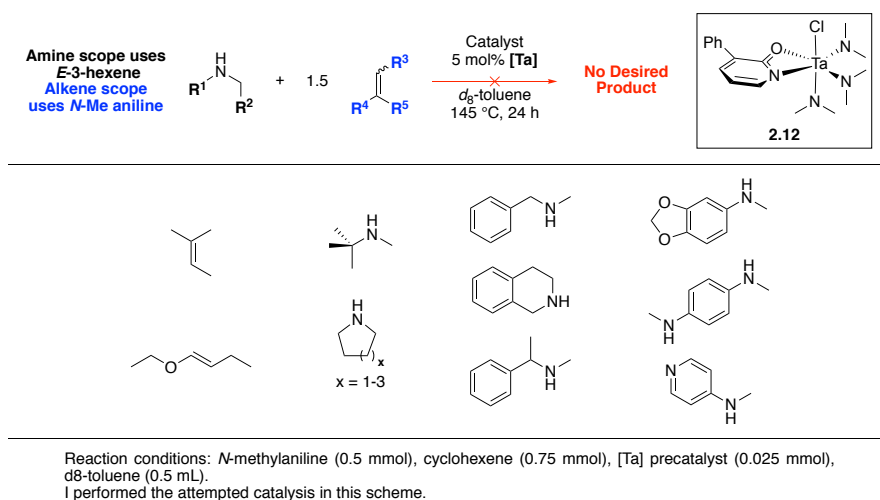
single diastereomer. Dialkyl *N*-methylcyclohexylamine, and *N*-methyl-*N*-butylamine result in 88% and 64% yields, respectively, but requires extended reaction times and 165 °C reaction temperature for the latter.



**Scheme 2.13** Amine substrate scope for hydroaminoalkylation catalyzed by **2.12**

Unfortunately, we did observe some substrate scope limitations. Reactivity was tested with 5 mol% **2.12** using *N*-methylaniline for alkene substrates and *E*-3-hexene for amine substrates (Scheme 2.14). The trisubstituted alkene, 2-methyl-2-butene, as well as a vinyl ether were both unreactive to hydroaminoalkylation. Multiple amines were also unreactive. *N*-methyl-*tert*-butyl amine, and heterocycles pyrrolidine, piperidine, and azetidine also did not react. Catalytic hydroaminoalkylation with 2-methyl-2-butene or *N*-methyl-*tert*-butyl amine have not been reported in the literature. We propose that steric hindrance prevents reactivity with these two substrates. *N*-heterocycles have successfully been used as substrates in Ta catalyzed hydroaminoalkylation.<sup>172,179</sup> At this time, we do not have an explanation for the lack of activity

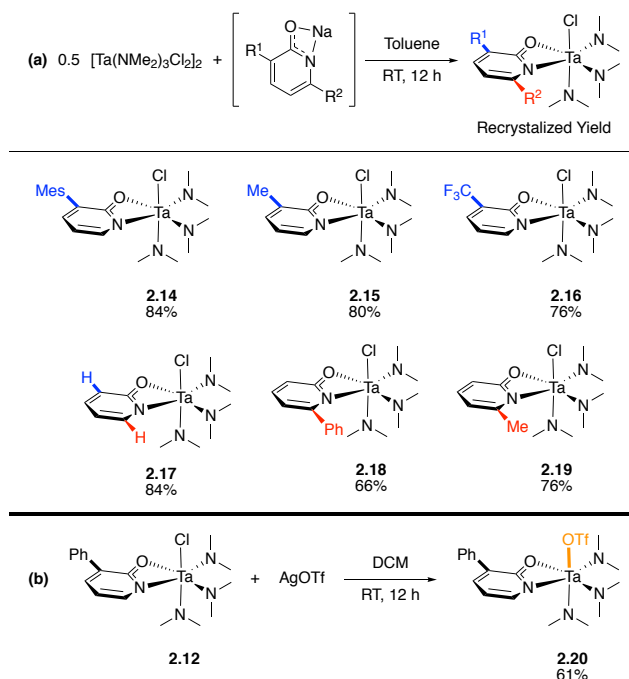
with **2.12**. Amines with benzylic methylenes were also unproductive substrates. However, we did observe that exposing catalytic amounts of *N*-methylbenzylamine to **2.12** results in decomposition of **2.12** and formation of new organotransition metal species. Attempts to isolate these species were unsuccessful. A catechol protected aniline derivative, 1,4-di-(*N*-methylamino)benzene, and 4-*N*-methylaminopyridine did not result in productive catalysis, but significant decomposition of these amine starting materials was observed.



**Scheme 2.14** Substrate scope limitations for hydroaminoalkylation catalyzed by **2.12**

## 2.2.2 Exploration of 2-Pyridonate Ligand Effects on Hydroaminoalkylation Catalysis

In an effort to better understand the effect of the pyridonate ligand, a systematic investigation of the steric and electronic properties of 2-pyridonate ligands was undertaken. Given the high reactivity of **2.12** with internal alkenes, we synthesized a variety of (2-pyridonate)Ta(NMe<sub>2</sub>)<sub>3</sub>Cl complexes (**2.14** – **2.19**, Scheme 2.15a). Previous work on 2-pyridonate Ti complexes have shown that substituent effects at the 3 and 6 positions on the pyridonate ligand can dramatically affect intramolecular hydroaminoalkylation.<sup>19</sup> In an effort to explore the role of the chloride ligand we also synthesized complex **2.20**, featuring an axial triflate ligand.



**Scheme 2.15** Synthesis of new Ta complexes **2.14-2.20**

Complexes **2.14** – **2.19** can be prepared via salt metathesis in the same manner as **2.12**. To prepare complex **9**, complex **1** can be reacted with silver triflate in dichloromethane to produce the desired tantalum triflate analogue (Scheme 2.15b). All resultant complexes were prepared in good yield and were fully characterized by  $^1\text{H}$  and  $^{13}\text{C}$  NMR spectroscopy, EI-MS, and EA. In the solution phase, the three inequivalent dimethylamido ligands in all complexes give rise to a single, broad resonance in both the  $^1\text{H}$  and  $^{13}\text{C}$  NMR spectra. This is due to rapid isomerization of the dimethylamido ligands.

Complex	2.12	2.15	2.16	2.18
Ta–N1 (Å)	2.288(4)	2.307(1)	2.295(3)	2.301(1)
Ta–O1 (Å)	2.129(2)	2.122(1)	2.155(2)	2.191(2)
N1–Ta–O1 (°)	59.30(9)	59.76(5)	59.4(1)	59.13(6)
Ta–Cl (Å)	2.4959(8)	2.4931(5)	2.476(1)	2.4643(6)
Av. Ta–NMe <sub>2</sub> (Å)	1.962(8)	1.97(1)	1.97(1)	1.97(1)
C1–N1 (Å)	1.344(4)	1.364(2)	1.349(4)	1.360(3)
C1–O1 (Å)	1.298(4)	1.315(2)	1.304(5)	1.302(2)

**Table 2.1 Comparison of key bond lengths and angles of the solid state molecular structures of 2.12, 2.15, 2.16, and 2.18**

Crystals suitable for single crystal X-ray diffraction of complexes **2.15**, **2.16**, and **2.18** were obtained (Figure 2.4). Each complex adopts a distorted octahedral geometry and shares similarity with the previously complex **2.12**. The facial arrangement of the dimethylamido ligands can be attributed to  $\pi$ -bonding effects, as the  $\pi$ -donating amido ligands are all trans to ligands with minimal  $\pi$ -donating ability. A comparison of key bond lengths and angles (Table 2.1), shows that any substituent induced variance in the binding of the pyridonate, chloride, or amido is small in the solid state. Of note, is the extended Ta–O1 bond lengths in complex **2.16** and **2.18** and concomitant shortening of the Ta–Cl bond lengths. Due to the fact that that **2.16** has an electron withdrawing trifluoromethyl group in the 3-position while **2.18** has an electron withdrawing phenyl group in the 6-position, we suggest this distortion is caused by electron withdrawing character coupled with steric effects in **2.18**. However, these changes are subtle and we are unable to rule out the possibility that crystal packing effects dominate the observed metrics. We were unable to obtain crystallographic data for all complexes and have assigned the geometries of the remaining complexes by analogy.



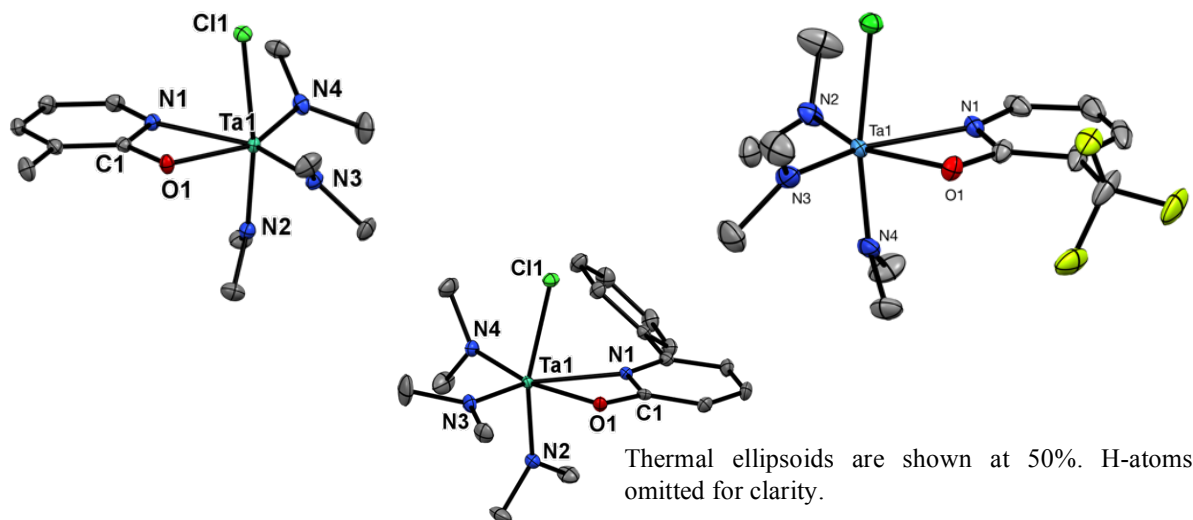
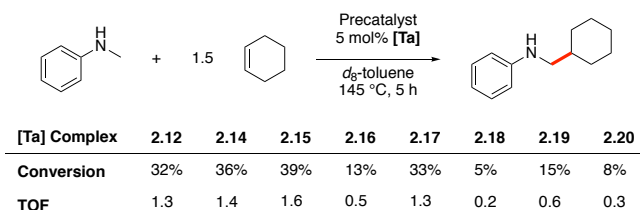


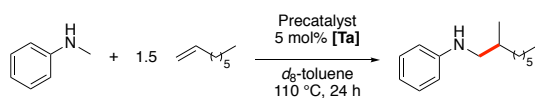
Figure 2.4 ORTEP representations of **2.15** (top-left), **2.16** (top-right), and **2.18** (bottom)

The catalytic activity of these complexes was assessed with the preferred benchmark reactions of *N*-methylaniline with cyclohexene (Scheme 2.16) and 1-octene (Scheme 2.17). Complex **2.12** has been shown to promote the reaction with cyclohexene in >95% conversion (145 °C, 20 h), and with 1-octene in 40% conversion (110 °C, 24 h). Reaction times of 5 h (Scheme 2.16) and 24 h (Scheme 2.17) were selected to give conversions that would allow for ready comparison of the ligand environments. Thus, the reported conversions do not represent optimized yields. Turnover frequencies (TOF) were calculated based on the given reaction times and do not represent exhaustive study. Turnover numbers were not determined.



Reaction conditions: *N*-methylaniline (0.5 mmol), cyclohexene (0.75 mmol), [Ta] pre-catalyst (0.025 mmol), *d*<sub>8</sub>-toluene (0.5 mL). Conversion determined by <sup>1</sup>H NMR spectroscopy. Average of two experiments, see experimental section. TOF (h<sup>-1</sup>) = turnover frequency = turnovers/time. TOF presented here is non-exhaustive.

Scheme 2.16 Hydroaminoalkylation activity of new precatalyst complexes with cyclohexene substrate



[Ta] Complex	2.12	2.13	2.15	2.17	2.18	2.19	2.20
Conversion	40%	>95%	92%	>95%	>95%	>95%	20%
TOF	1.6	3.8	3.7	3.8	3.8	3.8	0.8

Reaction conditions: N-methylaniline (0.5 mmol), cyclohexene (0.75 mmol), [Ta] pre-catalyst (0.025 mmol),  $d_8$ -toluene (0.5 mL). Conversion determined by  $^1\text{H}$  NMR spectroscopy. Average of two experiments, see experimental section. TOF ( $\text{h}^{-1}$ ) = turnover frequency = turnovers/time. TOF presented here is non-exhaustive.

#### Scheme 2.17 Hydroaminoalkylation activity of new precatalyst complexes with 1-octene substrate

Results with cyclohexene reveal that altering the steric parameters at the 3-position (**2.12**, 3-phenyl; **2.14**, 3-mesityl; **2.15**, 3-methyl; **2.17**, 3-hydro) of the pyridonate ring result in only minor differences in reactivity. Surprisingly, **2.16** (3-trifluoromethyl) results in low conversion. Analysis of the  $^{19}\text{F}$  NMR spectrum after the reaction showed various signals in the region of 50–100 ppm. This suggests the formation of Ta–F complexes,<sup>201</sup> *via* catalyst decomposition. Altering the 6-position (**2.18**, 6-phenyl; **2.19**, 3-methyl) of the pyridonate results in a significant decrease in reactivity. This detrimental effect on catalytic performance is proposed to be due to the added steric congestion at the metal center, thereby hindering reactivity with the sterically demanding internal alkene substrate. The use of **2.20** results in poor conversion. In this case, no Ta–F complexes could be observed by  $^{19}\text{F}$  NMR spectroscopy at the end of the catalytic reaction.

Using a terminal alkene, 1-octene, as a substrate provides significantly different results (Scheme 2.17). A marked increase in conversion occurs where the steric parameter is reduced in the 3-position of the pyridonate (**2.15** and **2.17**). Intriguingly, increasing the steric parameter of the pyridonate in the 6-position (**2.18** and **2.19**) also provides high conversion with this less sterically demanding terminal alkene substrate. As with the cyclohexene substrate, the triflate complex **2.20** provided disappointing reactivity with 1-octene. Complexes **2.15** and **2.17** are the first examples of highly active catalysts for both internal and terminal alkenes. These complexes offer a minimal increase over our previously reported complex **1** for reactivity with cyclohexene.

However, **2.15** and **2.17** are comparable to **2.13** and are significantly better than **2.12** for reactions with 1-octene. An attractive advantage to **2.15** and **2.17** is the fact that the 2-pyridone prolignands are commercially available and inexpensive.

To further elucidate the general reactivity of **2.15** and **2.17**, additional reactions with various alkene substrates were completed (Scheme 2.18). By reducing the reaction time to 20 hours with 1-octene (entry 1), the difference in reactivity between **2.15** and **2.17** could be better observed. Gratifyingly, **2.17** produces 86% yield (>95% conversion), while complex **2.15** is slightly less active (63% yield). Reactivity with different internal alkenes (entries 2-6) shows that complex **2.15** is more broadly useful than **2.17**. With cyclohexene (entry 2) and cycloheptene (entry 3), **2.15** provides yields of 81% and 93% respectively, in 4 hours less than it takes **2.12** to provide comparable yields (88% and 95% respectively). Complex **2.15** provides slightly less conversion in 24 h than **2.12** (83% vs. 92%) with *Z*-methylstyrene substrate (entry 5), but more significantly, reduced yields with *E*-3-hexene (entry 4) and (1*S*)- $\beta$ -pinene (entry 6); a 21% and 23% reduction in yield respectively. Both complexes **2.15** and **2.17** offer comparable regioselectivity with *Z*-methylstyrene (entry 5) and diastereoselectivity with (1*S*)- $\beta$ -pinene (entry 6), compared to reported complex **2.12**.

Entry	Products	Conds.	2.15	2.17
1		110 °C 20 h	63%	86%
2		145 °C 16 h	81%	44%
3		130 °C 16 h	93%	95%
4		145 °C 44 h	58%	31%
5		145 °C 24 h	83% (3.0:1) <sup>a,b</sup>	29% (3.7:1) <sup>a,b</sup>
6		145 °C 54 h	32% (20:1) <sup>c,d</sup>	14% (>20:1) <sup>c,d</sup>

Reaction conditions: *N*-methylaniline (0.5 mmol), alkene (0.75 mmol), [Ta] pre-catalyst (0.025 mmol), ferrocene (0.05 – 0.11 mmol), *d*<sub>8</sub>-toluene (0.5 mL). Yield determined by <sup>1</sup>H NMR spectroscopy with Cp<sub>2</sub>Fe internal standard. a) Major regioisomer shown. b) Ratio determined by <sup>1</sup>H NMR analysis. c) Major diastereomer shown. d) Ratio determined by UHPLC analysis. Average of two experiments, see experimental section.

**Scheme 2.18 Comparative hydroaminoalkylation reactivity of 2.15 and 2.17**

Complex **2.15** is a readily accessible, broadly reactive HAA pre-catalyst, and is the first catalyst system offering excellent reactivity profiles with both internal and terminal alkenes. However, efforts to optimize reaction yields for specific amine/alkene substrate combinations demanded empirical screening and few reliable reactivity trends could be determined. To improve our predictive ability to select and design optimized catalyst systems, mechanistic investigations were undertaken.

### 2.2.3 Mechanistic Interpretation

We, and others, have proposed a simplified catalytic cycle for hydroaminoalkylation as presented in Figure 2.2. Kinetic mechanistic research by Hultzs and co-workers on a tantalum BINOLate complex concluded that the rate determining step(s) for their system is either a

combined rate constant for conversion of **A** to **C**, or amido exchange with **C** to release product (Figure 2.2).<sup>174</sup> Their work also shows that the rate determining step is influenced by substrate.

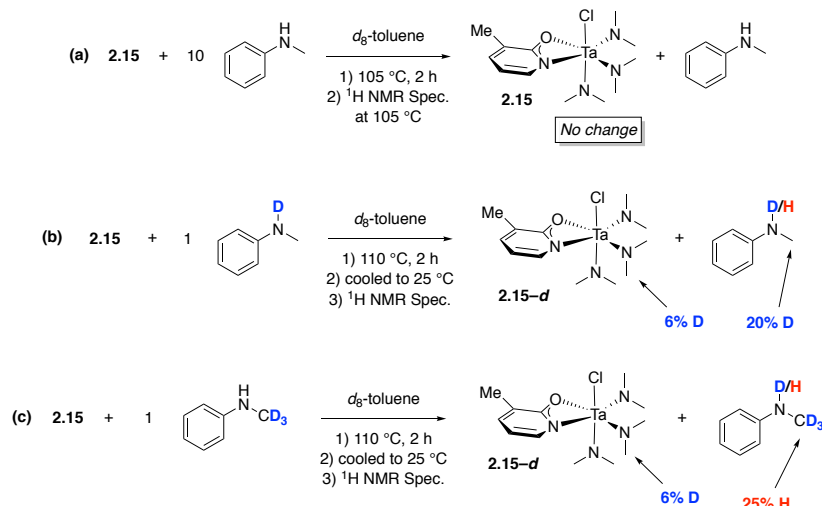
We propose that the introduction of the planar pyridonate and the chloro ligands (complex **2.12**) reduce the steric constraints for the insertion step (**A** to **B**), or protonolysis step (**B** to **C**) allowing for productive catalysis with sterically demanding internal alkenes. These two steps both involve high steric congestion of the metal center, where complexes of the type [(2-pyridonate)Ta(NMe<sub>2</sub>)<sub>3</sub>Cl], provide the necessary steric relief for catalytic turnover. The decreased reactivity shown by 6-phenyl (**2.18**) and 6-methyl (**2.19**) with cyclohexene can be explained by the increased steric constraints imparted by 6-substituted-2-pyridonates on the metal center.

When utilizing the less sterically demanding terminal alkene substrate, 1-octene, complex **2.12** shows markedly reduced reactivity when compared to **2.13**. We proposed that the overall steric congestion at the metal center in **2.13** (effected by the replacement of the chloro ligand with an amido ligand) is required for effective catalytic turnover when employing sterically less demanding terminal alkenes. Unlike the simple picture employed in Figure 2.2, we suggest the equilibrium between off-cycle and on-cycle tantalum species lies heavily towards the off-cycle species. This has the effect of lowering the reaction rate as the concentration of on-cycle species is low at any time during the reaction. Additionally, these off-cycle species are involved in multiple equilibria with rapid exchange of all amines present in solution. The increased congestion at the metal center in **2.13**, as well as in 6-substituted-2-pyridone complexes **2.18** and **2.19**, encourages product amine to be released from the metal center, resulting in a higher concentration of substrate amine bound as an amido ligand. We posit that this higher concentration of active species results in the observed increase in reactivity.

Intriguingly, the most sterically accessible pyridonate complexes **2.15** (3-methyl) and **2.17** (3,6-dihydro) provide high reactivity for both internal alkenes and 1-octene. In the context of the above rationalizations, the reactivity of **2.15** and **2.17** is unexpected. With internal alkenes, complex **2.12** and **2.15** provide similar reactivity (with modest improvements over **2.17**) with substrate dependent variations in reactivity. This suggests the 3-substitution of the 2-pyridonate ligand has limited effects with sterically demanding substrates. A major departure occurs with 1-octene substrate. Complex **2.17** exhibits higher reactivity than **2.15**, and both demonstrate comparable reactivity to **2.13**, despite lacking substituents that would impart increased steric crowding at the metal center. Both **2.15** and **2.17** offer improved conversion over that of complex **2.12**. Most likely, complex **2.15** and **2.17** alter the turnover limiting step(s) in a more complex way than is rationalized above.

#### **2.2.4 Investigations into Precatalyst Activation and Off-Cycle Equilibria**

Initial investigations focused on probing the amine exchange reaction during the precatalyst activation. To observe precatalyst activation, including amido ligand exchange and the C-H activation reactions, we heated a mixture of **2.15** with *N*-methylaniline at the catalytically relevant temperature of 110 °C (Scheme 2.19a). We expected to observe the formation of a complex with one or more anilido ligands and concomitant release of dimethylamine. This may have also resulted in the formation of *N*-phenyl tantalaziridine *in situ*. Interestingly, not only is there no evidence of tantalaziridine formation, there is no decomposition of **2.15**, no consumption of *N*-methylaniline, and no release of dimethylamine when observations are made at elevated temperatures in the NMR spectrometer with *in situ* monitoring. This shows that the sterically less demanding dimethylamido ligands (compared to *N*-methylanilido) are favoured as ligands for this tantalum complex.



Deuterium incorporation determined by  $^1\text{H NMR}$  spectroscopy and deuteration confirmed by  $^2\text{H NMR}$  spectroscopy.

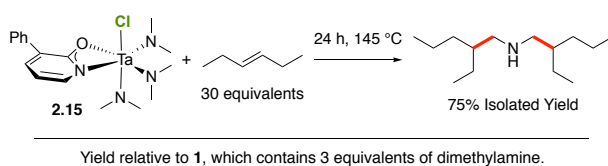
### Scheme 2.19 Deuterium Scrambling Experiment

Previous reports from our group demonstrated that tantalaziridine formation could be promoted by increased steric demand at the metal center, in one case by the addition of a second *N,O*-chelated, amidate ligand.<sup>172</sup> Further, Hultzsche *et al.* propose that C–H activation is facile and reversible in sterically encumbered BINOLate tantalum catalysts.<sup>174</sup> We were curious to see if we could observe facile C–H activation in our systems despite having significantly decreased steric bulk at the metal center.

A mixture of complex **2.15** with an excess of *d*-*N*-methylaniline was heated at  $110^\circ\text{C}$  for 2 hours (Scheme 2.19b). Here the deuterium of the amine group washes into the methyl groups of the pre-catalyst dimethylamido ligands and into the methyl group of the *N*-methylaniline substrate as observed by  $^2\text{H NMR}$  at 3.51 and 2.30 ppm respectively. Furthermore, a mixture of complex **2.15** with *N*-(methyl- $d_3$ )aniline heated to  $110^\circ\text{C}$  for 2 hours results in hydrogen being incorporated into the methyl group of the previously deuterated *N*-(methyl- $d_3$ )aniline (Scheme 2.19c). These results reveal that amido ligand exchange and C–H activation pathways are rapid

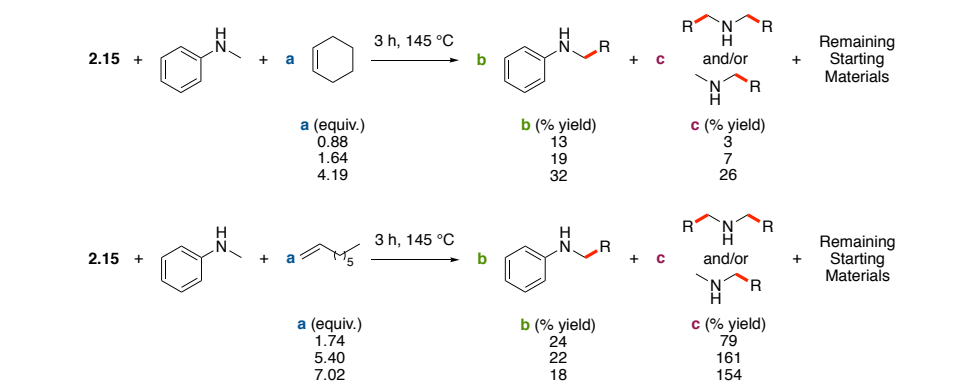
and reversible at catalytically relevant temperatures. Additionally, the experiments presented in Scheme 2.19 conclusively show that an equilibrium is present between **2.15** (precatalyst) and *N*-methylaniline, and this equilibrium strongly favors **2.15** (to the limit of detection of  $^1\text{H}$  NMR spectroscopy).

All the reactions in Scheme 2.19 have been carried out in the absence of alkene substrate. Previous work from our group has shown that the dimethylamido ligands of the precatalyst are not innocent during catalytic reactions, as they also undergo alkylation via hydroaminoalkylation.<sup>176,185</sup> Furthermore, complex **2.15** in the presence of excess 3-hexene and no exogenous amine results in high yields of dialkylated dimethylamine (Scheme 2.20).<sup>202</sup> Given the aforementioned facile and reversible amido ligand exchange and C-H activation reactions with **2.15**, we questioned how dimethyl amido ligands/free dimethyl amine may affect the desired catalytic alkylation of *N*-methylaniline. To this end, we set up a series of stoichiometric reactions with complex **2.15**, *N*-methylaniline and increasing amounts of either cyclohexene or 1-octene (Scheme 2.21). These experiments were then heated to 145 °C (cyclohexene) or 110 °C (1-octene) for 3 hours.



**Scheme 2.20 Isolation of dialkylated byproduct**





Equivalents for **a** values, and yields for **b** and **c** values (reported relative to initial amount of N-methylaniline) are calculated by  $^1\text{H}$  NMR spectroscopy with 1,3,5-trimethoxybenzene as an internal standard. A convoluted alkyl region of  $^1\text{H}$  NMR spectra prevents direct identification of the dimethylamine functionalized byproducts; they are calculated as such: functionalized byproducts = (alkene remaining) – (aniline product).

**Scheme 2.21 Stoichiometric experiments with variable equivalents of alkene to determine relative amounts of product and byproduct formation.**

Generally, we observe, a mixture of both products, suggesting the rate of functionalization of *N*-methylaniline and dimethylamine are comparable, and are in competition with each other for activation in the catalytic cycle. Furthermore, substrate dependent equilibria appear to dominate, as reactions with 1-octene yield significantly more alkylated dimethylamine byproducts than reactions with cyclohexene substrates. We also observe that as alkene equivalents increase, the amount of byproduct formation increases relative to the amounts of product. These experiments show that complex equilibria are at play in these catalytic reactions and amido ligand exchange allows for significant amounts of both product and byproduct formation at initial stages of the HAA reaction.

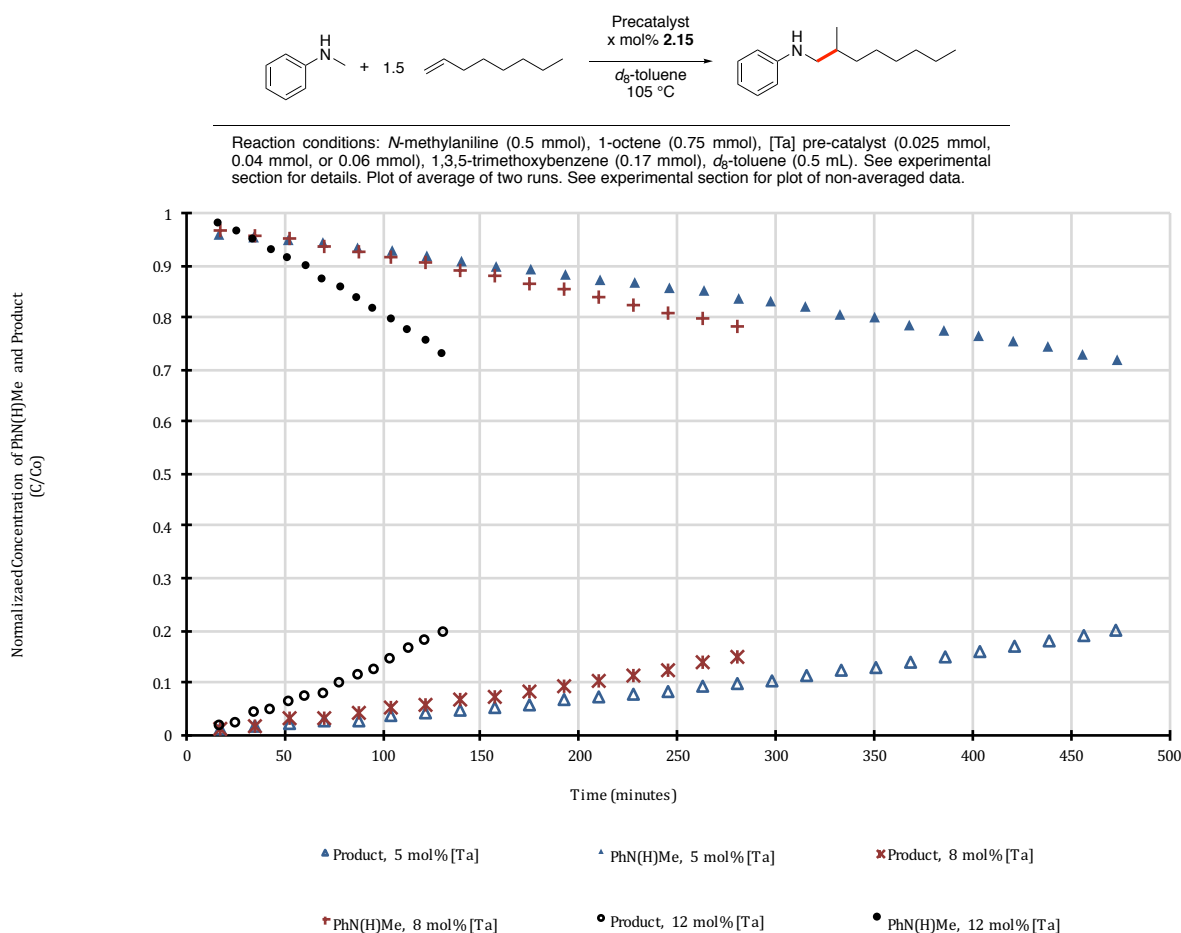


**Figure 2.5 Hydroaminoalkylation Reaction Monitoring with 5, 8, and 12 mol % of [Ta] Precatalyst 2.15**

Further evidence of such equilibria is presented in Figure 2.5. The catalytic reaction of *N*-methylaniline and 1-octene with **2.15** can be monitored by  $^1\text{H}$  NMR spectroscopy at 105 °C. Multiple attempts to monitor the reaction at 145 °C using the internal olefin cyclohexene, were unsuccessful. This included attempts to alter the reaction conditions by scale or by vessel for the purpose of real-time sampling, but resulted in inconsistent and poor yields (ca. <10%). Attempts to use *d*<sub>10</sub>-orthoxylenes and monitor the reaction at 140 °C by  $^1\text{H}$  NMR spectroscopy resulted in poor yields (ca. <10%) for similar reaction times. We believe these results are due to unquantified pressure effects. Product formation could be observed by the appearance of the diagnostic *ortho*-H proton signal at 6.41 ppm, with the concomitant consumption of starting *N*-methylaniline, as observed by the disappearance of the peak at 6.33 ppm. Due to the long reaction times, the reaction monitoring was limited to the first approximately 20% conversion with 5, 8, and 12 mol% pre-catalyst **2.15** (Figure 2.5).

Notably, this system displays an increasing rate with time, resulting in curved profiles observed for both product formation and starting material consumption. The observed profile is present in reactions with 5, 8, and 12 mol% pre-catalyst loading suggesting that increased catalyst loading does not alter this behaviour. This profile is consistent with an extended induction period. Induction periods are associated with the activation of precatalyst and are ideally short-lived. In this system, there is a period of increasing rate that continues to evolve up to 20% conversion. Unfortunately, these changing rates prevent quantitative kinetic assessments. However, the assembly of the data presented in Schemes 7 through 10 lead us to propose that the observed extended induction period is the result of extensive off-cycle equilibria between various tantalum amido species (Figure 2.6). The equilibrium studies between complex **2.15** and *N*-methylaniline define that the equilibrium lies heavily toward a combination of amido ligands that

minimizes steric crowding of the metal center. The slowly increasing rates are consistent with the alkylation of dimethylamido ligands, resulting in the formation of more sterically demanding amine by-products. These sterically demanding products in turn favor the formation of less sterically demanding *N*-methylanilido tantalum species. Thus, there is an observable increase in the rate of HAA of *N*-methylaniline. The equilibria between numerous and variable resting state species limits the formation of catalytically active tantalaziridine. We propose that these complicated and evolving equilibria result in the low observed turnover frequency of catalysis.

Finally, other reports of HAA have observed reversible  $sp^2$  hybridized C-H bond activation using deuterium labelling experiments.<sup>170,174,185</sup> This is proposed to proceed via the formation of a cyclometalated intermediate shown in Scheme 2.22. To determine if  $sp^2$

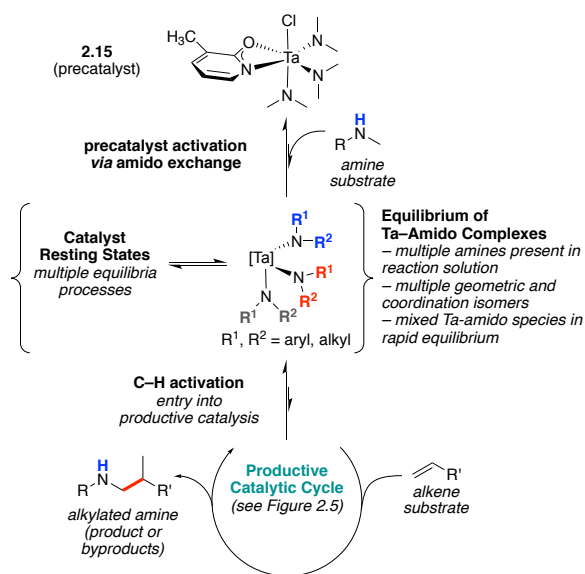
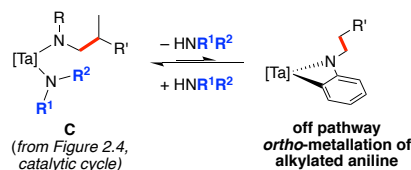


**Figure 2.6** Graphical representation of resting state equilibria

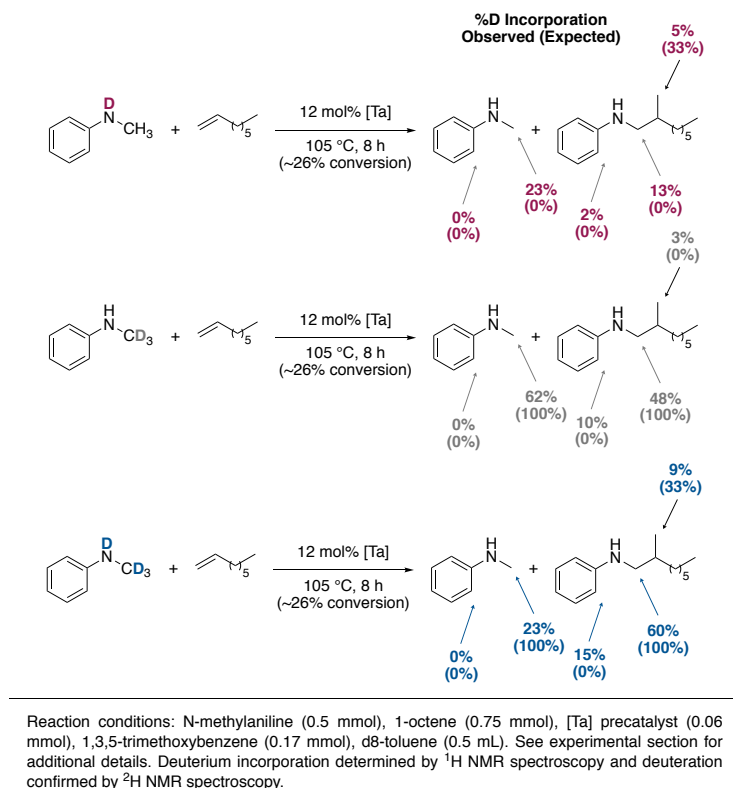


**Scheme 2.22** Ortho-deuteration off-pathway equilibrium

hybridized C-H activation is occurring with precatalyst **2.15**, we have also monitored the reaction with variably deuterated aniline substrates using 12 mol% precatalyst at 105 °C by  $^1\text{H}$  NMR spectroscopy until ~26% conversion of starting *N*-methylaniline (see experimental section for plot of results).

After monitoring, one reaction of each type was quenched and subjected to column chromatography. Both the starting *N*-methylaniline and the alkylation aniline product were isolated. Deuterium incorporation was confirmed by  $^2\text{D}$  NMR spectroscopy and quantified with  $^1\text{H}$  NMR spectroscopy. The results of deuterium quantification are summarized in Scheme 2.23.

The results of this experiment are also consistent with many off-cycle equilibria, as there are significant deviations in deuterium incorporation from the expected results based upon the mechanistic proposal presented in Figure 2.2. The observation of deuterium in the *ortho*-position of the phenyl ring of the final product confirms that both  $\text{sp}^3$  and  $\text{sp}^2$  C-H bond activation is occurring, however, productive catalysis only proceeds via the tantalaziridine reactive intermediate.



**Scheme 2.23 Analysis of Deuterium Incorporation into Product and Byproduct Aniline after Partial Catalytic Conversion with Variably Deuterated Aniline Substrates**

Our analysis of starting *N*-methylaniline represents the first report of analysis of this starting material after being subjected to catalytic HAA conditions. Interestingly, the unreacted starting *N*-methylaniline does not reversibly incorporate deuterium in the *ortho* position. This demonstrates that  $\text{sp}^3$  hybridized C–H (or C–D) activation is more favorable than  $\text{sp}^2$  C–H activation. However, once the methyl group of the starting material is converted to the methylene group in the product, subsequent  $\text{sp}^3$  hybridized C–H (or C–D) activation is hindered, allowing for C–H activation of the *ortho*-position to become energetically relevant. The observation that methyl  $\text{C}(\text{sp}^3)\text{--H}$  activation is favoured over methylene  $\text{C}(\text{sp}^3)\text{--H}$  activation is consistent with previous examples in the literature. Multiple examples of HAA from our group

and others have observed decreased catalytic activity with non *N*-methyl substrates. Substrates of this type remain a challenge and have been rarely reported.<sup>171-172,179,203</sup> Also of note, Hultzsch *et al.*, report scrambling of PhN(H)CD<sub>2</sub>CD<sub>3</sub> when heating alone with 2 mol% of a binolate tantalum catalyst.<sup>174</sup> In their report they observe significant deuterium incorporation into the *ortho*-position of the aryl ring, and loss of deuterium from the methylene ( $\alpha$  to the amine) position, consistent with our results presented here.

### 2.3 Conclusions

In summary, we have developed the first precatalyst, **2.12**, that is able to perform the hydroaminoalkylation reaction with broad substrate scope for internal alkenes. Additionally, **2.12** is the only precatalyst able to catalyze the hydroaminoalkylation reaction with sterically demanding *E*- and *Z*- internal alkenes to result in the  $\beta$ -branched products, avoiding the chain-walking that can occur with late-transition-metal catalysts. We have demonstrated that new substrate compatibilities have been made available through the combination of a 2-pyridonate-chloro ligated tantalum complex. We postulate that this combination of a planar 2-pyridonate and chloro ligand significantly reduced that steric congestion at the metal center allowing for improved reactivity with sterically demanding internal alkene substrates.

Complexes **2.15** and **2.17** are the first examples of hydroaminoalkylation catalysts that offer promising reactivity with both internal and terminal alkene substrates. Efforts to understand how ligand substitution affects catalyst activity resulted in the identification of complicating off-cycle equilibria that include (1) readily reversible trans-amination and C–H activation reactions in precatalyst activation, (2) unwanted byproduct formation resulting from alkylation of the dimethylamido ligands of the precatalyst, (3) complex mixtures of catalyst resting states resulting from the generation of multiple Ta amido complexes in situ, and (4) the observation

that C–H activation can occur at both  $sp^3$ - and  $sp^2$ -hybridized C–H bonds. Considered together, these factors play a significant role in limiting the generation of on-cycle tantalum species, thereby severely limiting catalytic turnover. Ongoing work is focused on new ligand environments that avoid the use of dimethylamido ligands to both increase the concentration of productive on-cycle tantalum species and increase the efficiency of catalytic hydroaminoalkylation.

## **2.4 Experimental Details**

### **2.4.1 General Considerations**

All air and moisture sensitive reactions were performed using standard inert atmosphere techniques using a Schlenk double manifold with  $N_2$  gas and high vacuum ( $10^{-2}$  mbar), or using a Mbraun LABmaster glovebox filled with a  $N_2$  atmosphere. All pieces of glassware were dried for at least 4 hours in a 160 °C oven, or dried over a propane flame before being used on the Schlenk manifold or being transferred into the glovebox. Toluene and hexanes were dried by passing through columns of activated alumina under  $N_2$  gas, collected into a Teflon sealed Strauss flask (or other appropriate Teflon sealed bomb type Schenk flask), and sparged with  $N_2$  gas for at least 30 minutes to remove dissolved  $O_2$  gas. Diethyl ether was dried over Na/benzophenone under  $N_2$  and distilled, once a deep purple colour was maintained, into a Teflon sealed Strauss flask. J. Young NMR tubes used for catalytic experiments had Teflon screw-type caps and were 8" x 5 mm tubes. Thin layer chromatography (TLC) was performed on EMD silica get 60 F254 plates. Visualization was achieved under a 254 nm UV light source and/or by staining with iodine or  $KMnO_4$  solution. Flash chromatography was performed using Silicycle SiliaFlash F60 silica gel (230-400 mesh), glass columns, and ACS grade solvents.



### 2.4.2 Instrumentation

$^1\text{H}$ ,  $^{13}\text{C}$ ,  $^{19}\text{F}$ , and  $^{31}\text{P}$  NMR spectra were recorded on a Bruker 300 MHz, 400 MHz, or 600 MHz Avance spectrometer at ambient temperature. Chemical shifts are given relative to the corresponding residual protio solvent for  $^1\text{H}$  spectra and to the carbon signal of the solvent for  $^{13}\text{C}$  spectra. Chemical shifts for  $^{19}\text{F}$  are externally referenced to neat  $\text{CFCl}_3$ . Chemical shifts for  $^{31}\text{P}$  are externally references to 85%  $\text{H}_3\text{PO}_4$ . Chemical shifts,  $\delta$ , are reported in parts per million (ppm) and coupling constants  $J$  are given in Hertz (Hz). The following abbreviations are used to indicate signal multiplicity: s = singlet, d = doublet, t = triplet, q = quartet, m = multiplet, and br = broad. For quantitative experiments,  $T_1$  relaxation times for peaks of interest were estimated utilizing a spin-echo pulse sequence, and relaxation delays were appropriately extended when collecting  $^1\text{H}$  NMR spectra. Mass spectra (MS) and elemental analyses (EA) were measured by the mass spectrometry and microanalysis service at the Department of Chemistry, University of British Columbia. Mass spectra were recorded on a Kratos MS-50 spectrometer using an electron impact (70 eV) source. Fragment signals are given in mass per charge number ( $m/z$ ). GCMS analyses. Elemental analyses were performed using a Thermo Flash 2000 Elemental Analyzer. The content of the specified element is expressed in percent (%). UHPLC analysis was conducted on an Agilent 1290 Series UHPLC with a multi wavelength UV detector and 6150 Series Quadrupole ESI/MS, using an Agilent Poroshell 120 column (SB-C18, 2.7  $\mu\text{m}$ , 2.1 x 50 mm) with a water:acetonitrile (0.1% TFA in acetonitrile) solvent system (gradient 80:20 to 0:100).

### 2.4.3 Materials

All chemicals were purchased from commercial sources and used as received unless otherwise specified. Chemicals from commercial sources that were not dried and shipped under inert

atmosphere, were appropriately dried and degassed of O<sub>2</sub> before being transferred to the glovebox or for use on the Schlenk manifold. All amines and alkenes were dried under N<sub>2</sub> atmosphere with CaH<sub>2</sub>, distilled, and degassed by the freeze-pump-thaw method. 2-pyridones were sublimed under vacuum on a Schlenk manifold at 80 – 100 °C with water cooling, before being transferred into the glovebox. Compounds **2.1**,<sup>19</sup> **2.2**,<sup>204</sup> **2.6**,<sup>172</sup> **2.11**,<sup>175</sup> **2.12**,<sup>24</sup> **2.13**,<sup>24</sup> [Ta(NMe<sub>2</sub>)<sub>3</sub>Cl<sub>2</sub>]<sub>2</sub>,<sup>205</sup> [Ta(NEt<sub>2</sub>)<sub>2</sub>Cl<sub>3</sub>]<sub>2</sub>,<sup>206</sup> TaMe<sub>3</sub>Cl<sub>2</sub>,<sup>207</sup> 3-phenyl-2-pyridone,<sup>19</sup> 3-mesityl-2-pyridone,<sup>19</sup> 6-phenyl-2-pyridone,<sup>208</sup> and *N*-(methyl-*d*<sub>3</sub>)aniline<sup>209</sup> were synthesized according to literature procedures. Final isolation of amines presented in Scheme 2.12 and Scheme 2.13, as discussed in the preface, were performed by Dr. Eugene Chong. Data and NMR spectra of these compounds can be obtained within these references.<sup>24,202</sup>

#### 2.4.4 Synthesis and Characterization of Compounds

**Synthesis of sodium-pyridonates.** In a glovebox, equimolar amounts of 2-pyridone (*ca.* 2.00 mmol) and NaHMDS (*ca.* 2.00 mmol) were slurried with ~ 6 mL toluene in a 20 mL scintillation vial, and stirred at ambient temperature for 12 hours. The volatiles were removed *in vacuo* to reveal a sticky white salt. ~2 mL of hexanes was added to form a slurry, and the volatiles were removed *in vacuo*. This was repeating one to two additional times and the resulting white to off-white powder was thoroughly *in vacuo*. These products were used without further purification or characterization.

**General procedure for the synthesis of complexes 2.14 – 2.19.** In a glovebox, a white suspension of the sodium pyridonate salt in toluene (~ 3 mL) was added to a stirring suspension of yellow [Ta(NMe<sub>2</sub>)<sub>3</sub>Cl<sub>2</sub>]<sub>2</sub> in toluene (~ 3 mL) at ambient temperature. The resulting suspension was stirred for 12 hours at ambient temperature, and then filtered through a plug a celite. The resulting clear yellow solution was concentrated *in vacuo*. The resulting sticky, pale yellow solid

was dissolved in minimal warm toluene (~ 1.5 mL), and cooled first to ambient temperature, and then cooled for 10 minutes at -35 °C. This dark yellow solution was then layered with hexanes (~ 3 mL) and stored in the freezer at -35 °C to promote crystallization. Products generally recrystallized within 24 hours. After thoroughly drying the crushed, recrystallized product *in vacuo*, samples were used for characterization.

**Chlorotris(dimethylamido)( $\kappa^2$ -*N,O*-3-(2,4,6-trimethylphenyl)-2-pyridonato)tantalum(V)**

**(2.14).** Using the general procedure described above, sodium 3-(2,4,6-trimethylphenyl)-2-pyridonate salt (0.045 g, 0.19 mmol) was added to [Ta(NMe<sub>2</sub>)<sub>3</sub>Cl<sub>2</sub>]<sub>2</sub> (0.074 g, 0.01 mmol). A single recrystallization resulted in 0.090 g (84% yield) of yellow crystals.

<sup>1</sup>H-NMR and <sup>13</sup>C-NMR spectra reveal fluxional behavior for the 2,6-dimethyl groups of the 2,4,6-trimethylphenyl group as exhibited by additional resonances in both spectrum (one sharp and one broad). The 4-methyl group of the same aryl ring also exhibits this behavior but results in a single broad resonance.

**<sup>1</sup>H-NMR** (400 MHz, C<sub>6</sub>D<sub>6</sub>):  $\delta$  7.71 (dd,  $J$  = 5.4, 1.9 Hz, 1H), 7.11 (dd,  $J$  = 7.3, 1.9 Hz, 1H), 6.82 (br. s, 2H), 6.38 (dd,  $J$  = 7.3, 5.4 Hz, 1H), 3.50 (br. s, 18H), 2.37 (br. s, 3H), 2.14/2.11 (s/br. s., 6H). **<sup>13</sup>C{<sup>1</sup>H}-NMR** (101 MHz, C<sub>6</sub>D<sub>6</sub>):  $\delta$  168.1, 141.4, 140.4, 138.2 (br. s), 137.2, 135.8 (br. s), 132.6, 129.0, 125.6, 113.0, 46.8, 21.2, 21.0 (br. s), 20.8 (br. s). **MS** (EI):  $m/z$  560 [M<sup>+</sup>], 516 [M<sup>+</sup> - NMe<sub>2</sub>]. **EA**: Calc'd for C<sub>20</sub>H<sub>32</sub>ClN<sub>4</sub>OTa: C 42.83, H 5.75, N 9.99; Found: C 43.12, H 5.80, N 9.80.

**Chlorotris(dimethylamido)( $\kappa^2$ -*N,O*-3-methyl-2-pyridonato)tantalum(V) (2.15).** Using the general procedure described above, sodium 3-methyl-2-pyridonate salt (0.026 g, 0.20 mmol) was added to [Ta(NMe<sub>2</sub>)<sub>3</sub>Cl<sub>2</sub>]<sub>2</sub> (0.076 g, 0.10 mmol). A single recrystallization resulted in 0.073 g (80% yield) of yellow crystals.

**<sup>1</sup>H-NMR** (400 MHz, C<sub>6</sub>D<sub>6</sub>): δ 7.60-7.58 (m, 1H), 6.94-6.91 (m, 1H), 6.23 (dd, *J* = 7.2, 5.5 Hz, 1H), 3.55 (br. s, 18H), 2.02 (s, 3H). **<sup>13</sup>C{<sup>1</sup>H}-NMR** (101 MHz, C<sub>6</sub>D<sub>6</sub>): δ 169.5, 140.0, 138.7, 122.1, 112.8, 46.7, 14.6. **MS** (EI): *m/z* 456 [*M*<sup>+</sup>], 412 [*M*<sup>+</sup>–NMe<sub>2</sub>] **EA**: Calc'd for C<sub>12</sub>H<sub>24</sub>ClN<sub>4</sub>OTa: C 31.56, H 5.30, N 12.27; Found: C 31.64, H 5.58, N 12.24.

**Chlorotris(dimethylamido)(κ<sup>2</sup>-*N,O*-3-trifluoromethyl-2-pyridonato)tantalum(V) (2.16).**

Using the general procedure described above, sodium 3-trifluoromethyl-2-pyridonate salt (0.037 g, 0.19 mmol) was added to [Ta(NMe<sub>2</sub>)<sub>3</sub>Cl<sub>2</sub>]<sub>2</sub> (0.076 g, 0.10 mmol). A single recrystallization resulted in 0.078 g (76% yield) of yellow crystals.

**<sup>1</sup>H-NMR** (600 MHz, C<sub>6</sub>D<sub>6</sub>): δ 7.55-7.53 (m, 1H), 7.30-7.29 (m, 1H), 5.94-5.92 (m, 1H), 3.45 (br. s, 18H). **<sup>13</sup>C{<sup>1</sup>H}-NMR** (151 MHz, C<sub>6</sub>D<sub>6</sub>): δ 145.1, 133.0 (q, <sup>2</sup>*J*<sub>CF</sub> = 4.5 Hz), 128.4, 111.5, 46.7. Could not locate CF<sub>3</sub> or C(O)N carbons. **<sup>19</sup>F-NMR** (282 MHz, C<sub>6</sub>D<sub>6</sub>): δ -62.93. **MS** (EI): *m/z* 510 [*M*<sup>+</sup>], 466 [*M*<sup>+</sup>–NMe<sub>2</sub>] **EA**: Calc'd for C<sub>12</sub>H<sub>21</sub>N<sub>4</sub>ClF<sub>3</sub>OTa: C 28.22, H 4.14, N 10.97; Found: C 27.98, H 4.06, N 10.44.

**Chlorotris(dimethylamido)(κ<sup>2</sup>-*N,O*-2-pyridonato)tantalum(V) (2.17).** Using the general procedure described above, sodium 2-pyridonate salt (0.025 g, 0.21 mmol) was added to [Ta(NMe<sub>2</sub>)<sub>3</sub>Cl<sub>2</sub>]<sub>2</sub> (0.082 g, 0.11 mmol). A single recrystallization resulted in 0.080 g (84% yield) of yellow crystals.

**<sup>1</sup>H-NMR** (400 MHz, C<sub>6</sub>D<sub>6</sub>): δ 7.63 (ddd, *J* = 5.5, 1.8, 0.9 Hz, 1H), 6.96 (ddd, *J* = 8.6, 7.1, 1.8 Hz, 1H), 6.32 (ddd, *J* = 8.6, 0.9, 0.9 Hz, 1H), 6.18 (ddd, *J* = 7.1, 5.5, 0.9 Hz, 1H), 3.54 (br. s, 18H). **<sup>13</sup>C{<sup>1</sup>H}-NMR** (101 MHz, C<sub>6</sub>D<sub>6</sub>): δ 170.5, 141.4, 140.7, 112.7, 112.6, 46.6.

**MS** (EI): *m/z* 442 [*M*<sup>+</sup>], 398 [*M*<sup>+</sup>–NMe<sub>2</sub>] **EA**: Calc'd for C<sub>11</sub>H<sub>22</sub>ClN<sub>4</sub>OTa: C 29.84, H 5.01, N 12.66; Found: C 29.72, H 5.03, N 12.25.

**Chlorotris(dimethylamido)( $\kappa^2$ -*N,O*-6-phenyl-2-pyridonato)tantalum(V) (2.18).** Using the general procedure described above, sodium 6-phenyl-2-pyridonate salt (0.035 g, 0.18 mmol) was added to [Ta(NMe<sub>2</sub>)<sub>3</sub>Cl<sub>2</sub>]<sub>2</sub> (0.070 g, 0.09 mmol). A single recrystallization resulted in 0.062 g (66% yield) of yellow crystals.

**<sup>1</sup>H-NMR** (300 MHz, C<sub>6</sub>D<sub>6</sub>):  $\delta$  7.89-7.85 (m, 2H), 7.24-7.18 (m, 2H), 7.13 (d,  $J$  = 2.4 Hz, 1H), 7.03 (dd,  $J$  = 8.5, 7.4 Hz, 1H), 6.50 (dd,  $J$  = 7.4, 0.8 Hz, 1H), 6.34 (dd,  $J$  = 8.5, 0.8 Hz, 1H), 3.51 (br. s, 18H). **<sup>13</sup>C{<sup>1</sup>H}-NMR** (75 MHz, C<sub>6</sub>D<sub>6</sub>):  $\delta$  170.8, 153.5, 140.9, 139.4, 128.9, 128.6, 128.5, 111.5, 111.4, 48.29. **MS** (EI):  $m/z$  474 [M<sup>+</sup>-NMe<sub>2</sub>] Satisfactory elemental analysis could not be obtained for this product. **EA**: Calc'd for C<sub>17</sub>H<sub>26</sub>ClN<sub>4</sub>OTa: C 39.36, H 5.05, N 10.80; Found: C 38.70, H 5.23, N 10.35.

**Chlorotris(dimethylamido)( $\kappa^2$ -*N,O*-6-methyl-2-pyridonato)tantalum(V) (2.19).** Using the general procedure described above, sodium 6-methyl-2-pyridonate salt (0.025 g, 0.19 mmol) was added to [Ta(NMe<sub>2</sub>)<sub>3</sub>Cl<sub>2</sub>]<sub>2</sub> (0.073 g, 0.09 mmol). A single recrystallization resulted in 0.066 g (76% yield) of yellow crystals.

**<sup>1</sup>H-NMR** (400 MHz, C<sub>6</sub>D<sub>6</sub>):  $\delta$  6.95 (dd,  $J$  = 8.5, 7.3 Hz, 1H), 6.20 (m, 1H), 6.08 (m, 1H), 3.60 (br. s, 18H), 2.10 (s, 3H). **<sup>13</sup>C{<sup>1</sup>H}-NMR** (101 MHz, C<sub>6</sub>D<sub>6</sub>):  $\delta$  170.9, 151.9, 141.1, 111.9, 109.7, 47.3, 21.8. **MS** (EI):  $m/z$  412 [M<sup>+</sup>-NMe<sub>2</sub>] **EA**: Calc'd for C<sub>12</sub>H<sub>24</sub>ClN<sub>4</sub>OTa: C 31.56, H 5.30, N 12.27; Found: C 31.91, H 5.37, N 12.47.

**Tris(dimethylamido)triflato( $\kappa^2$ -*N,O*-3-phenyl-2-pyridonato)tantalum(V) (2.20).** In a glovebox, a 10 mL Schlenk tube was charged with **1** (0.071 g, 0.14 mmol) and AgOTf (0.035 g, 0.14 mmol). The flask was moved to the Schlenk line, charged with 3 mL dichloromethane to create a cloudy yellow solution, and stirred at ambient temperature for 12 h. Volatiles were removed *in vacuo* and the flask returned to the glovebox. The yellow white solid was extracted

with 10 mL toluene and filtered through a celite plug. The resulting clear yellow solution was concentrated *in vacuo*. The resulting sticky, pale yellow solid was dissolved in minimal warm toluene (~ 1.5 mL), and cooled first to ambient temperature, and then cooled for 10 minutes at -35 °C. This dark yellow solution was then layered with hexanes (~ 3 mL) and stored in the freezer at -35 °C to promote recrystallization. Products generally recrystallized within 24 hours. After thoroughly drying the crushed, recrystallized product *in vacuo*, samples were used for characterization. A single recrystallization resulted in 0.053 g (61% yield) of yellow crystals.

**<sup>1</sup>H-NMR** (300 MHz; C<sub>6</sub>D<sub>6</sub>): δ 7.86-7.82 (m, 2H), 7.64 (dd, *J* = 5.5, 1.8 Hz, 1H), 7.37 (dd, *J* = 7.5, 1.8 Hz, 1H), 7.25-7.20 (m, 2H), 7.11-7.06 (m, 1H), 6.37 (dd, *J* = 7.5, 5.5 Hz, 1H), 3.43 (br. s, 18H). **<sup>13</sup>C{<sup>1</sup>H}-NMR** (101 MHz; C<sub>6</sub>D<sub>6</sub>): δ 169.0, 140.9, 140.8, 135.3, 128.9, 128.8, 128.1, 125.4, 122.2, 119.1, 114.5, 46.3. **<sup>19</sup>F-NMR** (282 MHz; C<sub>6</sub>D<sub>6</sub>): δ -78.2 **MS** (EI): *m/z* 632 [M<sup>+</sup>], 588 [M<sup>+</sup>-NMe<sub>2</sub>], 483 [M<sup>+</sup>-OTf] **EA**: Calc'd for C<sub>18</sub>H<sub>26</sub>F<sub>3</sub>N<sub>3</sub>O<sub>4</sub>STa: C 34.19, H 4.14, N 8.86; Found: C 33.88, H 4.05, N 8.50.

***N*-deutero aniline derivatives.** The requirement of dry substrates for these catalytic reactions does not allow for standard preparation of *N*-deutero substrates by exchange (with MeOD or DCl/D<sub>2</sub>O), as drying with CaH<sub>2</sub> would be required. To avoid possible loss of deuteration during drying, this procedure was developed to maintain dry substrate for catalysis.

***N*-d-*N*-methylaniline.** All manipulations were conducted in a glovebox or on a Schlenk manifold under N<sub>2</sub> with proper Schlenk technique. In a glovebox, a 50 mL pear-shaped Schlenk flask was charged with dried and degassed *N*-methylaniline (2.290 g, 27.2 mmol), 15 mL diethyl ether, and a stir bar. The mixture was stirred to ensure a homogenous mixture. The flask was attached to the Schlenk line and cooled to 0 °C. With stirring, 17.2 mL of nBuLi solution (27.5 mmol, 1.6 M in hexanes) was added dropwise *via* syringe and stainless steel needle. The reaction

was allowed to slowly warm to ambient temperature and stirred for 2 h. Separately, a small Schlenk flask was charged with D<sub>2</sub>O, and sparged with N<sub>2</sub> for 30 min. After the 2 h stir period, 0.97 equivalents of D<sub>2</sub>O (0.529 g, 0.48 mL, 26.4 mmol), was added dropwise *via* syringe and stainless steel needle. The reaction was allowed to stir for 2 h. After the 2 h stir period, a short-path distillation apparatus with a Teflon sealed Schlenk flask connected for collection of the product, was attached to the reaction flask. Vacuum was applied slowly, through the distillation apparatus, and the hexanes and diethyl ether were allowed to evaporate. Once complete, the product was distilled under dynamic vacuum (30 °C, 10<sup>-2</sup> mbar), the receiving flask placed under N<sub>2</sub> gas, sealed, transferred into the glovebox, and the product transferred to a 20 mL scintillation vial. <sup>1</sup>H NMR spectrum revealed trace amounts of hexanes and diethyl ether, which can be removed *in vacuo* with stirring, inside the glovebox, to yield 1.733 g (59% yield) of the product. <sup>1</sup>H NMR spectroscopy reveals >98% deuteration with no evidence for *N*-H protons. <sup>2</sup>D NMR spectroscopy confirms *N-deutero* incorporation.

**<sup>1</sup>H-NMR** (400 MHz; C<sub>6</sub>D<sub>6</sub>): δ 7.21-7.16 (m, 2H), 6.78-6.74 (m, 1H), 6.42-6.39 (m, 2H), 2.30 (s, 3H). **<sup>2</sup>H-NMR** (61 MHz; C<sub>6</sub>H<sub>6</sub>): δ 2.84 (s, 1D)

***N-d-N-(methyl-d<sub>3</sub>)aniline***. All manipulations were conducted in a glovebox or on a Schlenk manifold under N<sub>2</sub> with proper Schlenk technique. In a glovebox, a 50 mL pear-shaped Schlenk flask was charged with dried and degassed *N*-(methyl-d<sub>3</sub>)aniline (2.337 g, 21.2 mmol), 15 mL diethyl ether, and a stir bar. The mixture was stirred to ensure homogeneity. The flask was attached to the Schlenk line and cooled to 0 °C. With stirring, 13.5 mL of <sup>n</sup>BuLi solution (21.6 mmol, 1.6 M in hexanes) was added dropwise *via* syringe and stainless steel needle. The reaction was allowed to slowly warm to ambient temperature and stirred for 2 h. Separately, a small Schlenk flask was charged with ~ 1-2 mL of D<sub>2</sub>O, and sparged with N<sub>2</sub> for 30 min. After the 2 h

stir period, 0.98 equivalents of D<sub>2</sub>O (0.416 g, 0.37 mL, 20.8 mmol), was added dropwise *via* syringe and stainless steel needle. The reaction was allowed to stir for 2 h. After the 2 h stir period, a short-path distillation apparatus with a Teflon sealed Schlenk flask connected for collection of the product, was attached to the reaction flask. Vacuum was applied slowly, through the distillation apparatus, and the hexanes and diethyl ether were allowed to evaporate. Once complete, the product was distilled under dynamic vacuum (30 °C, 10<sup>-2</sup> mbar), the receiving flask placed under N<sub>2</sub> gas, sealed, transferred into the glovebox, and the product transferred to a 20 mL scintillation vial. <sup>1</sup>H NMR spectrum revealed trace amounts of hexanes and diethyl ether, which were removed *in vacuo* with stirring, inside the glovebox, to yield 2.012 g (87% yield) of the product. <sup>1</sup>H NMR spectroscopy indicates >98% deuteration with no evidence for N-H protons. <sup>2</sup>D NMR spectroscopy confirms *N-deutero* incorporation.

**<sup>1</sup>H-NMR** (400 MHz; *d*<sub>8</sub>-Tol): δ 7.14-7.09 (m, 2H), 6.71-6.67 (m, 1H), 6.35-6.32 (m, 2H) **<sup>2</sup>H-NMR** (61 MHz; Tol): δ 2.81 (s, 1D), 2.33 (s, 3D)

#### 2.4.5 Reaction and Experimental Details:

**Catalytic Screening Reactions (Scheme 2.16 and Scheme 2.17):** In a glovebox, the pre-catalyst (0.025 mmol) was dissolved in *d*<sub>8</sub>-toluene (500 μL, 0.477 mg) in a 5 mL scintillation vial. *N*-methylaniline (0.50 mmol) and alkene (0.75 mmol) were weighed into a separate 5 mL scintillation vial. Using a glass disposable pipette, the solution of pre-catalyst was transferred between the two vials multiple times to ensure a complete dissolution and creation of a homogeneous mixture. The resulting solution was transferred to a J. Young NMR tube and the tube closed with a screw-type Teflon cap. The <sup>1</sup>H NMR spectrum was recorded, and the J. Young NMR tube was placed in a preheated oil bath at the specified temperature for the specified time. After the specified time, the tube was removed, allowed to cool to ambient



temperature, and a  $^1\text{H}$  NMR spectrum was recorded. Conversion was determined from this spectrum by integration of the *ortho*-proton signal of *N*-methylaniline centered at  $\delta$  6.33, and the appearance of product *ortho*-proton signals of product centered at  $\delta$  6.41.

**Substrate Scope Investigations (Scheme 2.18):** In a glovebox, the pre-catalyst (0.025 mmol) was dissolved in  $d_8$ -toluene (500  $\mu\text{L}$ , 477 mg) in a 5 mL scintillation vial.  $\text{Cp}_2\text{Fe}$  (0.05-0.10 mmol) was weighed into a separate 5 mL scintillation vial and the mass recorded (used to calculate yield after the reaction was completed). *N*-methylaniline (0.50 mmol) and alkene (0.75 mmol) were weighed into the same 5 mL scintillation vial as the  $\text{Cp}_2\text{Fe}$ . Using a glass disposable pipette, the solution of pre-catalyst was transferred between the two vials multiple times to ensure a complete dissolution and creation of a homogeneous mixture. The resulting solution was transferred to a J. Young NMR tube and the tube closed with a screw-type Teflon cap. The  $^1\text{H}$  NMR spectrum was recorded, and the J. Young NMR tube was placed in a preheated oil bath at the specified temperature for the specified time. After the specified time, the tube was removed, allowed to cool to ambient temperature, and a  $^1\text{H}$  NMR spectrum was recorded. Yield was determined by  $^1\text{H}$  NMR spectroscopy by calculating the moles of *N*-methylaniline (*ortho*-protons at  $\delta$  6.33) in the  $t = 0$  h spectrum relative to the known moles of  $\text{Cp}_2\text{Fe}$  (singlet at  $\delta$  3.99) and by calculating the moles of product (*ortho*-protons at  $\delta$  6.41) at the end of the reaction relative to the known moles of  $\text{Cp}_2\text{Fe}$ .

**Deuterium Scrambling Experiments (Scheme 2.19):** In a glovebox, **2.15** (15.0 mg, 0.033 mmol), *N*-methylaniline (or isotopically labelled variant) (0.033 mmol), and 1,3,5-trimethoxybenzene (5.5 mg, 0.033 mmol) were dissolved in  $d_8$ -toluene (500  $\mu\text{L}$ , 477 mg) in a 5 mL scintillation vial. The homogeneous solution was transferred into a J. Young NMR tube and sealed with a Teflon screw-type cap. The  $^1\text{H}$  NMR spectrum was collected, and the tube placed in

a preheated 110 °C oil bath for 2 h. After the time, the tube was removed, cooled, and a  $^1\text{H}$  NMR spectrum was collected. Experiments c) and d) were repeated in the same manner but in toluene, so that  $^2\text{H}$  NMR spectra could be obtained. In a), no change was observed in the integration of **2.15** or *N*-methylaniline relative to the 1,3,5-trimethoxybenzene internal standard. In b), the experiment was set up as described but with 10 equivalents of *N*-methylaniline (35.2 mg, 0.328 mmol). Instead of being placed into a pre-heated oil bath, the tube was placed into an NMR spectrometer, heated to 105 °C and allowed to stabilize for 15 minutes once the probe temperature was stable. A  $^1\text{H}$  NMR spectrum was collected every 30 minutes for 2 h. As in a), no change was observed in the integration of **2.15** or *N*-methylaniline relative to the 1,3,5-trimethoxybenzene internal standard. In c) and d), deuterium incorporation was determined by  $^1\text{H}$  NMR spectroscopy.  $^2\text{H}$  NMR spectra confirm the presence of deuterium in the dimethylamido ligands of **4** (deuterium signal at  $\delta$  3.51), the presence of an aniline *N-d* (deuterium signal at  $\delta$  2.82), and the presence of deuterium incorporated at methyl position of the aniline (deuterium signal at  $\delta$  2.30).

**Stoichiometric Experiments with Variable Alkene Equivalents (Scheme 2.21):** In a glovebox, **2.15** (12.5 mg, 0.027 mmol), *N*-methylaniline (2.9 mg, 0.027 mmol), variable amounts of either cyclohexene or 1-octene (~1–7 equivalents), and 1,3,5-trimethoxybenzene (1.5 mg, 0.009 mmol) were dissolved in *d*<sub>8</sub>-toluene (500  $\mu\text{L}$ , 477 mg) in a 5 mL scintillation vial. The homogeneous solution was transferred into a J. Young NMR tube and sealed with a Teflon screw-type cap. The  $^1\text{H}$  NMR spectrum was collected, and the tube was placed in a preheated oil bath for 3 h (with cyclohexene at 145 °C; with 1-octene at 110 °C). After 3 h, the tube was removed and a  $^1\text{H}$  NMR spectrum was collected. Initial alkene equivalents (proton signal at  $\delta$  5.66 for cyclohexene and at  $\delta$  5.76 ppm for 1-octene) were calculated from the  $t = 0$  h spectrum

relative to the known amount of 1,3,5-trimethoxybenzene internal standard (proton signal at  $\delta$  6.14). Product (*ortho*-protons signal at  $\delta$  6.14) and remaining alkene were calculated from the  $t = 3$  h spectrum relative to the known amount of 1,3,5-trimethoxybenzene. A convoluted alkyl region of  $^1\text{H}$  NMR spectra prevents direct identification of the dimethylamine functionalized byproducts; they are calculated as such: functionalized byproducts = (alkene remaining) – (aniline product).

**Reaction Monitoring (Scheme 10 and 12):** In a glovebox, pre-catalyst **2.15** (5 mol%: 11.4 mg, 0.025 mmol; 8 mol%: 18.3 mg, 0.040 mmol; 12 mol%: 27.4 mg, 0.060 mmol) was dissolved in  $d_8$ -toluene (500  $\mu\text{L}$ , 477 mg) in a 5 mL scintillation vial. 1,3,5-trimethoxybenzene (28.0 mg, 0.167 mmol) was weighed into a separate 5 mL scintillation vial (used to calculate yields after the reaction was completed). *N*-methylaniline, or isotopically labelled variant, (0.50 mmol) and 1-octene (84.2 mg, 0.75 mmol) were weighed into the same 5 mL scintillation vial as the 1,3,5-trimethoxybenzene. Using a glass disposable pipette, the solution of pre-catalyst was transferred between the two vials multiple times to ensure a complete dissolution and creation of a homogeneous mixture. These samples were consistently measured to have a volume of 0.55 mL by 1.0 mL syringe. The resulting solution was transferred to a J. Young NMR tube and the tube closed with a screw-type Teflon cap. The tube was then placed into the NMR spectrometer that was already pre-heated to 105  $^{\circ}\text{C}$ . This time point was taken to be  $t = 0$  min. The sample was allowed  $\sim 10$  minutes to reach equilibrium, followed by shimming of the magnet, and tuning and matching of the instrument. An  $^1\text{H}$  NMR spectrum was collected every 17.6 minutes with the first  $^1\text{H}$  NMR spectrum recorded at 17.4 minutes. Yield of *N*-methylaniline (*ortho*-protons at  $\delta$  6.33) and product (*ortho*-protons at  $\delta$  6.41) was determined by integration relative to the known amount of 1,3,5-trimethoxy benzene internal standard (aryl-protons at  $\delta$  6.04). Due to deuterium

scrambling into the *ortho*-position of the product, only the yield of the starting material aniline is reported when using deuterated aniline substrates. Each kinetic monitoring experiment was repeated to confirm the reaction profile.

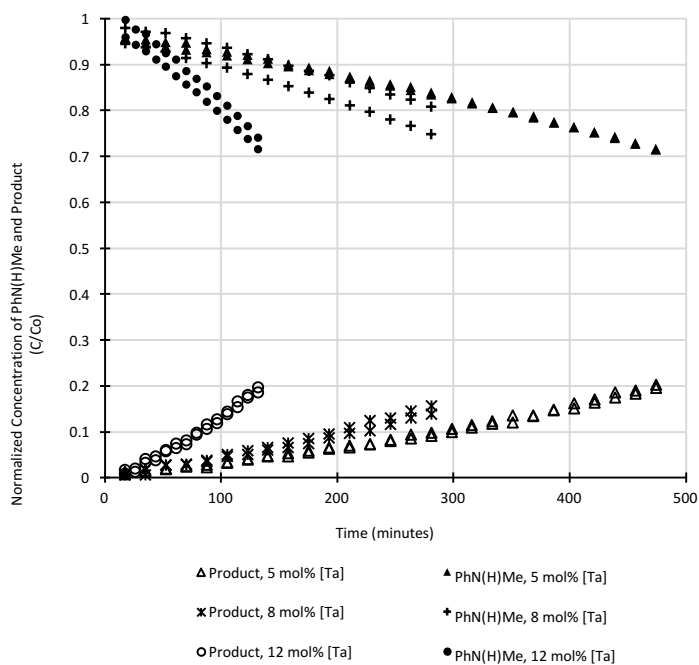


**Figure 2.7** Plot of reaction monitoring experiments with 5, 8, and 12 mol% 2.15 as precatalyst for the hydroaminoalkylation reaction between N-methylaniline and 1-octene. Overlay of both experiments.

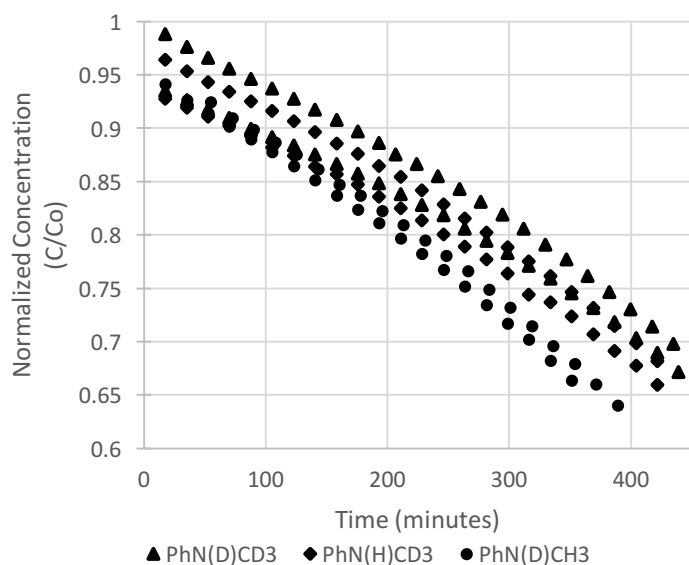


**Figure 2.8** Plot of reaction monitoring experiments with 12 mol% **2.15** as precatalyst for the hydroaminoalkylation reaction between *N*-methylaniline (variably deuterated) and 1-octene. Overlay of both experiments.

**Analysis of Deuterium Incorporation (Scheme 2.23):** After collecting kinetic data, the reactions with the deuterated substrates were quenched with 2 mL methanol, transferred to 20 mL scintillation vial, and the solvents removed on a rotary evaporator. The product aniline and the *N*-methylaniline starting material were isolated by column chromatography (10% EtOAc in hexanes, silica). Deuterium incorporation was determined by  $^1\text{H}$  NMR spectroscopy and deuteration confirmed by  $^2\text{H}$  NMR spectroscopy.

# Chapter 3: Phosphoramidate Niobium Complexes for the Hydroaminoalkylation of Alkenes with Secondary Amines – Synthesis of Novel Niobium Complexes and Catalytic Reactivity

## 3.1 Introduction

As discussed in detail in Chapter 2, the hydroaminoalkylation reaction offers a powerful tool for the  $\alpha$ -alkylation of simple secondary amine substrates. Additionally, our research into 2-pyridonate tantalum complexes demonstrates that ligand effects can result in significant changes in catalytic activity. While there has been significant development on Ta complexes as precatalysts for hydroaminoalkylation, there are only few reports of niobium complexes as precatalysts for this reaction (Figure 3.1).<sup>173-174,181-182,185</sup>

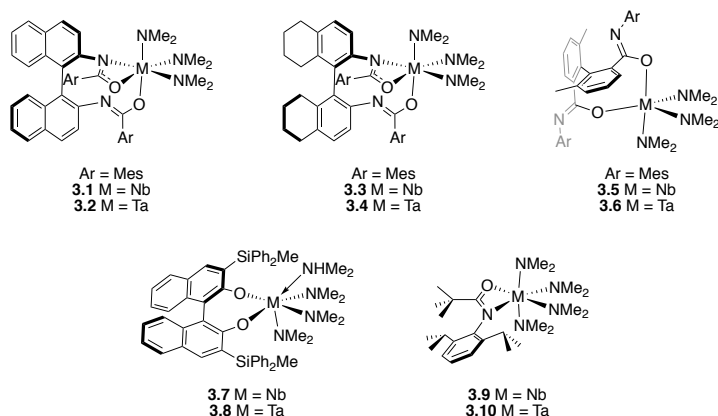
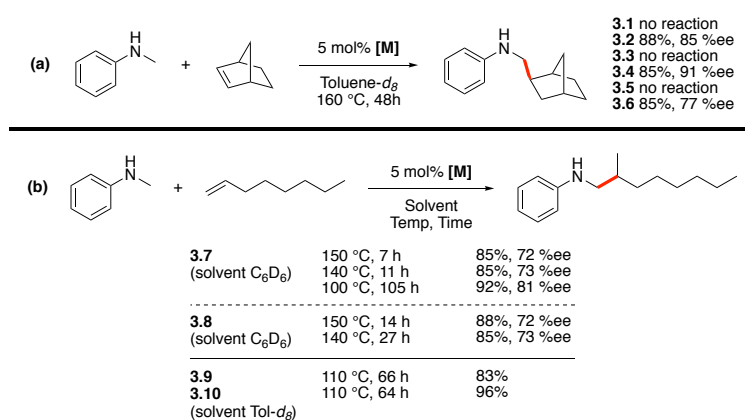


**Figure 3.1 Nb complexes reported for hydroaminoalkylation and their direct Ta analogues**

### 3.1.1 Niobium Catalyzed Hydroaminoalkylation

Early reports of Nb precatalysts for hydroaminoalkylation have studied chiral, tethered-biaryl-diamidate ligands,<sup>173,181</sup> and chiral BINOLate ligands for the enantioselective hydroaminoalkylation.<sup>174,182</sup> Complexes **3.1**, **3.3**, and **3.5** were reported to not be reactive for hydroaminoalkylation, whereas the direct Ta analogues **3.2**, **3.4**, **3.6** are active and achieve good

enantioselectivities (Scheme 3.1a). In contrast, Nb and Ta BINOLate complexes **3.7** and **3.8** are both active for catalytic hydroaminoalkylation (Scheme 3.1b). Here it was found that Nb complex **3.7** achieved similarly high yields to Ta complex **3.8** while requiring approximately half the reaction time. Recently, an amidate ligated Nb complex **3.9** was reported and compared with its direct Ta analogue **3.10** for hydroaminoalkylation reactivity (Scheme 3.1b).<sup>185</sup> Compared to **3.9**, Ta complex **3.10** achieves a higher yield with a slightly increased rate.



**Scheme 3.1 Comparative hydroaminoalkylation reactivity of Nb and Ta precatalysts**

Complexes **3.7** and **3.8** were further investigated in an attempt to understand the origin of the increased rate observed with a Nb precatalyst over the Ta precatalyst. Through deuterium labelling experiments, it was observed that significantly less deuterium scrambling occurs with Nb complex **3.7** compared with Ta complex **3.8** (Scheme 3.2). Here, it is proposed that the deuterium scrambling is the result of off-cycle equilibria, similar to those detailed in Chapter 2. These off-cycle pathways may contribute to the reduced observed reaction rate for Ta complex **3.8**.





temperature range for early-transition-metal-catalyzed hydroaminoalkylation with precatalysts containing amido ligands.<sup>26,165,185</sup>

### 3.2 Scope of Chapter

While the achievement of room temperature reactivity with **3.11** is impressive, this complex suffers greatly from decomposition under catalytic conditions. More specifically, only gentle heating is tolerated (up to 70 °C), which limits substrate scope significantly.<sup>175</sup> Additionally, this is in contrast to many of the Ta amido complexes that can be heated at high temperatures (greater than 150 °C), for long reaction times, to achieve high yields with substrates that exhibit slow rates such as piperidine.<sup>172,179</sup>

To overcome this drawback, a precatalyst with the correct coordination mode of a phosphoramidate ancillary ligand(s) with the remaining ligands as amido ligands, may achieve an increased rate at a given temperature while resisting catalyst death under catalytic conditions over longer reaction times. Additionally, the improved activity and significant reduction in deuterium scrambling with Nb precatalyst **3.7** over Ta precatalyst **3.8** suggests Nb may be well suited for hydroaminoalkylation chemistry. Similar structural features are found between Nb complex **3.9** and Ta complex **3.10**, where the ancillary *1,3-N,O*-chelating amidate ligand has a planar N-C-O fragment when bound to Nb or Ta. The phosphoramidate ligands can impart a significantly different steric environment about the metal center due to the tetrahedral geometry about the phosphorous atom, which has been postulated to improve catalytic performance.<sup>175,185</sup>

This chapter details efforts toward the synthesis of highly active phosphoramidate Nb complexes for the hydroaminoalkylation of alkenes with secondary amines. A desirable precatalyst would have an improve rate over known precatalysts with established substrate combinations, and would also have improved yields and rate with challenging substrates such as

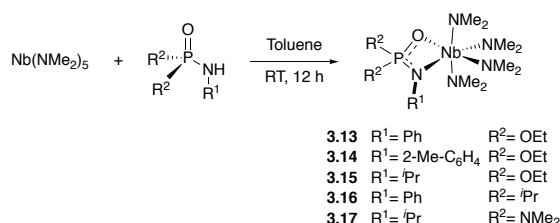
*N*-containing saturated heterocycles, highly nucleophilic dialkyl amines, and sterically demanding amine and alkene substrates.<sup>24,165,171-172</sup> Presented herein are the synthesis of a variety of phosphoramidate Nb complexes, and their subsequent catalytic reactivity for the hydroaminoalkylation reaction.

### 3.3 Results and Discussion

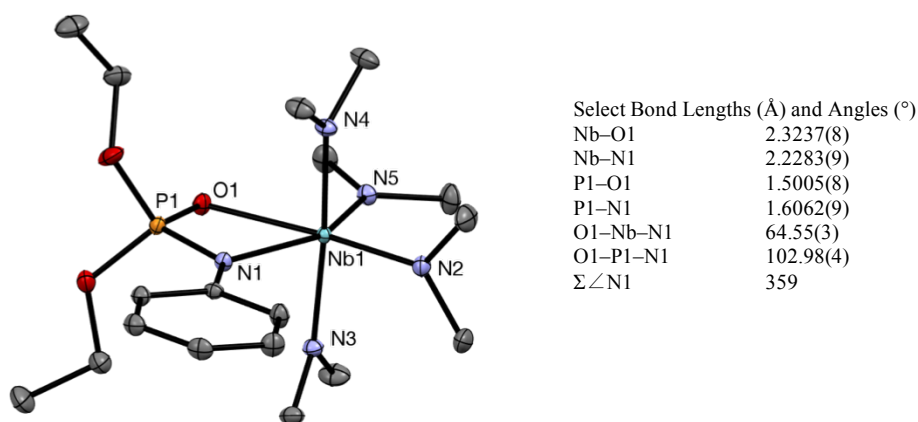
#### 3.3.1 Synthesis of Phosphoramidate Nb Complexes

A protonolysis reaction was used to synthesize phosphoramidate ligated Nb complexes **3.13** – **3.17** (Scheme 3.4).<sup>165,172-173,181,185</sup> Here, phosphoramidate protio-ligand is reacted with Nb(NMe<sub>2</sub>)<sub>5</sub> to create the phosphoramidate ligated Nb complex and an equivalent of dimethylamine. Complex **3.13** could be recrystallized and a solid-state molecular structure was obtained (Figure 3.2). The solid-state molecular structure of **3.13** reveals a pseudo-octahedral structure. The phosphoramidate ligand binds as a  $\kappa^2$ -*1,3-N,O*-chelate in a similar manner to the solid-state structure of phosphoramidate Ta complex **3.11**, and amidate Nb and Ta complexes **3.9** and **3.10**. Notably, N1 is almost perfectly planar suggesting *sp*<sup>2</sup> hybridization. This is consistent with the coordination of both phosphoramidate and amidate ligands on Nb and Ta. All amido ligands are nearly perfectly planar about nitrogen suggesting *sp*<sup>2</sup> hybridization. These provide both  $\sigma$ - and  $\pi$ -bonding interactions, and act as highly donating ligands. A comparison with complex **3.11** shows that complex **3.13** has longer Nb–O1 (2.3237(8) vs. 2.190(2) Å) and Nb–N1 bonds (2.2282(9) vs. 2.135(2) Å). This lengthening is likely caused by **3.13** being more electron rich due to the highly donating amido ligands. Consequently, **3.13** exhibits a slightly tighter bite angle (64.55(3)° vs. 66.68(9)°), and slightly shorter P1–O1 (1.5005(8) vs. 1.516(2) Å) and P1–N1 (1.6062(9) vs. 1.616(2)) bond lengths. When compared to the binding of the amidate ligand in **3.9**, the phosphoramidate ligand in **3.11** adopts a more symmetric binding mode with Nb–O1

and Nb–N1 (2.3237(8) and 2.2283(9) Å) being closer in distance than the amidate ligand with Nb–O1 and Nb–N1 (2.1133(8) and 2.4653(9) Å). This suggests that the oxygen of the phosphoramidate ligand is, comparatively, less donating likely owing to the high P–O bond strength. The  $^{31}\text{P}\{^1\text{H}\}$  NMR spectrum of **3.13** reveals a single signal at 4.4 ppm, as expected based on the solid-state structure. The  $^1\text{H}$  NMR spectrum is also consistent with the solid-state structure. A single broad resonance at 3.36 ppm is observed for the dimethylamido ligands suggesting fluxional behavior due to facile exchange of the amido ligands.



**Scheme 3.4** Synthesis of phosphoramidate Nb complexes **3.13** – **3.17**



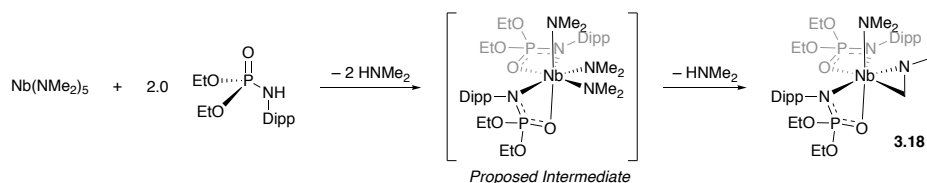
Thermal ellipsoids are shown at 50%. H-atoms omitted.

**Figure 3.2** ORTEP representation of **3.13** with select bond lengths and angles

In contrast, **3.14** – **3.17** were obtained as sticky solids that were resistant to recrystallization and complete purification.  $^{31}\text{P}\{^1\text{H}\}$  NMR spectroscopy reveals only a single resonance and the absence of the starting material phosphoramidate. Complexes **3.14** – **3.16** demonstrate trace baseline impurities in their  $^1\text{H}$  and  $^{13}\text{C}\{^1\text{H}\}$  spectra, while **3.17** has

unidentified impurities in both the  $^1\text{H}$  and  $^{13}\text{C}\{^1\text{H}\}$  NMR spectra. The NMR spectra for these complexes is analogous to that of **3.13** and their structure is presumed to be similar to that of **3.13**.

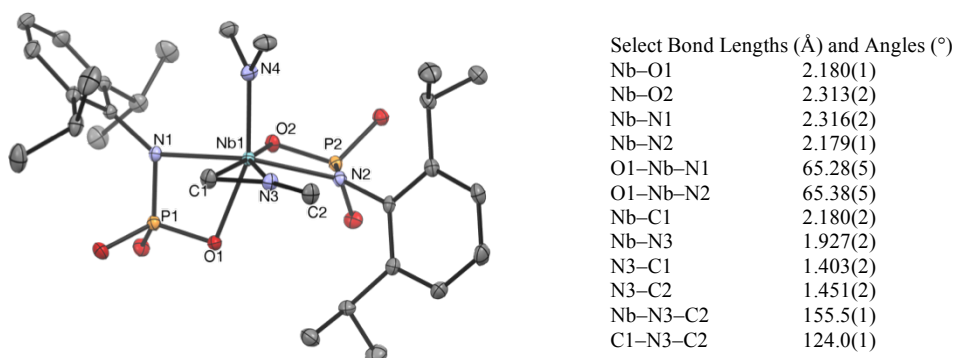
Curiously, attempts to synthesize the analogous complex with a phosphoramidate ligand containing a more sterically demanding *N*-2,6-diisopropylphenyl group produces a different product than expected. A 1:1 reaction of phosphoramidate: $\text{Nb}(\text{NMe}_2)_5$  resulted in the formation of a new bis-ligated complex, and 0.5 equivalents of  $\text{Nb}(\text{NMe}_2)_5$  remaining. A reaction of 2:1 ligand to Nb results in the expected consumption of all  $\text{Nb}(\text{NMe}_2)_5$  and the same new complex (Scheme 3.5). Fortunately, complex **3.18** can be recrystallized and the solid-state molecular structure obtained to determine the structure of the complex. The molecular structure reveals that **3.18** is a diphosphoramidate niobaziridine that results from two protonolysis reactions from ligation of the phosphoramidate ligands and a sterically driven hydrogen-atom abstraction event forming the niobaziridine fragment (Scheme 3.5).



**Scheme 3.5** Synthesis of niobaziridine complex **3.18**

Complex **3.18** is 7-coordinate in the solid-state with a pseudo pentagonal bipyramidal geometry (Figure 3.3). The niobaziridine moiety contains a C1–N3 bond length of 1.403(2) Å indicating some multiple bond character. While this binding might also be described as a Nb(III)– $\eta^2$ -imine, assignment of a Nb(V) complex is the best interpretation, as the Nb–C1 and Nb–N3 bond lengths, and angles of the 3-membered metallaacycle are in complete agreement with reported Ta(V) tantalaziridines supported by amidate ligands.<sup>172,185,210</sup> Additionally, N3 is

planar and  $sp^2$  hybridized, and likely a  $4e^-$  donor to create a  $18e^-$  complex. Each phosphoramidate ligand contains significant differences in binding as evidenced by the Nb–O bond lengths (Nb–O1 of 2.180(1) Å and Nb–O2 2.313(2) Å) and Nb–N bond lengths (Nb–N1 of 2.316(2) Å and Nb–N2 2.179(1) Å). Given the high steric constraints about the metal center, these changes in bond lengths likely arise due to steric interactions over significant changes in binding enthalpy of Nb–O or Nb–N bonds.



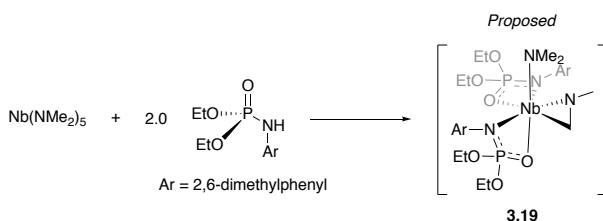
Thermal ellipsoids are shown at 50%. H-atoms and  $OCH_2CH_3$  omitted.

**Figure 3.3** ORTEP representation of 3.18 and select bond lengths and angles

$^1H$  and  $^{31}P\{^1H\}$  NMR spectra confirm this structure in the solution state. While both spectra reveal two separate phosphoramidate ligand environments at 25 °C,  $^1H$  2D-NOESY experiment at 25 °C reveals chemical exchange peaks for the inequivalent phosphoramidate ligands indicating the complex is fluxional and ligand interconversion occurs on the NMR time scale.

Consumption of 2 equivalents of ligand to Nb center also occurs with a *N*-2,6-dimethylphenyl phosphoramidate ligand (Scheme 3.6). The crude material results in a  $^{31}P\{^1H\}$  spectrum with two major signals at 8.1 and –0.5 with 1:1 integration values. The  $^1H$  NMR spectrum is complex, and exhibits broad peaks suggestive of fluxional behavior. Unfortunately, variable temperature NMR experiments (–75 °C to 90 °C) did not result in simplification of the

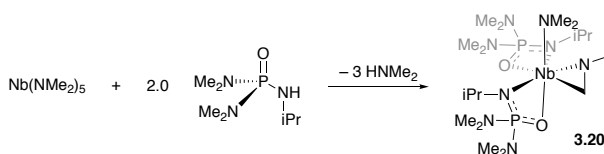
$^1\text{H}$  NMR spectrum. Although this complex could be recrystallized, no crystals suitable for resolved X-ray diffraction could be obtained. However, based on analogy to **3.18**, niobaziridine **3.19** is proposed. This assignment is based on the two  $^{31}\text{P}$  NMR signals at similar chemical shifts to the fully characterized niobaziridine **3.18**. Without further information regarding chemical structure, the assignment is tentative. To ensure accurate concentrations of niobium, catalytic reactions were prepared *in situ* using 2:1 pro-ligand: $\text{Nb}(\text{NMe}_2)_5$  for catalytic screening (*vide infra*).



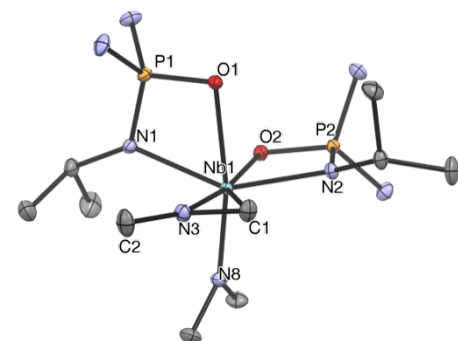
**Scheme 3.6** Reaction of  $\text{Nb}(\text{NMe}_2)_5$  with two equivalents of phosphoramidate

In an attempt to synthesize an additional niobaziridine, two equivalents of a *N*-phenyl phosphoramidate and one equivalent of  $\text{Nb}(\text{NMe}_2)_5$  results in a complicated and broad  $^1\text{H}$  NMR spectrum, and a  $^{31}\text{P}\{^1\text{H}\}$  spectrum with multiple broad signals between 10 – 0 ppm. VT  $^1\text{H}$  and  $^{31}\text{P}\{^1\text{H}\}$  NMR experiments were attempted but no conclusions regarding structure could be made. As above, *in situ* preparations of 2:1 pro-ligand: $\text{Nb}(\text{NMe}_2)_5$  were used for catalytic screening (*vide infra*).

Scheme 3.7 shows the synthesis of an additional niobaziridine **3.20** where the ethoxy substituents of the phosphoramidate have been substituted with dimethylamido groups. The solid-state molecular structure, as well as solution state NMR spectra, reveal an analogous structure to **3.18** (Figure 3.4). The  $\text{N1}-\text{P1}-\text{O1}$  and  $\text{N2}-\text{P2}-\text{O2}$  angles are smaller by  $\sim 2^\circ$  compared to **3.18** due to the increased steric parameter of dimethylamido backbone (vs. ethoxy backbone in **3.18**).



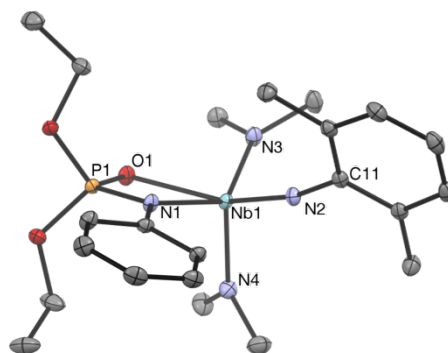
**Scheme 3.7** Synthesis of niobaziridine **3.20**



**3.20**

Select Bond Lengths (Å) and Angles (°)

Nb–O1	2.2211(9)
Nb–O2	2.2545(9)
Nb–N1	2.2411(9)
Nb–N2	2.1755(8)
Nb–C1	2.180(2)
Nb–N3	1.940(1)
N3–C1	1.404(1)
N3–C2	1.439(2)
Nb–N3–C2	153.36(8)
C1–N3–C2	126.3(1)



**3.21**

Select Bond Lengths (Å) and Angles (°)

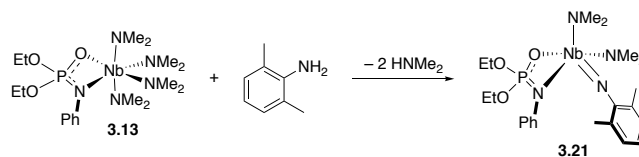
Nb–O1	2.278(1)
Nb–N1	2.206(1)
P1–O1	1.507(1)
P1–N1	1.611(1)
Nb–N2	1.790(1)
Nb–N3	2.005(1)
Nb–N4	1.978(1)
Nb–N2–C11	167.3(1)

Thermal ellipsoids are shown at 50%. H-atoms omitted for both. N(CH<sub>3</sub>)<sub>2</sub> omitted for **3.20** (left).

**Figure 3.4** ORTEP representations of **3.20** (left) and **3.21** (right) with select bond lengths and angles

The relative thermal stability of niobaziridine **3.18** is notable in comparison to that of mono(phosphoramidate) niobium complex **3.13**. In a sealed J. Young NMR tube in Tol-*d*<sub>8</sub>, the niobaziridine species is not observed to decompose over 48 hours at 165 °C and less than 10% is observed to decompose over 72 hours of heating at the same temperature, as observed by <sup>31</sup>P{<sup>1</sup>H} spectroscopy. On the other hand, complex **3.13** completely decomposes after only 12 hours at 110 °C, as observed by the formation of a complex <sup>31</sup>P{<sup>1</sup>H} NMR spectrum and a disappearance of the signal for **3.13**.

To date, there are no reports of imido complexes used as precatalysts for hydroaminoalkylation. Incorporation of an imido ligand may provide additional thermal robustness to the precatalyst complex, potentially increasing turnover number or allowing for improved substrate scope with increased reaction temperatures. Phosphoramidate imido complex **3.21** can be prepared from the reaction between 2,6-dimethylaniline and **3.13** (Scheme 3.8). The solid-state molecular structure reveals a pseudo trigonal bipyramidal structure with the multiply bonded imido (N2) and O2 of the phosphoramidate in the axial positions (Figure 3.4). The phosphoramidate ligand binds in a similar manner to those previously discussed with only minor changes from the binding in **3.13** suggesting the amido ligand has limited impact on the electronic character of the metal center. The Nb–N2–C11 bond angle is 167.30° implying N2 has significant sp-hybrid character, and that the imido ligand acts 6e<sup>−</sup> donor to access an 18e<sup>−</sup> complex. Both amido ligands are planar at nitrogen, consistent with previous structures.



**Scheme 3.8 Synthesis of phosphoramidate imido Nb complex 3.21**

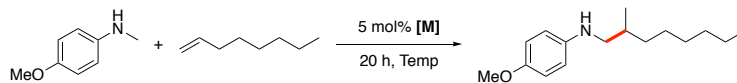
### 3.3.2 Catalytic Hydroaminoalkylation Reactivity of Phosphoramidate Nb Complexes

The synthesized mono phosphoramidate Nb complexes were tested for their reactivity as precatalysts in a hydroaminoalkylation reaction between *N*-methyl-*para*-methoxyaniline and 1-octene (Table 3.1).<sup>165,175,203</sup> Reactivity was assessed at 5 mol% [Nb] loading at various temperatures. The precursor Nb(NMe<sub>2</sub>)<sub>5</sub> was tested in a control reaction (entry 6). Previous work from the Schafer group has demonstrated phosphoramidate Ta complexes are also active precatalysts for hydroaminoalkylation.<sup>211</sup> Entry 7 provides the direct comparison to entry 1, while entry 8 represents Ta precatalyst with the highest reported activity. Conversion was determined



by  $^1\text{H}$  NMR spectroscopy as a ratio between starting amine and product amine. Reports of conversions and isolated yields with Group 5 precatalysts have established that conversions are valuable indicators of catalytic activity for catalyst screening purposes.<sup>24-25,171-172,175,203</sup>

Entry 1 demonstrates good reactivity with **3.13** at 130 °C with decreasing reactivity down to 90 °C. A control reaction exhibits 33% conversion at 130 °C and no reactivity at 110 °C, confirming the ligand plays a significant role in the catalysis (entry 6). Modification of the *N*-functionality of the phosphoramidate ligand to increase the steric parameter decreases reactivity (entry 2, *o*-tolyl; entry 3, isopropyl). Modification of the ligand backbone substituents to increased steric parameters of isopropyl (entry 4) and to a significantly more electron donating dimethylamido backbone (entry 5), results in limited reactivity. Nb complex **3.13** (entry 1) demonstrates a marked improvement in activity compared to directly analogous Ta complex (entry 7). Additionally, this complex provides comparable activity at 90 °C to the best reported Ta complex (entry 8). However, a comparison at 100 °C reveals a significant decrease in activity of the Nb complex.



Entry	Precatalyst	T (°C)	Conversion (%) <sup>a</sup>
1	 3.13	130	82
		110	71
		100	46
		90	31
2	 3.14	110	57
		90	13
3	 3.15	110	38
		90	9
4	 3.16	110	45
		90	21
5	 3.17	110	16
6	Nb(NMe <sub>2</sub> ) <sub>5</sub>	130	33
		110	n.r. <sup>c</sup>
7 <sup>b</sup>		110	60
		90	9
8 <sup>b</sup>		100	98
		90	37

Reaction conditions: *N*-methylaniline (0.5 mmol), 1-octene (0.75 mmol), [Ta] pre-catalyst (0.025 mmol, 5 mol%), *d*8-toluene (0.5 mL). See experimental section for details. <sup>a</sup>Determined by <sup>1</sup>H NMR spectroscopy. <sup>b</sup>Results from the Schafer group.<sup>211</sup> <sup>c</sup>n.r. = no reaction.

**Table 3.1 Evaluation of monophosphoramidate Nb complexes as precatalysts for hydroaminoalkylation**

Next, the diphosphoramidate complexes and the phosphoramidate imido complex were access for reactivity (Table 3.2). Entry 1 and 2 evaluate the catalytic activity of the isolated niobaziridine complexes. Both provide limited reactivity with **3.20** exhibiting diminished reactivity compared to **3.18**, consistent with the comparison between **3.13** and **3.17** (Table 3.1, entries 1 and 5). Notably, these niobaziridines are proposed to be active species in the catalytic cycle (see Chapter 2.1). While their reactivity is poor, the observation that niobaziridine species are active precatalysts suggests that these phosphoramidate Nb complexes follow the same generalized mechanism that has been proposed for Ta precatalysts. The phosphoramidate imido species **3.21** (entry 5) is not reactive for the hydroaminoalkylation reaction. One proposal for the lack of observed reactivity with **3.21** is that there is not sufficient steric congestion at the metal center to encourage appreciable niobaziridine formation as the single, multiple bonded imido ligand has replaced two dimethylamido ligands.

Interestingly, the *in situ* preparations with two equivalents of phosphoramidate to Nb, provide moderate (entry 3) and excellent (entry 4) yields at 90 °C. Given the exact nature of these precatalyst structures is unknown, it is difficult to assess the structure-activity relationship. We propose that the second equivalent of phosphoramidate enhances reactivity by creating a more electrophilic metal center by means of replacing a highly donating dimethylamido ligand. This has been demonstrated to enhance reactivity by utilization of chloro ligands in Ta complexes.<sup>24,171,175</sup> Entry 4 also creates an optimal steric environment about the metal center, where increasing the steric parameter of the *N*-substituent (*N*-2,6-dimethylphenyl, entry 3; *N*-Dipp, entry 1) favours a highly stabilized niobaziridine structures that are kinetically inert due to the increased steric parameters of the phosphoramidate ligands. The *in situ* preparation with *N*-phenyl phosphoramidate (Table 3.2, entry 1) provides the highest reactivity at 90 °C, and offers a

significant improvement in activity compared the best reported Ta phosphoramidate complex (Table 3.1, entry 8).

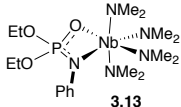
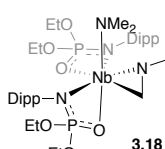
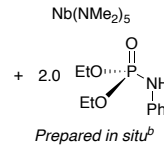
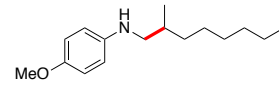
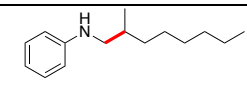
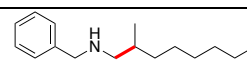
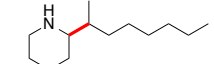
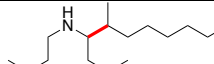
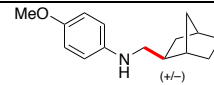
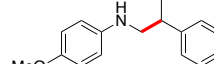
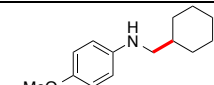
Entry	Precatalyst	T (°C)	Conversion (%) <sup>a</sup>
1	 3.18	110	61
		90	17
2	 3.20	110	<5
3 <sup>b</sup>	Nb(NMe <sub>2</sub> ) <sub>5</sub> + 2.0 Ar = 2,6-dimethyl phenyl Prepared <i>in situ</i>	110	75
		90	37
4 <sup>b</sup>	Nb(NMe <sub>2</sub> ) <sub>5</sub> + 2.0 Prepared <i>in situ</i>	110	>98
		90	78
5	 3.21	110	n.r. <sup>c</sup>

Reaction conditions: *N*-methylaniline (0.5 mmol), 1-octene (0.75 mmol), [Ta] pre-catalyst (0.025 mmol, 5 mol%), *d*<sub>8</sub>-toluene (0.5 mL). See experimental section for details. <sup>a</sup>Determined by <sup>1</sup>H NMR spectroscopy. <sup>b</sup>Prepared *in situ* at 5% for Nb, 10 mol% phosphoramidate; see experimental for details. <sup>c</sup>n.r. = no reaction.

**Table 3.2 Evaluation of diphosphoramidate and imido Nb complexes as precatalyst for hydroaminoalkylation**

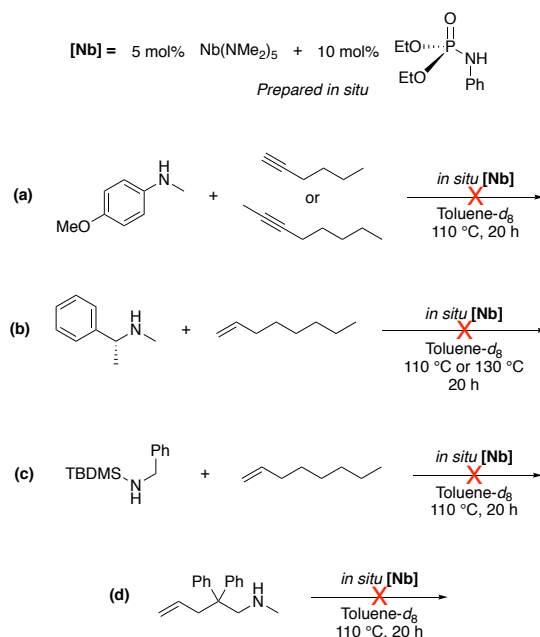
To further assess these Nb precatalysts, **3.13**, **3.18**, and the system generated *in situ* from entry 9, various substrates were examined (Table 3.3). As in the initial screening, the *in situ* generated system provides the highest reactivity across the evaluated substrate scope. Moving from the *para*-methoxyaniline derivative to aniline (entry 2) decreases reactivity. This trend has

been observed for the reactivity of known phosphoramidate Ta complex **3.11**.<sup>175</sup> Dialkylamine substrates, known to be difficult for hydroaminoalkylation, only exhibit trace reactivity at elevated temperatures (entry 3 and 4). It should be noted that the lack of efficient reactivity here could be caused by catalyst design, or by catalyst death at elevated temperatures. For context, using piperidine as a substrate requires 134 h at 165 °C to produce 74% yield using amidate Ta complex **3.10**.<sup>172</sup> While reactivity with the strained norbornene is excellent (entry 6), reactivity with styrene (entry 7), and cyclohexene (entry 8) are poor.

$\text{NH} + \text{CH}_2=\text{CH-R} \xrightarrow[\text{Toluene-}d_8, \text{Temp, 20h}]{5 \text{ mol\% [Nb]}} \text{NH-CH(R)-CH}_3$					
Conversion <sup>a</sup>					
Entry	Product	Temp (°C)	 3.13	 3.18	 Nb(NMe <sub>2</sub> ) <sub>5</sub> + 2.0 EtO-P(=O)(NHPh)-OEt <i>Prepared in situ</i> <sup>b</sup>
1		110	71	61	>98
2		110	43	36	67
3		110	26	10	29
4		165	n.a. <sup>c</sup>	<10	<10
5		165	n.a. <sup>c</sup>	<10	<10
6		110	71	57	90
7		110	<10	<10	18
8		165	n.a. <sup>c</sup>	<10	16

Reaction conditions: *N*-methylaniline (0.5 mmol), 1-octene (0.75 mmol), [Ta] pre-catalyst (0.025 mmol, 5 mol%), *d*<sub>8</sub>-toluene (0.5 mL). See experimental section for details. <sup>a</sup>Determined by <sup>1</sup>H NMR spectroscopy. <sup>b</sup>Prepared *in situ* at 5 mol% for Nb, 10 mol% phosphoramidate; see experimental for details. <sup>c</sup>n.a. = not attempted.

**Table 3.3 Evaluation of substrate scope of Nb catalyzed hydroaminoalkylation**



**Scheme 3.9 Substrate combinations that are not reactive for hydroaminoalkylation with a phosphoramidate**

#### **Nb catalytic system**

A number of limitations in substrate scope were identified utilizing the *in situ* prepared Nb precatalyst system that has been demonstrated in Table 3.2 as the most active system (Scheme 3.9). It was found that alkynes, unknown as a hydroaminoalkylation substrate, were unreactive to generate the desired allylamines (Scheme 3.9a). In an attempt to observe chirality transfer, *N*-methyl-methylbenzyl amine was attempted but unsuccessful (Scheme 3.9b). Additionally, *N*-silylbenzylamine and a secondary amino-alkene substrate were both unreactive for hydroaminoalkylation (Scheme 3.9 c and d).

### **3.4 Conclusions**

We have demonstrated that a number of phosphoramidate Nb complexes can be synthesized and isolated. Interestingly, increasing the steric bulk of the *N*-substituent of the phosphoramidate pro-ligand from phenyl to 2,6-dimethylphenyl or 2,6-diisopropylphenyl

drastically alters the protonolysis reaction in that two equivalents of ligand coordinate to each equivalent of metal center, even with excess Nb(NMe<sub>2</sub>)<sub>5</sub> present in solution. One of these species (**3.18**) was identified to be a diphosphoramidate niobaziridine, a proposed intermediate in the catalytic cycle for hydroaminoalkylation.

Rewardingly, these complexes were active towards hydroaminoalkylation. An *in situ* preparation of 2:1 phosphoramidate:Nb was found to be a highly active precatalyst system. Direct determination of the structure of the precatalyst has not yet been possible, but variable temperature NMR experiments reveal a highly fluxional system. Additionally, this system provides high reactivity for multiple substrates at 90 °C. However, challenging substrates such as dialkyl amines or internal alkenes give only trace reactivity even at elevated temperatures. At this time, it is unclear whether or not, or to what extent catalyst decomposition plays a significant role at the temperatures required for challenging substrate.

These results also demonstrate that these Nb precatalysts are more active than their Ta analogues, and suggests that Nb analogues of known Ta catalytic systems could be exploited for improved reactivity.<sup>165</sup> Many efforts on Ta suggest a mono-ligated 1,3-*N,O*-chelated complexes provide for best reactivity, while a bis-ligated 1,3-*N,O*-chelated complex provides significantly reduced activity.<sup>24-25,172,175,185</sup> In contrast, the most active phosphoramidate Nb system discussed here requires 2 equivalents of phosphoramidate ligand. This demonstrates that ligand design for Nb complexes can significantly differ from that of Ta complexes for hydroaminoalkylation and direct analogy between the reactivity of Nb and Ta complexes should not be assumed.

### 3.5 Experimental Details

General considerations and instrumentation details can be found in Chapter 2.4.1 and 2.4.2, respectively.



### 3.5.1 Materials

All chemicals were purchased from commercial sources and used as received unless otherwise specified. Chemicals from commercial sources that were not dried and shipped under inert atmosphere, were appropriately dried and degassed of O<sub>2</sub> before being transferred to the glovebox or for use on the Schlenk manifold. All amines and alkenes were dried under N<sub>2</sub> atmosphere with CaH<sub>2</sub>, distilled, and degassed by the freeze-pump-thaw method. Solid phosphoramides were sublimed under vacuum on a Schlenk manifold at 80 – 100 °C with water cooling, and liquid phosphoramides were distilled from CaH<sub>2</sub> and degassed before being transferred into the glovebox. *N*-2,6-diisopropylphenyl diethyl phosphoramidate decomposed during attempts to sublime the compound and was instead dried over 48 h under vacuum (10<sup>-2</sup> mbar) at ambient temperature. Phosphoramides were synthesized according to literature procedures.<sup>175</sup> Note: attempts to obtain air sensitive EI-MS of these compounds were not successful as they were found to lose dimethylamido ligands and the parent ion could not be detected. However, for purified complexes, solid-state molecular structures obtained from single crystal X-ray diffraction and elemental analysis confirm structure and purity.

### 3.5.2 Synthetic and Experimental Details

**Synthesis of (*N*-phenyl-*O,O'*-diethylphosphoramidato)tetrakis(dimethylamido)Nb(V) (3.13).** In a glovebox, a solution of *N*-phenyl-*O,O'*-diethylphosphoramidate (0.066 g, 0.287 mmol) in toluene (~ 4 mL) was added to a stirring solution of deep brown Nb(NMe<sub>2</sub>)<sub>5</sub> (0.090 g, 0.287 mmol) in toluene (~ 6 mL). The resulting solution was stirred for 12 hours. The solution was then concentrated *in vacuo*. The sticky semi-solid was dissolved in a minimal amount of toluene at ambient temperature and stored in the freezer at -35 °C to promote recrystallization. After 24 h, the product could be recovered as red crystals (0.104 g, 0.210 mmol, 73%).

**<sup>1</sup>H-NMR** (600 MHz, C<sub>6</sub>D<sub>6</sub>): δ 7.33-7.31 (m, 2H), 7.20 (dd, *J* = 7.6, 0.6 Hz, 2H), 6.88 (tt, *J* = 7.3, 1.1 Hz, 1H), 4.04-3.93 (m, 4H), 3.36 (s, 24H), 1.08 (td, *J* = 7.1, 0.6 Hz, 6H). **<sup>13</sup>C{<sup>1</sup>H}-NMR** (151 MHz, C<sub>6</sub>D<sub>6</sub>): δ 147.6 (d, *J*<sub>CP</sub> = 2.4 Hz), 129.6 (d, *J*<sub>CP</sub> = 1.5 Hz), 120.8 (d, *J*<sub>CP</sub> = 16.4 Hz), 119.4, 62.80 (d, *J*<sub>CP</sub> = 6.6 Hz), 49.1 (br. s), 16.5 (d, *J*<sub>CP</sub> = 6.7 Hz). **<sup>31</sup>P{<sup>1</sup>H}-NMR** (122 MHz, C<sub>6</sub>D<sub>6</sub>): δ 5.0 (s). **EA**: Calc'd for C<sub>18</sub>H<sub>39</sub>N<sub>5</sub>NbO<sub>3</sub>P: C 43.46, H 7.90, N 14.08; Found: C 43.83, H 8.10, N 14.43.

**General procedure for the synthesis of complexes 3.14 – 3.17.** In a glovebox, a solution of the corresponding phosphoramidate (0.096 mmol) in toluene (~ 2 mL) was added to a stirring solution of deep brown Nb(NMe<sub>2</sub>)<sub>5</sub> (0.030 g, 0.096 mmol) in toluene (~ 3 mL). The resulting red-orange solution was stirred for 12 hours. The solution was then concentrated *in vacuo*. Hexanes (~ 3 mL) was added and the solution concentrated *in vacuo*. This was repeated three times in an attempt to dissolve residual solvent in an effort to create a solid compound. Attempts at recrystallization from toluene or toluene/hexanes mixtures at ambient temperature or -35 °C were unsuccessful. Crude yields are reported, however, due to residual solvent or small impurities, crude yields are over 100%.

**(*N*-(2-methylphenyl)-*O,O'*-diethylphosphoramidato)tetrakis(dimethylamido)Nb(V) (3.14).**

Using the general procedure above, *N*-(2-methylphenyl)-*O,O'*-diethylphosphoramidate (0.023 g, 0.096) was added to Nb(NMe<sub>2</sub>)<sub>5</sub> (0.030 g, 0.096 mmol) resulting in a red-orange semi-solid (crude yield of 0.047 g, 96%).

**<sup>1</sup>H-NMR** (400 MHz, C<sub>6</sub>D<sub>6</sub>): δ 7.31-7.28 (m, 1H), 7.20-7.18 (m, 2H), 6.90-6.88 (m, 1H), 4.02 (qd, apt. quintet, *J*<sub>HH</sub> = 7.1, *J*<sub>HP</sub> = 7.1 Hz, 4H), 3.183 (br. s, 12H), 3.179 (br. s, 12H), 2.62 (s, 4H), 1.14 (td, *J*<sub>HH</sub> = 7.1, *J*<sub>HP</sub> = 0.7 Hz, 6H). **<sup>13</sup>C{<sup>1</sup>H}-NMR** (101 MHz, C<sub>6</sub>D<sub>6</sub>): δ 149.4 (s), 131.5 (d, *J*<sub>CP</sub> = 19.9 Hz), 130.6 (s), 126.4 (d, *J*<sub>CP</sub> = 13.0 Hz), 123.7 (d, *J*<sub>CP</sub> = 9.2 Hz), 118.3 (s), 62.1 (d, *J*<sub>CP</sub>

= 7.1 Hz), 47.6 (s), 47.0 (s), 19.9 (d,  $J_{CP}$  = 8.3 Hz), 16.7 (d,  $J_{CP}$  = 7.6 Hz).  $^{31}\text{P}\{^1\text{H}\}$ -NMR (162 MHz,  $\text{C}_6\text{D}_6$ ):  $\delta$  1.25 (s).

**(*N*-phenyl-*O,O'*-diisopropylphosphoramidato)tetrakis(dimethylamido)Nb(V) (3.15).** Using the general procedure above, *N*-phenyl-*O,O'*-diisopropylphosphoramidate (0.025 g, 0.096 mmol) was added to  $\text{Nb}(\text{NMe}_2)_5$  (0.030 g, 0.096 mmol) resulting in a red-orange semi-solid (crude yield of 0.055 g, 123%).

$^1\text{H}$ -NMR (400 MHz,  $\text{C}_6\text{D}_6$ ):  $\delta$  7.33-7.29 (m, 2H), 7.19-7.15 (m, 2H), 6.88-6.84 (m, 1H), 4.67-4.59 (m, 2H), 3.35 (br. s, 18H), 1.25 (d,  $J$  = 6.1 Hz, 6H), 1.17 (d,  $J$  = 6.2 Hz, 6H).  $^{13}\text{C}\{^1\text{H}\}$ -NMR (101 MHz,  $\text{C}_6\text{D}_6$ ):  $\delta$  147.7 (d,  $J_{CP}$  = 3.1 Hz), 129.5 (s, 4C), 120.8 (d,  $J_{CP}$  = 16.9 Hz), 119.3 (s, 2C), 71.0 (d,  $J_{CP}$  = 6.9 Hz), 49.1 (br. s), 24.2 (d,  $J_{CP}$  = 6.1 Hz), 24.0 (d,  $J_{CP}$  = 3.0 Hz).  $^{31}\text{P}\{^1\text{H}\}$ -NMR (162 MHz,  $\text{C}_6\text{D}_6$ ):  $\delta$  3.55 (s).

**(*N*-isopropyl-*O,O'*-diethylphosphoramidato)tetrakis(dimethylamido)Nb(V) (3.16).** Using the general procedure above, *N*-isopropyl-*O,O'*-diethylphosphoramidate (0.019 g, 0.096 mmol) was added to  $\text{Nb}(\text{NMe}_2)_5$  (0.030 g, 0.096 mmol) resulting in a red-orange semi-solid (crude yield of 0.051 g, 115%).

$^1\text{H}$ -NMR (400 MHz,  $\text{C}_6\text{D}_6$ ):  $\delta$  4.01-3.91 (m, 4H), 3.78-3.64 (m, 1H), 3.40 (s, 18H), 1.45 (d,  $J_{HH}$  = 6.6 Hz, 6H), 1.11 (td,  $J_{HH}$  = 7.1,  $J_{HP}$  = 0.4 Hz, 6H).  $^{13}\text{C}\{^1\text{H}\}$ -NMR (101 MHz,  $\text{C}_6\text{D}_6$ ):  $\delta$  62.4 (d,  $J_{CP}$  = 7.4 Hz), 52.5 (d,  $J_{CP}$  = 9.2 Hz), 49.2 (br. s), 48.1 (br. s), 26.7 (d,  $J_{CP}$  = 6.0 Hz), 16.4 (d,  $J_{CP}$  = 7.8 Hz).  $^{31}\text{P}\{^1\text{H}\}$ -NMR (162 MHz,  $\text{C}_6\text{D}_6$ ):  $\delta$  56.9 (s).

**(*N*-isopropylbis(dimethylamino)phosphoramidato)tetrakis(dimethylamido)Nb(V) (3.17).** Using the general procedure above, *N*-isopropylbis(dimethylamino)phosphoramidate (0.019 g, 0.096 mmol) was added to  $\text{Nb}(\text{NMe}_2)_5$  (0.019 g, 0.096) resulting in a red-orange semi-solid (crude yield of 0.059 g, 133%).

We observe some unknown significant impurities in the  $^1\text{H}$  NMR and  $^{31}\text{C}$  spectra as well as small baseline impurities.  **$^1\text{H}$ -NMR** (400 MHz,  $\text{C}_6\text{D}_6$ ):  $\delta$  3.67 (sept,  $J = 6.5$  Hz), 3.42 (br. s, 18H), 3.19 (d,  $J = 8.4$  Hz, 3H, unknown assignment), 2.44 (d,  $J = 9.2$  Hz, 12H), 1.28 (dd,  $J_{HH} = 6.5$ ,  $J_{PH} = 0.4$  Hz, 6H).  **$^{13}\text{C}\{^1\text{H}\}$ -NMR** (101 MHz,  $\text{C}_6\text{D}_6$ ):  $\delta$  (101 MHz,  $\text{C}_6\text{H}_6$ ):  $\delta$  48.5, 48.4 (br. s), 47.7 (d,  $J_{CP} = 3.1$  Hz), 47.0, 37.5 (d,  $J_{CP} = 4.5$  Hz), 32.0, 27.1 (d,  $J_{CP} = 10.7$  Hz), 23.1, 14.4.  **$^{31}\text{P}\{^1\text{H}\}$ -NMR** (162 MHz,  $\text{C}_6\text{D}_6$ ):  $\delta$  26.33 (s).

**Synthesis of bis(*N*-(2,6-diisopropylphenyl)-*O,O'*-diethylphosphoramidato)dimethylamido-*N*-methylniobaziridine (3.18).** In a glovebox, a solution of *N*-(2,6-diisopropylphenyl)-*O,O'*--diethylphosphoramidate (0.540 g, 1.724 mmol) in toluene ( $\sim 10$  mL) was added to a stirring solution of deep brown  $\text{Nb}(\text{NMe}_2)_5$  (0.270 g, 0.862 mmol) in toluene ( $\sim 1$  mL). The resulting solution was stirred for 12 hours. The solution was then concentrated *in vacuo*. The sticky semi-solid was dissolved in a minimal amount of toluene at ambient temperature and then cooled for 10 minutes at  $-35$   $^\circ\text{C}$ . The yellow solution was then layered with a small amount of hexanes ( $\sim 0.5$  mL) and stored in the freezer at  $-35$   $^\circ\text{C}$  to promote recrystallization. The product recrystallized over 24 h to yield pale yellow crystals (0.483 g, 69%).  **$^1\text{H}$ -NMR** (600 MHz,  $\text{C}_6\text{D}_6$ ):  $\delta$  7.32-7.28 (m, 3H), 7.24-7.20 (m, 2H), 7.19-7.17 (m, 1H), 4.76-4.55 (m, 3H), 4.16-4.10 (m, 1H), 4.08-4.00 (m,  $J = 6.7$  Hz, 1H), 3.97-3.93 (m, 1H), 3.89-3.70 (m, 5H), 3.58-3.54 (m, 1H), 3.11 (s, 3H), 2.86 (s, 6H), 2.59 (d,  $J = 5.2$  Hz, 1H), 2.35 (d,  $J = 5.2$  Hz, 1H), 1.57 (d,  $J = 6.6$  Hz, 3H), 1.48-1.46 (m, 6H), 1.38-1.36 (m, 6H), 1.31 (d,  $J = 6.9$  Hz, 3H), 1.29 (d,  $J = 6.9$  Hz, 3H), 1.24 (t,  $J = 7.0$  Hz, 3H), 1.21 (d,  $J = 6.7$  Hz, 3H), 1.16 (t,  $J = 7.0$  Hz, 3H), 1.01 (t,  $J = 7.1$  Hz, 3H), 0.94 (t,  $J = 7.1$  Hz, 3H).  **$^{13}\text{C}\{^1\text{H}\}$ -NMR** (151 MHz,  $\text{C}_6\text{D}_6$ ):  $\delta$  147.62 (d,  $J_{CP} = 7.0$  Hz), 147.43 (d,  $J_{CP} = 6.3$  Hz), 147.29 (d,  $J_{CP} = 7.3$  Hz), 145.50 (d,  $J_{CP} = 6.0$  Hz), 141.37 (d,  $J_{CP} = 6.7$  Hz), 140.28 (d,  $J_{CP} = 7.2$  Hz), 125.50 (d,  $J_{CP} = 3.6$  Hz), 124.73 (d,  $J_{CP} = 3.2$  Hz), 124.23 (m),

124.15 (d,  $J_{CP}$  = 4.1 Hz), 123.80 (m), 123.62 (d,  $J_{CP}$  = 3.3 Hz), 63.36 (d,  $J_{CP}$  = 8.3 Hz), 63.12 (d,  $J_{CP}$  = 6.6 Hz), 62.94 (t,  $J_{CP}$  = 3.4 Hz), 62.92 (t,  $J_{CP}$  = 4.5 Hz), 54.00 (s), 46.80 (s), 27.48 (d,  $J_{CP}$  = 1.0 Hz), 27.35 (s), 27.18 (s), 26.99 (s), 25.85 (s), 25.71 (d,  $J_{CP}$  = 1.0 Hz), 25.52 (s), 25.40 (s), 25.36 (s), 24.91 (d,  $J_{CP}$  = 1.6 Hz), 24.86 (s), 16.78 (d,  $J_{CP}$  = 4.8 Hz), 16.67 (d,  $J_{CP}$  = 3.9 Hz), 16.24 (d,  $J_{CP}$  = 6.8 Hz), 16.09 (d,  $J_{CP}$  = 6.7 Hz).  $^{31}\text{P}\{^1\text{H}\}$ -NMR (162 MHz,  $\text{C}_6\text{D}_6$ ):  $\delta$  9.0, -0.2.

**EA:** Calc'd for  $\text{C}_{36}\text{H}_{65}\text{N}_4\text{NbO}_6\text{P}_2$ : C 53.73, H 8.14, N 6.96; Found: C 53.94, H 8.44, N 6.76.

**Synthesis of bis(*N*-isopropylbis(dimethylamino)phosphoramidato)dimethylamido-*N*-methylniobaziridine (3.20).** In a glovebox, a solution of *N*-(*N*-isopropylbis(dimethylamino)phosphoramidate) (0.185 g, 0.958 mmol) in toluene (~ 4 mL) was added to a stirring solution of deep brown  $\text{Nb}(\text{NMe}_2)_5$  (0.150 g, 0.479 mmol) in toluene (~ 1 mL). The resulting solution was stirred for 12 hours. The solution was then concentrated *in vacuo*. The sticky semi-solid was dissolved in a minimal amount of toluene at ambient temperature and then cooled for 10 minutes at -35 °C. The yellow solution was then layered with a small amount of hexanes (~ 0.5 mL) and stored in the freezer at -35 °C to promote recrystallization. The product recrystallized over 24 h to yield pale yellow crystals (0.176 g, 65%).  $^1\text{H}$ -NMR (600 MHz,  $\text{C}_6\text{D}_6$ ):  $\delta$  4.08 (s, 3H), 3.90 (br. s, 1H), 3.63 (br. s, 1H), 3.40 (br. s, 6H), 2.65 (d,  $J$  = 8.8 Hz, 6H), 2.62 (d,  $J$  = 9.4 Hz, 6H), 2.54 (d,  $J$  = 9.4 Hz, 6H), 2.41 (d,  $J$  = 8.8 Hz, 6H), 1.38-1.31 (m, 12H).  $^{13}\text{C}\{^1\text{H}\}$ -NMR (151 MHz,  $\text{C}_6\text{D}_6$ ):  $\delta$  52.8 (s), 49.6 (s), 48.7 (s), 47.7 (s), 37.67 (t,  $J_{CP}$  = 3.3 Hz), 37.65 (t,  $J_{CP}$  = 3.3 Hz), 37.5 (d,  $J_{CP}$  = 4.9 Hz), 37.3 (d,  $J_{CP}$  = 4.4 Hz), 28.4 (d,  $J_{CP}$  = 5.0 Hz), 26.7 (d,  $J_{CP}$  = 11.2 Hz), 26.1 (d,  $J_{CP}$  = 7.5 Hz), 25.8 (d,  $J_{CP}$  = 3.5 Hz).  $^{31}\text{P}\{^1\text{H}\}$ -NMR (121 MHz,  $\text{C}_6\text{D}_6$ ):  $\delta$  34.6 (br. s), 24.6 (br. s). **EA:** Calc'd for  $\text{C}_{18}\text{H}_{49}\text{N}_8\text{NbO}_2\text{P}_2$ : C 38.30, H 8.75, N 19.85; Found: C 38.45, H 8.79, N 19.86.

**Synthesis of (N-phenyl-O,O'-diethylphosphoramidato)bis(dimethylamido)2,6-dimethylphenylimidoNb(V) (3.21).** In the glovebox, a Schlenk flask was charged with a solution of **3.13** (0.115 g, 0.231 mmol) in 5 mL toluene. While stirring, a solution of 2,6-dimethylaniline (0.028 g, 0.231 mmol) in 5 mL toluene was added dropwise over 15 minutes. The Schlenk flask was then sealed with a greased stopper and greased key, secured with elastics, removed from the box, and heated (while sealed) at 50 °C for 12 hours. The Schlenk flask was then returned to room temperature, attached to the Schlenk manifold, and concentrated *in vacuo* to a yellow solid. The evacuated Schlenk flask was then returned to the glovebox. The crude solid was dissolved in minimal amount of toluene at ambient temperature and then cooled for 10 minutes at -35 °C. The yellow solution was then layered with a small amount of hexanes (~ 0.5 mL) and stored in the freezer at -35 °C to promote recrystallization. The product recrystallized over 24 h to yield pale yellow crystals (0.030 g, 25%). **<sup>1</sup>H-NMR** (300 MHz, Tol-*d*<sub>8</sub>): δ 7.36-7.32 (m, 2H), 6.98-6.96 (m, 2H), 6.92-6.89 (m, 2H), 6.75-6.69 (m, 2H), 3.94-3.76 (m, 4H), 3.53 (s, 12H), 2.47 (s, 6H), 0.99 (td, *J*<sub>HH</sub> = 7.1, *J*<sub>HP</sub> = 0.6 Hz, 6H). **<sup>13</sup>C{<sup>1</sup>H}-NMR** (75 MHz, Tol-*d*<sub>8</sub>): δ 133.8, 122.9, 122.6, 122.4, 121.9, 63.08 (d, *J*<sub>CP</sub> = 4.8 Hz), 49.65, 19.46, 15.96 (d, *J*<sub>CP</sub> = 6.2 Hz). (aryl peaks hidden by solvent, solvent used due to solubility). **<sup>31</sup>P{<sup>1</sup>H}-NMR** (121 MHz, Tol-*d*<sub>8</sub>): δ 11.92. **EA:** Calc'd for C<sub>22</sub>H<sub>36</sub>N<sub>4</sub>NbO<sub>3</sub>P: C 50.00, H 6.87, N 10.60; Found: C 50.55, H 6.73, N 9.98.

**General procedure for catalytic hydroaminoalkylation reactions with isolated niobium complexes.** In the glovebox at room temperature, 0.025 mmol (5 mol%) of metal pre-catalyst was dissolved in 0.30 g toluene-*d*<sub>8</sub> in 1-dram vial. In a separate 1-dram vial, 0.5 mmol of amine substrate was dissolved in 0.30 g toluene-*d*<sub>8</sub>. In a third 1-dram vial, 0.75 mmol of alkene (or

alkyne) was weighed. The solution of amine was then added to the alkene (or alkyne) and mixed thoroughly to ensure a homogenous mixture. The substrate solution was then added to the pre-catalysts solution, and mixed thoroughly to ensure a homogeneous mixture. The reaction mixture was then transfer to a J. Young NMR tube and sealed with a Teflon screw-type cap. A  $^1\text{H}$  NMR spectrum was then recorded for reference, as  $t = 0$  h. The NMR tube was placed in a thermostated oil bath on a hot plate, preset for the desired reaction temperature. After the desired reaction time, the J. Young NMR tube was removed from the hot oil bath and a  $^1\text{H}$  NMR spectrum was recorded. Conversion was determined by integration of peak(s) of desire product to peak(s) of substrate amine, and reported as conversion with respect to the amine substrate (conversion = normalized integration of product amine / sum of normalized integration of product and substrate amines). Chemical shifts of products were obtained from literature values.<sup>9,10,22,23</sup>

In situations where the pre-catalyst complex is not defined, *in situ* preparation was used to insure the concentration of metal species was accurately defined. In the glovebox at room temperature, 0.025 mmol of  $\text{Nb}(\text{NMe}_2)_5$  was dissolved in 0.30 g toluene- $d_8$ . In a second 1-dram vial, 0.050 mmol of phosphoramidate ligand was dissolved in 0.30 g toluene- $d_8$ . The protioligand solution was then added to and thoroughly mixed with the solution of  $\text{Nb}(\text{NMe}_2)_5$ . The solution was then added to a J. Young NMR tube and sealed with a Teflon screw-type cap. The NMR tube was shaken vigorously for ~3 minutes, after which  $^1\text{H}$  and  $^{31}\text{P}\{^1\text{H}\}$  NMR spectra were recorded to confirm the absence of starting reagents. Utilizing this procedure, in no instances were starting reagents observed in the NMR spectra. The J. Young NMR tube was then taken back into the glovebox. In separate 1-dram vials, the amine substrate and alkene (or alkyne) substrate were

weighed. Following this, the contents of the NMR tube was first added to the amine substrate, and mixed thoroughly to ensure a homogenous mixture. This mixture was then added to the alkene (or alkyne) substrate, and mixed thoroughly to ensure a homogenous mixture. This mixture was then charged to the same J. Young NMR tube. From here the procedure recorded above for reactions with isolated niobium complexes was followed.

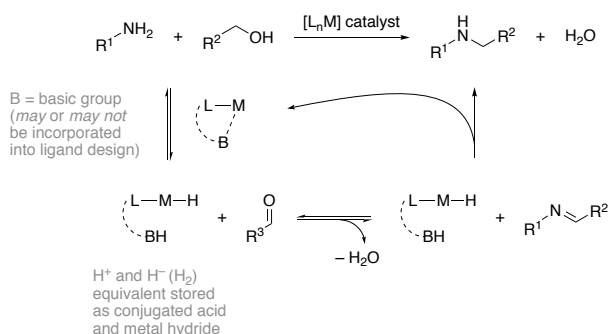


## **Chapter 4: 6-Substituted-2-Pyridonate and 2-Pyridonate Ligated Ru, Rh, and Ir Complexes for the Activation of Unprotected Amines – Efforts Towards Hydroaminoalkylation Catalysis for the $\alpha$ -Functionalization of Amines**

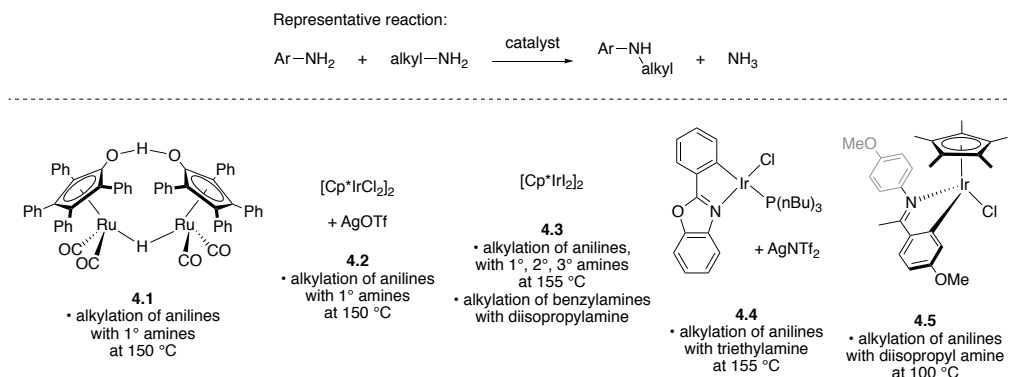
### **4.1 Introduction**

#### **4.1.1 Alkylation of Amines through Hydrogen-Borrowing Catalysis**

Recently, hydrogen-borrowing catalysis, also termed hydrogen auto-catalysis or hydrogen auto-transfer, has garnered significant interest in the literature for the *N*-alkylation of amines with alcohols (Scheme 4.2).<sup>212-217</sup> This chemistry has been reported for a variety of late transition metal homogeneous and heterogeneous catalysts, including those utilizing 2-hydroxypyridine ligands (or ligands containing the 2-hydroxypyridine fragment) as detailed in Chapter 1. Here, the alcohol is converted to a carbonyl by deprotonation and  $\alpha$ -C–H activation resulting in the effective loss of one equivalent of H<sub>2</sub> in the form of a proton and a metal hydride species (Scheme 4.2). The mechanism of this step likely depends on the complex and ligand design. For 2-pyridonate Ir species, DFT calculations suggest a concerted mechanism (often more specifically referred to as metal-ligand cooperativity or a bifunctional ligand-assisted mechanism) over a step-wise,  $\beta$ -H elimination mechanism. Subsequently, the amine and carbonyl undergo condensation to produce an imine and water, and, finally, the imine species is reduced by the ‘H<sub>2</sub>’ equivalent to the *N*-alkylated amine product.



**Scheme 4.2** *N*-alkylation of amines with alcohols *via* hydrogen borrowing catalysis



**Scheme 4.1** *N*-alkylation of amines with alkylamines *via* hydrogen-borrowing catalysis

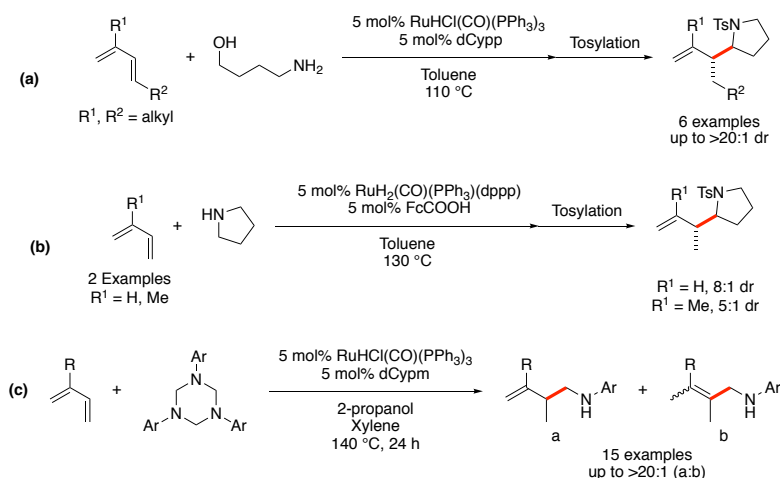
Interestingly, specific complexes were also found to be able to perform the *N*-alkylation of amines utilizing a sacrificial amine as the alkylation reagent (Scheme 4.1).<sup>218-223</sup> These reactions require higher temperatures (100-155 °C) as the C–H activation of amines to produce the an intermediate imine product is more challenging than the alcohol to carbonyl conversion.<sup>224</sup> The precatalyst systems **4.1** – **4.5** in (Scheme 4.1) all produce *N*-alkylation of anilines to the secondary *N*-alkylaniline utilizing primary, secondary, or tertiary amines as the alkyl source. Precatalyst **4.5** provides the only examples of alkylation of benzylamines, where they utilize diisopropylamine. Substrate scope is (almost exclusively) limited to the formation of non-nucleophilic and sterically hindered *N*-alkylanilines as these do not appear to readily form the intermediate iminium cation necessary to produce the tertiary *N,N*-dialkylaniline product. While

not necessarily a practical synthetic route, unlike the same reaction with alcohols, the effective dehydrogenation of an amine to produce a metal hydride and proton equivalent is of interest as these types of intermediates can be utilized in other catalytic processes, such as hydroaminoalkylation.

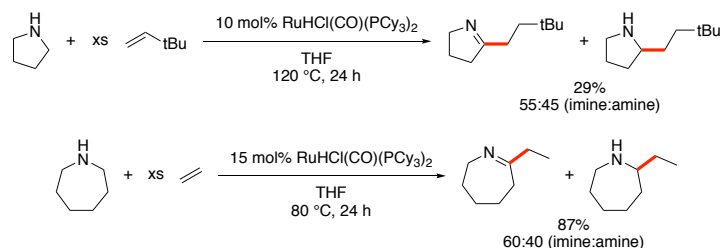
The Krische group has exploited and advanced the hydrogen-borrowing approach to produce  $\alpha$ -alkylated *N*-heterocycles from amino-alcohols and dienes (Scheme 4.4).<sup>195</sup> The products here are the same as would result from a hydroaminoalkylation reaction between the *N*-heterocycle and the diene. This Ru catalyzed reaction occurs via a modified hydrogen-borrowing mechanism: first, dehydrogenation of the alcohol produces an aldehyde and a Ru–H; second, cyclization to the cyclic imine occurs; third, insertion of the diene into the Ru–H bond generates a Ru-allyl species; fourth, C–C coupling occurs generating a Ru-amido complex; fifth, protonation of the Ru-amido species regenerates the catalyst and releases the product. A single example is provided where pyrrolidine is functionalized directly (Scheme 4.4b). This concept has also been expanded to a similar system where *N*-arylmethanimines (generated *in situ* from *N*-aryltriazene) are  $\alpha$ -functionalized by dienes using 2-propanol as the reducing agent in a related transfer hydrogenation (Scheme 4.4c).<sup>196</sup> This produces products that can conceptually be derived from hydroaminoalkylation (from *N*-methylaniline and diene) or hydroaminomethylation (from aniline, diene, CO, and H<sub>2</sub>).

Another report from the Yi group demonstrates the possibility of hydroaminoalkylation through this approach with the  $\alpha$ -alkylation of amines with alkenes (Scheme 4.3).<sup>137</sup> This is presumed to occur through a similar mechanism as described above. Here, the major product is the  $\alpha$ -alkylated imine, with the desired  $\alpha$ -alkylated amine as the byproduct. Presumably, the

imine product results from a dehydrogenation of the amine product, likely using the large excess of alkene (6 – 10 equivalents to amine) as the hydrogen acceptor.



**Scheme 4.4 Ru-catalyzed synthesis of  $\alpha$ -alkylated amines**

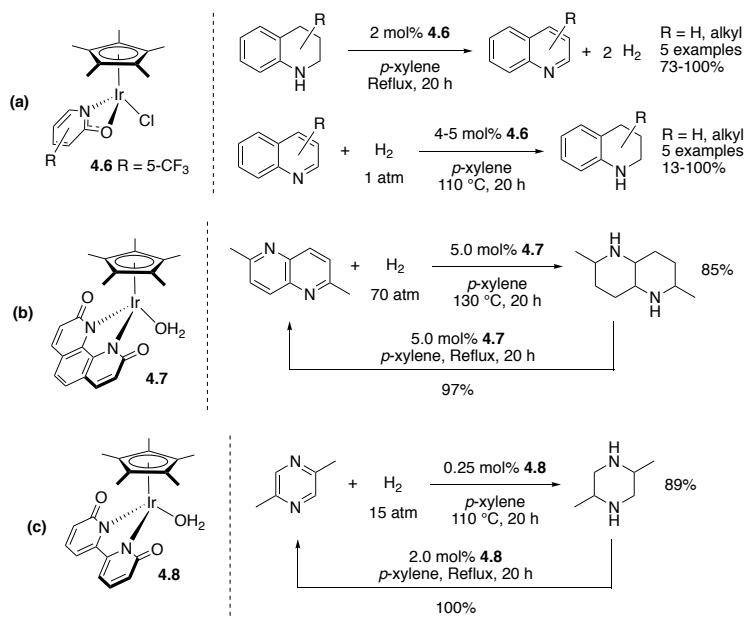


**Scheme 4.3  $\alpha$ -Alkylation of cyclic amines with alkenes**

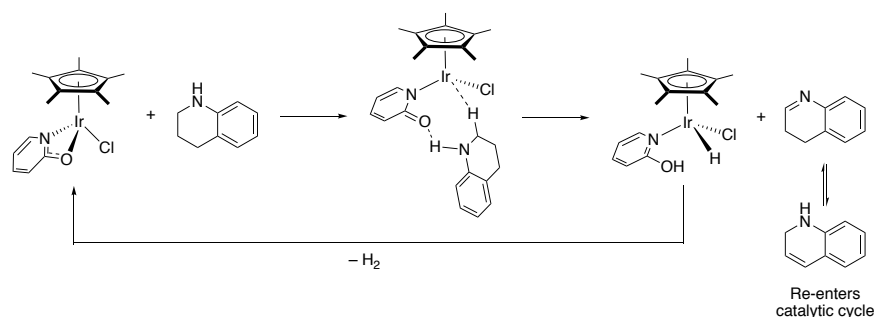
#### 4.1.2 Acceptorless Dehydrogenation of Amines

A metal-hydride intermediate generated from the dehydrogenation of an amine can also be intercepted by a C-C unsaturation (such as an alkene) leading to the catalytic transfer dehydrogenation and subsequent hydrogenation of the unsaturation.<sup>224</sup> Recently, multiple examples have been discovered where the metal-hydride can be intercepted by an appropriately acidic proton to generate  $H_2$ ; when done catalytically, this reaction is termed the acceptorless dehydrogenation of amines.<sup>78-80,225-234</sup> While thermodynamically unfavorable, the release of gaseous hydrogen drives the reaction forward and avoids the use of an acceptor or stoichiometric oxidant to generate an imine.

2-Hydroxypyridine/2-pyridonate ligands have been used in Ir complexes for both the acceptorless dehydrogenation, and the reverse hydrogenation reaction under hydrogen atmosphere (Scheme 4.5). Notably, complete dehydrogenation occurs utilizing these catalyst systems. DFT calculations based on complex **4.6** propose a concerted dehydrogenation step (vs.  $\beta$ -hydrogen elimination steps), followed by isomerization of the *N*-heterocycle to allow for another  $\alpha$ -C–H activation (vs. C–H activation at other positions) (Scheme 4.6).<sup>235</sup> The interconversion of 2,6-dimethylpyrazine and 2,6-dimethylpiperazine (Scheme 4.5b) is proposed for use in H<sub>2</sub> storage systems as the reaction can be performed under neat conditions in both directions, and 2,6-dimethylpiperazine has a high gravimetric H<sub>2</sub> capacity of 5.3 weight percent.<sup>80</sup>



**Scheme 4.5** Acceptorless dehydrogenation of *N*-heterocycles by 2-pyridonate Ir complexes



**Scheme 4.6 Mechanism for the acceptorless dehydrogenation of 1,2,3,4-tetrahydroquinoline proposed by DFT calculations**

A variety of additional complexes are also utilized for the acceptorless dehydrogenation of amines (Figure 4.1). Complexes **4.1**, and **4.9** – **4.11** have been reported for the acceptorless dehydrogenation *N*-heterocycles.<sup>228,230-232</sup> Complex **4.11** has also been reported for the reverse, hydrogenation reaction. Notably, complex **4.9** is reported to dehydrogenate primary amines to the nitrile product in good to high yields with high selectivity.<sup>230</sup> Complexes **4.12** – **4.14** have been reported for the dehydrogenation of primary amines, however, newly formed imine and amine condense to form the *N*-substituted imine and releasing an equivalent of ammonia.<sup>225-226,229</sup> With the exception of complex **4.15**, all other complexes catalyze acceptorless dehydrogenative reactions at >110 °C. Rh complex **4.15** operates at room temperature but under photolytic conditions (450 W Hg lamp).<sup>227</sup> Arene supported Ru complexes **4.16** and **4.17** were studied comparatively to see if tethered amine groups (**4.16**) could play a significant role in acceptorless dehydrogenation. Catalytic reactions with benzylamine reveal a mixture of nitrile, imine, and dibenzylamine products with similar ratios and rates for both **4.16** and **4.17**.<sup>233</sup> Complex **4.18** was found to dehydrogenate benzylamine to mixtures of imine, dibenzylamine, and small amounts of tribenzylamine.<sup>234</sup>

## 4.2 Scope of Chapter

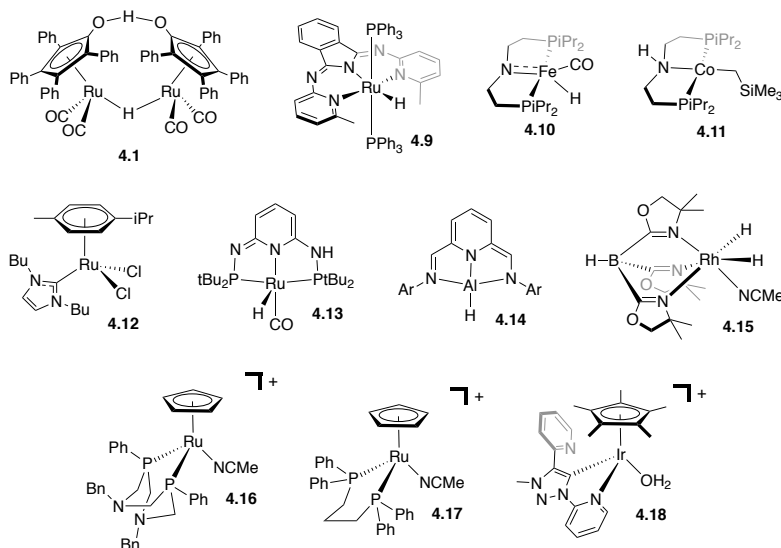
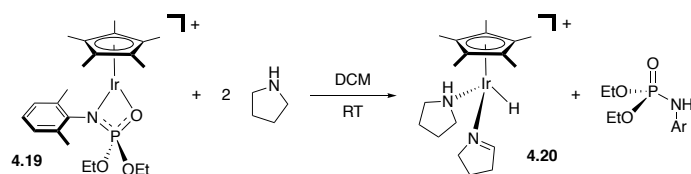


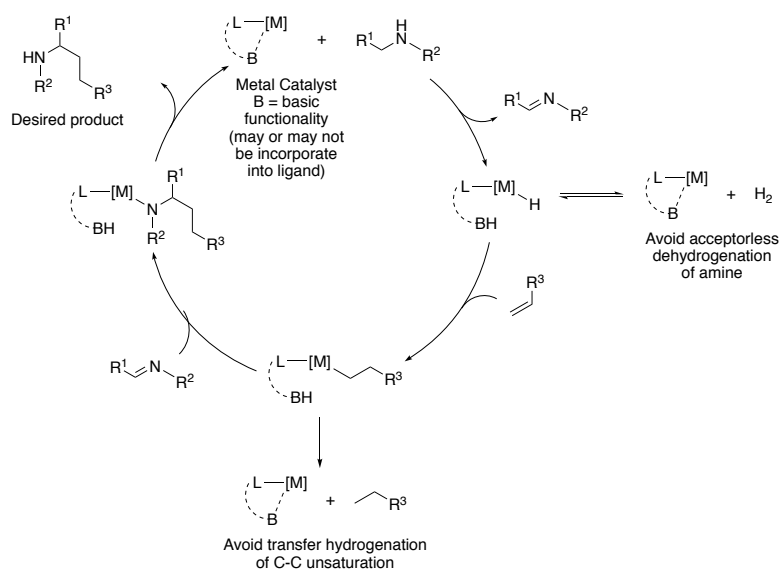
**Figure 4.1** Transition-metal complexes reported to catalyze the acceptorless dehydrogenation of amines

Recently, our group has reported the stoichiometric dehydrogenation of pyrrolidine and piperidine using a 1,3-*N,O*-chelated phosphoramidate Ir(III) complex **4.19** to produce Ir–H complex **4.20** and one equivalent of phosphoramidate (Scheme 4.7).<sup>236</sup> Notably, this reaction occurs at room temperature. This result, combined with the significant use of the 2-pyridonate motif used for dehydrogenation/hydrogenation chemistry (outlined above and in Chapter 1), lead us to propose that 2-pyridonate or tethered-2-pyridonate ligands may be effective ligands on Ru, Rh, or Ir complexes for use in the hydroaminoalkylation of unprotected amines utilizing a synthetic strategy similar to that described above for the Ru-catalyzed reactions (*vide supra*).



**Scheme 4.7** Stoichiometric dehydrogenation of pyrrolidine by a 1,3-*N,O*-chelated phosphoramidate Ir complex

Multiple steps must be achieved, and multiple side reactions must be suppressed to realize a general catalytic methodology for this reaction. A ligand and complex design approach was adopted to work toward this goal. Scheme 4.8 outlines the catalytic cycle for the hydrogen-borrowing approach to hydroaminoalkylation using a secondary amine and alkene. The first step in the catalytic cycle could potentially be addressed by extending the chemistry realized with **4.19** (Scheme 4.8) but with 2-pyridonate ligands as they have improved donor properties in the 2-hydroxypyridine form to allow for coordination to the metal center. Acceptorless dehydrogenation from the release of  $H_2$  is a potential off-cycle pathway. After insertion of the alkene into the M–H, protonation of the M–C bond, resulting in a transfer hydrogenation of the alkene, could occur. The basic functionality (B, Scheme 4.8) must be designed such that its conjugate acid (BH, Scheme 4.8) is not acidic enough to protonate the M–H or M–C bond. Alternatively, the basic functionality may be chosen to have poor binding affinity for the metal complex thereby creating an alternative thermodynamic preference to avoid the undesired side-reactions. The desired catalytic metal complex must then provide the correct environment to



**Scheme 4.8** Proposed catalytic cycle for the late-transition metal catalyzed hydroaminoalkylation of amines



accommodate insertion of the imine into the M–C bond to achieve C–C bond formation. Finally, protonation of the amide ligand provides the  $\alpha$ -alkylated, hydroaminoalkylation product.

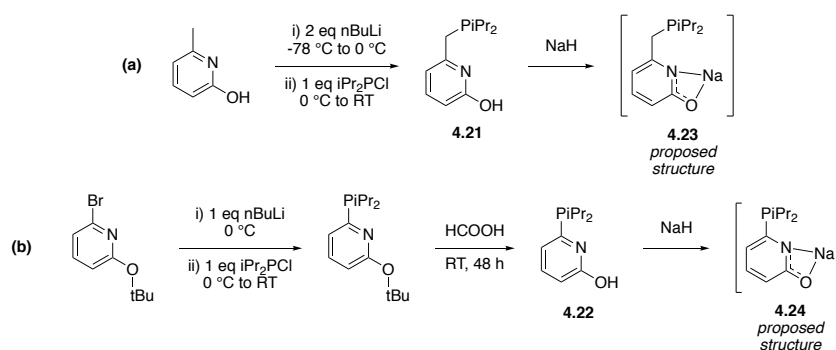
To this end, this chapter details the synthesis of 6-phosphinomethyl- and 6-phosphino-2-pyridone ligands and their use in the subsequent synthesis of Ru, Rh, and Ir complexes. These complexes as well as known 2-pyridonate complexes are explored for their reactivity toward secondary amines specifically targeting the catalytic  $\alpha$ -alkylation with dienes and acceptorless dehydrogenation chemistry.

## 4.3 Results and Discussion

### 4.3.1 Arene Supported Ru, Rh, and Ir Complexes and Reactivity

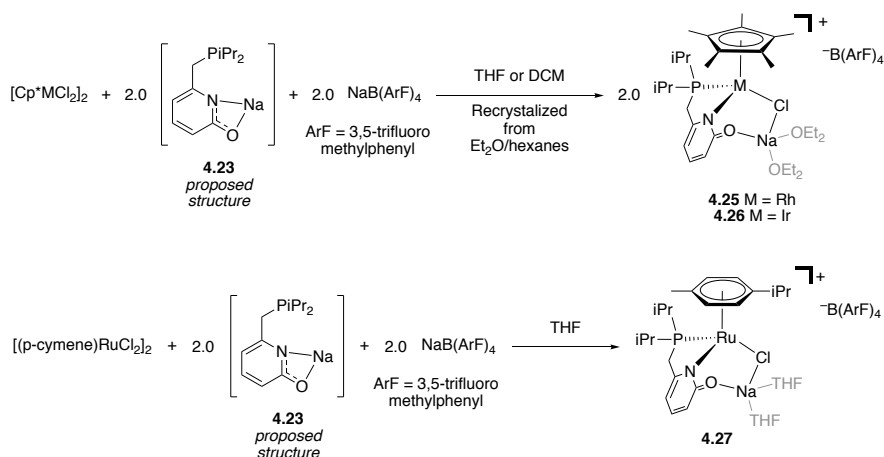
The efforts of Krische and co-workers,<sup>195-196</sup> and Yi and co-workers,<sup>137</sup> to achieve hydroaminoalkylation chemistry make use of electron-rich phosphine ligands (e.g. bis(dicyclohexylphosphino)propane, bis(dicyclohexylphosphino)methane, tricyclohexylphosphine). Taking inspiration from their work, we endeavored to synthesize bidentate ligands incorporating both an electron-rich phosphine tethered to a 2-pyridone fragments. Additionally, we wanted to explore ligand derivatives that could provide us with variation in the chelate ring size to explore how that may affect complex synthesis and/or reactivity. Literature procedures for the synthesis of diphenylphosphino-2-pyridone ligands were adapted to synthesize the new variants **4.21** and **4.23** that incorporate more electron rich diisopropylphosphine moiety (Scheme 4.9).<sup>33,237</sup> It was found that these ligands could be easily deprotonated with NaH to generate the sodium-2-pyridonate derivatives (**4.23** and **4.24**) for use in salt metathesis reactions.

Reactions of the Na salt **4.23** with [Cp\*RhCl<sub>2</sub>]<sub>2</sub>, [Cp\*IrCl<sub>2</sub>]<sub>2</sub>, and [(*p*-cymene)RuCl<sub>2</sub>]<sub>2</sub> starting materials, followed by the one-pot addition of NaB(ArF)<sub>4</sub> (ArF = 3,5-triflu

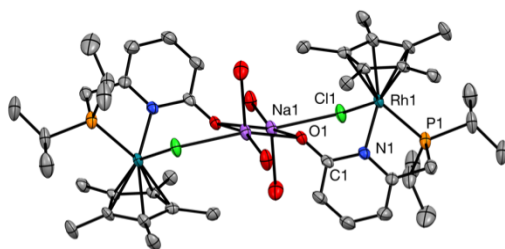


**Scheme 4.9 Synthesis of bidentate phosphine-2-pyridone ligands**

oromethylphenyl), results in the formation of new cationic complexes **4.25**, **4.26**, and **4.27** (Scheme 4.10). Single crystals of the Rh complex **4.25** suitable for single crystal X-ray diffraction were obtained with the tetraphenylborate anion, which recrystallizes as a dimeric structure. X-ray diffraction data obtained for **4.25** and **4.26** reveal three-legged piano-stool complexes, instead of the expected two-legged piano-stool, unsaturated complex (Figure 4.2). Both structures reveal coordination of one Na ion per metal center, supported by the carbonyl oxygen of the 2-pyridonate ligand, the chloride, and solvent molecules. Analysis of the solid-state molecular structures reveals an anionic  $\kappa^2$ -*P,N*-2-pyridonate binding mode and similar bonding metrics for both Rh and Ir. The 2-pyridonate fragment is found to be in a conjugated amide structure, with a C1–O1 bond length (1.260(4) Å for **4.25**, 1.246(8) Å for **4.26**) representative of a carbonyl functional group. While the solid-state molecular structure of complex **4.25** was obtained with a different anion ( $\text{BPh}_4^-$  vs.  $\text{B}(\text{ArF})_4^-$ ), elemental analysis of the products [**4.25**][ $\text{B}(\text{ArF})_4^-$ ] and [**4.26**][ $\text{B}(\text{ArF})_4^-$ ] confirms the molecular formulas as illustrated in Scheme 4.10. The incorporation of the Na ion suggests a highly Lewis basic oxygen in the 2-pyridonate moiety, potentially suitable for deprotonation, as proposed.

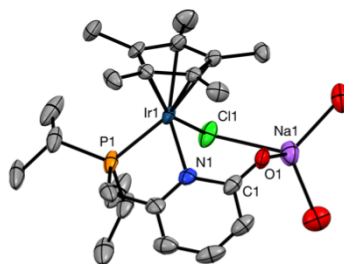


**Scheme 4.10** Synthesis of Rh, Ir and Ru complexes **4.25**, **4.26**, and **4.27**



**[4.25][BPh<sub>4</sub>]** THF, H-atoms, and BPh<sub>4</sub> removed for clarity. Thermal ellipsoids are shown at 50%.

Select bond lengths (Å)  
 Rh–P 2.315(1)      C1–O1 1.260(4)  
 Rh–N 2.129(3)      C1–N1 1.384(4)  
 Rh–Cl 2.4122(9)



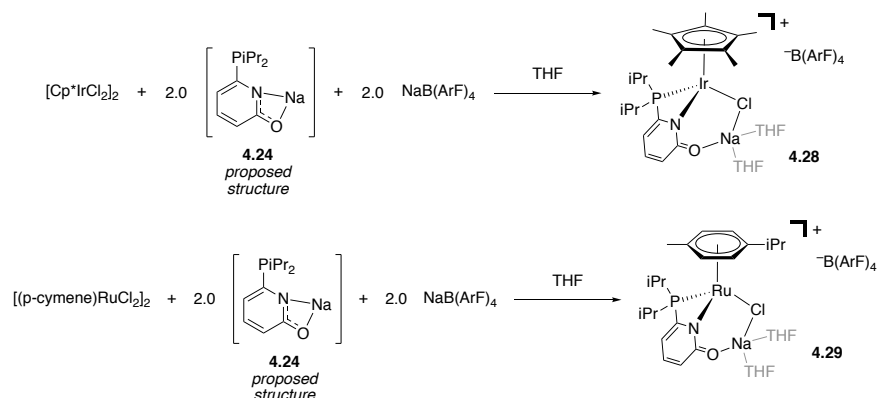
**[4.26][B(ArF)<sub>4</sub>]** Et<sub>2</sub>O, H-atoms, and B(ArF)<sub>4</sub> removed for clarity. Thermal ellipsoids are shown at 50%.

Select bond lengths (Å)  
 Ir–P 2.306(2)      C1–O1 1.246(8)  
 Ir–N 2.137(4)      C1–N1 1.390(9)  
 Ir–Cl 2.421(1)

**Figure 4.2** ORTEP representations of the solid-state molecular structures of **4.25** and **4.26**

<sup>1</sup>H NMR spectroscopy of **4.25** and **4.26** confirms the solid-state structures are present in solution as the isopropyl groups of the phosphine are inequivalent as expected. If an unsaturated, two-legged piano stool complex was formed in solution, the isopropyl group may be expected to present as equivalent. <sup>1</sup>H and <sup>31</sup>P{<sup>1</sup>H} NMR spectroscopy of **4.25** exhibit significant broadening of the signals indicative of a fluxional species. In particular, <sup>31</sup>P{<sup>1</sup>H} NMR signal has poor intensity and suffers from significant broadening, but does present as the doublet expected from Rh coupling (<sup>1</sup>J<sub>PRh</sub> = 129.3 Hz). Signals for Et<sub>2</sub>O in the <sup>1</sup>H NMR spectrum appear sharp, suggesting the solvent (THF-*d*<sub>8</sub>) replaces the Na coordinated Et<sub>2</sub>O in the structure in solution.

While the Ru complex **4.27** proved resistant to recrystallization,  $^1\text{H}$  and  $^{31}\text{P}\{^1\text{H}\}$  NMR spectroscopy revealed a single product of high purity with spectroscopic signatures of the ligand environment almost identical to that in **4.26**. The structure of **4.27** is thus assigned based on analogy to the Rh and Ir analogues. In the case of Ru, significant amounts of THF (the solvent used for synthesis) that are observed and are likely coordinated to the Na ion.

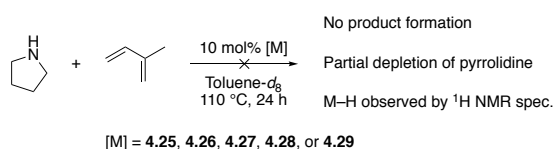


**Scheme 4.11** Synthesis of small-bite-angle complexes **4.28** and **4.29**

Arene-supported complexes derived from ligand **4.22** would likely form a small-bite-angle 4-membered chelate upon complexation. The strain introduced in a small bite angle chelate may allow for different reactivity from the complexes prepared from **4.23**. In particular, this could allow for the ligand to more readily adopt a  $\kappa^1\text{-P}$  binding mode upon formation of the neutral 2-pyridone, allowing for an open coordination site at the metal center. The same synthetic pathway as above was employed utilizing ligand salt **4.24** to generate complexes **4.28** and **4.29** (Scheme 4.11). Unfortunately, these complexes were resistant to recrystallization. Fortunately, the  $^1\text{H}$  and  $^{31}\text{P}\{^1\text{H}\}$  spectra for both complexes exhibit a single complex in high purity, consistent with the representation in Scheme 4.11. The  $^1\text{H}$  NMR spectra reveal asymmetric complexes with independent isopropyl groups, analogous to that found in structurally characterized complexes **4.25** and **4.26**.  $^{31}\text{P}\{^1\text{H}\}$  spectroscopy confirms a small bite angle with

both complexes having a significantly upfield and negative chemical shift (**4.28**,  $\delta$  -27.8; **4.29**,  $\delta$  -6.3). The negative  $^{31}\text{P}\{^1\text{H}\}$  NMR resonance is consistent with and indicative of a  $\kappa^2\text{-P,N}$  binding mode.<sup>238</sup>

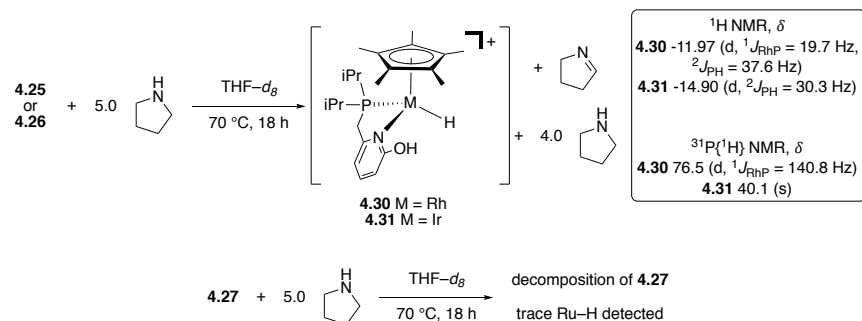
As the Krische group has seen success with pyrrolidine and dienes,<sup>195</sup> the hydroaminoalkylation of isoprene with pyrrolidine was attempted with complexes **4.25** – **4.29** (Scheme 4.12). No coupling of pyrrolidine and isoprene was observed by  $^1\text{H}$  NMR spectroscopy or detected by HPLC/ESI-MS. Interestingly, a small depletion of pyrrolidine was observed and formation of signals consistent with a metal hydride was observed in the  $^1\text{H}$  NMR spectrum.



**Scheme 4.12 Attempted hydroaminoalkylation of isoprene with pyrrolidine**

The dehydrogenation of pyrrolidine was further evaluated by reacting each complex with 5 equivalents of pyrrolidine (Scheme 4.13). The Rh and Ir complexes were completely converted to their corresponding metal hydride species (**4.30** and **4.31**) with a concomitant loss of 1 equivalent of pyrrolidine as determined by  $^1\text{H}$  and  $^{31}\text{P}$  NMR spectroscopy. The  $^1\text{H}$  NMR spectra reveal a phosphine coupled doublet of doublets for the Rh complex (**4.30**,  $\delta$  -11.97,  $^1J_{\text{RhP}} = 19.7$  Hz,  $^2J_{\text{PH}} = 37.6$  Hz), and doublet for the Ir complex (**4.31**,  $\delta$  -14.90,  $^2J_{\text{PH}} = 30.3$  Hz) for the hydride signals. The same reaction can also be performed in toluene- $d_8$ . Heating for an additional 48 h at 110 °C brings about no change in the reaction mixture, with no further depletion of amine, indicating a highly stable hydride species. The same reaction with the Ru complex **4.27** (THF- $d_8$ , 70 °C, 18 h) results in only trace hydride formation as well as other unidentified species. Interestingly, in excess pyrrolidine the expected –OH resonance is not observed in the

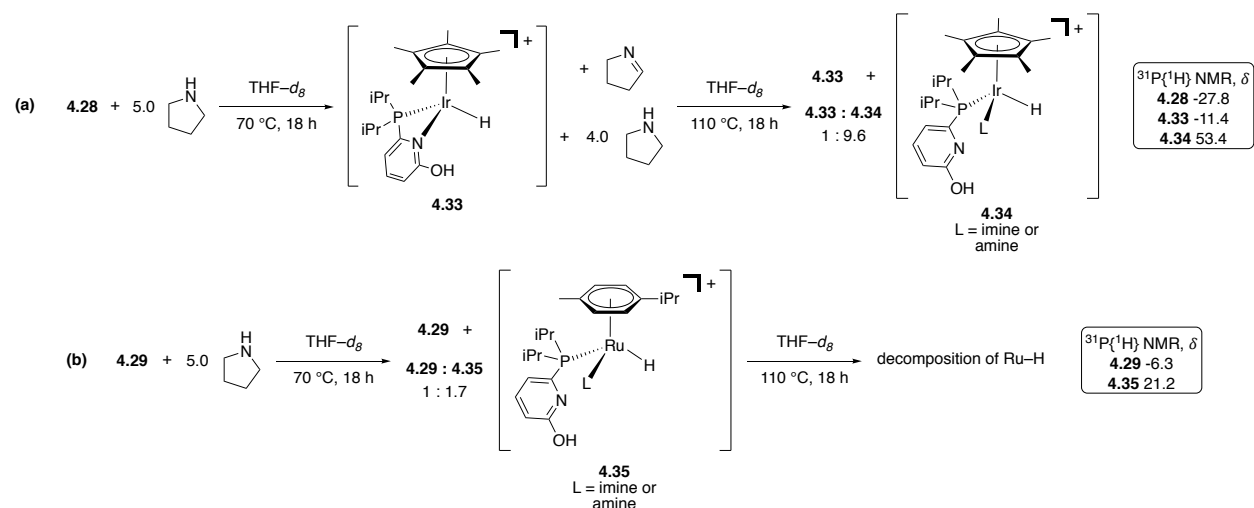
$^1\text{H}$  NMR spectra. This could potentially be due to hydrogen bonding interactions with free pyrrolidine in solution. However, this can be observed in an isolated sample of **4.31** (*vide infra*).



**Scheme 4.13** Reaction of **4.25**, **4.26**, and **4.27** with 5 equivalents of pyrrolidine

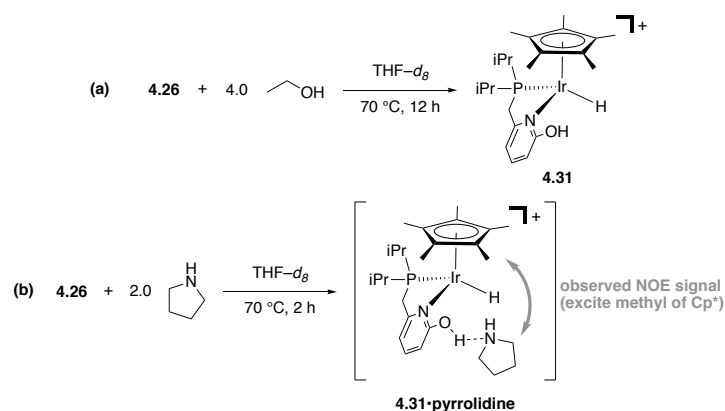
Reactivity of **4.28** and **4.29** show different reactivity due to their small-bite-angle. Both complexes were dissolved in THF- $d_8$  with 5 equivalents of pyrrolidine in a sealed J. Young NMR tube then heated for 18 h at 70 °C, followed by additional heating for 18 h at 110 °C (Scheme 4.14). Complex **4.28** is first transformed into Ir-H **4.33** ( $^{31}\text{P}\{^1\text{H}\}$   $\delta$  -11.4), with the loss of one equivalent of pyrrolidine. Additional heating at 110 °C results in a mixture of **4.33** and  $\kappa^1$ -*P* bound **4.34**, where the binding mode is suggested based on the significantly downfield shift of the  $^{31}\text{P}\{^1\text{H}\}$  NMR resonance ( $^{31}\text{P}\{^1\text{H}\}$   $\delta$  53.4, Scheme 4.14a). The Ru complex **4.29** results in formation of  $\kappa^1$ -*P* bound **4.35** (assigned by the upfield shift of the signal in the  $^{31}\text{P}\{^1\text{H}\}$  NMR spectrum) in a 1.6:1 ratio of **4.35** to **4.29** (Scheme 4.14b). Interestingly, no Ru-H species with a  $\kappa^2$ -*P,N* binding mode is observed. Further heating at 110 °C results in decomposition of the Ru complexes, as evidenced by baseline signals only being observable in the  $^{31}\text{P}\{^1\text{H}\}$  NMR spectrum. No further conversion of the pyrrolidine is apparent by  $^1\text{H}$  NMR spectroscopy. Both of the proposed  $\kappa^1$ -*P* complexes [**4.34**] and [**4.35**] are assigned a neutral donor, **L**, based on general electron counting rules (to create an 18  $e^-$  complex). However, the number of signals in the  $^1\text{H}$  NMR spectra prevents further assignment of complexation. These results demonstrate the small-

bite-angle derivatives offer hemi-labile coordination/de-coordination. Additionally, the Ir variant requires a higher activation energy than the Ru example to access de-coordination of the pyridine fragment. Similar to the large-bite-angle complexes, no acceptorless dehydrogenation is observed in these reactions.



**Scheme 4.14** Reaction of **4.28** and **4.29** with 5 equivalents of pyrrolidine

With precedence for 2-pyridonate Ir complexes to be active catalysts for acceptorless dehydrogenation (see Chapter 4.2.1), we further explored **4.26** toward this reaction. A frozen solution of **4.26** in a sealed J. Young NMR tube was backfilled with  $\sim 1$  atm of  $\text{H}_2$ . Heating to  $110\text{ }^{\circ}\text{C}$  over 24 h resulted in no reaction. This demonstrates that if  $\text{H}_2$  release was occurring in the above stoichiometric dehydrogenations, it is not reversible. We also found that a reaction of **4.25** with excess piperidine and diethylamine resulted in the same Ir-H **4.31** (THF- $d_8$ ,  $80\text{ }^{\circ}\text{C}$ , 18 h). Curiously, *N*-methylaniline only produces 30% of hydride **4.31** under the same reaction conditions. This slow reaction rate could be due to an induction period required to break apart the Na-Cl complex or, alternatively, could indicate a requirement for an electron rich amine in the dehydrogenation step. In all cases, no catalytic acceptorless dehydrogenation or additional conversion of the amine was observed.



**Scheme 4.15** Synthesis and isolation of **4.31** and **4.31•pyrrolidine**

To explore the reactivity of **4.31** in the absence of excess pyrrolidine, **4.31** can be isolated from the reaction of **4.26** and excess ethanol, followed by recrystallization (Scheme 4.15a). An attempt to isolate **4.31** from a reaction of 1 equivalent of **4.26** and 1 equivalent of pyrrolidine resulted in only 50% conversion to the hydride species **4.31**. Addition of one additional equivalent results in full conversion to **4.31**. After workup (removal of volatiles, washing with hexanes, and removal of trace volatiles again), the  $^1\text{H}$  NMR spectra reveals a remaining equivalent of pyrrolidine, with a downfield shift of the  $\alpha$ -methylene proton signals compared to free pyrrolidine (Scheme 4.15b). Further, a 1D  $^1\text{H}$  NOE experiment, with irradiation of the Cp\* protons, results in an NOE signal for the  $\alpha$ -protons of the pyrrolidine (in addition to NOE signals of the phosphine/2-pyridone ligand). Comparing isolated **4.31** and **4.31•pyrrolidine**,  $^1\text{H}$  and  $^{31}\text{P}\{^1\text{H}\}$  spectroscopy reveal very similar chemical shifts for both complexes, however, **4.31•pyrrolidine** exhibits broadened peaks, that is particularly evident in the  $^{31}\text{P}\{^1\text{H}\}$  resonance. Additionally, the OH resonance for **4.31** can be found in the  $^1\text{H}$  NMR spectrum at 7.78 ppm ( $\text{CDCl}_3$ ). Comparatively, the OH resonance cannot be located in the  $^1\text{H}$  NMR spectrum of **4.31•pyrrolidine**, due to exchange of the hydrogen bonding interaction causing extreme broadening of the signal. The changes in the NMR spectra suggest a similar binding mode in



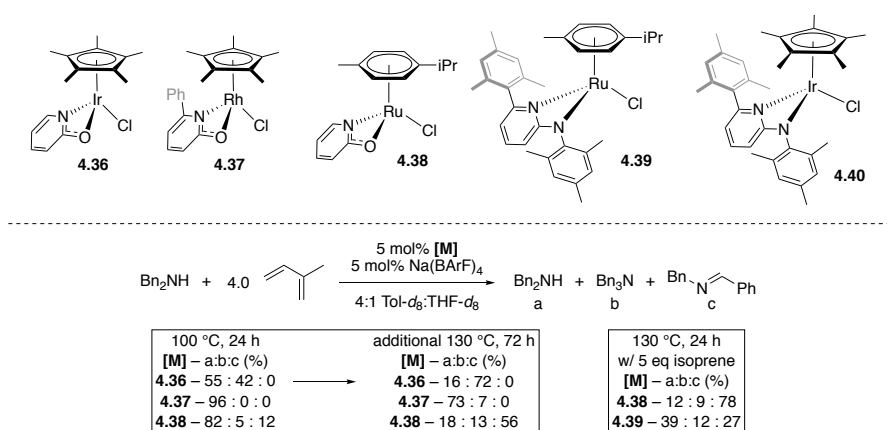
each, with the pyrrolidine involved in a hydrogen bonding interaction with the hydroxy functionality (Scheme 4.15b).

Isolated complex **4.31** was tested in a variant of refluxing solvents to evaluate if H<sub>2</sub> release or other decomposition is possible. However, reactions in THF-*d*<sub>8</sub>, D<sub>2</sub>O, toluene-*d*<sub>8</sub>, 2,2,2-trifluoroethanol, and *o*-xylene-*d*<sub>10</sub> in a J. Young NMR tube reveal no decomposition of complex **4.31** by <sup>31</sup>P{<sup>1</sup>H} NMR spectroscopy. Also, **4.31** showed no reaction with 3 equivalents of *t*-butylsulfinimide (THF-*d*<sub>8</sub>, 70 °C, 24 h). These results suggest the Ir–H complex does not have the required basicity to release H<sub>2</sub> or allow for hydrogenation of an unsaturation by **4.31**.

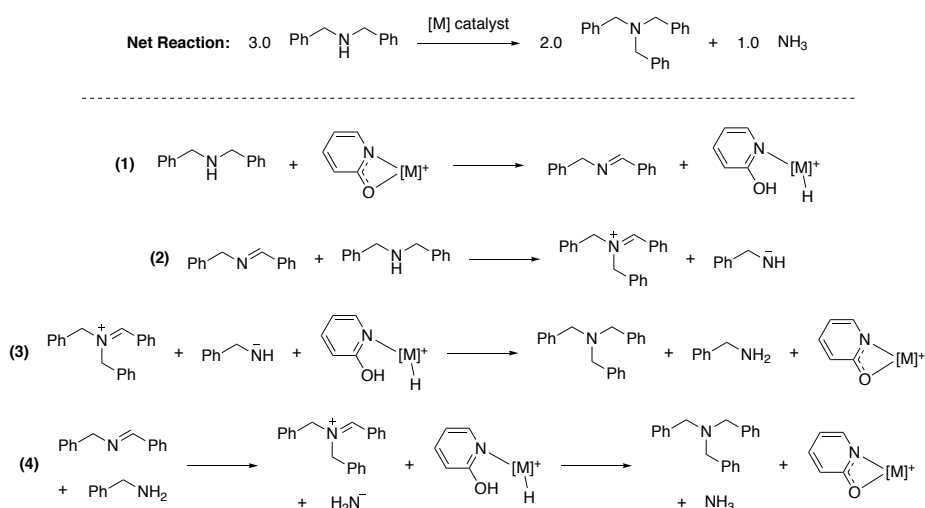
While these complexes proved inactive for the desired catalytic hydroaminoalkylation, or the acceptorless dehydrogenation of amines, these results suggest cationic complexes are highly active for stoichiometric dehydrogenation of secondary amines and ethanol. Given the lack of reactivity, we postulated that the bidentate ligands may have suppressed reactivity by not providing an open coordination site, or if the use of a phosphine donor created highly stable metal hydride that is unreactive. Curiously, the known complex **4.36** is reactive for the acceptorless dehydrogenation of *N*-heterocycles, but is not reported for reactivity with additional amines.<sup>78</sup> To this end, catalytic reactions were attempted with complexes **4.36** – **4.40** with one equivalent NaB(ArF)<sub>4</sub> to generate a cationic complex *in situ*. Dibenzylamine was chosen as the amine source due to its NMR spectral simplicity, allowing for ease of analysis of the products.

Catalytic reactions between dibenzylamine and isoprene were attempted with 5 mol% **4.36** – **4.38** with 5 mol% NaB(ArF)<sub>4</sub> in a J. Young NMR tube at 100 °C for 24 h, and following <sup>1</sup>H NMR experiment at ambient temperature, was heated for an additional 72 h at 130 °C (Scheme 4.16). Interestingly, Ir complex **4.36** generates only tribenzylamine product in a final conversion of 72% (by <sup>1</sup>H NMR analysis; product presence confirmed by GC/MS). The

tribenzylamine product likely results from a series of steps: 1) generation of *N*-benzylbenzaldimine and a M–H; 2) attack by an equivalent of dibenzylamine to form *N,N*-dibenzyl-benzaldiminium cation; 3) the *N,N*-dibenzyl-benzaldiminium cation is then sufficiently activated to be hydrogenated by the M–H and protonation results in tribenzylamine; 4) released benzylamine can attack an equivalent of *N*-benzylbenzaldimine producing the *N,N*-dibenzylbenzaldiminium cation and releasing an equivalent of ammonia to result in only



**Scheme 4.16 Attempted hydroaminoalkylation of isoprene with dibenzylamine**



**Scheme 4.17 Generation of tribenzylamine from dibenzylamine**

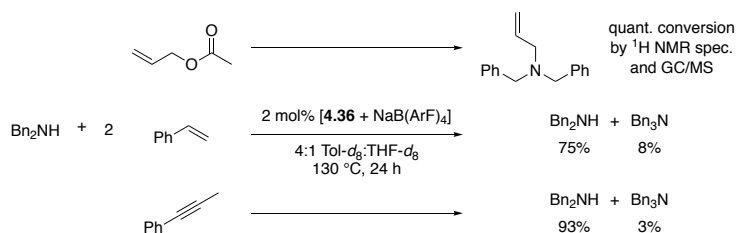
formation of the tribenzylamine (Scheme 4.17).

The Rh complex **4.37** only demonstrates trace reactivity for this transformation, and further experimentation with Rh was abandoned. The Ru complex **4.38** provides significant conversion of dibenzylamine to give tribenzylamine (13%), and the imine product (56%). The formation of the imine product is likely the result of dehydrogenation of the amine with concomitant transfer hydrogenation to the isoprene. At this time, the fate of the isoprene has yet not been determined. Reactions with **4.38** in the absence of an acceptor unsaturation result in only the formation of benzylamine confirming the transfer hydrogenation (*vide infra*, Scheme 4.18a). Unfortunately, in all these reactions, the desired  $\alpha$ -alkylation product was not observed by  $^1\text{H}$  NMR spectroscopy or by GC/MS. We hypothesized that the 2-pyridone ligand was overly acidic, resulting in protonation of the generated Ru–allyl species (from insertion of isoprene into the generated Ru–H). To avoid this, Ru complex **4.39** was prepared and subjected to slightly modified conditions (along with **4.38**). However, no  $\alpha$ -alkylation product was observed and it was found that **4.39** performed worse for the dehydrogenation of dibenzylamine than **4.38** (Scheme 4.16).

While not successful for hydroaminoalkylation chemistry, we wondered if the chemistry could be adapted to achieve acceptorless dehydrogenation of amines. Reactivity of dibenzylamine was explored, in the absence of isoprene, with these Ir and Ru complexes as well as complex **4.40**, a new derivative adapted from previous 2-aminopyridinate complexes of Ir (Scheme 4.18a).<sup>239</sup> The complex **4.40** was included as a more basic derivative to potentially avoid the hydrogen bonding observed in **4.31•pyrrolidine**, which may hinder hydrogen release in a catalytic acceptorless dehydrogenation. These reactions were conducted in degassed and evacuated J. Young NMR tubes to allow for significant head-space to facilitate  $\text{H}_2$  release. In the



Ru complex **4.38** was additionally tested with dibenzylamine and other unsaturations under catalytic conditions (Scheme 4.19). With allyl acetate, quantitative conversion to the *N*-allyl tertiary amine is formed as determined by  $^1\text{H}$  NMR spectroscopy and GC/MS analysis. Reaction with styrene or 1-phenylpropyne result in only minimal conversion of dibenzylamine, minimal amounts of tribenzylamine, no imine product, and no  $\alpha$ -alkylation products.



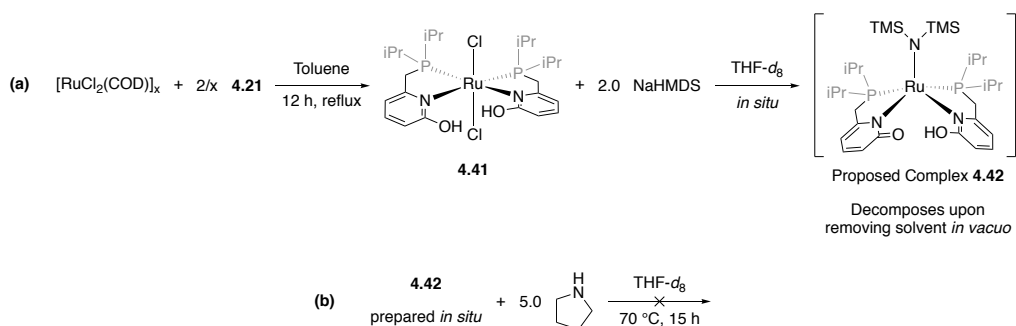
Scheme 4.19 Attempted catalytic reactions between dibenzylamine and C–C unsaturations

### 4.3.2 Initial Investigations into Non-Arene Ligated Late-Transition-Metal Complexes for Hydroaminoalkylation

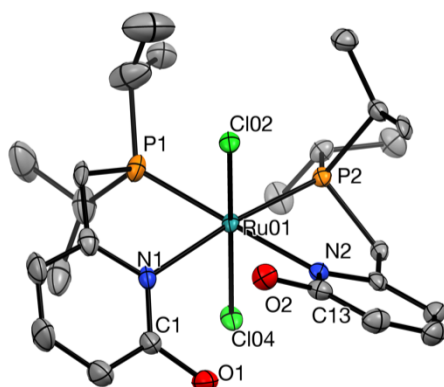
The cationic complexes described above have demonstrated facile stoichiometric dehydrogenation of amines, catalytic conversion of dibenzylamine to tribenzylamine, and catalytic dehydrogenation of amine to imine using a diene hydrogen acceptor. This reactivity can be attributed to the use of the 2-pyridonate ligand framework to assist in the dehydrogenation. As cationic complexes, they are inherently electron deficient. Unfortunately, this seems to limit the hydricity of the generated M–H, making them unsuitable for the desired hydroaminoalkylation of amines. Based on the reported successes of non-arene supported Ru phosphine complexes to demonstrate reactivity for the hydroaminoalkylation reaction (see Chapter 4.1.1).<sup>195,242</sup> we endeavored to synthesize similar Ru complexes using ligand **4.21** or its sodium salt **4.23**.

Refluxing 2 equivalents of **4.21** with polymeric [RuCl<sub>2</sub>(COD)]<sub>x</sub> in toluene results in complex **4.41** (Scheme 4.20). This complex could be recrystallized and the solid-state molecular structure was obtained by single crystal X-ray diffraction (Figure 4.3). This complex

recrystallizes in a pseudo-octahedral geometry with axial chloride ligands, and a *cis*-phosphine arrangement of the phosphino-2-hydroxypyridine ligands. Compared to the 2-pyridonate fragment in **4.25** and **4.26**, we observe a lengthened C1–O1 bond at 1.352(7) Å (C13–O2 is 1.351(7) Å) compared to 1.260(4) Å and 1.246(8) Å respectively. Furthermore, **4.41** has a shortened C1–N1 bond of 1.341(7) Å and C13–N2 bond of 1.335(7) Å (1.138(4) Å in **4.25**; 1.390(9) Å in **4.26**). Both of these results are consistent with the assignment of a  $\kappa^1$ -*N*-2-



**Scheme 4.20** Synthesis and reactivity of **4.41**



H-atoms removed. Thermal ellipsoids are shown at 50%.

Select bond lengths reported as averages (Å):

Ru–P 2.287  
 Ru–N 2.224  
 Ru–Cl 2.427  
 C(2-position)–N 1.338  
 C(2-position)–O 1.351

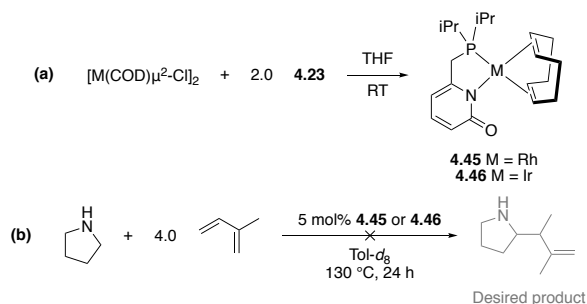
**Figure 4.3** ORTEP representation of the solid-state molecular structure of **4.41**

hydroxypyridine fragments.

Complex **4.41** was found to react with 2 equivalents of NaHMDS to produce the proposed complex **4.42** (Scheme 4.20a). This complex could not be purified as it was found to decompose upon removal of solvent and was resistant to recrystallization. The structure of **4.42**

is proposed on the basis of the NMR spectra. The  $^{31}\text{P}\{^1\text{H}\}$  spectrum reveals two coupled doublets, and the  $^1\text{H}$  NMR spectrum reveals a downfield singlet at 14.59 ppm (integration of 1H, THF- $d_8$ ), indicative of a 2-hydroxypyridine proton (9.73 ppm in **4.41**, THF- $d_8$ ). The  $^1\text{H}$  NMR spectrum also indicates two inequivalent phosphino-2-hydroxypyridine ligand environments. A reaction of *in situ* prepared **4.42** produces no reaction with excess pyrrolidine, and was not further evaluated (Scheme 4.20b).

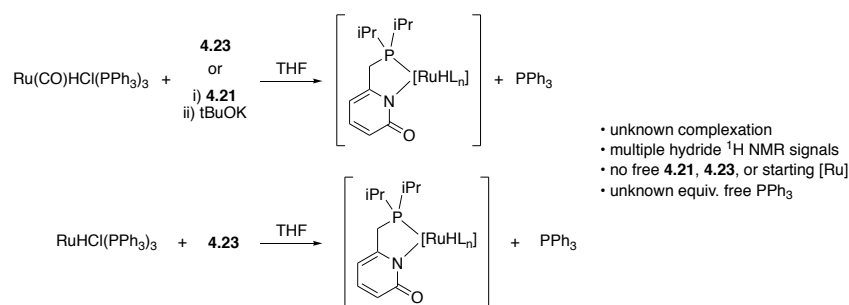
Rh(I) and Ir(I) complexes **4.43** and **4.44** were synthesized by salt metathesis of 2 equivalents of **4.23** and the corresponding  $[\text{M}(\text{COD})\text{Cl}_2]_2$  dimer (COD = 1,5-cyclooctadiene) (Scheme 4.21a). Unfortunately, these complexes could not be recrystallized.  $^1\text{H}$  and  $^{31}\text{P}\{^1\text{H}\}$  spectra show a single product of high purity that is consistent with the square-planar structure shown. Unlike the previous complexes where Na-Cl is coordinated, there is no significant THF (reaction solvent) signals in the  $^1\text{H}$  NMR spectrum that would likely be required to support coordination of a Na ion. These complexes were not active precatalysts for the hydroaminoalkylation of isoprene with pyrrolidine (Scheme 4.21b).



**Scheme 4.21 (a) Synthesis of Rh(I) and Ir(I) complexes 4.45 and 4.46; (b) attempted use of M(I) as precatalysts for hydroaminoalkylation**

The attempted salt metathesis reactions with known Ru complex and **4.23** results in mixtures of unidentifiable complexes (Scheme 4.22). However, free  $\text{PPh}_3$  and no free **4.21** or **4.23** is detected in the  $^{31}\text{P}\{^1\text{H}\}$  NMR spectra of these attempted reactions, indicating

complexation of the phosphino-2-pyridonate ligand does occur. As discussed previously, work by Krische and co-workers did not rely on preformed complexes, but instead *in situ* generation of the active catalyst system.<sup>195-196</sup> Due to our lack of success in isolating Ru complexes, we instead turned to attempted  $\alpha$ -alkylation reactions between piperidine and 2,3-dimethyl-1,3-butadiene with *in situ* generation of these systems (Scheme 4.23). Here, 5 mol% of known  $\text{Ru}(\text{CO})\text{H}(\text{PPh}_3)_3$  was combined with 5 mol% of one of ligands **4.21**, **4.22**, or **4.45 – 4.47**. Developments from Krische and co-workers have found the use of diphosphinopropane ligands to be successful, and the same series of reactions were attempted with the addition of 5 mol% dppp (dppp = 1,3-bis(diphenylphosphino)propane) added as well. To test whether the carbonyl ligand significantly altered catalytic activity, 5 mol% of the known  $\text{RuHCl}(\text{PPh}_3)_3$  with addition of 5 mol% of one of the sodium-2-pyridonate salts (**4.23**, **4.24**, or **4.48**) were also tested as a catalyst system. To our disappointment though, these reactions were all unsuccessful. By  $^1\text{H}$  NMR spectroscopy or HPLC/ESI analysis, no hydroaminoalkylation product formation was observed, nor was any significant consumption of the starting materials apparent.

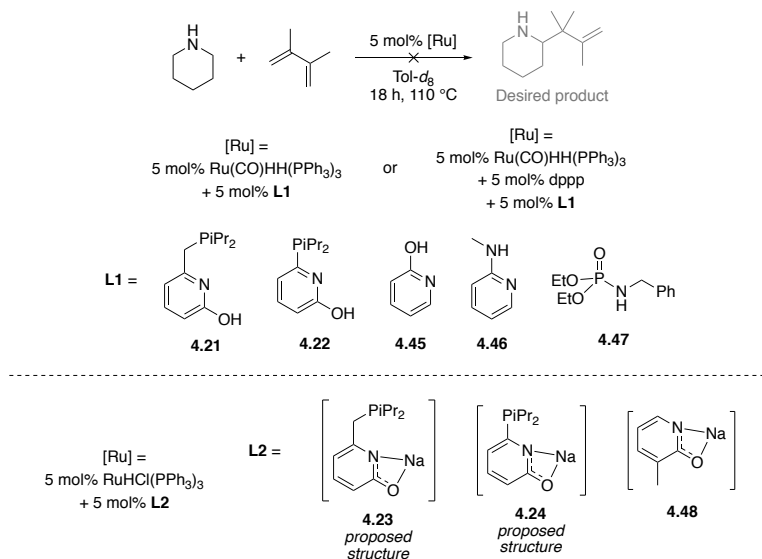


**Scheme 4.22 Attempted synthesis of phosphino-2-pyridonate ligated Ru–H complexes**

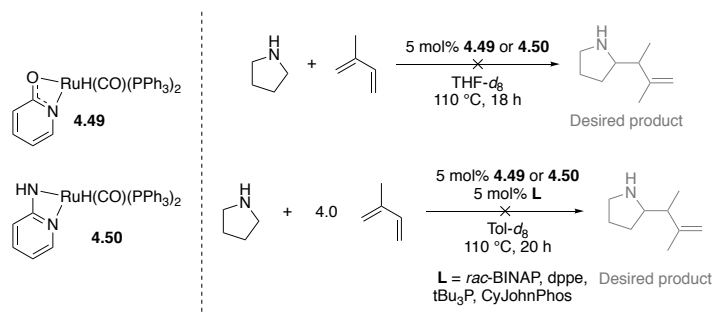
Starting from isolated complexes would remove significant amounts of  $\text{PPh}_3$  from the reaction. Excess phosphine could be hindering the reactivity by out-competing the amine substrate for coordination/interaction with the metal center. Known Ru complexes **4.49** and **4.50**



were synthesized and tested as catalyst for the reaction between pyrrolidine and isoprene (Scheme 4.24). However, no  $\alpha$ -alkylation products or notable conversion of the starting materials were observed.



**Scheme 4.23 Attempted hydroaminoalkylation of 2,3-dimethyl-1,3-butadiene with piperidine *in situ* generated Ru catalysts**



**Scheme 4.24 Attempted hydroaminoalkylation of isoprene with pyrrolidine using Ru complexes 4.43 and 4.44**

## 4.4 Conclusions

In summary, we have successfully synthesized a variety of  $\kappa^2$ -*P,N*-bidentate phosphino-2-pyridonate arene supported cationic complexes. Interestingly, the oxygen of the 2-pyridonate ligand fragment proves to be highly Lewis basic, stabilizing a Na-Cl adduct within the solid-state molecular structure. These complexes were demonstrated to stoichiometrically generate metal

hydride complexes. Unfortunately, the generated metal hydrides are not reactive and did not allow for catalytic hydroaminoalkylation of amines, or the catalytic acceptorless dehydrogenation of amines.

To test the effect of removing the phosphine donor, cationic complexes were derived *in situ* from Ru, Rh, and Ir 2-pyridonate and 2-aminopyridinate complexes and sodium tetraarylborate. These *in situ* systems were tested for as precatalyst for the catalytic hydroaminoalkylation, and catalytic acceptorless dehydrogenation of amines. Attempts at the catalytic acceptorless dehydrogenation of dibenzylamine resulted in formation of tribenzylamine. Reactions of dibenzylamine and diene with catalytic Ir also resulted in formation of tribenzylamine. In contrast, using catalytic Ru resulted in formation of *N*-benzylbenzaldimine, *via* transfer hydrogenation of the diene.

Finally, initial investigations were undertaken to synthesize alternative complexes using ligand **4.21**. While complexation with Ru occurs, isolation of the products proved difficult. Instead, numerous *in situ* derived catalytic systems were tested for the hydroaminoalkylation of amines with dienes, but attempts have been unsuccessful to date. Square planar Rh(I) and Ir(I) complexes were synthesized bearing a phosphino-2-pyridonate ligand. These complexes were also not active precatalysts for the hydroaminoalkylation reaction.

## **4.5 Experimental Details**

General considerations and instrumentation details can be found in Chapter 2.4.1 and 2.4.2, respectively.

### **4.5.1 Materials**

All chemicals were purchased from commercial sources and used as received unless otherwise specified. Chemicals from commercial sources that were not dried and shipped under inert

atmosphere, were appropriately dried and degassed of O<sub>2</sub> before being transferred to the glovebox or for use on the Schlenk manifold. All amines and alkenes were dried under N<sub>2</sub> atmosphere with CaH<sub>2</sub>, distilled, and degassed by the freeze-pump-thaw method. Commercially available 2-pyridones were sublimed under vacuum on a Schlenk manifold at 80 – 100 °C with water cooling. *N*-2,6-diisopropylphenyl diethyl phosphoramidate decomposed during attempts to sublime the compound and was instead dried over 48 h under vacuum (10<sup>-2</sup> mbar) at ambient temperature. NaB(ArF)<sub>4</sub> was generously provided by Prof. Hein's research group (UBC Vancouver). [Cp\*RhCl<sub>2</sub>]<sub>2</sub> was generously donated by Prof. Legzdins' research group (UBC Vancouver). *N*-(2,4,6-trimethylphenyl)-2-amino-6-(2,4,6-trimethylphenyl)pyridine,<sup>243</sup> 2-bromo-6-*tert*-butoxypyridine,<sup>244</sup> *N*-(*rac*-2-methylpropane-2-sulfinyl)benzaldimine,<sup>245</sup> **4.36**,<sup>78</sup> **4.37**,<sup>70</sup> **4.38**,<sup>246</sup> **4.49**,<sup>247</sup> **4.50**,<sup>247</sup> 1,2,3,4,5-pentamethylcyclopentadiene (Cp\*H),<sup>248</sup> [RuCl<sub>2</sub>(COD)]<sub>n</sub>,<sup>249</sup> [Cp\*IrCl<sub>2</sub>]<sub>2</sub>,<sup>250</sup> [Ir(COD)Cl<sub>2</sub>]<sub>2</sub>,<sup>251</sup> [Rh(COD)Cl<sub>2</sub>]<sub>2</sub>,<sup>252</sup> Ru(CO)HH(PPh<sub>3</sub>)<sub>3</sub>,<sup>253</sup> Ru(dppp)(CO)H(PPh<sub>3</sub>)<sub>3</sub>,<sup>254</sup> Ru(CO)HCl(PPh<sub>3</sub>)<sub>3</sub>,<sup>255</sup> and RuHCl(PPh<sub>3</sub>)<sub>3</sub>,<sup>256</sup> were synthesized according to literature procedures.

#### 4.5.2 Synthetic and Experimental Details

**Synthesis of 6-(diisopropylphosphino)methyl-2-pyridone, 4.21.**<sup>33</sup> Using a Schlenk double manifold and standard technique, a dried 100 mL Schlenk flask was placed under N<sub>2</sub> atmosphere. Under positive N<sub>2</sub> flow, 6-methyl-2-pyridone (2.000 g, 18.32 mmol) was added to the flask, 20 mL THF was then added, the slurry stirred vigorously, and cooled to -78 °C. A solution of *n*BuLi (23.2 mL, 37.11 mmol, 1.6 M in hexanes) was added dropwise over 10-15 minutes to produce an orange solution. Upon addition, the solution was warmed to 0 °C and stirred for ~ 3h until all 6-methyl-2-pyridone had dissolved. The solution was then cooled back to -78 °C. In the glovebox, chlorodiisopropylphosphine (2.867 g, 18.78 mmol) was added to a 30 mL Schlenk flask with 10-

15 mL THF to create a clear solution. This flask was then removed from the glovebox and connected to the Schlenk manifold. The solution of chlorodiisopropylphosphine was then added to the stirred solution of deprotonated 2-pyridone (at -78 °C) dropwise by cannula over 30 minutes. The solution was allowed to stir and warm to room temperature slowly over 12 h to produce a pale-yellow solution. The reaction was quenched with 0.5 mL of  $\text{NH}_4\text{Cl}_{(\text{aq})}$  (sparged with  $\text{N}_2$  for 30 min) to produce a cloudy white solution. The solution was concentrated *in vacuo* to result in a sticky yellow solid, to which 15 mL  $\text{H}_2\text{O}$  (sparged with  $\text{N}_2$  for 30 min) was added resulting in a partially cloudy yellow solution. Under  $\text{N}_2$  atmosphere, the phosphine was extracted with EtOAc (2 x 40 mL, sparged for 30 min), dried over sodium sulfate. This was filtered *via* cannula filtration (oven dried glass-fiber filter), and the sodium sulfate washed with an additional 10 mL portion of EtOAc. The combined EtOAc was concentrated to an off-white solid *in vacuo*. The Schlenk flask was then transferred into the glovebox, where the solid was transferred to a 20 mL vial. The product was recrystallized from THF/hexanes at -35 °C in two crops resulting in 2.392 g (58%) of a white solid.  $^1\text{H-NMR}$  (300 MHz,  $\text{CDCl}_3$ ):  $\delta$  12.92 (s, 1H), 7.30 (dd,  $J = 9.1, 7.0$  Hz, 1H), 6.32 (d,  $J = 9.0$  Hz, 1H), 6.20 (d,  $J = 7.0$  Hz, 1H), 2.72 (d,  $J = 1.1$  Hz, 2H), 1.77 (quintd,  $J = 7.1, 1.5$  Hz, 2H), 1.03 (m, 12H).  $^{13}\text{C}\{^1\text{H}\}\text{-NMR}$  (75 MHz,  $\text{CDCl}_3$ ):  $\delta$  165.7, 148.8 (d,  $J = 10.5$  Hz), 141.6, 116.4 (d,  $J = 1.7$  Hz), 106.3 (d,  $J = 9.9$  Hz), 26.7 (d,  $J = 23.8$  Hz), 23.6 (d,  $J = 14.2$  Hz), 19.6 (d,  $J = 14.4$  Hz), 19.01 (d,  $J = 10.7$  Hz).  $^{31}\text{P}\{^1\text{H}\}\text{-NMR}$  (121 MHz,  $\text{CDCl}_3$ ):  $\delta$  11.4. **MS** (ESI):  $m/z$  242.1 [ $\text{MOH}^+$ ]. **EA**: Calc'd for  $\text{C}_{12}\text{H}_{20}\text{NOP}$ : C 63.98, H 8.95, N 6.22; Found: C 62.76, H 9.41, N 6.05.

**Synthesis of 6-diisopropylphosphinyl-2-pyridone, 4.22.**<sup>33,237</sup> Using a Schlenk double manifold and standard technique, a dried 100 mL Schlenk flask was placed under  $\text{N}_2$  atmosphere. Under positive  $\text{N}_2$  flow, 2-bromo-6-*tert*-butoxypyridine (2.400 g, 10.43 mmol) was added to the flask,

and 50 mL Et<sub>2</sub>O was then added, the slurry stirred vigorously, and cooled to -0 °C. A solution of nBuLi (6.84 mL, 10.95 mmol, 1.6 M in hexanes) was added dropwise over 10-15 minutes to produce an orange/red solution. The solution was then stirred for 1 h at 0 °C. In the glovebox, chlorodiisopropylphosphine (1.671 g, 10.95 mmol) was added to a 30 mL Schlenk flask with 5-10 mL Et<sub>2</sub>O to create a clear solution. This flask was then removed from the glovebox and connected to the Schlenk manifold. The solution of chlorodiisopropylphosphine was then added to the stirred solution of lithiated pyridine (at 0 °C) dropwise by cannula over 30 minutes. The solution was allowed to stir and warm to room temperature slowly over 12 h to produce a pale-yellow solution. The reaction was quenched with 0.30 mL methanol (sparged for 30 min) to produce a colorless solution. All volatiles were removed *in vacuo*. The solid was extracted with 50 mL hexanes and filtered *via* cannula filtration (oven dried glass-fiber filter). The solvent was again removed *in vacuo* to give a white solid. To the flask, 20 mL formic acid solution (88%, sparged for 30 min) was added and stirred for 48 h. The formic acid solution was then distilled off at 40 °C *in vacuo* to leave a sticky yellow solid. The flask was allowed to remain under vacuum at ambient temperature overnight. The Schlenk flask was then transferred into the glovebox, the solid transferred to a water-cooled sublimation glassware, and sublimed *in vacuo* on the Schlenk manifold at 85 °C overnight to produce 1.40 g of the product as a bright-yellow, waxy solid (64%). <sup>1</sup>H-NMR (300 MHz, CDCl<sub>3</sub>): δ 12.14 (s, 1H), 7.28 (ddd, *J* = 9.2, 6.7, 1.3 Hz, 1H), 6.49 (ddd, *J* = 9.2, 5.7, 1.1 Hz, 1H), 6.34 (ddd, *J* = 6.7, 5.7, 1.0 Hz, 1H), 2.23 (quintd, *J* = 7.0, 3.1 Hz, 2H), 1.06 (dd, *J* = 15.9, 6.9 Hz, 6H), 0.89 (dd, *J* = 12.1, 6.9 Hz, 6H). <sup>13</sup>C{<sup>1</sup>H}-NMR (75 MHz, CDCl<sub>3</sub>): δ 165.4 (d, *J* = 2.2 Hz), 146.6 (d, *J* = 33.2 Hz), 139.8 (d, *J* = 7.8 Hz), 120.9, 114.6 (d, *J* = 21.0 Hz), 22.9 (d, *J* = 11.5 Hz), 20.0 (d, *J* = 19.8 Hz), 19.4 (d, *J* = 9.3 Hz).

**$^{31}\text{P}\{^1\text{H}\}$ -NMR** (121 MHz,  $\text{CDCl}_3$ ):  $\delta$  11.8. **MS** (ESI):  $m/z$  228.1 [ $\text{MOH}^+$ ]. **EA**: Calc'd for  $\text{C}_{11}\text{H}_{18}\text{NOP}$ : C 62.54, H 8.59, N 6.63; Found: C 62.63, H 8.70, N 6.52.

**Synthesis of sodium-2-pyridonate, 4.23, and 4.24.** In a glovebox, a THF ( $\sim 3$  mL) solution of 2-pyridone, **4.21**, or **4.23** ( $\sim 1$  mmol scale) was added dropwise to a vigorously stirring suspension of NaH (1.1 equivalents) in THF ( $\sim 10$  mL). The suspension was stirred for 12 h, and then filtered through celite. The volatiles were removed from the clear solution *in vacuo* to reveal a sticky white salt.  $\sim 2$  mL of hexanes was added to form a slurry, and the volatiles were removed *in vacuo*. This was repeating three additional times and the resulting white powder was dried thoroughly *in vacuo*. These products were used without further purification.

**Synthesis of  $[\kappa^2\text{-P,N-6-diisopropylphosphinomethyl-2-pyridonate-}\eta^5\text{-(1,2,3,4,5-pentamethylcyclopentadienyl)Rh(III)\cdot NaCl(Et}_2\text{O)}_2][\text{tetrakis(3,5-trifluoromethylphenyl)borate}]$  4.25.** In a glovebox, a solution of **4.23** (0.028 g, 0.113 mmol) in THF ( $\sim 3$  mL) was added to a stirring suspension deep red  $[\text{Cp}^*\text{RhCl}_2]_2$  (0.035 g, 0.057 mmol) in THF ( $\sim 3$  mL) at ambient temperature. The resulting suspension was stirred for 2 hours at ambient temperature resulting in a deep red solution. Then, a solution of  $\text{NaB}(\text{ArF})_4$  (0.100 g, 0.133 mmol) in THF ( $\sim 2$  mL) was added and the solution stirred for 12 h. The resulting dark orange solution was concentrated *in vacuo*. The resulting orange-brown solid was dissolved in minimal  $\text{Et}_2\text{O}$  ( $\sim 2$  mL), and filtered through celite. The solution was then cooled for 10 minutes at  $-35$   $^\circ\text{C}$ . This dark orange-brown solution was then layered with hexanes ( $\sim 7$  mL) and stored in the freezer at  $-35$   $^\circ\text{C}$  to promote recrystallization. This yielded an orange-brown powder of 0.048 g (27%). It was found that a similar *in situ* procedure at smaller scale ( $\sim 0.008$  mmol Rh) in total volume  $\sim 0.7$  mL  $\text{THF-}d_8$  was found to be of high purity by  $^1\text{H}$  and  $^{31}\text{P}$  NMR and behaved the same as isolated **4.25**. Crystals suitable for single crystal X-ray diffraction were synthesized in the

same manner but with NaBPh<sub>4</sub> (instead of Na(B(ArF)<sub>4</sub>). This required two recrystallizations from Et<sub>2</sub>O layered with hexanes at -35 °C. Significant fluxional behavior is observed, making assignment of peaks difficult. Spectra are further complicated by the presence of significant amounts of Et<sub>2</sub>O. Fluxionality of the complex can further be observed by the significant depletion in signal integration of the [Rh]<sup>+</sup> compared to the signals for Et<sub>2</sub>O or [B(ArF)<sub>4</sub>]<sup>-</sup>. Compare to Ir complex **4.26**. <sup>1</sup>H-NMR (300 MHz, THF-*d*<sub>8</sub>): δ 7.79 (s, 8H), 7.58 (s, 4H), 7.17 (br. s, 1H), 6.35 (d, *J* = 5.7 Hz, 1H), 6.23 (br. s, 1H), 3.75-3.65 (m, 1H), 3.35-3.27 (m, 1H), 2.77-2.66 (m, 1H), 2.47-2.39 (m, 1H), 1.67 (d, *J* = 2.7 Hz, 15H), 1.53 (dd, *J* = 15.8, 7.4 Hz, 3H), 1.42 (dd, *J* = 12.8, 7.0 Hz, 3H), 1.24-1.15 (m, 6H). <sup>13</sup>C{<sup>1</sup>H}-NMR (75 MHz, THF-*d*<sub>8</sub>): δ 163.4 (q, <sup>1</sup>*J*<sub>CB</sub> = 49.8 Hz, B(ArF<sub>4</sub>)), 136.2 (br. s, B(ArF<sub>4</sub>)), 130.7 (qq, <sup>2</sup>*J*<sub>CF</sub> = 31.5, <sup>2</sup>*J*<sub>CB</sub> = 2.9 Hz B(ArF<sub>4</sub>)), 126.1 (q, <sup>1</sup>*J*<sub>CF</sub> = 272.2 Hz, B(ArF<sub>4</sub>)), 118.8 (m B(ArF<sub>4</sub>)), 101.3, 37.7, 36.13, 36.09, 33.2, 30.6, 27.0, 24.1, 21.6, 16.3, 15.0, 12.4, 10.37, 10.35, 9.9 (note: fluxional behavior creates significant difficulties in locating all carbon signals). <sup>31</sup>P{<sup>1</sup>H}-NMR (121 MHz, THF-*d*<sub>8</sub>): δ 56.31 (d, *J*<sub>PRh</sub> = 129.3 Hz). <sup>19</sup>F{<sup>1</sup>H}-NMR (282 MHz, THF-*d*<sub>8</sub>): δ -65.23. MS (EI): Unable to obtain data, decomposition of sample observed upon collection. EA: Calc'd for C<sub>62</sub>H<sub>66</sub>BClF<sub>24</sub>NNaO<sub>3</sub>PRh: C 48.60, H 4.34, N 0.91; Found: C 49.54, H 4.25, N 0.91.

**Synthesis of [κ<sup>2</sup>-*P,N*-6-diisopropylphosphinomethyl-2-pyridonate-η<sup>5</sup>-(1,2,3,4,5-pentamethylcyclopentadienyl)Ir(III)•NaCl(Et<sub>2</sub>O)<sub>2</sub>][tetrakis(3,5-trifluoromethylphenyl)borate] **4.26**.** In a glovebox, a solution of **4.23** (0.019 g, 0.075 mmol) in THF (~ 3 mL) was added to a stirring suspension of orange [Cp\*IrCl<sub>2</sub>]<sub>2</sub> (0.030 g, 0.038 mmol) in THF (~ 3 mL) at ambient temperature. The resulting suspension was stirred for 2 hours at ambient temperature resulting in an orange solution. Then, a solution of NaB(ArF)<sub>4</sub> (0.067 g, 0.075 mmol) in THF (~ 2 mL) was added and the solution stirred for 12 h. The resulting yellow

solution was concentrated *in vacuo*. The resulting yellow solid was dissolved in minimal Et<sub>2</sub>O (~ 2 mL), and filtered through celite. The solution was then cooled for 10 minutes at -35 °C. This dark orange-brown solution was then layered with hexanes (~ 7 mL) and stored in the freezer at -35 °C to promote recrystallization. This yielded a yellow powder of 0.045 g (37%). It was found that a similar *in situ* procedure at smaller scale (~ 0.008 mmol Ir) in total volume ~0.7 mL THF-*d*<sub>8</sub> was found to be of high purity by <sup>1</sup>H and <sup>31</sup>P NMR and behaved the same as isolated **4.25**. Crystals suitable for single crystal X-ray diffraction could be grown by utilizing a more dilute Et<sub>2</sub>O solution layered with hexanes at -35 °C. **<sup>1</sup>H-NMR** (400 MHz, THF-*d*<sub>8</sub>): δ 7.79 (s, 8H), 7.57 (s, 4H), 7.08 (dd, *J* = 8.5, 6.8 Hz, 1H), 6.31 (d, *J* = 6.8 Hz, 1H), 6.09 (d, *J* = 8.5 Hz, 1H), 3.82 (dd, *J* = 15.9, 12.4 Hz, 1H), 3.38 (q, *J* = 7.0 Hz, 4H), 3.17 (dd, *J* = 15.8, 8.7 Hz, 1H), 2.62 (m, 2H), 1.68 (d, *J* = 1.9 Hz, 15H), 1.48 (dd, *J* = 15.8, 7.3 Hz, 3H), 1.40 (dd, *J* = 13.5, 7.1 Hz, 3H), 1.23 (dd, *J* = 14.6, 7.2 Hz, 3H), 1.15 (dd, *J* = 12.7, 7.2 Hz, 3H), 1.12 (t, *J* = 7.0 Hz, 6H). **<sup>13</sup>C{<sup>1</sup>H}-NMR** (101 MHz, THF-*d*<sub>8</sub>): δ 172.0, 163.4 (q, <sup>1</sup>*J*<sub>CB</sub> = 49.8 Hz, B(ArF<sub>4</sub>)), 158.1, 139.1, 136.2 (br. s, B(ArF<sub>4</sub>)), 130.7 (qq, <sup>2</sup>*J*<sub>CF</sub> = 31.5, <sup>2</sup>*J*<sub>CB</sub> = 2.9 Hz B(ArF<sub>4</sub>)), 126.1 (q, <sup>1</sup>*J*<sub>CF</sub> = 272.2 Hz, B(ArF<sub>4</sub>)), 118.8 (m B(ArF<sub>4</sub>)), 116.1, 94.6 (d, *J* = 2.60), 66.9, 41.9 (d, *J* = 32.5 Hz), 28.2 (d, *J* = 30.2 Hz), 27.0 (d, *J* = 25.1 Hz), 20.6 (d, *J* = 30.8 Hz), 20.4 (d, *J* = 16.0 Hz), 19.5 (d, *J* = 6.5 Hz), 16.3, 10.1. **<sup>31</sup>P{<sup>1</sup>H}-NMR** (162 MHz, THF-*d*<sub>8</sub>): δ 23.3. **MS** (EI): *m/z* 552 [*M*<sup>+</sup>]. **EA**: Calc'd for C<sub>62</sub>H<sub>66</sub>BClF<sub>24</sub>NNaO<sub>3</sub>PIr: C 45.92, H 4.10, N 0.86; Found: C 45.71, H 3.89, N 0.81.

**Synthesis of [κ<sup>2</sup>-*P,N*-6-diisopropylphosphinomethyl-2-pyridonate-η<sup>6</sup>-(*p*-cymene)Ru(II)•NaCl(THF)<sub>2</sub>][tetrakis(3,5-trifluoromethylphenyl)borate] **4.27**.** In a glovebox, a solution of **4.23** (0.014 g, 0.056 mmol) in THF (~ 3 mL) and a suspension of deep red [(*p*-cymene)RuCl<sub>2</sub>]<sub>2</sub> (0.017 g, 0.028 mmol) in THF (~ 3 mL) were both chilled to -35 °C in the freezer. The cold solution of ligand salt was then added, dropwise, to the stirring, cold



suspension of Ru. After the addition, the suspension was returned to the freezer for 15 min. The solution was then stirred for 5 h, until the Ru had completely dissolved to form a red solution. Then, a solution of NaB(ArF)<sub>4</sub> (0.049 g, 0.056 mmol) in THF (~ 2 mL) was added and the solution stirred for 12 h. The resulting orange-red solution was filtered through celite and concentrated to an orange-red powder *in vacuo*, resulting in a crude yield of 0.085 g (100%). **<sup>1</sup>H-NMR** (400 MHz, THF-*d*<sub>8</sub>): δ 7.79 (s, 8H), 7.57 (s, 4H), 7.08 (ddd, *J* = 8.5, 6.8, 0.7 Hz, 1H), 6.28 (d, *J* = 6.3 Hz, 1H), 6.21 (d, *J* = 6.8 Hz, 1H), 6.12 (d, *J* = 8.5 Hz, 1H), 5.98 (d, *J* = 5.3 Hz, 1H), 5.92 (d, *J* = 6.3 Hz, 1H), 5.55 (d, *J* = 5.3 Hz, 1H), 3.65-3.61 (m, 1H), 3.08 (dd, *J* = 15.9, 8.6 Hz, 1H), 2.91-2.82 (m, 1H), 2.72-2.65 (m, 1H), 2.44-2.34 (m, *J* = 7.2 Hz, 1H), 1.76 (s, 3H), 1.68 (dd, *J* = 15.3, 7.4 Hz, 3H), 1.49 (dd, *J* = 13.2, 7.1 Hz, 3H), 1.22 (d, *J* = 7.0 Hz, 3H), 1.19 (dd, *J* = 14.5, 7.1 Hz, 3H), 1.15 (d, *J* = 6.9 Hz, 3H), 1.05 (dd, *J* = 15.2, 7.2 Hz, 3H). **<sup>31</sup>P{<sup>1</sup>H}-NMR** (121 MHz, THF-*d*<sub>8</sub>): δ 57.6. **<sup>19</sup>F-NMR** (377 MHz, THF-*d*<sub>8</sub>): δ -63.42.

**Synthesis of [κ<sup>2</sup>-*P,N*-6-diisopropylphosphinyl-2-pyridonate-η<sup>5</sup>-(1,2,3,4,5-pentamethylcyclopentadienyl)Ir(III)•NaCl(THF)<sub>2</sub>][tetrakis(3,5-trifluoromethylphenyl)borate] 4.28.** In a glovebox, a solution of **4.24** (0.021 g, 0.088 mmol) in THF (~ 3 mL) was added to a stirring suspension of orange [Cp\*IrCl<sub>2</sub>]<sub>2</sub> (0.035 g, 0.044 mmol) in THF (~ 3 mL) at ambient temperature. The resulting suspension was stirred for 2 hours at ambient temperature resulting in an orange solution. Then, a solution of NaB(ArF)<sub>4</sub> (0.078 g, 0.088 mmol) in THF (~ 2 mL) was added and the solution stirred for 12 h. The resulting yellow solution was filtered through celite and concentrated *in vacuo*. This resulted in a yellow solid in crude yield of 0.156 g (111%). **<sup>1</sup>H-NMR** (400 MHz, THF-*d*<sub>8</sub>): δ 7.79 (s, 8H), 7.57 (s, 4H), 7.27 (ddd, *J* = 9.0, 6.4, 4.0 Hz, 1H), 6.33 (d, *J* = 9.0 Hz, 1H), 6.08 (dd, *J* = 6.4, 4.6 Hz, 1H), 3.11 (ddt, *J* = 14.7, 11.5, 7.3 Hz, 1H), 2.71 (ddt, *J* = 14.2, 8.9, 7.1 Hz, 1H), 1.90 (d, *J* = 2.5 Hz, 15H), 1.45-

1.31 (m, 12H).  $^{31}\text{P}\{^1\text{H}\}$ -NMR (162 MHz, THF- $d_8$ ):  $\delta$  -25.87.  $^{19}\text{F}$ -NMR (377 MHz, THF- $d_8$ ):  $\delta$  -63.08.

**Synthesis of  $[\kappa^2\text{-}P,N\text{-}6\text{-diisopropylphosphinyl-2-pyridonate-}\eta^6\text{-(}p\text{-cymene)Ru(II)\cdot NaCl(THF)}_2\text{][tetrakis(3,5-trifluoromethylphenyl)borate}]$  4.29.** In a glovebox, a solution of **4.24** (0.013 g, 0.056 mmol) in THF ( $\sim$  3 mL) and a suspension of deep red  $[(p\text{-cymene)RuCl}_2]_2$  (0.017 g, 0.018 mmol) in THF ( $\sim$  3 mL) where both chilled to  $-35^\circ\text{C}$  in the freezer. The cold solution of ligand salt was then added, dropwise, to the stirring, cold suspension of Ru. After the addition, the suspension was returned to the freezer for 15 min. The solution was then stirred for 5 h, until the Ru had completely dissolved to form a red solution. Then, a solution of  $\text{NaB}(\text{ArF})_4$  (0.049 g, 0.056 mmol) in THF ( $\sim$  2 mL) was added and the solution stirred for 12 h. The resulting orange-red solution was filtered through celite and concentrated to an orange-red powder *in vacuo*, resulting in a crude yield of 0.088 g (105%).  $^1\text{H}$ -NMR (400 MHz, THF- $d_8$ ):  $\delta$  7.79 (s, 8H), 7.57 (s, 4H), 7.22 (ddd,  $J$  = 8.7, 6.2, 3.7 Hz, 1H), 6.58 (d,  $J$  = 6.3 Hz, 1H), 6.34 (d,  $J$  = 8.7 Hz, 1H), 6.20 (d,  $J$  = 5.9 Hz, 1H), 6.10 (t,  $J$  = 6.2 Hz, 1H), 5.69 (d,  $J$  = 6.3 Hz, 1H), 5.62 (d,  $J$  = 5.9 Hz, 1H), 2.88-2.78 (m, 2H), 2.68-2.58 (m, 1H), 2.07 (s, 3H), 1.53 (dd,  $J$  = 15.2, 7.0 Hz, 3H), 1.41 (dd,  $J$  = 15.5, 7.1 Hz, 3H), 1.36 (dd,  $J$  = 17.0, 7.2 Hz, 3H), 1.31 (dd,  $J$  = 17.6, 7.4 Hz, 3H), 1.21 (d,  $J$  = 6.9 Hz, 3H), 1.16 (d,  $J$  = 7.0 Hz, 3H).  $^{31}\text{P}\{^1\text{H}\}$ -NMR (162 MHz, THF- $d_8$ ):  $\delta$  -4.39.  $^{19}\text{F}$ -NMR (377 MHz, THF- $d_8$ ):  $\delta$  -63.42.

**Synthesis of  $[\kappa^2\text{-}P,N\text{-}6\text{-diisopropylphosphinomethyl-2-pyridonate-}\eta^5\text{-(1,2,3,4,5-pentamethylcyclopentadienyl)hydridoIr(III)][tetrakis(3,5-trifluoromethylphenyl)borate}]$  4.31.** Complex **4.26** was prepared *in situ* as above using **4.23** (0.016 g, 0.065 mmol),  $[\text{Cp}^*\text{IrCl}_2]_2$  (0.026 g, 0.032 mmol), and  $\text{NaB}(\text{ArF})_4$  (0.057 g, 0.065 mmol) in THF (total volume 1.0 mL). This solution was placed in a J. Young NMR tube and 2  $\mu\text{L}$  EtOH (0.015 g, 0.324 mmol, dry and

degassed), the tube sealed, and heated for 12 h in a 70 °C oil bath. The reaction can be monitored by  $^{31}\text{P}\{^1\text{H}\}$  NMR spectroscopy to confirm completion. Once complete, the tube was taken into a glovebox, transferred to a vial, filtered through celite, and the volatiles were removed *in vacuo*. The pale yellow solid was dissolved in a minimal amount of THF (~ 1 mL), layered with hexanes (~ 3 mL), and placed in the freezer at -35 °C to encourage crystallization. This resulted in 0.069 mg (75%) of pale yellow crystals.  **$^1\text{H}$ -NMR** (400 MHz,  $\text{CDCl}_3$ ):  $\delta$  7.78 (s, 1H), 7.70 (s, 8H), 7.52 (s, 4H), 7.48 (dd,  $J$  = 8.2, 7.3 Hz, 1H), 6.94 (d,  $J$  = 7.3 Hz, 1H), 6.82 (d,  $J$  = 8.2 Hz, 1H), 3.68-3.61 (m, 1H), 3.25 (dd,  $J$  = 16.9, 8.5 Hz, 1H), 2.56-2.47 (m, 1H), 1.99-1.95 (m, 1H), 1.91 (s, 16H), 1.31 (dd,  $J$  = 15.5, 7.1 Hz, 3H), 1.27 (dd,  $J$  = 16.7, 7.2 Hz, 3H), 0.87 (dd,  $J$  = 17.8, 6.7 Hz, 3H), 0.39 (dd,  $J$  = 15.8, 6.9 Hz, 3H), -13.77 (d,  $J$  = 27.5 Hz, 1H).  **$^{13}\text{C}$ -NMR** (101 MHz,  $\text{CDCl}_3$ ):  $\delta$  163.4 (d,  $J$  = 2.7 Hz), 161.8 (q,  $J$  = 49.8 Hz, B(ArF<sub>4</sub>)), 159.1 (d,  $J$  = 2.3 Hz), 141.7, 134.9, 129.1 (qq,  $J$  = 31.54, 2.7 Hz, B(ArF<sub>4</sub>)), 124.7 (q,  $J$  = 272.5 Hz, B(ArF<sub>4</sub>)), 117.6 (m, B(ArF<sub>4</sub>)), 114.6 (d,  $J$  = 7.9 Hz, 1C), 107.7, 94.5, 41.3 (d,  $J$  = 29.1 Hz), 24.7 (d,  $J$  = 21.8 Hz), 24.4 (d,  $J$  = 20.7 Hz), 19.0 (d,  $J$  = 2.2 Hz), 18.6 (s), 18.4 (d,  $J$  = 4.4 Hz), 17.2 (d,  $J$  = 1.7 Hz), 10.2.  **$^{31}\text{P}\{^1\text{H}\}$ -NMR** (162 MHz,  $\text{CDCl}_3$ ):  $\delta$  38.32. **MS** (EI): unable to obtain data as complex decomposed upon addition to the instrument. **EA**: Calc'd for  $\text{C}_{54}\text{H}_{48}\text{BF}_{24}\text{NOPIr}$ : C 45.77, H 3.41, N 0.99; Found: C 45.67, H 3.51, N 0.86.

**Synthesis of  $[\kappa^2\text{-}P,N\text{-}6\text{-diisopropylphosphinomethyl-2-pyridonate-}\eta^5\text{-(1,2,3,4,5-pentamethylcyclopentadienyl)hydridoIr(III)}\cdot\text{pyrrolidine}][\text{tetrakis(3,5-trifluoromethylphenyl)borate}]$  4.31**•pyrrolidine. The reaction was prepared in the same manner as **4.31** except that 7  $\mu\text{L}$  pyrrolidine (0.012 g, 0.150 mmol) and was heated for 2 h at 70 °C. The reaction can be monitored by  $^{31}\text{P}\{^1\text{H}\}$  NMR spectroscopy. Once complete, the tube was taken into a glovebox, transferred to a vial, filtered through celite, and the volatiles were

removed *in vacuo*. The solid was washed with hexanes (3 x 1.5 mL) and thoroughly dried *in vacuo* resulting in a pale yellow solid in quantitative yield. **<sup>1</sup>H-NMR** (300 MHz, THF-*d*<sub>8</sub>): δ 7.79 (s, 8H), 7.57 (s, 4H), 7.10 (dd, *J* = 8.1, 7.0 Hz, 1H), 6.44 (d, *J* = 7.0 Hz, 1H), 6.11 (d, *J* = 8.1 Hz, 1H), 3.48 (dd, *J* = 16.9, 10.1 Hz, 1H), 3.30 (dd, *J* = 16.8, 11.1 Hz, 1H), 3.22-3.17 (m, 4H), 2.52-2.40 (m, 1H), 2.19-2.11 (m, 1H), 2.03 (dd, *J* = 1.8, 0.9 Hz, 15H), 1.95-1.90 (m, 4H), 1.25 (m, *J* = 15.4, 7.1 Hz, 3H), 1.19 (m, *J* = 14.2, 7.0 Hz, 3H), 1.01 (dd, *J* = 17.0, 6.9 Hz, 3H), 0.82 (dd, *J* = 14.9, 6.8 Hz, 3H), -14.93 (d, *J* = 30.3 Hz, 1H). **<sup>31</sup>P{<sup>1</sup>H}-NMR** (121 MHz, THF-*d*<sub>8</sub>): δ 41.25.

**Synthesis of sodium-[*N*-(2,4,6-trimethylphenyl)-6-(2,4,6-trimethylphenyl)-2-aminopyridinate].** In a glovebox, a THF (~ 3 mL) yellow solution of *N*-(2,4,6-trimethylphenyl)-6-(2,4,6-trimethylphenyl)-2-aminopyridine (~ 1 mmol scale) was to a suspension of NaH (1.1 equivalents) in THF (~ 5 mL) in a 15 mL Teflon sealed Schlenk bomb. The Schlenk bomb was sealed, removed from the glovebox, and stirred for 12 h at 70 °C. The bomb was returned to the glovebox and the suspension filtered through celite to produce a clear yellow solution. The volatiles were removed *in vacuo* to reveal a sticky yellow salt. ~2 mL of hexanes was added to form a slurry, and the volatiles were removed *in vacuo*. This was repeating three additional times and the resulting yellow powder was dried thoroughly *in vacuo*. This product was used without further purification. <sup>1</sup>H NMR spectroscopy revealed 0.32 eq. THF incorporated into the powder that cannot be removed *in vacuo*.

**Synthesis of chloro(κ<sup>2</sup>-*N,N'*-*N*-(2,4,6-trimethylphenyl)-6-(2,4,6-trimethylphenyl)-2-aminopyridinato)-η<sup>6</sup>-(*p*-cymene)Ru(II) 4.39.** In a glovebox, a solution of sodium-[*N*-(2,4,6-trimethylphenyl)-6-(2,4,6-trimethylphenyl)-2-aminopyridinate] (0.061 g, 0.163 mmol) in THF (~ 5 mL) and a suspension of deep red [(*p*-cymene)RuCl<sub>2</sub>]<sub>2</sub> (0.050 g, 0.082 mmol) in THF (~ 5 mL)

where both chilled to -35 °C in the freezer. The cold solution of ligand salt was then added, dropwise, to the stirring, cold suspension of Ru. After the addition, the suspension was returned to the freezer for 15 min. The solution was then stirred for 12 h at ambient temperature. The resulting orange-red solution was filtered through celite, concentrated 4 mL, and 8 mL of hexanes were slowly added causing partial precipitation of an orange powder. The solution was stored at -35 °C overnight resulting in the formation of more orange powder. The solution was decanted, the product washed with hexanes (2 x 3 mL), and dried *in vacuo* resulting in 0.064 g (65%) of bright orange product. **<sup>1</sup>H-NMR** (400 MHz, THF-*d*<sub>8</sub>): δ 7.02-6.98 (m, 2H), 6.96 (br. s, 1H), 6.82 (br. d, *J* = 2.5 Hz, 2H), 5.76 (dd, *J* = 7.0, 1.0 Hz, 1H), 5.39 (d, *J* = 6.0 Hz, 1H), 5.24 (dd, *J* = 8.6, 1.0 Hz, 1H), 5.14 (d, *J* = 5.5 Hz, 1H), 4.80 (d, *J* = 5.5 Hz, 1H), 4.68 (d, *J* = 6.0 Hz, 1H), 2.36 (s, 3H), 2.28 (s, 3H), 2.25 (s, 6H), 2.22 (s, 3H), 2.18 (s, 3H), 1.78-1.73 (m, 1H), 1.55 (s, 3H), 1.16 (d, *J* = 6.9 Hz, 3H), 0.78 (d, *J* = 7.0 Hz, 3H). **<sup>13</sup>C{<sup>1</sup>H}-NMR** (101 MHz, THF-*d*<sub>8</sub>): δ 171.4, 157.4, 141.8, 138.4, 138.2, 136.8, 136.5, 135.8, 134.4, 132.4, 130.1, 129.20, 129.13, 127.7, 106.7, 105.5, 102.1, 97.5, 85.4, 79.1, 78.5, 76.2, 30.9, 24.0, 21.66, 21.59, 21.43, 21.0, 20.8, 20.35, 20.20, 17.7. **MS** (EI): *m/z* 600 [*M*<sup>+</sup>-H], 565 [*M*<sup>+</sup>-H-Cl]. **EA**: Calc'd for C<sub>33</sub>H<sub>39</sub>ClN<sub>2</sub>Ru: C 66.04, H 6.55, N 4.67; Found: C 65.88, H 6.49, N 4.61.

**Synthesis of chloro(κ<sup>2</sup>-*N,N'*-*N*-(2,4,6-trimethylphenyl)-6-(2,4,6-trimethylphenyl)-2-aminopyridinato)-η<sup>5</sup>-(1,2,3,4,5-pentamethylcyclopentadienyl)Ir(III) 4.40.**<sup>239</sup> In a glovebox, a solution of sodium-[*N*-(2,4,6-trimethylphenyl)-6-(2,4,6-trimethylphenyl)-2-aminopyridinate] (0.055 g, 0.138 mmol) in THF (~ 5 mL) and a suspension of orange [Cp\*IrCl<sub>2</sub>]<sub>2</sub> (0.055 g, 0.069 mmol) in THF (~ 5 mL) where both chilled to -35 °C in the freezer. The cold solution of ligand salt was then added, dropwise, to the stirring, cold suspension of Ru. After the addition, the suspension was returned to the freezer for 15 min. The solution was then stirred for 12 h at

ambient temperature. The resulting yellow-orange solution was filtered through celite, concentrated to 4 mL, and 8 mL of hexanes were slowly added causing partial precipitation of an yellow powder. The solution was stored at -35 °C overnight resulting in the formation of more yellow powder. The solution was decanted, the product washed with hexanes (2 x 3 mL), and dried *in vacuo* resulting in 0.079 g (82%) of bright yellow product. **<sup>1</sup>H-NMR** (400 MHz, C<sub>6</sub>D<sub>6</sub>): δ 6.95 (br. s, 1H), 6.91 (br. s, 1H), 6.85 (br. s, 1H), 6.79-6.75 (m, 2H), 5.76 (dd, *J* = 7.0, 1.0 Hz, 1H), 5.43 (dd, *J* = 8.6, 1.0 Hz, 1H), 2.75 (s, 3H), 2.67 (s, 3H), 2.27 (s, 3H), 2.23 (s, 3H), 2.19 (s, 3H), 2.12 (s, 3H), 1.08 (s, 15H). **<sup>13</sup>C{<sup>1</sup>H}-NMR** (101 MHz, C<sub>6</sub>D<sub>6</sub>): δ 173.1, 155.9, 138.69, 138.50, 137.60, 137.46, 136.82, 136.74, 136.62, 134.8, 132.9, 130.0, 128.9, 128.7, 127.6, 107.8, 107.5, 83.6, 22.1, 21.34, 21.18, 21.08, 20.5, 19.7, 8.8. **MS** (EI): *m/z* 692 [M<sup>+</sup>], 654 [M<sup>+</sup>-H-Cl]. **EA**: Calc'd for C<sub>33</sub>H<sub>40</sub>ClN<sub>2</sub>Ir: C 57.25, H 5.82, N 4.05; Found: C 55.69, H 5.78, N 3.93.

**Synthesis of *trans*-dichloro-*cis*-bis(κ<sup>2</sup>-*P,N*-6-diisopropylphosphinomethyl-2-pyridonate)Ru(II) 4.41.** In the glovebox [RuCl<sub>2</sub>(COD)]<sub>n</sub> (0.110 g, 0.392 mmol) and **4.21** (0.177 g, 0.785 mmol) were charged to a 10 mL Schlenk flask with 3 mL toluene to create a dark brown slurry. The flask was sealed, removed from the glovebox, and stirred at 110 °C for 12 h resulting in an orange-brown suspension. The flask was connected to a Schlenk manifold and the volatiles were removed *in vacuo* to leave an orange-brown solid. The flask was returned to the glovebox where it was washed with Et<sub>2</sub>O (2 x 1.5 mL) and then hexanes (2 x 1.5 mL) to give 0.191 g of the orange-brown product (78%). Single crystals suitable to X-ray diffraction were grown from a saturated toluene solution layered with hexanes at -35 °C over several days. **<sup>1</sup>H-NMR** (300 MHz, THF-*d*<sub>8</sub>): δ 9.73 (s, 2H), 7.60 (dd, *J* = 8.2, 7.5 Hz, 2H), 7.10 (d, *J* = 7.5 Hz, 2H), 6.50 (d, *J* = 8.2 Hz, 2H), 4.40-4.32 (m, 2H), 3.53-3.43 (m, 2H), 2.71-2.59 (m, *J* = 6.8 Hz, 2H), 2.51-2.38 (m, 2H), 1.42 (dd, *J* = 12.2, 7.2 Hz, 6H), 1.39 (dd, *J* = 12.2, 7.2 Hz, 6H), 1.10 (dd, *J* = 14.1, 7.1 Hz,

6H), 0.94 (dd,  $J = 12.4, 7.1$  Hz, 6H).  $^{13}\text{C}\{^1\text{H}\}$ -NMR (75 MHz, THF- $d_8$ ):  $\delta$  169.1, 162.2, 140.4, 115.6 (t,  $J = 4.8$  Hz), 109.1 (t,  $J = 1.1$  Hz), 37.8-37.4 (m), 28.4 (dd,  $J = 8.8, 8.7$  Hz), 27.8 (dd,  $J = 9.9, 9.8$  Hz), 20.7, 19.5, 19.3 (t,  $J = 1.4$  Hz), 18.9.  $^{31}\text{P}\{^1\text{H}\}$ -NMR (121 MHz, THF- $d_8$ ):  $\delta$  68.0. MS (EI):  $m/z$  622 [ $\text{M}^+$ ], 586 [ $\text{M}^+ - \text{H} - \text{Cl}$ ]. EA: Calc'd for  $\text{C}_{24}\text{H}_{40}\text{Cl}_2\text{N}_2\text{O}_2\text{P}_2\text{Ru}$ : C 46.31, H 6.48, N 4.50; Found: C 45.48, H 6.42, N 4.47.

***In situ* preparation of proposed complex [4.42].** In the glove box, complex **4.41** (0.010 g, 0.0161 mmol) was dissolved in 0.3 mL THF- $d_8$  in a 5 mL vial. In another vial, NaHMDS (0.006 g, 0.0322 mmol) was dissolved in 0.3 mL THF- $d_8$ . Using a pipette, the solution of NaHMDS was added and thoroughly mixed with the solution of **4.41** for 2-3 minutes. This solution was added to a J. Young NMR tube and NMR analysis taken. NMR spectroscopy revealed complete conversion of **4.41** into a new product proposed as [4.42]. Attempts (up to 5x larger scale) to isolate the complex found the removal of the volatiles *in vacuo* decomposes the product, as evidenced by NMR spectroscopy after dissolving the resulting solid in THF- $d_8$ .  $^1\text{H}$ -NMR (300 MHz, THF- $d_8$ ):  $\delta$  14.59 (s, 1H), 6.72 (dd,  $J = 8.4, 6.5$  Hz, 1H), 6.44 (dd,  $J = 8.9, 6.7$  Hz, 1H), 6.23 (d,  $J = 6.5$  Hz, 1H), 6.13 (d,  $J = 6.7$  Hz, 1H), 5.42 (d,  $J = 8.9$  Hz, 1H), 5.24 (d,  $J = 8.4$  Hz, 1H), 3.29-3.20 (m, 1H), 3.02-2.92 (m, 3H), 2.13 (d,  $J = 26.5$  Hz, 1H), 1.96 (d,  $J = 29.6$  Hz, 1H), 1.68-1.58 (m, 3H), 1.42-1.23 (m, 15H), 1.03 (dd,  $J = 13.3, 7.2$  Hz, 3H), 0.88 (dd,  $J = 14.2, 7.3$  Hz, 3H), 0.04 (s, 32H). Significant broadening in the spectrum is observed obscuring integrations.  $^{31}\text{P}\{^1\text{H}\}$ -NMR (121 MHz, THF- $d_8$ ):  $\delta$  79.9 (d,  $J = 36.3$  Hz), 67.9 (d,  $J = 36.2$  Hz).

**Synthesis of  $\eta^2\text{-}\eta^2\text{-(1,5-cyclooctadiene)}\text{-(}\kappa^2\text{-}P,N\text{-6-diisopropylphosphinomethyl-2-pyridonate)Rh(I) 4.45.$**  In a glovebox, a solution of **4.23** (0.026 g, 0.104 mmol) in THF (~ 3 mL) was added to a stirring suspension of deep red  $[\text{Cp}^*\text{RhCl}_2]_2$  (0.026 g, 0.052 mmol) in THF (~ 3 mL) at ambient temperature. The resulting suspension was stirred for 2 hours at ambient

temperature resulting in an orange solution. The resulting orange solution was filtered through celite and concentrated *in vacuo*. This resulted in an orange solid in crude yield of 0.051 g (113%). **<sup>1</sup>H-NMR** (400 MHz, THF-*d*<sub>8</sub>): δ 6.82-6.80 (m, 1H), 6.77 (m, 2H), 5.83 (d, *J* = 8.6 Hz, 1H), 5.77 (d, *J* = 6.4 Hz, 1H), 3.79 (m, 2H), 3.12 (d, *J* = 10.7 Hz, 2H), 2.35-2.10 (m, 8H), 2.08-2.01 (m, 2H), 1.23 (dd, *J* = 15.1, 7.1 Hz, 6H), 1.12 (dd, *J* = 13.6, 7.0 Hz, 6H). **<sup>31</sup>P{<sup>1</sup>H}-NMR** (162 MHz, THF-*d*<sub>8</sub>): δ 54.3 (d, *J* = 154.6 Hz).

**Synthesis of  $\eta^2\text{-}\eta^2\text{-(1,5-cyclooctadiene)}\text{-(}\kappa^2\text{-}P,N\text{-6-diisopropylphosphinomethyl-2-pyridonate)Ir(I) 4.46$ .** In a glovebox, a solution of **4.23** (0.026 g, 0.104 mmol) in THF (~ 3 mL) was added to a stirring suspension of orange [Cp\*IrCl<sub>2</sub>]<sub>2</sub> (0.035 g, 0.052 mmol) in THF (~ 3 mL) at ambient temperature. The resulting suspension was stirred for 2 hours at ambient temperature resulting in a yellow-orange solution. The resulting yellow-orange solution was filtered through celite and concentrated *in vacuo*. This resulted in a yellow-orange solid in crude yield of 0.058 g (105%). **<sup>1</sup>H-NMR** (400 MHz, THF-*d*<sub>8</sub>): δ 6.86 (ddd, *J* = 8.8, 6.4, 0.6 Hz, 1H), 6.45 (m, 2H), 5.95 (d, *J* = 8.8 Hz, 1H), 5.92 (d, *J* = 6.4 Hz, 1H), 3.34-3.32 (m, 2H), 3.19 (d, *J* = 10.4 Hz, 2H), 2.34-2.21 (m, *J* = 7.3, 6.9 Hz, 2H), 2.14-2.04 (m, 4H), 1.95-1.84 (m, 4H), 1.22 (dd, *J* = 15.3, 7.1 Hz, 6H), 1.11 (dd, *J* = 14.0, 7.0 Hz, 6H). **<sup>31</sup>P{<sup>1</sup>H}-NMR** (162 MHz, THF-*d*<sub>8</sub>): δ 38.9.

**Attempted Catalytic Reactions:** Reactions were prepared in a glovebox and conducted in a J. Young NMR tube at ~ 0.07 mmol scale for metal complex (~ 0.005 – 0.010 g) in ~ 0.5-0.6 mL of the indicated solvent(s) with 1,3,5-trimethoxybenzene as a standard. Metal complexes, **[M]**, substrate, and reaction solvent were first mixed in a 5 mL vial. Liquid substrates were measured using a gas-tight 50 uL syringe. The resulting solution/suspension was then transferred to the J. Young tube, sealed, and removed from the glovebox. Upon removal, NMR spectrum were obtained for reference (t = 0 h), then the reaction placed into a temperature regulated oil bath for



the designated time. Reactions from Scheme 4.16, Scheme 4.18, and Scheme 4.19 first had the [M] precursor thoroughly mixed with NaB(ArF)<sub>4</sub> in the reaction solvent for ~ 3 minutes by pipette to create a homogenous suspension before adding the substrate(s). Reactions from Scheme 4.24 and Scheme 4.23 were conducted in 5 mL vials sealed with Teflon lined, screw-type caps. The [M] precursor and ligand(s) were thoroughly stirred in the reaction solvent for ~10 minutes before adding the substrates, sealing the reaction vial, and heating in a temperature regulated aluminum block outside the glovebox. After the reactions were complete, a combination of NMR spectroscopy, UHPLC/ESI, and/or GC/MS analyses were performed.

## Chapter 5: Conclusion

### 5.1 Summary

This thesis has focused on the development of organotransition metal complexes featuring 1,3-*N,O*-chelating ligands. These complexes were tested as precatalysts in the homogenous catalytic  $\alpha$ -alkylation of amines with C-C unsaturations, termed hydroaminoalkylation. Chapter 1 reviewed transition-metal complexes that feature 2-pyridone/2-pyridonate ligands. The review highlights complexes that are used in catalytic reactions. Chapter 2 utilized 2-pyridonate ancillary ligands as a catalyst design feature to develop novel catalytic systems expanding the scope of Ta catalyzed hydroaminoalkylation to include sterically demanding internal alkenes. Further investigations have revealed that the functionalization of the 2-pyridonate ligand can significantly impact reactivity, and that off-cycle equilibria limit the rate of catalysis. Chapter 3 explored new phosphoramidate ligated Nb complexes for hydroaminoalkylation catalysis. Chapter 4 investigates Ru, Rh, and Ir complexes featuring both phosphino-2-pyridonate and 2-pyridonate ligands for their reactivity towards amines and initial efforts to realize a general late-transition-metal hydroaminoalkylation catalyst system.

In collaboration with Dr. Eugene Chong, a former Schafer group member, we explored the hydroaminoalkylation reactivity of a 6-phenyl-2-pyridonate chloro tri(amido) tantalum complex **2.12**. This complex was found to provide excellent reactivity and broad substrate for the hydroaminoalkylation of internal alkenes with unprotected secondary amines. This reactivity represents the first hydroaminoalkylation catalyst that allows for general reactivity with internal alkenes, without isomerization of the alkene, to produce  $\beta$ -branched amine products. A direct comparison with 2-pyridonate tetra(amido) tantalum complex **2.13** was made. It was found that **2.13** reacts poorly with internal alkenes, but has excellent reactivity with terminal alkenes. Based

on this, we propose that the steric accessibility created by the planar 2-pyridonate, and chloro ligands are key features for reactivity with sterically demanding internal alkene substrates.

Derivatives of **2.12** were synthesized with modification of the 3- and 6-position of the 2-pyridonate ligand. It was found that commercially available 3-methyl-2-pyridonate and 2-pyridonate maintained high reactivity with cyclohexene while improving reactivity with 1-octene compared to **2.12**. Complexes with 2-pyridonate ligands with 6-substitution had significantly hindered reactivity with cyclohexene, while offering high reactivity with 1-octene, which is consistent with our steric proposal. The 6-position of the 2-pyridonate ligand is positioned close to the metal center and could readily impart significant steric bulk about the Ta active site.

A series of experiments, including reaction monitoring and deuterium labelling studies, were used to gain mechanistic insight for this new type of precatalyst. It was demonstrated that off-cycle species dominate the tantalum speciation. Deuterium labelling also demonstrates facile C–H activation through scrambling of the deuterium label. Further, significant competition between the amine substrate and the amido ligands of the precatalyst was observed. Reaction monitoring confirmed this, as a significant induction period was observed.

Chapter 3 explored the use of an alternative 1,3-*N,O*-chelating phosphoramidate ancillary ligand on Nb complexes. A series of complexes was synthesized by protonolysis and activity for catalytic hydroaminoalkylation was tested. It was found that the highest activity was observed with an *in situ* prepared catalyst system of 2 equivalents phosphoramidate ligand to 1 equivalent Nb(NMe<sub>2</sub>)<sub>5</sub>. These Nb precatalysts show a slight improvement in activity when compared to analogous Ta complexes. Additionally, diphosphoramidate niobaziridine complexes could be synthesized, and proved to be active for hydroaminoalkylation. The activity of these niobaziridines, while poor, supports that phosphoramidate amido Nb complexes likely follow the

same proposed mechanism for that of other early-transition-metal hydroaminoalkylation catalysts.

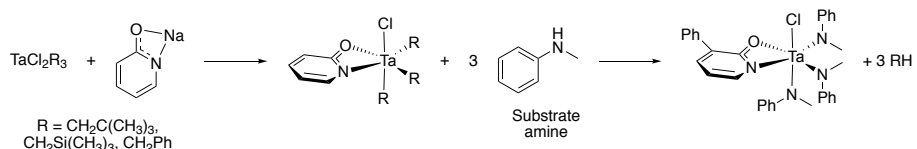
Chapter 4 detailed my initial investigations into the synthesis and reactivity of tethered phosphino-2-pyridonate and 2-pyridonate late-transition metal complexes toward their use in hydroaminoalkylation chemistry. New *P,N*-chelated cationic Cp\*Rh, Cp\*Ir, and (*p*-cymene)Ru complexes were found to react with pyrrolidine to produce M–H complexes. However, these complexes were not active for catalytic hydroaminoalkylation or catalytic acceptorless dehydrogenation of amines. The use of 2-pyridonate and 2-aminopyridinate cationic complexes, generated *in situ*, were found to catalyze the reaction of dibenzylamine into tribenzylamine. While no hydroaminoalkylation chemistry was observed in the presence of diene, the Ru variant was found to catalyze the dehydrogenation of dibenzylamine to the imine, transferring the ‘H<sub>2</sub>’ equivalent to the diene. Attempts to synthesize non-arene supported complexes was met with limited success but resulted in a bis(phosphino-2-pyridone)Ru(II) complex, and phosphino-2-pyridonate Rh(I) and Ir(I) complexes. Unfortunately, attempts to utilize these complexes, as well as *in situ* generated Ru complexes with these ligands sets, did not result in catalytic hydroaminoalkylation.

## **5.2 Future Directions**

### **5.2.1 Early-Transition Metal Catalyzed Hydroaminoalkylation**

The discovery of the 2-pyridonate chloro tris(amido) tantalum ligand environment allowed for expansion of hydroaminoalkylation substrate scope to include internal alkenes. This advance should help guide new precatalyst development. The amido ligands have been found to significantly compete for hydroaminoalkylation reactivity, and require the use of excess amounts alkene to ensure complete functionalization of the desired substrate amine, as well as the amido

ligands. This could be avoided through the replacement of amido ligands with alkyl ligands in the precatalyst.  $\text{TaMe}_3\text{Cl}_2$  and complex **2.11** have both been found to catalyze hydroaminoalkylation.<sup>175-176</sup> However, both complexes are thermally and light sensitive potentially limiting their synthetic utility. Fortunately, previously reported  $\text{TaCl}_2\text{R}_3$  ( $\text{R} = \text{CH}_2\text{C}(\text{CH}_3)_3$ ,  $\text{CH}_2\text{Si}(\text{CH}_3)_3$ ,  $\text{CH}_2\text{Ph}$ ) complexes are stable at ambient temperatures and stable to light.<sup>257-259</sup> Complexes analogous to our reported **2.12** could potentially be synthesized using these precursors (Scheme 5.1). Additionally,  $\text{TaCl}_3\text{R}_2$  complexes are also readily available, offering the possibility to explore complexes with two chloro ligands.<sup>257-259</sup> Upon reaction with substrate amine, these complexes would undergo protonolysis releasing unreactive alkane.

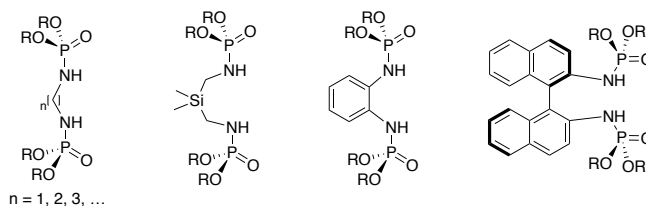


**Scheme 5.1 Synthesis of Ta alkyl complexes analogous to 2.12**

A logical extension to the use of 2-pyridonate ligands, is the use of 2-aminopyridinate ligands. As outlined in Chapter 2, 2-aminopyridinate Ti complexes have been utilized for hydroaminoalkylation.<sup>169,204,260</sup> Compared to 2-pyridonates, the modular synthesis of 2-aminopyridines allows for the *N*-substitution and the 6-substitution to be readily modified to further control the steric and/or electronic parameters.<sup>243,261</sup>

The results and conclusions presented in Chapter 3 demonstrate that a Nb metal center ligated by two phosphoramidate ligands with minimal steric parameters is a highly effective catalytic system for hydroaminoalkylation. This is in direct contrast to tethered, diamidate complexes of Nb that were found to be unreactive for hydroaminoalkylation,<sup>181</sup> as well as results on diamidate complexes of Ta that have been found to exhibit poor activity as precatalysts for hydroaminoalkylation.<sup>172,185</sup>

The results from Chapter 3 suggest that tethered diphosphoramidate Nb complexes could be highly active catalyst (Scheme 5.2). Previous work on Zr complexes with tethered diureates for hydroamination demonstrate the potential use of these types of motifs in early-transition-metal catalysis.<sup>262</sup> A similar *N,N*-tethered ligand set would allow for significant variation in tether length and flexibility that would in turn allow for precise control over the steric environment and bite angle to optimize reactivity. For example, incorporation of a silyl group in the tether would allow for increased flexibility, while incorporation of an aryl group would provide a more rigid tether structure. A tethered ligand should also offer potential improvements in catalyst stability. The incorporation of a chiral linkage could allow for enantioselective reactivity. For example, biaryl motifs have been successfully utilized in enantioselective hydroaminoalkylation as diamidates and as BINOLate Ta complexes.<sup>172-174,181-182</sup> However, these examples suffer from high reaction temperatures resulting in moderate enantioselectivities for all but a few substrates. The 90 °C reactivity provided by phosphoramidate Nb complexes may allow for significant improvement to enantioselectivities.



**Scheme 5.2 Potential tethered diphosphoramidate protio-ligands for use in Nb catalyzed hydroaminoalkylation**

### 5.2.2 Late-Transition Metal Catalyzed Hydroaminoalkylation

Unfortunately, our efforts in Chapter 4 to realize a late-transition-metal catalyzed hydroaminoalkylation were unsuccessful. It was demonstrated that facile stoichiometric dehydrogenation of amines could be facilitated by ligands incorporating the 2-pyridonate motif combined with electron-deficient cationic metal complexes. Efforts to move away from arene-

supported complexes were met with little success. A significant drawback was the inability to produce isolable and characterized non-arene complexes based on the bidentate phosphino-2-pyridone ligands employed. Well-defined complexes could have guided future ligand and catalyst design through additional stoichiometric studies to probe the fundamental steps involved in hydroaminoalkylation. Future work could focus on multi-dentate ligand incorporating the 2-pyridone functionality. Additionally, a ligand framework that could also be modified to incorporate the analogous 2-aminopyridine functionality is desirable. A 2-amino group could be sterically and electronically modified to potentially modulate reactivity.

Complexes that incorporate tridentate *N,N,N*-chelates, such as complexes **1.22**, **1.31**, **1.38**, **1.39**, **1.41**, or **1.42** detailed in Chapter 1,<sup>31,35-36,38</sup> have already been explored for their reactivity in hydrogenation/dehydrogenation chemistry with alcohols/carbonyls. However, their reactivity with amines has not been reported. A related *N*-mesityl-2-aminopyridine derivative has also been synthesized (Figure 5.1, **5.1**).<sup>263</sup> These complexes could be starting points to investigate their potential for catalytic hydroaminoalkylation. Additionally, these ligand sets could be expanded to synthesize their Rh and Ir analogues. These derivatives all coordinate in a meridional geometry about the metal center. As an alternative, the trispyridylamine ligand set has been expanded to include 2-hydroxypyridines and 2-aminopyridines. Complexes of Fe, Cu (Figure 5.1, **5.2**), and Ru (Figure 5.1, **5.3**) have already been reported,<sup>264-266</sup> while trispyridylamine Rh and Ir complexes are also reported.<sup>267</sup> Intriguingly, the trispyridylamine ligand has been shown to be hemi-labile, where a pyridyl arm can become uncoordinated from the metal center allowing for an open coordination site.<sup>267</sup>

While our results demonstrate that cationic complexes can readily facilitate the stoichiometric dehydrogenation of amines, the resulting metal hydride does not have the required

hydricity to realize the desired hydroaminoalkylation chemistry. The use of these hard nitrogen donors may provide for non-cationic complexes that are electron poor to accommodate the dehydrogenation step, but have increased hydricity over cationic complexes to effect hydroaminoalkylation chemistry.

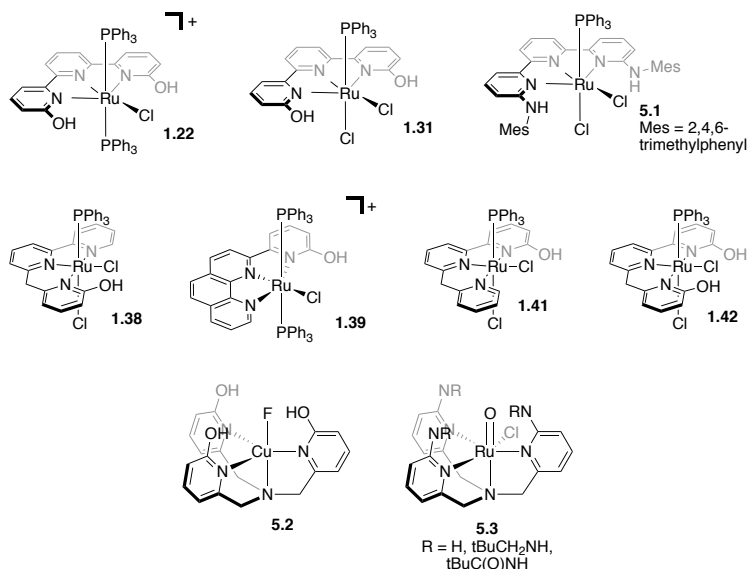


**Figure 5.1** Examples of alternative ligand sets for future work toward late-transition-metal catalyzed hydroaminoalkylation chemistry

### 5.3 Concluding Remarks

This thesis has demonstrated how a combination of ligand and complex design can significantly alter reactivity. Further, this thesis demonstrates that 1,3-*N,O*-chelating 2-pyridonate and phosphoramidate ligands are well-suited as ancillary ligands for Ta and Nb catalyzed hydroaminoalkylation of alkenes with secondary amines. In contrast, phosphino-2-pyridonate and 2-pyridonate ligands have been shown to act as a coordinated base when coordinated to late-transition metal complexes, allowing for interesting reactivity with amines.



## References

- (1) Lawrence, S. A., *Amines: Synthesis, Properties and Applications*. Cambridge University Press: Cambridge, 2004.
- (2) Ricci, A., *Amino Group Chemistry: From Synthesis to the Life Sciences*. Wiley-VCH Verlag GmbH & Co. KGaA: Weinheim, 2008.
- (3) Nugent, T. C., *Chiral Amine Synthesis*. Wiley-VCH Verlag GmbH and Co. KGaA: Weinheim, 2010.
- (4) Roughley, S. D.; Jordan, A. M. *J. Med. Chem.* **2011**, *54*, 3451-3479.
- (5) Vitaku, E.; Smith, D. T.; Njardarson, J. T. *J. Med. Chem.* **2014**, *57*, 10257-10274.
- (6) Thomas, S. W.; Swager, T. M. *Macromolecules* **2005**, *38*, 2716-2721.
- (7) Lin, H.-y.; Liou, G.-S. *J. Polym. Sci. A* **2009**, *47*, 285-294.
- (8) Froidevaux, V.; Negrell, C.; Caillol, S.; Pascault, J. P.; Boutevin, B. *Chem. Rev.* **2016**, *116*, 14181-14224.
- (9) Perry, M. R.; Ebrahimi, T.; Morgan, E.; Edwards, P. M.; Hatzikiriakos, S. G.; Schafer, L. L. *Macromolecules* **2016**, *49*, 4423-4430.
- (10) Hao, H.; Thompson, K. A.; Hudson, Z. M.; Schafer, L. *Chem. Eur. J.* **2017**, *10.1002/chem.201704500*.
- (11) Dutcher, B.; Fan, M.; Russell, A. G. *ACS Appl. Mater. Interfaces* **2015**, *7*, 2137-2148.
- (12) Hartwig, J. F., *Organotransition Metal Chemistry: From Bonding to Catalysis*. University Science Books: Sausalito, Calif., 2010.
- (13) Sheldon, R. A. *Green Chem.* **2007**, *9*, 1273-1283.
- (14) Cook, M. J.; Katritzky, A. R.; Hepler, L. G.; Matsui, T. *Tetrahedron Lett.* **1976**, *17*, 2685-2688.
- (15) Cox, R. H.; Bothner-By, A. A. *J. Phys. Chem.* **1969**, *73*, 2465-2468.
- (16) Frank, J.; Katritzky, A. R. *J. Chem. Soc., Perkin Trans. 2* **1976**, 1428-1431.
- (17) Dono, K.; Huang, J.; Ma, H.; Qian, Y. *J. Appl. Polym. Sci.* **2000**, *77*, 3247-3251.
- (18) Takashima, Y.; Nakayama, Y.; Hashiguchi, M.; Hosoda, T.; Yasuda, H.; Hirao, T.; Harada, A. *Polymer* **2006**, *47*, 5762-5774.
- (19) Chong, E.; Schafer, L. L. *Org. Lett.* **2013**, *15*, 6002-6005.
- (20) Webster, R. L.; Noroozi, N.; Hatzikiriakos, S. G.; Thomson, J. A.; Schafer, L. L. *Chem. Commun.* **2013**, *49*, 57-59.
- (21) Gilmour, D. J.; Webster, R. L.; Perry, M. R.; Schafer, L. L. *Dalton Trans.* **2015**, *44*, 12411-12419.
- (22) Bexrud, J. A.; Eisenberger, P.; Leitch, D. C.; Payne, P. R.; Schafer, L. L. *J. Am. Chem. Soc.* **2009**, *131*, 2116-2118.
- (23) Bexrud, J. A.; Schafer, L. L. *Dalton Trans.* **2010**, *39*, 361-363.
- (24) Chong, E.; Brandt, J. W.; Schafer, L. L. *J. Am. Chem. Soc.* **2014**, *136*, 10898-10901.
- (25) Brandt, J. W.; Chong, E.; Schafer, L. L. *ACS Catal.* **2017**, *7*, 6323-6330.
- (26) Edwards, P. M.; Schafer, L. L. *Org. Lett.* **2017**, *19*, 5720-5723.
- (27) Dubey, A.; Nencini, L.; Fayzullin, R. R.; Nervi, C.; Khusnutdinova, J. R. *ACS Catal.* **2017**, *7*, 3864-3868.
- (28) Kelson, E. P.; Phengsy, P. P. *Dalton Trans.* **2000**, 4023-4024.
- (29) van Ravensteijn, B. G. P.; Schild, D.-J.; Kegel, W. K.; Klein Gebbink, R. J. M. *ChemCatChem* **2017**, *9*, 440-450.

- (30) Nieto, I.; Livings, M. S.; Sacci, J. B.; Reuther, L. E.; Zeller, M.; Papish, E. T. *Organometallics* **2011**, *30*, 6339-6342.
- (31) Moore, C. M.; Szymczak, N. K. *Chem. Commun.* **2013**, *49*, 400-402.
- (32) Baysal, A.; Aydemir, M.; Durap, F.; Ozkar, S.; Yildirim, L. T.; Ocak, Y. S. *Polyhedron* **2015**, *89*, 55-61.
- (33) Jiang, F.; Achard, M.; Roisnel, T.; Dorcet, V.; Bruneau, C. *Eur. J. Inorg. Chem.* **2015**, *2015*, 4312-4317.
- (34) Baran, M. F.; Durap, F.; Aydemir, M.; Baysal, A. *Appl. Organomet. Chem.* **2016**, *30*, 1030-1035.
- (35) Moore, C. M.; Bark, B.; Szymczak, N. K. *ACS Catal.* **2016**, *6*, 1981-1990.
- (36) Shi, J.; Hu, B.; Gong, D.; Shang, S.; Hou, G.; Chen, D. *Dalton Trans.* **2016**, *45*, 4828-4834.
- (37) Paul, B.; Chakrabarti, K.; Kundu, S. *Dalton Trans.* **2016**, *45*, 11162-11171.
- (38) Shi, J.; Hu, B.; Chen, X.; Shang, S.; Deng, D.; Sun, Y.; Shi, W.; Yang, X.; Chen, D. *ACS Omega* **2017**, *2*, 3406-3416.
- (39) Shi, J.; Shang, S.; Hu, B.; Chen, D. *Appl. Organomet. Chem.* **2017**, 10.1002/aoc.4100.
- (40) Flood, T. C.; Lim, J. K.; Deming, M. A. *Organometallics* **2000**, *19*, 2310-2317.
- (41) Lugan, N.; Lavigne, G.; Soulie, J. M.; Fabre, S.; Kalck, P.; Saillard, J. Y.; Halet, J. F. *Organometallics* **1995**, *14*, 1712-1731.
- (42) Werle, T.; Schaeffler, L.; Maas, G. *J. Organomet. Chem.* **2005**, *690*, 5562-5569.
- (43) Grohmann, M.; Buck, S.; Schaeffler, L.; Maas, G. *Adv. Synth. Catal.* **2006**, *348*, 2203-2211.
- (44) Grohmann, M.; Maas, G. *Tetrahedron* **2007**, *63*, 12172-12178.
- (45) Harvey, M. E.; Musaev, D. G.; Du Bois, J. *J. Am. Chem. Soc.* **2011**, *133*, 17207-17216.
- (46) Corbin, J. R.; Schomaker, J. M. *Chem. Commun.* **2017**, *53*, 4346-4349.
- (47) Sahli, Z.; Sundararaju, B.; Achard, M.; Bruneau, C. *Green Chem.* **2013**, *15*, 775-779.
- (48) Geri, J. B.; Szymczak, N. K. *J. Am. Chem. Soc.* **2015**, *137*, 12808-12814.
- (49) Chakrabarti, K.; Paul, B.; Maji, M.; Roy, B. C.; Shee, S.; Kundu, S. *Org. Biomol. Chem.* **2016**, *14*, 10988-10997.
- (50) Chakrabarti, K.; Maji, M.; Panja, D.; Paul, B.; Shee, S.; Das, G. K.; Kundu, S. *Org. Lett.* **2017**, *19*, 4750-4753.
- (51) Roy, B. C.; Chakrabarti, K.; Shee, S.; Paul, S.; Kundu, S. *Chem. Eur. J.* **2016**, *22*, 18147-18155.
- (52) Sahoo, A. R.; Jiang, F.; Bruneau, C.; Sharma, G. V. M.; Suresh, S.; Roisnel, T.; Dorcet, V.; Achard, M. *Catal. Sci. Technol.* **2017**, *7*, 3492-3498.
- (53) Sahoo, A. R.; Lalitha, G.; Murugesu, V.; Bruneau, C.; Sharma, G. V. M.; Suresh, S.; Achard, M. *J. Org. Chem.* **2017**, *82*, 10727-10731.
- (54) Selvamurugan, S.; Ramachandran, R.; Prakash, G.; Nirmala, M.; Viswanathamurthi, P.; Fujiwara, S.; Endo, A. *Inorg. Chim. Acta* **2017**, *454*, 46-53.
- (55) Schworer, B.; Fernandez, V. M.; Zirngibl, C.; Thauer, R. K. *Eur. J. Biochem.* **1993**, *212*, 255-261.
- (56) Vogt, S.; Lyon, E. J.; Shima, S.; Thauer, R. K. *J. Biol. Inorg. Chem.* **2008**, *13*, 97-106.
- (57) Hiromoto, T.; Warkentin, E.; Moll, J.; Ermler, U.; Shima, S. *Angew. Chem., Int. Ed.* **2009**, *48*, 6457-6460.
- (58) Shima, S.; Pilak, O.; Vogt, S.; Schick, M.; Stagni, M. S.; Meyer-Klaucke, W.; Warkentin, E.; Thauer, R. K.; Ermler, U. *Science* **2008**, *321*, 572-575.

- (59) Shima, S.; Chen, D.; Xu, T.; Wodrich, M. D.; Fujishiro, T.; Schultz, K. M.; Kahnt, J.; Ataka, K.; Hu, X. *Nat. Chem.* **2015**, *7*, 995-1002.
- (60) Yang, X. *Chem. Commun.* **2015**, *51*, 13098-13101.
- (61) Ge, H.; Jing, Y.; Yang, X. *Inorg. Chem.* **2016**, *55*, 12179-12184.
- (62) Xu, T.; Yin, C.-J. M.; Wodrich, M. D.; Mazza, S.; Schultz, K. M.; Scopelliti, R.; Hu, X. *J. Am. Chem. Soc.* **2016**, *138*, 3270-3273.
- (63) Fujita, K.-i.; Tanino, N.; Yamaguchi, R. *Org. Lett.* **2007**, *9*, 109-111.
- (64) Royer, A. M.; Rauchfuss, T. B.; Wilson, S. R. *Inorg. Chem.* **2008**, *47*, 395-397.
- (65) Fujita, K.-i.; Yoshida, T.; Imori, Y.; Yamaguchi, R. *Org. Lett.* **2011**, *13*, 2278-2281.
- (66) Kawahara, R.; Fujita, K.-i.; Yamaguchi, R. *J. Am. Chem. Soc.* **2012**, *134*, 3643-3646.
- (67) Kawahara, R.; Fujita, K.-i.; Yamaguchi, R. *Angew. Chem., Int. Ed.* **2012**, *51*, 12790-12794.
- (68) Zeng, G.; Sakaki, S.; Fujita, K.-i.; Sano, H.; Yamaguchi, R. *ACS Catal.* **2014**, *4*, 1010-1020.
- (69) Fujita, K.-i.; Tamura, R.; Tanaka, Y.; Yoshida, M.; Onoda, M.; Yamaguchi, R. *ACS Catal.* **2017**, *7*, 7226-7230.
- (70) Munjanja, L.; Yuan, H.; Brennessel, W. W.; Jones, W. D. *J. Organomet. Chem.* **2017**, *847*, 28-32.
- (71) Fujita, K.-i.; Uejima, T.; Yamaguchi, R. *Chem. Lett.* **2013**, *42*, 1496-1498.
- (72) Fujita, K.-i.; Ito, W.; Yamaguchi, R. *ChemCatChem* **2014**, *6*, 109-112.
- (73) Ngo, A. H.; Adams, M. J.; Do, L. H. *Organometallics* **2014**, *33*, 6742-6745.
- (74) Fujita, K.-i.; Kawahara, R.; Aikawa, T.; Yamaguchi, R. *Angew. Chem., Int. Ed.* **2015**, *54*, 9057-9060.
- (75) Dai, X.-J.; Li, C.-J. *J. Am. Chem. Soc.* **2016**, *138*, 5433-5440.
- (76) Li, F.; Lu, L.; Liu, P. *Org. Lett.* **2016**, *18*, 2580-2583.
- (77) Sahoo, A. R.; Jiang, F.; Bruneau, C.; Sharma, G. V. M.; Suresh, S.; Achard, M. *RSC Adv.* **2016**, *6*, 100554-100558.
- (78) Yamaguchi, R.; Ikeda, C.; Takahashi, Y.; Fujita, K.-i. *J. Am. Chem. Soc.* **2009**, *131*, 8410-8412.
- (79) Fujita, K.; Tanaka, Y.; Kobayashi, M.; Yamaguchi, R. *J. Am. Chem. Soc.* **2014**, *136*, 4829-4832.
- (80) Fujita, K.-i.; Wada, T.; Shiraishi, T. *Angew. Chem., Int. Ed.* **2017**, *56*, 10886-10889.
- (81) Wang, R.; Fan, H.; Zhao, W.; Li, F. *Org. Lett.* **2016**, *18*, 3558-3561.
- (82) Fan, H.; Zhang, W.; Zhao, W.; Li, F. *ChemistrySelect* **2017**, *2*, 5735-5739.
- (83) Himeda, Y.; Onozawa-Komatsuzaki, N.; Sugihara, H.; Kasuga, K. *Organometallics* **2007**, *26*, 702-712.
- (84) Hull, J. F.; Himeda, Y.; Wang, W. H.; Hashiguchi, B.; Periana, R.; Szalda, D. J.; Muckerman, J. T.; Fujita, E. *Nat. Chem.* **2012**, *4*, 383-388.
- (85) Wang, W.-H.; Hull, J. F.; Muckerman, J. T.; Fujita, E.; Himeda, Y. *Energy Environ. Sci.* **2012**, *5*, 7923-7926.
- (86) Wang, W.-H.; Muckerman, J. T.; Fujita, E.; Himeda, Y. *ACS Catal.* **2013**, *3*, 856-860.
- (87) Badiei, Y. M.; Wang, W.-H.; Hull, J. F.; Szalda, D. J.; Muckerman, J. T.; Himeda, Y.; Fujita, E. *Inorg. Chem.* **2013**, *52*, 12576-12586.
- (88) Wang, L.; Onishi, N.; Murata, K.; Hirose, T.; Muckerman, J. T.; Fujita, E.; Himeda, Y. *ChemSusChem* **2017**, *10*, 1071-1075.
- (89) Wang, W.-H.; Xu, S.; Manaka, Y.; Suna, Y.; Kambayashi, H.; Muckerman, J. T.; Fujita, E.; Himeda, Y. *ChemSusChem* **2014**, *7*, 1976-1983.

- (90) Wang, W.-H.; Ertem, M. Z.; Xu, S.; Onishi, N.; Manaka, Y.; Suna, Y.; Kambayashi, H.; Muckerman, J. T.; Fujita, E.; Himeda, Y. *ACS Catal.* **2015**, *5*, 5496-5504.
- (91) Conifer, C. M.; Law, D. J.; Sunley, G. J.; Haynes, A.; Wells, J. R.; White, A. J. P.; Britovsek, G. J. P. *Eur. J. Inorg. Chem.* **2011**, *2011*, 3511-3522.
- (92) Conifer, C. M.; Taylor, R. A.; Law, D. J.; Sunley, G. J.; White, A. J. P.; Britovsek, G. J. P. *Dalton Trans.* **2011**, *40*, 1031-1033.
- (93) Brewster, T. P.; Ou, W. C.; Tran, J. C.; Goldberg, K. I.; Hanson, S. K.; Cundari, T. R.; Heinekey, D. M. *ACS Catal.* **2014**, *4*, 3034-3038.
- (94) Qu, P.; Sun, C.; Ma, J.; Li, F. *Adv. Synth. Catal.* **2014**, *356*, 447-459.
- (95) Liang, R.; Li, S.; Wang, R.; Lu, L.; Li, F. *Org. Lett.* **2017**, *19*, 5790-5793.
- (96) Wang, R.; Ma, J.; Li, F. *J. Org. Chem.* **2015**, *80*, 10769-10776.
- (97) Suna, Y.; Ertem, M. Z.; Wang, W.-H.; Kambayashi, H.; Manaka, Y.; Muckerman, J. T.; Fujita, E.; Himeda, Y. *Organometallics* **2014**, *33*, 6519-6530.
- (98) Ngo, A. H.; Ibanez, M.; Do, L. H. *ACS Catal.* **2016**, *6*, 2637-2641.
- (99) Wu, W.-P.; Xu, Y.-J.; Zhu, R.; Cui, M.-S.; Li, X.-L.; Deng, J.; Fu, Y. *ChemSusChem* **2016**, *9*, 1209-1215.
- (100) Xu, Z.; Yan, P.; Li, H.; Liu, K.; Liu, X.; Jia, S.; Zhang, Z. C. *ACS Catal.* **2016**, *6*, 3784-3788.
- (101) Xu, Y.-J.; Shi, J.; Wu, W.-P.; Zhu, R.; Li, X.-L.; Deng, J.; Fu, Y. *Appl. Catal., A* **2017**, *543*, 266-273.
- (102) Xu, Z.; Yan, P.; Jiang, H.; Liu, K.; Zhang, Z. C. *Chin. J. Chem.* **2017**, *35*, 581-585.
- (103) DePasquale, J.; Nieto, I.; Reuther, L. E.; Herbst-Gervasoni, C. J.; Paul, J. J.; Mochalin, V.; Zeller, M.; Thomas, C. M.; Addison, A. W.; Papish, E. T. *Inorg. Chem.* **2013**, *52*, 9175-9183.
- (104) Lewandowska-Andralojc, A.; Polyansky, D. E.; Wang, C.-H.; Wang, W.-H.; Himeda, Y.; Fujita, E. *Phys. Chem. Chem. Phys.* **2014**, *16*, 11976-11987.
- (105) Menendez Rodriguez, G.; Bucci, A.; Hutchinson, R.; Bellachioma, G.; Zuccaccia, C.; Giovagnoli, S.; Idriss, H.; Macchioni, A. *ACS Energy Lett.* **2017**, *2*, 105-110.
- (106) Chakraborty, S.; Piszal, P. E.; Brennessel, W. W.; Jones, W. D. *Organometallics* **2015**, *34*, 5203-5206.
- (107) Chouzier, S.; Gruber, M.; Djakovitch, L. *J. Mol. Catal. A: Chem.* **2004**, *212*, 43-52.
- (108) Djakovitch, L.; Rouge, P. *J. Mol. Catal. A: Chem.* **2007**, *273*, 230-239.
- (109) Tomas-Mendivil, E.; Diez, J.; Cadierno, V. *Catal. Sci. Technol.* **2011**, *1*, 1605-1615.
- (110) Priyarega, S.; Raja, D. S.; Babu, S. G.; Karvembu, R.; Hashimoto, T.; Endo, A.; Natarajan, K. *Polyhedron* **2012**, *34*, 143-148.
- (111) Jhong, H.-M.; Liu, Y.-H.; Peng, S.-M.; Liu, S.-T. *Eur. J. Inorg. Chem.* **2016**, *2016*, 5449-5455.
- (112) Zhu, M.; Fujita, K.-i.; Yamaguchi, R. *Chem. Commun.* **2011**, *47*, 12876-12878.
- (113) Wang, Y.-H.; Xu, M.-C.; Liu, J.; Zhang, L.-J.; Zhang, X.-M. *Tetrahedron* **2015**, *71*, 9598-9601.
- (114) Zhang, L.-J.; Wang, Y.-H.; Liu, J.; Xu, M.-C.; Zhang, X.-M. *RSC Adv.* **2016**, *6*, 28653-28657.
- (115) Gerlach, D. L.; Bhagan, S.; Cruce, A. A.; Burks, D. B.; Nieto, I.; Truong, H. T.; Kelley, S. P.; Herbst-Gervasoni, C. J.; Jernigan, K. L.; Bowman, M. K.; Pan, S.; Zeller, M.; Papish, E. T. *Inorg. Chem.* **2014**, *53*, 12689-12698.
- (116) Zhang, T.; Wang, C.; Liu, S.; Wang, J.-L.; Lin, W. *J. Am. Chem. Soc.* **2014**, *136*, 273-281.

- (117) Karmakar, A.; Paul, A.; Mahmudov, K. T.; Guedes da Silva, M. F. C.; Pombeiro, A. J. L. *New J. Chem.* **2016**, *40*, 1535-1546.
- (118) Llabres i. Xamena, F. X.; Abad, A.; Corma, A.; Garcia, H. *J. Catal.* **2007**, *250*, 294-298.
- (119) Opelt, S.; Krug, V.; Sonntag, J.; Hunger, M.; Klemm, E. *Microporous Mesoporous Mater.* **2011**, *147*, 327-333.
- (120) Opelt, S.; Krug, V.; Sonntag, J.; Hunger, M.; Klemm, E. *Microporous Mesoporous Mater.* **2012**, *147*, 327-333.
- (121) Schuster, S.; Klemm, E.; Bauer, M. *Chem. Eur. J.* **2012**, *18*, 15831-15837.
- (122) Tabares, L. C.; Navarro, J. A. R.; Salas, J. M. *J. Am. Chem. Soc.* **2001**, *123*, 383-387.
- (123) Llabres i. Xamena, F. X.; Casanova, O.; Galiasso Tailleur, R.; Garcia, H.; Corma, A. *J. Catal.* **2008**, *255*, 220-227.
- (124) Luz, I.; Leon, A.; Boronat, M.; Llabres i. Xamena, F. X.; Corma, A. *Catal. Sci. Technol.* **2013**, *3*, 371-379.
- (125) Luz, I.; Llabres i. Xamena, F. X.; Corma, A. *J. Catal.* **2010**, *276*, 134-140.
- (126) Luz, I.; Llabres i. Xamena, F. X.; Corma, A. *J. Catal.* **2012**, *285*, 285-291.
- (127) Priyadarshini, S.; Amal Joseph, P. J.; Kantam, M. L.; Sreedhar, B. *Tetrahedron* **2013**, *69*, 6409-6414.
- (128) Luz, I.; Corma, A.; Llabres i. Xamena, F. X. *Catal. Sci. Technol.* **2014**, *4*, 1829-1836.
- (129) Maiti, D.; Fors, B. P.; Henderson, J. L.; Nakamura, Y.; Buchwald, S. L. *Chem. Sci.* **2011**, *2*, 57-68.
- (130) Paradies, J., Palladium-Catalyzed Aromatic Carbon–Nitrogen Bond Formation. In *Metal-Catalyzed Cross-Coupling Reactions and More*, Meijere, A. d.; Bräse, S.; Oestreich, M., Eds. Wiley-VCH Verlag GmbH & Co.: Weinheim, Germany, 2014; Vol. 1, pp 995-1066.
- (131) Schafer, L. L.; Yim, J. C.-H.; Yonson, N., Transition-Metal-Catalyzed Hydroamination Reactions. In *Metal-Catalyzed Cross-Coupling Reactions and More*, Meijere, A. d.; Bräse, S.; Oestreich, M., Eds. Wiley-VCH Verlag GmbH & Co.: Weinheim, Germany, 2014; Vol. 1, pp 1135-1258.
- (132) Crozet, D.; Urrutigoñy, M.; Kalck, P. *ChemCatChem* **2011**, *3*, 1102-1118.
- (133) Murahashi, S.; Yoshimura, N.; Tsumiyama, T.; Kojima, T. *J. Am. Chem. Soc.* **1983**, *105*, 5002-5011.
- (134) Chatani, N.; Asaumi, T.; Ikeda, T.; Yorimitsu, S.; Ishii, Y.; Kakiuchi, F.; Murai, S. *J. Am. Chem. Soc.* **2000**, *122*, 12882-12883.
- (135) Murahashi, S.; Komiya, N.; Terai, H.; Nakae, T. *J. Am. Chem. Soc.* **2003**, *125*, 15312-15313.
- (136) DeBoef, B.; Pastine, S. J.; Sames, D. *J. Am. Chem. Soc.* **2004**, *126*, 6556-6557.
- (137) Yi, C. S.; Yun, S. Y.; Guzei, I. A. *Organometallics* **2004**, *23*, 5392-5395.
- (138) Li, Z.; Li, C.-J. *J. Am. Chem. Soc.* **2004**, *126*, 11810-11811.
- (139) Li, Z.; Li, C.-J. *Org. Lett.* **2004**, *6*, 4997-4999.
- (140) Li, Z.; Li, C.-J. *Eur. J. Org. Chem.* **2005**, *2005*, 3173-3176.
- (141) Li, Z.; Li, C.-J. *J. Am. Chem. Soc.* **2005**, *127*, 3672-3673.
- (142) Li, Z.; Li, C.-J. *J. Am. Chem. Soc.* **2005**, *127*, 6968-6969.
- (143) Ohta, M.; Quick, M. P.; Yamaguchi, J.; Wunsch, B.; Itami, K. *Chem. Asian J.* **2009**, *4*, 1416-1419.
- (144) Prokopcova, H.; Bergman, S. D.; Aelvoet, K.; Smout, V.; Herrebout, W.; Van der Veken, B.; Meerpoel, L.; Maes, B. U. *Chem. Eur. J.* **2010**, *16*, 13063-13067.

- (145) He, J.; Hamann, L. G.; Davies, H. M.; Beckwith, R. E. *Nat Commun* **2015**, *6*, 5943.
- (146) Prier, C. K.; Rankic, D. A.; MacMillan, D. W. *Chem. Rev.* **2013**, *113*, 5322-5363.
- (147) Condie, A. G.; Gonzalez-Gomez, J. C.; Stephenson, C. R. *J. Am. Chem. Soc.* **2010**, *132*, 1464-1465.
- (148) McNally, A.; Prier, C. K.; MacMillan, D. W. *Science* **2011**, *334*, 1114-1117.
- (149) Zuo, Z.; Ahneman, D. T.; Chu, L.; Terrett, J. A.; Doyle, A. G.; MacMillan, D. W. *Science* **2014**, *345*, 437-440.
- (150) Ahneman, D. T.; Doyle, A. G. *Chem. Sci.* **2016**, *7*, 7002-7006.
- (151) Joe, C. L.; Doyle, A. G. *Angew. Chem., Int. Ed.* **2016**, *55*, 4040-4043.
- (152) Nicholls, T. P.; Constable, G. E.; Robertson, J. C.; Gardiner, M. G.; Bissember, A. C. *ACS Catal.* **2015**, *6*, 451-457.
- (153) Dangel, B. D.; Johnson, J. A.; Sames, D. *J. Am. Chem. Soc.* **2001**, *123*, 8149-8150.
- (154) McNally, A.; Haffemayer, B.; Collins, B. S.; Gaunt, M. J. *Nature* **2014**, *510*, 129-133.
- (155) He, C.; Gaunt, M. J. *Angew. Chem., Int. Ed.* **2015**, *54*, 15840-15844.
- (156) Smalley, A. P.; Gaunt, M. J. *J. Am. Chem. Soc.* **2015**, *137*, 10632-10641.
- (157) Li, Q.; Liskey, C. W.; Hartwig, J. F. *J. Am. Chem. Soc.* **2014**, *136*, 8755-8765.
- (158) Lee, M.; Sanford, M. S. *J. Am. Chem. Soc.* **2015**, *137*, 12796-12799.
- (159) Calleja, J.; Pla, D.; Gorman, T. W.; Domingo, V.; Haffemayer, B.; Gaunt, M. J. *Nat. Chem.* **2015**, *7*, 1009-1016.
- (160) Topczewski, J. J.; Cabrera, P. J.; Saper, N. I.; Sanford, M. S. *Nature* **2016**, *531*, 220-224.
- (161) Wu, Y.; Chen, Y. Q.; Liu, T.; Eastgate, M. D.; Yu, J. Q. *J. Am. Chem. Soc.* **2016**, *138*, 14554-14557.
- (162) Xu, Y.; Young, M. C.; Wang, C.; Magness, D. M.; Dong, G. *Angew. Chem., Int. Ed.* **2016**, *55*, 9084-9087.
- (163) Clerici, M. G.; Maspero, F. *Synthesis* **1980**, 305-306.
- (164) Nugent, W. A.; Ovenall, D. W.; Holmes, S. J. *Organometallics* **1983**, *2*, 162-164.
- (165) Chong, E.; Garcia, P.; Schafer, L. L. *Synthesis* **2014**, *46*, 2884-2896.
- (166) Bexrud, J. A.; Eisenberger, P.; Leitch, D. C.; Payne, P. R.; Schafer, L. L. *J. Am. Chem. Soc.* **2009**, *131*, 2116-2118.
- (167) Kubiak, R.; Prochnow, I.; Doye, S. *Angew. Chem., Int. Ed.* **2009**, *48*, 1153-1156.
- (168) Prochnow, I.; Kubiak, R.; Frey, O. N.; Beckhaus, R.; Doye, S. *ChemCatChem* **2009**, *1*, 162-172.
- (169) Dörfler, J.; Bytyqi, B.; Hüller, S.; Mann, N. M.; Brahms, C.; Schmidtman, M.; Doye, S. *Adv. Synth. Catal.* **2015**, *357*, 2265-2276.
- (170) Herzon, S. B.; Hartwig, J. F. *J. Am. Chem. Soc.* **2007**, *129*, 6690-6691.
- (171) Herzon, S. B.; Hartwig, J. F. *J. Am. Chem. Soc.* **2008**, *130*, 14940-14941.
- (172) Eisenberger, P.; Ayinla, R. O.; Lauzon, J. M. P.; Schafer, L. L. *Angew. Chem., Int. Ed.* **2009**, *48*, 8361-8365.
- (173) Zi, G.; Zhang, F.; Song, H. *Chem. Commun.* **2010**, *46*, 6296.
- (174) Reznichenko, A. L.; Hultsch, K. C. *J. Am. Chem. Soc.* **2012**, *134*, 3300-3311.
- (175) Garcia, P.; Lau, Y. Y.; Perry, M. R.; Schafer, L. L. *Angew. Chem., Int. Ed.* **2013**, *52*, 9144-9148.
- (176) Zhang, Z.; Hamel, J.-D.; Schafer, L. L. *Chem. Eur. J.* **2013**, *19*, 8751-8754.
- (177) Kubiak, R.; Prochnow, I.; Doye, S. *Angew. Chem., Int. Ed.* **2010**, *49*, 2626-2629.
- (178) Jaspers, D.; Saak, W.; Doye, S. *Synlett* **2012**, *23*, 2098-2102.

- (179) Payne, P. R.; Garcia, P.; Eisenberger, P.; Yim, J. C.-H.; Schafer, L. L. *Org. Lett.* **2013**, *15*, 2182-2185.
- (180) Eisenberger, P.; Schafer, L. L. *Pure Appl. Chem.* **2010**, *82*, 1503-1515.
- (181) Zhang, F.; Song, H.; Zi, G. *Dalton Trans.* **2011**, *40*, 1547.
- (182) Reznichenko, A. L.; Emge, T. J.; Audörsch, S.; Klauber, E. G.; Hultzsche, K. C.; Schmidt, B. *Organometallics* **2011**, *30*, 921-924.
- (183) Nako, A. E.; Oyamada, J.; Nishiura, M.; Hou, Z. M. *Chem. Sci.* **2016**, *7*, 6429-6434.
- (184) Liu, F.; Luo, G.; Hou, Z.; Luo, Y. *Organometallics* **2017**, *36*, 1557-1565.
- (185) Lauzon, J. M.; Eisenberger, P.; Roşca, S.-C.; Schafer, L. L. *ACS Catal.* **2017**, *7*, 5921-5931.
- (186) Jun, C.-H. *Chem. Commun.* **1998**, 1405-1406.
- (187) Chatani, N.; Asaumi, T.; Yorimitsu, S.; Ikeda, T.; Kakiuchi, F.; Murai, S. *J. Am. Chem. Soc.* **2001**, *123*, 10935-10941.
- (188) Pan, S.; Endo, K.; Shibata, T. *Org. Lett.* **2011**, *13*, 4692-4695.
- (189) Bergman, S. D.; Storr, T. E.; Prokopcova, H.; Aelvoet, K.; Diels, G.; Meerpoel, L.; Maes, B. U. *Chem. Eur. J.* **2012**, *18*, 10393-10398.
- (190) Pan, S.; Matsuo, Y.; Endo, K.; Shibata, T. *Tetrahedron* **2012**, *68*, 9009-9015.
- (191) Pan, S. G.; Shibata, T. *ACS Catal.* **2013**, *3*, 704-712.
- (192) Schmitt, D. C.; Lee, J.; Dechert-Schmitt, A. M.; Yamaguchi, E.; Krische, M. J. *Chem. Commun.* **2013**, *49*, 6096-6098.
- (193) Lahm, G.; Opatz, T. *Org. Lett.* **2014**, *16*, 4201-4203.
- (194) Schinkel, M.; Wang, L.; Bielefeld, K.; Ackermann, L. *Org. Lett.* **2014**, *16*, 1876-1879.
- (195) Chen, T. Y.; Tsutsumi, R.; Montgomery, T. P.; Volchkov, I.; Krische, M. J. *J. Am. Chem. Soc.* **2015**, *137*, 1798-1801.
- (196) Oda, S.; Franke, J.; Krische, M. J. *Chem. Sci.* **2016**, *7*, 136-141.
- (197) Thullen, S. M.; Rovis, T. *J. Am. Chem. Soc.* **2017**, *139*, 15504-15508.
- (198) He, J.; Li, S.; Deng, Y.; Fu, H.; Laforteza, B. N.; Spangler, J. E.; Homs, A.; Yu, J. Q. *Science* **2014**, *343*, 1216-1220.
- (199) Tran, A. T.; Yu, J. Q. *Angew. Chem., Int. Ed.* **2017**, *56*, 10530-10534.
- (200) Yamauchi, D.; Nishimura, T.; Yorimitsu, H. *Angew. Chem., Int. Ed.* **2017**, *56*, 7200-7204.
- (201) Marchetti, F.; Pampaloni, G.; Zacchini, S. *J. Fluorine Chem.* **2010**, *131*, 21-28.
- (202) Chong, E. Early Transition Metal Complexes of Pyridine Derivatives: Applications in the Catalytic Synthesis of Amines and *N*-Heterocycles. Ph.D. Dissertation, University of British Columbia, Vancouver, BC, Canada, 2014.
- (203) Garcia, P.; Payne, P. R.; Chong, E.; Webster, R. L.; Barron, B. J.; Behrle, A. C.; Schmidt, J. A. R.; Schafer, L. L. *Tetrahedron* **2013**, *69*, 5737-5743.
- (204) Dörfler, J.; Doye, S. *Angew. Chem., Int. Ed.* **2013**, *52*, 1806-1809.
- (205) Chisholm, M. H.; Huffman, J. C.; Tan, L. S. *Inorg. Chem.* **1981**, *20*, 1859-1866.
- (206) Chao, Y. W.; Wexler, P. A.; Wigley, D. E. *Inorg. Chem.* **1989**, *28*, 3860-3868.
- (207) Schrock, R. R.; Sharp, P. R. *J. Am. Chem. Soc.* **1978**, *100*, 2389-2399.
- (208) Gallagher, T.; Smith, C.; Hirschhäuser, C.; Malcolm, G.; Nasrallah, D. *Synlett* **2014**, *25*, 1904-1908.
- (209) Fusco, R.; Sannicolò, F. *J. Org. Chem.* **1984**, *49*, 4374-4378.
- (210) Lauzon, J. M. P.; Schafer, L. L. *Dalton Trans.* **2012**, *41*, 11539.

- (211) Lau, Y. Y. Catalytic Synthesis of N-Heterocycles and  $\alpha$ -Alkylated Amines by Hydroamination and Hydroaminoalkylation. Ph.D. Dissertation, University of British Columbia, Vancouver, BC, Canada, 2016.
- (212) Hamid, M. H. S. A.; Slatford, P. A.; Williams, J. M. J. *Adv. Synth. Catal.* **2007**, *349*, 1555-1575.
- (213) Guillena, G.; D, J. R.; Yus, M. *Chem. Rev.* **2010**, *110*, 1611-1641.
- (214) Bähn, S.; Imm, S.; Neubert, L.; Zhang, M.; Neumann, H.; Beller, M. *ChemCatChem* **2011**, *3*, 1853-1864.
- (215) Leonard, J.; Blacker, A. J.; Marsden, S. P.; Jones, M. F.; Mulholland, K. R.; Newton, R. *Org. Process Res. Dev.* **2015**, *19*, 1400-1410.
- (216) Yang, Q.; Wang, Q.; Yu, Z. *Chem. Soc. Rev.* **2015**, *44*, 2305-2329.
- (217) Gunanathan, C.; Milstein, D. *Science* **2013**, *341*, 1229712.
- (218) Hollmann, D.; Bahn, S.; Tillack, A.; Beller, M. *Angew. Chem., Int. Ed.* **2007**, *46*, 8291-8294.
- (219) Hollmann, D.; Bähn, S.; Tillack, A.; Parton, R.; Altink, R.; Beller, M. *Tetrahedron Lett.* **2008**, *49*, 5742-5745.
- (220) Prades, A.; Corberan, R.; Poyatos, M.; Peris, E. *Chem. Eur. J.* **2008**, *14*, 11474-11479.
- (221) Saidi, O.; Blacker, A. J.; Farah, M. M.; Marsden, S. P.; Williams, J. M. *Angew. Chem., Int. Ed.* **2009**, *48*, 7375-7378.
- (222) Wang, D.; Zhao, K.; Xu, C.; Miao, H.; Ding, Y. *ACS Catal.* **2014**, *4*, 3910-3918.
- (223) Zou, Q.; Wang, C.; Smith, J.; Xue, D.; Xiao, J. *Chem. Eur. J.* **2015**, *21*, 9656-9661.
- (224) Dobereiner, G. E.; Crabtree, R. H. *Chem. Rev.* **2010**, *110*, 681-703.
- (225) Prades, A.; Peris, E.; Albrecht, M. *Organometallics* **2011**, *30*, 1162-1167.
- (226) He, L.-P.; Chen, T.; Gong, D.; Lai, Z.; Huang, K.-W. *Organometallics* **2012**, *31*, 5208-5211.
- (227) Ho, H. A.; Manna, K.; Sadow, A. D. *Angew. Chem., Int. Ed.* **2012**, *51*, 8607-8610.
- (228) Muthaiah, S.; Hong, S. H. *Adv. Synth. Catal.* **2012**, *354*, 3045-3053.
- (229) Myers, T. W.; Berben, L. A. *J. Am. Chem. Soc.* **2013**, *135*, 9988-9990.
- (230) Tseng, K. N.; Rizzi, A. M.; Szymczak, N. K. *J. Am. Chem. Soc.* **2013**, *135*, 16352-16355.
- (231) Chakraborty, S.; Brennessel, W. W.; Jones, W. D. *J. Am. Chem. Soc.* **2014**, *136*, 8564-8567.
- (232) Xu, R.; Chakraborty, S.; Yuan, H.; Jones, W. D. *ACS Catal.* **2015**, *5*, 6350-6354.
- (233) Stubbs, J. M.; Hazlehurst, R. J.; Boyle, P. D.; Blacquiere, J. M. *Organometallics* **2017**, *36*, 1692-1698.
- (234) Valencia, M.; Pereira, A.; Muller-Bunz, H.; Belderrain, T. R.; Perez, P. J.; Albrecht, M. *Chem. Eur. J.* **2017**, 10.1002/chem.201700676.
- (235) Li, H.; Jiang, J.; Lu, G.; Huang, F.; Wang, Z.-X. *Organometallics* **2011**, *30*, 3131-3141.
- (236) Drover, M. W.; Schafer, L. L.; Love, J. A. *Dalton Trans.* **2017**, *46*, 8621-8625.
- (237) Breit, B.; Seiche, W. *J. Am. Chem. Soc.* **2003**, *125*, 6608-6609.
- (238) Govindaswamy, P.; Mozharivskyj, Y. A.; Kollipara, M. R. *Polyhedron* **2004**, *23*, 3115-3123.
- (239) Zamorano, A.; Rendon, N.; Lopez-Serrano, J.; Valpuesta, J. E.; Alvarez, E.; Carmona, E. *Chem. Eur. J.* **2015**, *21*, 2576-2587.
- (240) Hu, Y.; Norton, J. R. *J. Am. Chem. Soc.* **2014**, *136*, 5938-5948.

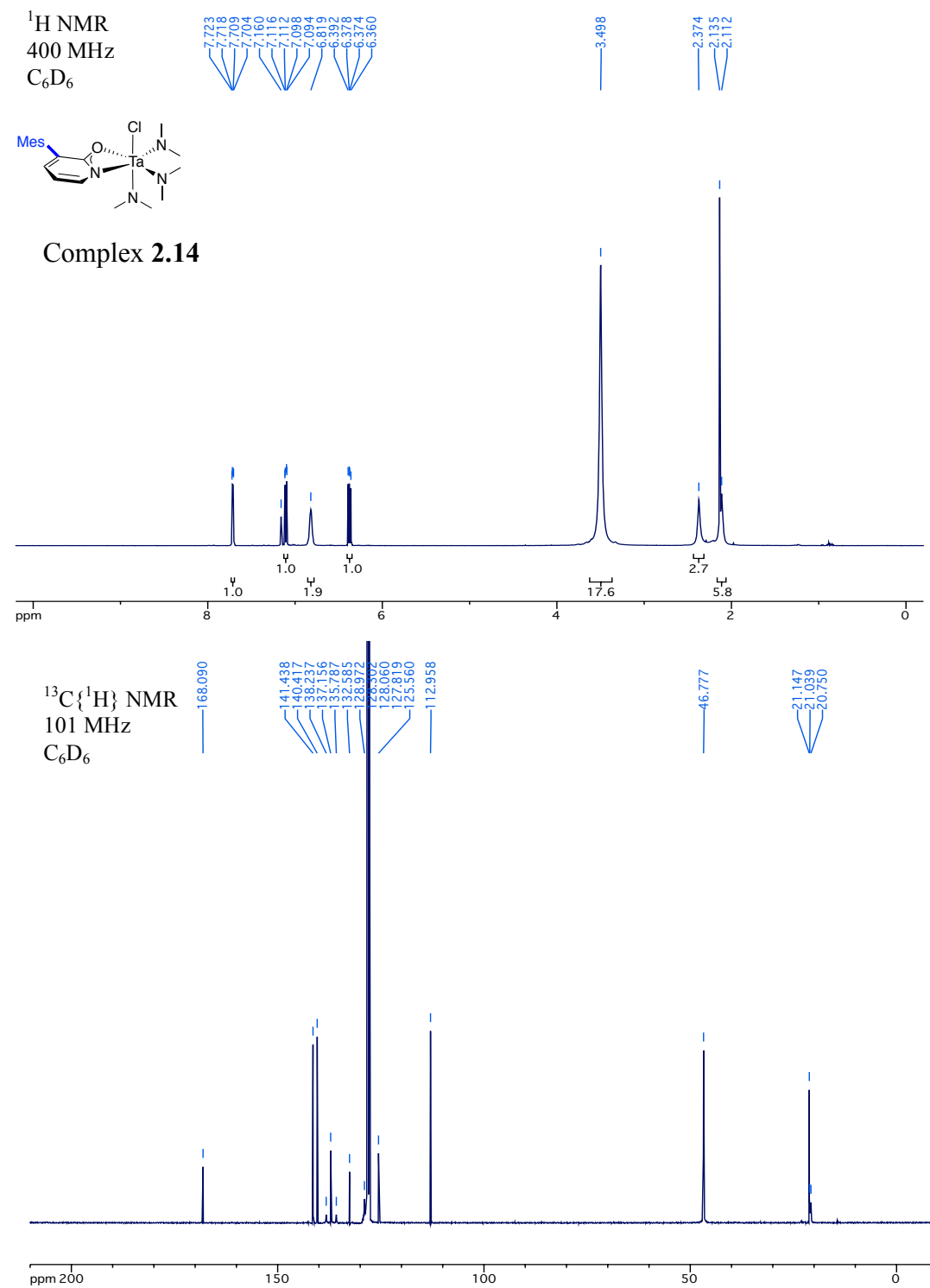


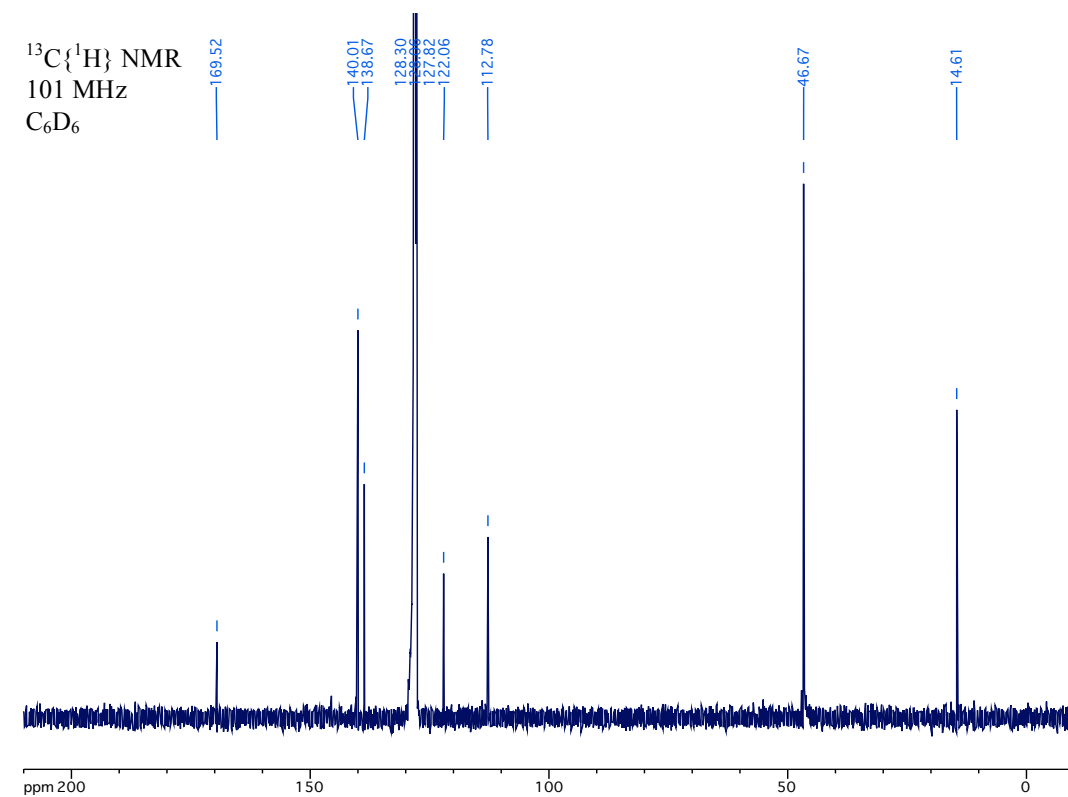
- (241) Wiedner, E. S.; Chambers, M. B.; Pitman, C. L.; Bullock, R. M.; Miller, A. J.; Appel, A. M. *Chem. Rev.* **2016**, *116*, 8655-8692.
- (242) Yi, C. S.; Yun, S. Y. *Organometallics* **2004**, *23*, 5392-5395.
- (243) Scott, Natalie M.; Schareina, T.; Tok, O.; Kempe, R. *Eur. J. Inorg. Chem.* **2004**, 3297-3304.
- (244) Rocha, S. V.; Finney, N. S. *J. Org. Chem.* **2013**, *78*, 11255-11261.
- (245) Petrone, D. A.; Yoon, H.; Weinstabl, H.; Lautens, M. *Angew. Chem., Int. Ed.* **2014**, *53*, 7908-7912.
- (246) Lahuerta, P.; Latorre, J.; Sanaú, M.; Cotton, F. A.; Schwotzer, W. *Polyhedron* **1988**, *7*, 1311-1316.
- (247) Alteparmakian, V.; Mura, P.; Olby, B. G.; Robinson, S. D. *Inorg. Chim. Acta* **1985**, *104*, L5-L6.
- (248) Threlkel, R. S.; Bercaw, J. E.; Seidler, P. F.; Stryker, J. M.; Bergman, R. G. *Org. Synth.* **1987**, *65*, 42.
- (249) Albers, M. O.; Singleton, E.; Yates, J. E. *Inorg. Synth.* **1989**, *26*, 250-251.
- (250) White, C.; Yates, A.; Maitlis, P. M. *Inorg. Synth.* **1992**, *29*, 230.
- (251) Choudhury, J.; Podder, S.; Roy, S. *J. Am. Chem. Soc.* **2005**, *127*, 6162-6163.
- (252) Schenck, T. G.; Downes, J. M.; Milne, C. R. C.; Mackenzie, P. B.; Boucher, H.; Whelan, J.; Bosnich, S. *Inorg. Chem.* **1985**, *24*, 2334-2337.
- (253) Ahmad, N.; Levison, J. J.; Robinson, S. D.; Uttley, M. F. *Inorg. Synth.* **1974**, *15*, 48-50.
- (254) Jung, C. W.; Garrou, P. E. *Organometallics* **1982**, *1*, 658-666.
- (255) Neumann, K. T.; Klimczyk, S.; Burhardt, M. N.; Bang-Andersen, B.; Skrydstrup, T.; Lindhardt, A. T. *ACS Catal.* **2016**, *6*, 4710-4714.
- (256) Abbel, R.; Abdur-Rashid, K.; Faatz, M.; Hadzovic, A.; Lough, A. J.; Morris, R. H. *J. Am. Chem. Soc.* **2005**, *127*, 1870-1882.
- (257) Schrock, R. R. *J. Organomet. Chem.* **1976**, *122*, 209-225.
- (258) Schrock, R. R.; Fellmann, J. D. *J. Am. Chem. Soc.* **1978**, *100*, 3359-3370.
- (259) Messerle, L. W.; Jennische, P.; Schrock, R. R.; Stucky, G. *J. Am. Chem. Soc.* **1980**, *102*, 6744-6752.
- (260) Dorfler, J.; Preuss, T.; Schischko, A.; Schmidtman, M.; Doye, S. *Angew. Chem., Int. Ed.* **2014**, *53*, 7918-7922.
- (261) Kempe, R. *Eur. J. Inorg. Chem.* **2003**, 2003, 791-803.
- (262) Leitch, D. C.; Payne, P. R.; Dunbar, C. R.; Schafer, L. L. *J. Am. Chem. Soc.* **2009**, *131*, 18246-18247.
- (263) Dahl, E. W.; Louis-Goff, T.; Szymczak, N. K. *Chem. Commun.* **2017**, *53*, 2287-2289.
- (264) Ogo, S.; Wada, S.; Watanabe, Y.; Iwase, M.; Wada, A.; Harata, M.; Jitsukawa, K.; Masuda, H.; Einaga, H. *Angew. Chem., Int. Ed.* **1998**, *37*, 2102-2104.
- (265) Jitsukawa, K.; Oka, Y.; Yamaguchi, S.; Masuda, H. *Inorg. Chem.* **2004**, *43*, 8119-8129.
- (266) Moore, C. M.; Szymczak, N. K. *Chem. Commun.* **2015**, *51*, 5490-5492.
- (267) Krom, M.; Peters, Theo P. J.; Coumans, Ruud G. E.; Sciarone, Timo J. J.; Hoogboom, J.; ter Beek, Sandra I.; Schlebos, Paul P. J.; Smits, Jan M. M.; de Gelder, R.; Gal, Anton W. *Eur. J. Inorg. Chem.* **2003**, 2003, 1072-1087.
- (268) Burla, M. C.; Caliendo, R.; Camalli, M.; Carrozzini, B.; Cascarano, G. L.; De Caro, L.; Giacovazzo, C.; Polidori, G.; Spagna, R. *J. Appl. Crystallogr.* **2005**, *38*, 381-388.

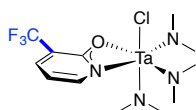
- (269) Dolomanov, O. V.; Bourhis, L. J.; Gildea, R. J.; Howard, J. A. K.; Puschmann, H. *J. Appl. Crystallogr.* **2009**, *42*, 339-341.
- (270) Sheldrick, G. M. *Acta Crystallogr. C.* **2015**, *71*, 3-8.
- (271) Macrae, C. F.; Edgington, P. R.; McCabe, P.; Pidcock, E.; Shields, G. P.; Taylor, R.; Towler, M.; van de Streek, J. *J. Appl. Crystallogr.* **2006**, *39*, 453-457.

## Appendices

### Appendix A NMR Spectra

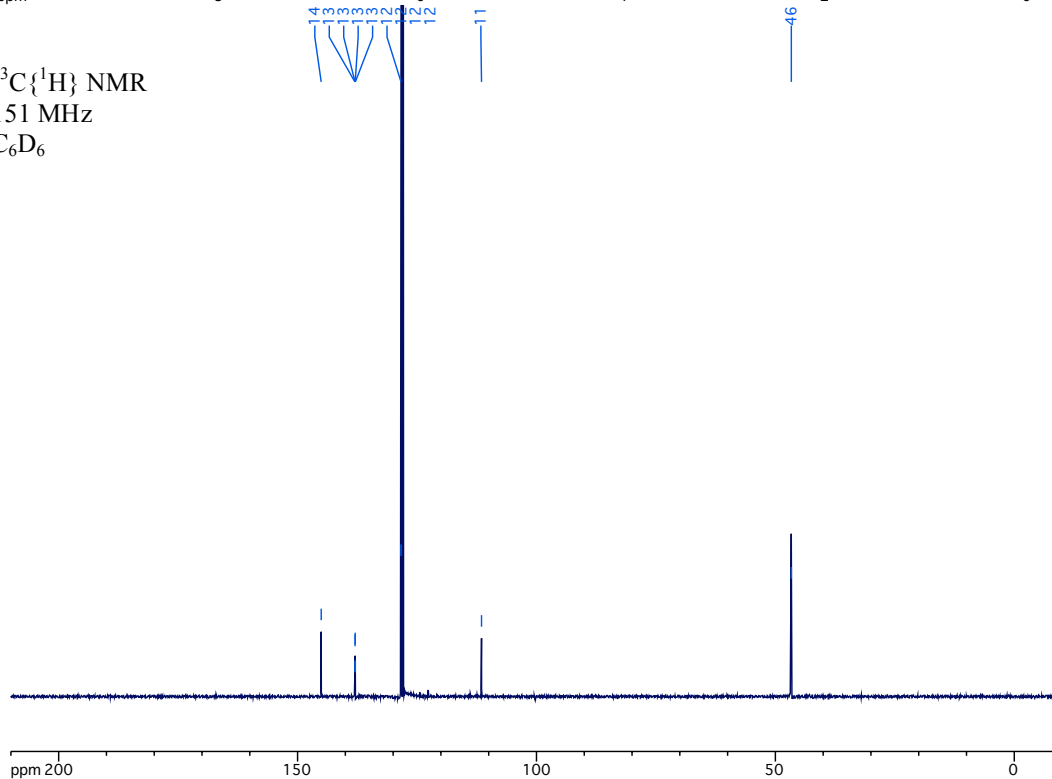




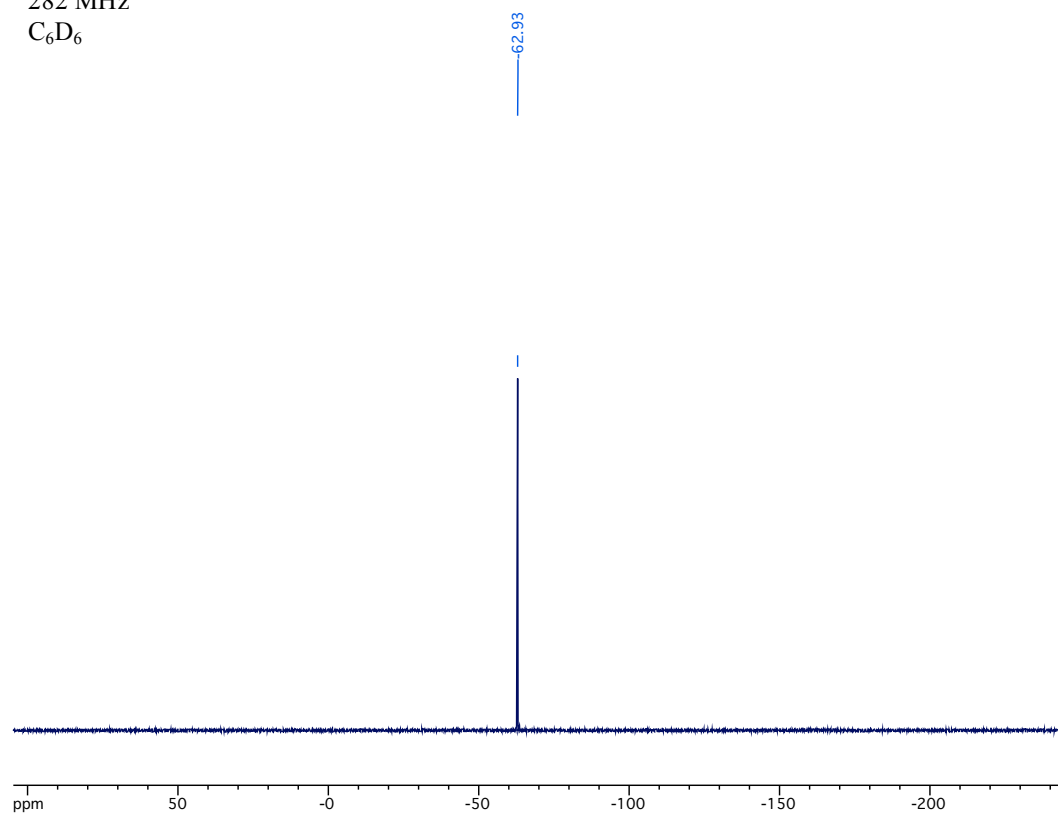


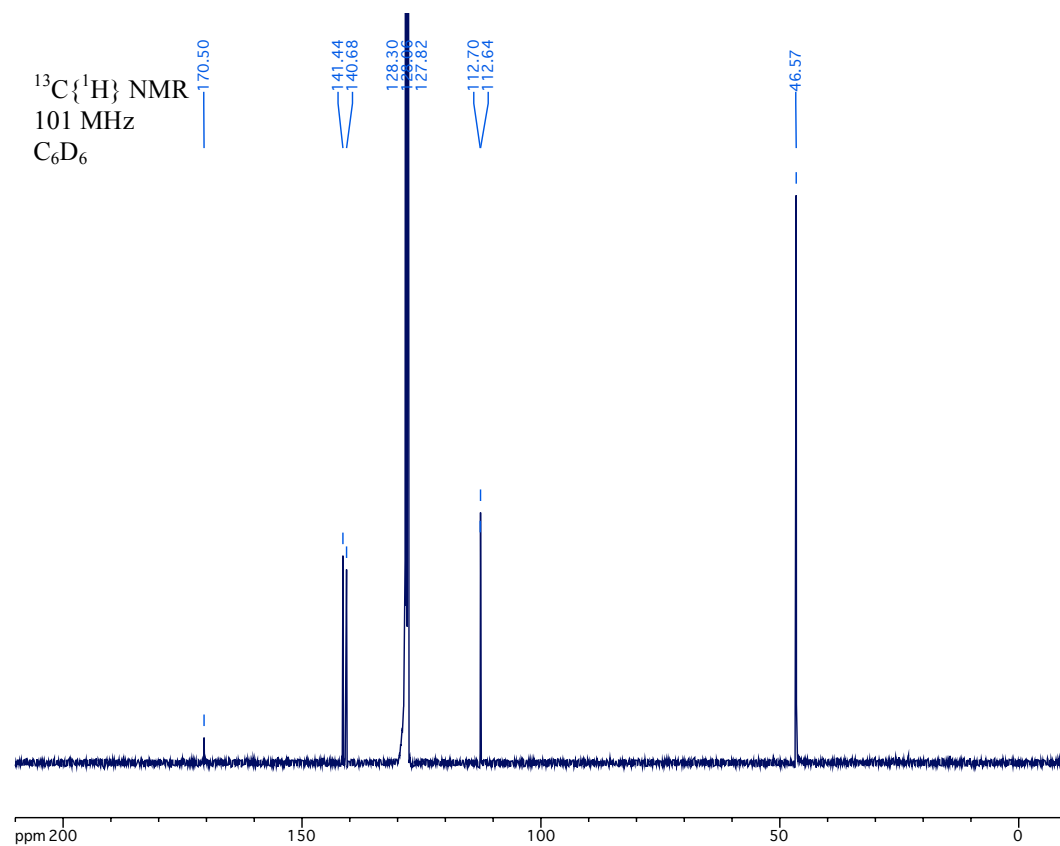
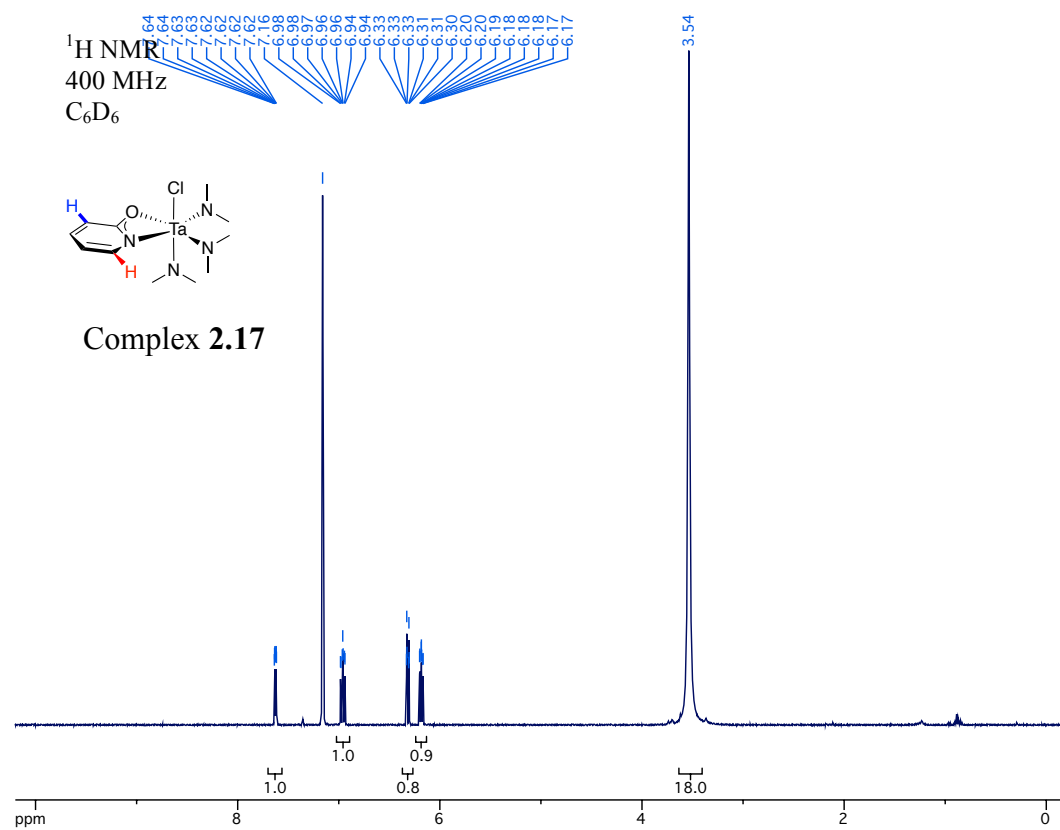
**Complex 2.16**

$^1\text{H}$  NMR spectrum ( $\text{CDCl}_3$ ) of Complex 2.16. The spectrum shows a triplet at  $\delta$  7.8 ppm (1H), a multiplet at  $\delta$  7.5 ppm (1H), a multiplet at  $\delta$  6.8 ppm (1H), a multiplet at  $\delta$  3.8 ppm (18.9H), and a small peak at  $\delta$  1.2 ppm. Integration values are shown below the peaks: 1.0 for the triplet at 7.8 ppm, 1.0 for the multiplet at 7.5 ppm, 1.0 for the multiplet at 6.8 ppm, and 18.9 for the multiplet at 3.8 ppm. The x-axis is labeled from 0 to 10 ppm.

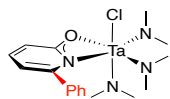


$^{19}\text{F}$  NMR  
282 MHz  
 $\text{C}_6\text{D}_6$

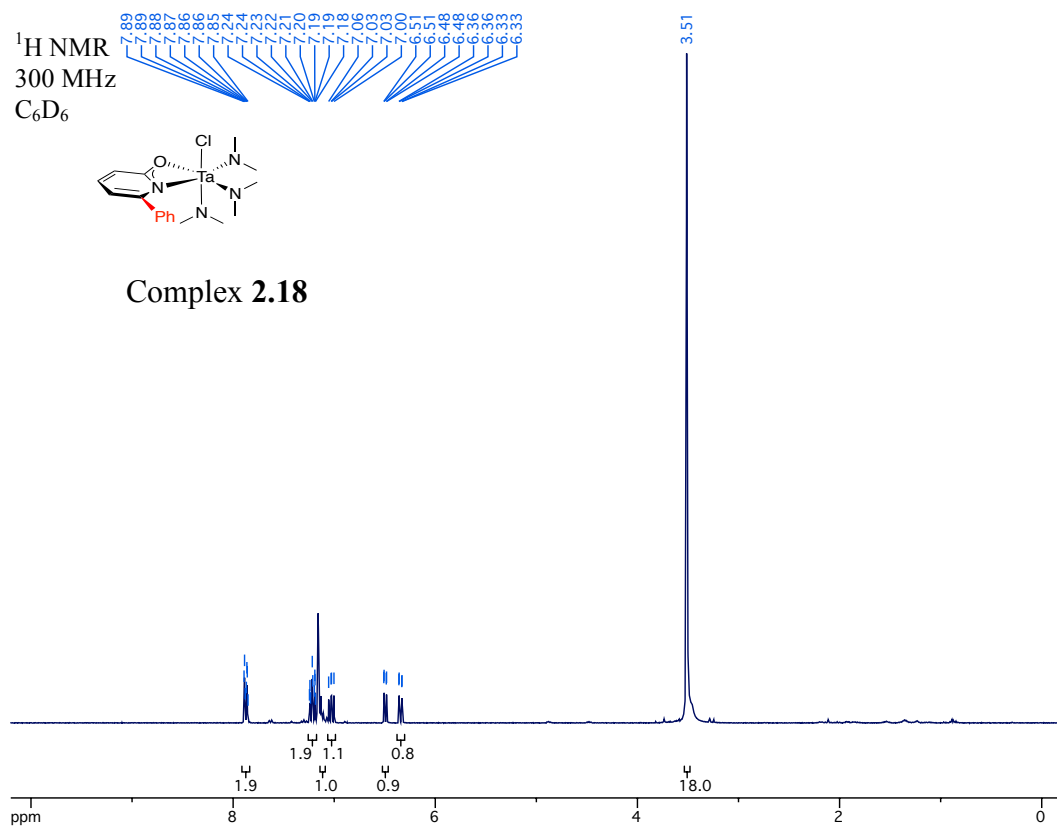




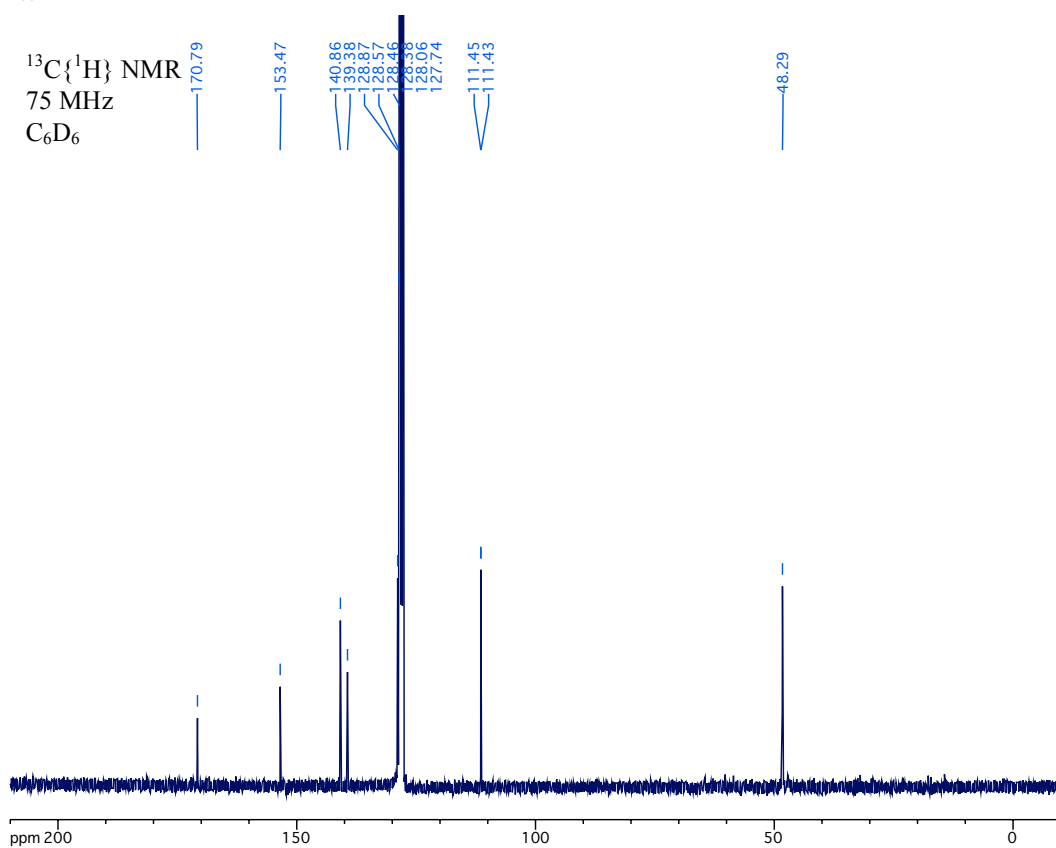
$^1\text{H}$  NMR  
300 MHz  
 $\text{C}_6\text{D}_6$



Complex **2.18**

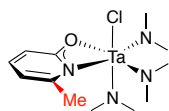


$^{13}\text{C}\{^1\text{H}\}$  NMR  
75 MHz  
 $\text{C}_6\text{D}_6$

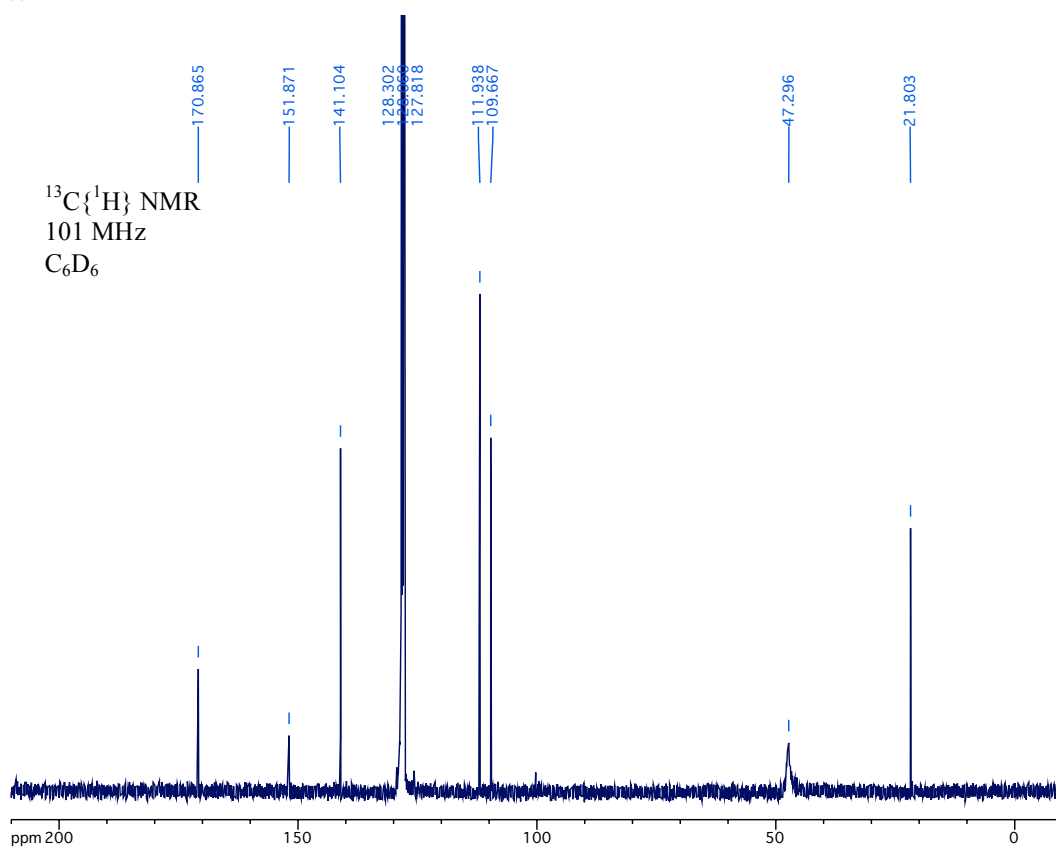
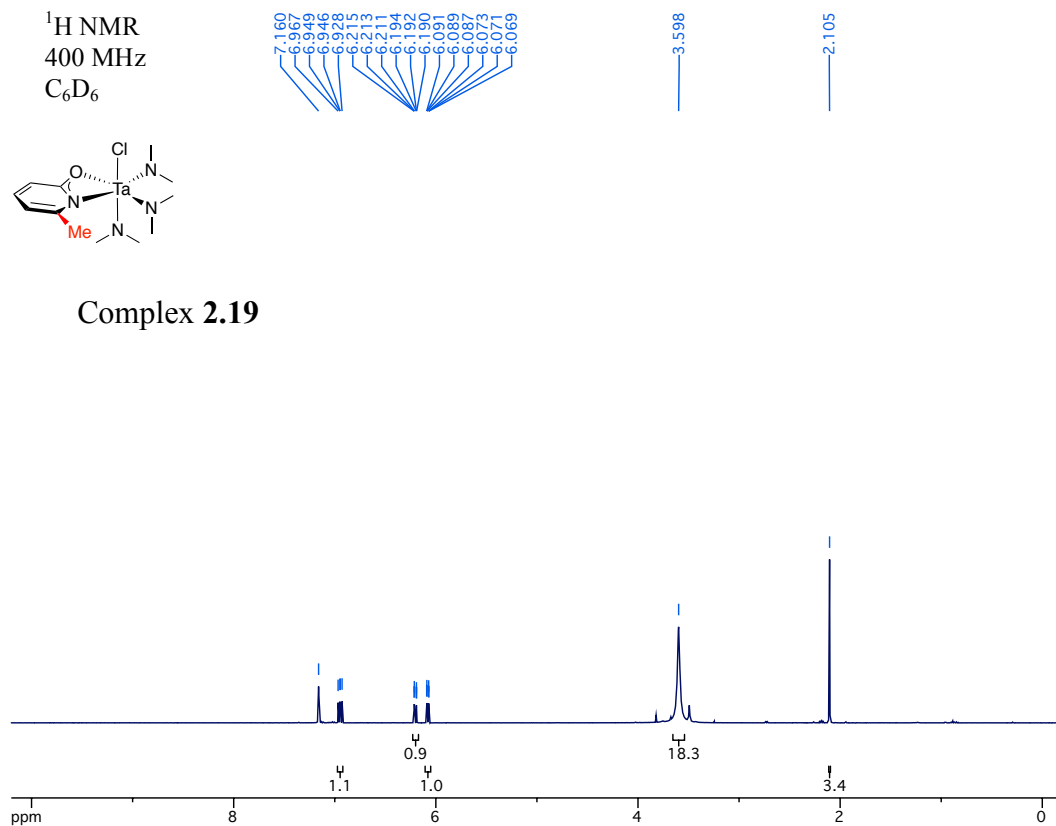




$^1\text{H}$  NMR  
400 MHz  
 $\text{C}_6\text{D}_6$

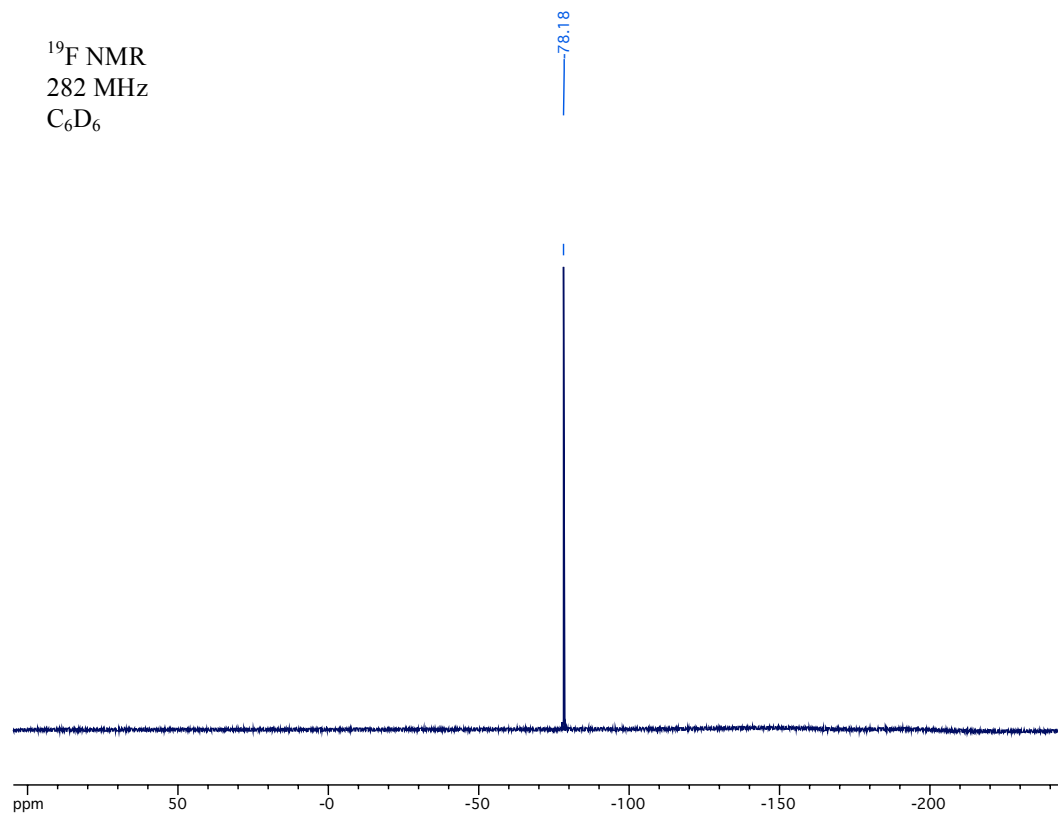


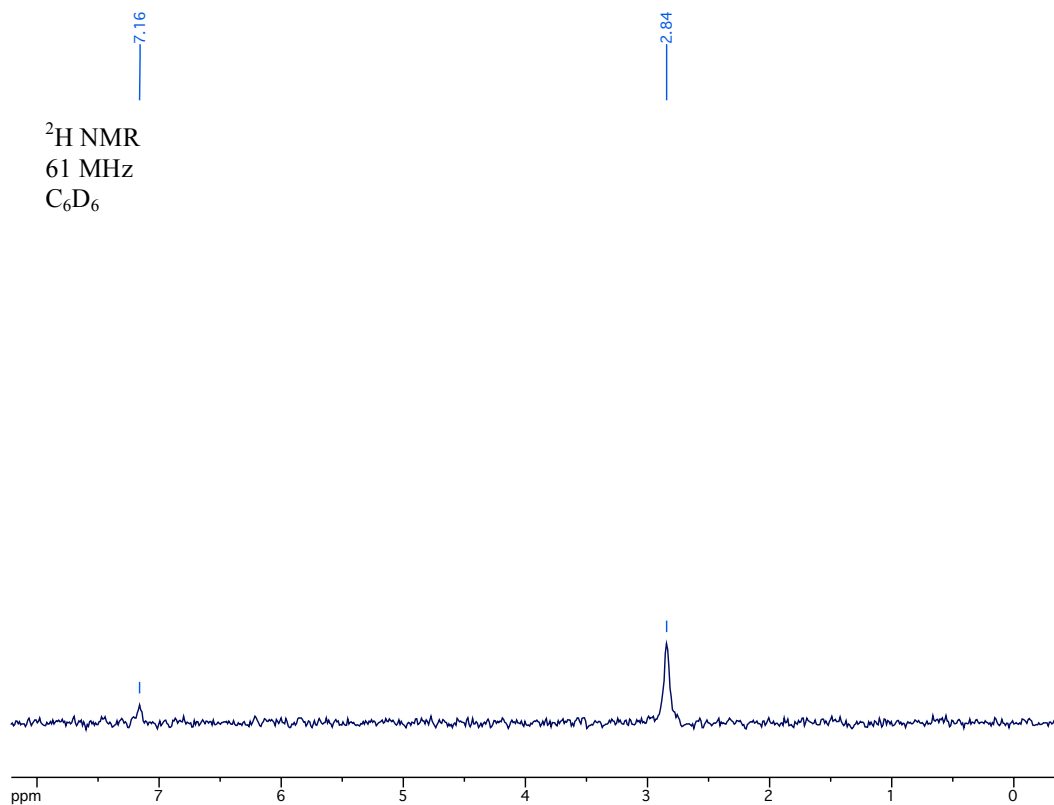
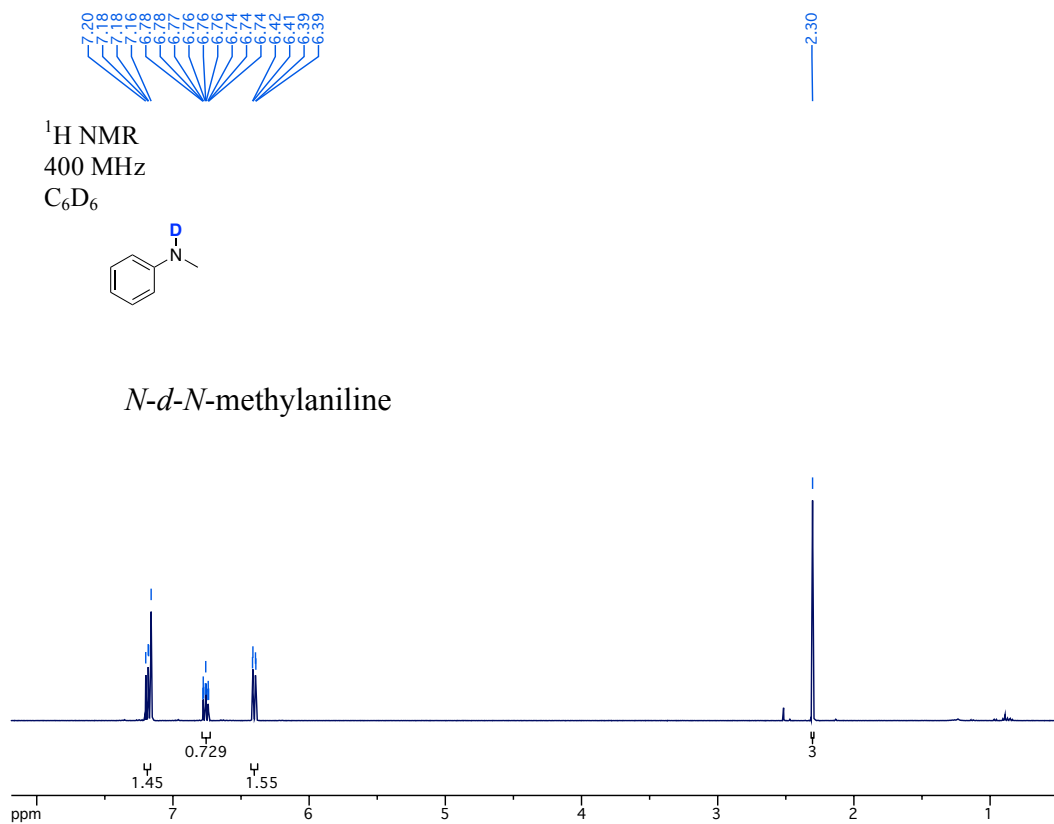
Complex **2.19**

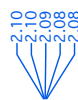
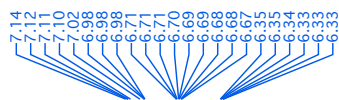




$^{19}\text{F}$  NMR  
282 MHz  
 $\text{C}_6\text{D}_6$

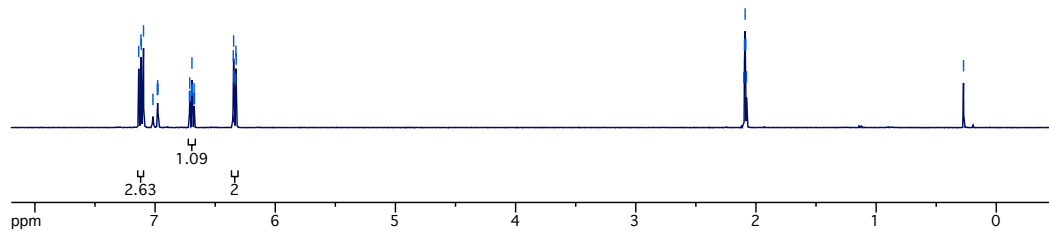
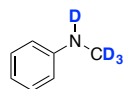




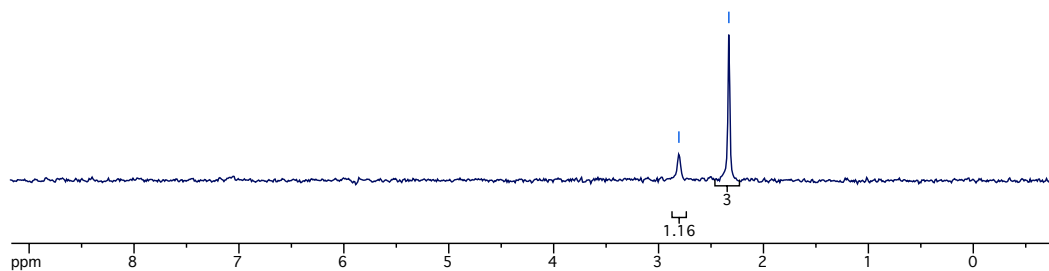


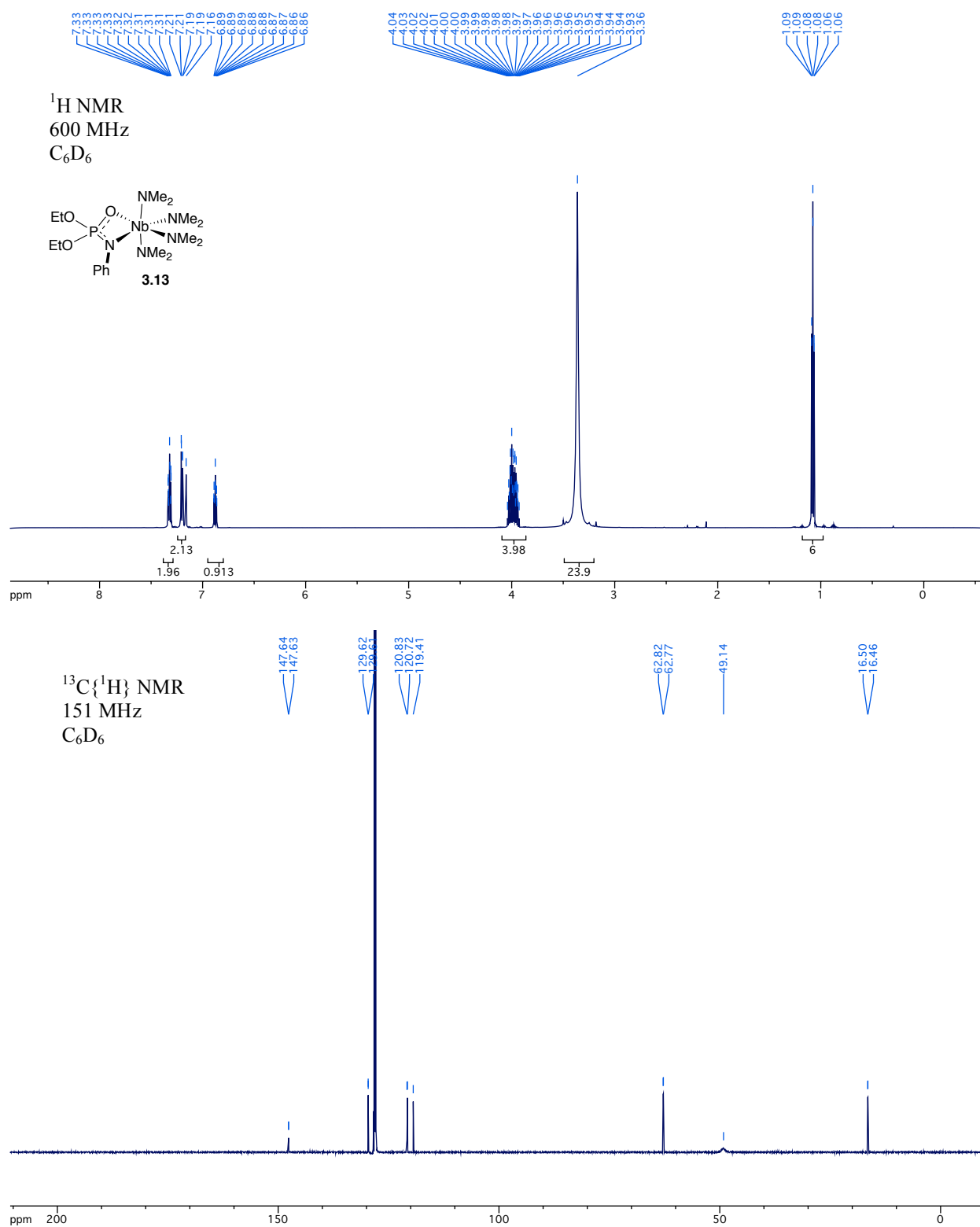
$^1\text{H}$  NMR  
400 MHz  
 $\text{Tol-}d_8$

*N-d-N*-(methyl- $d_3$ )aniline

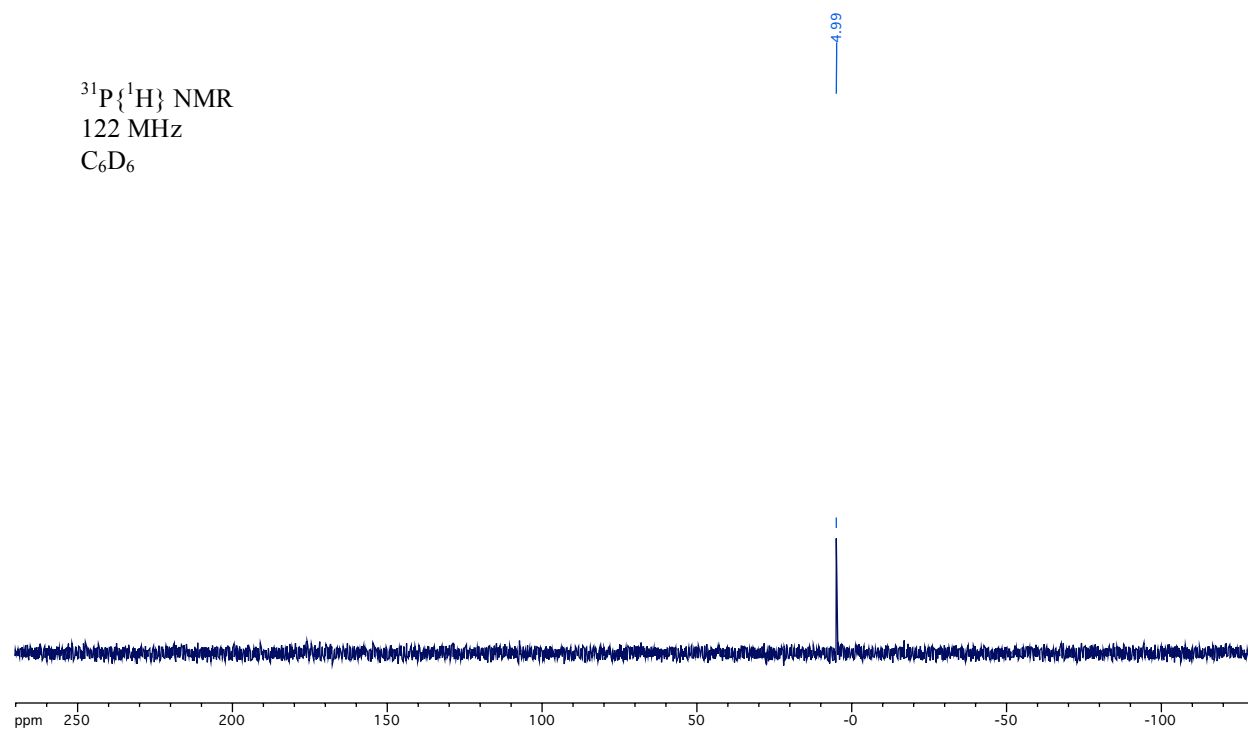


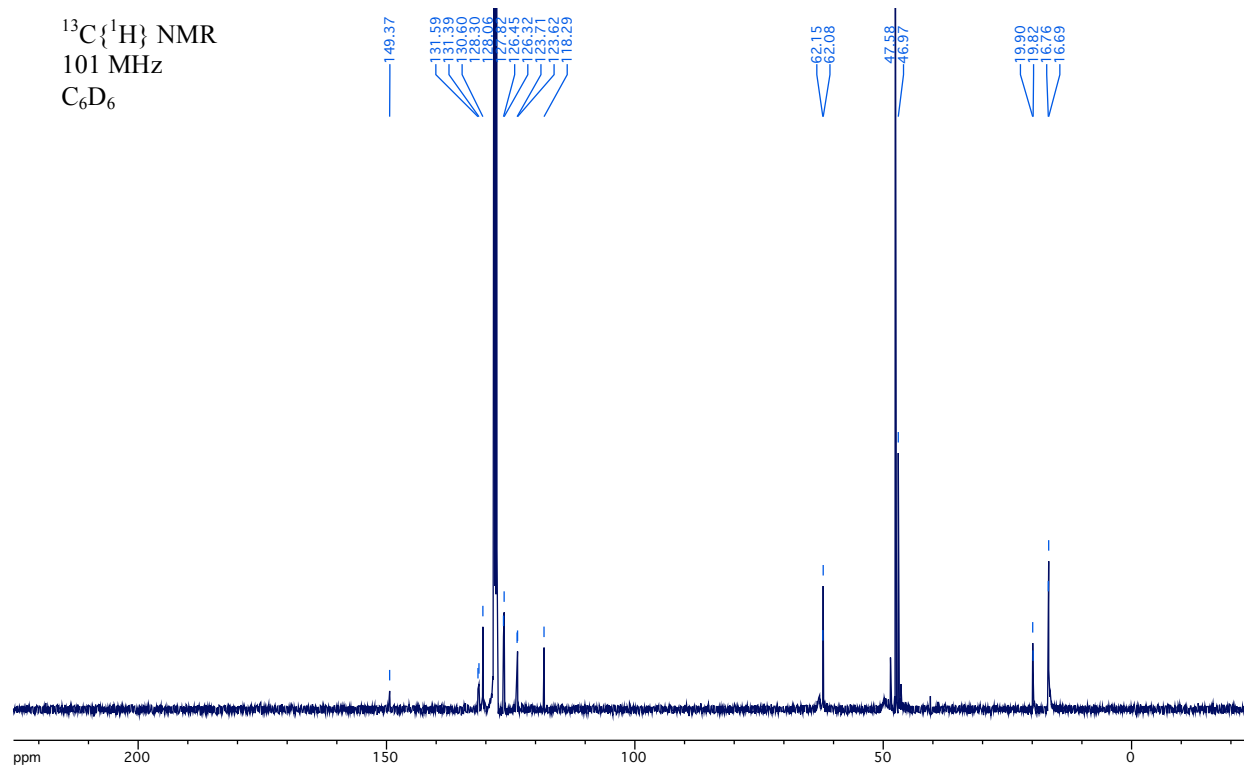
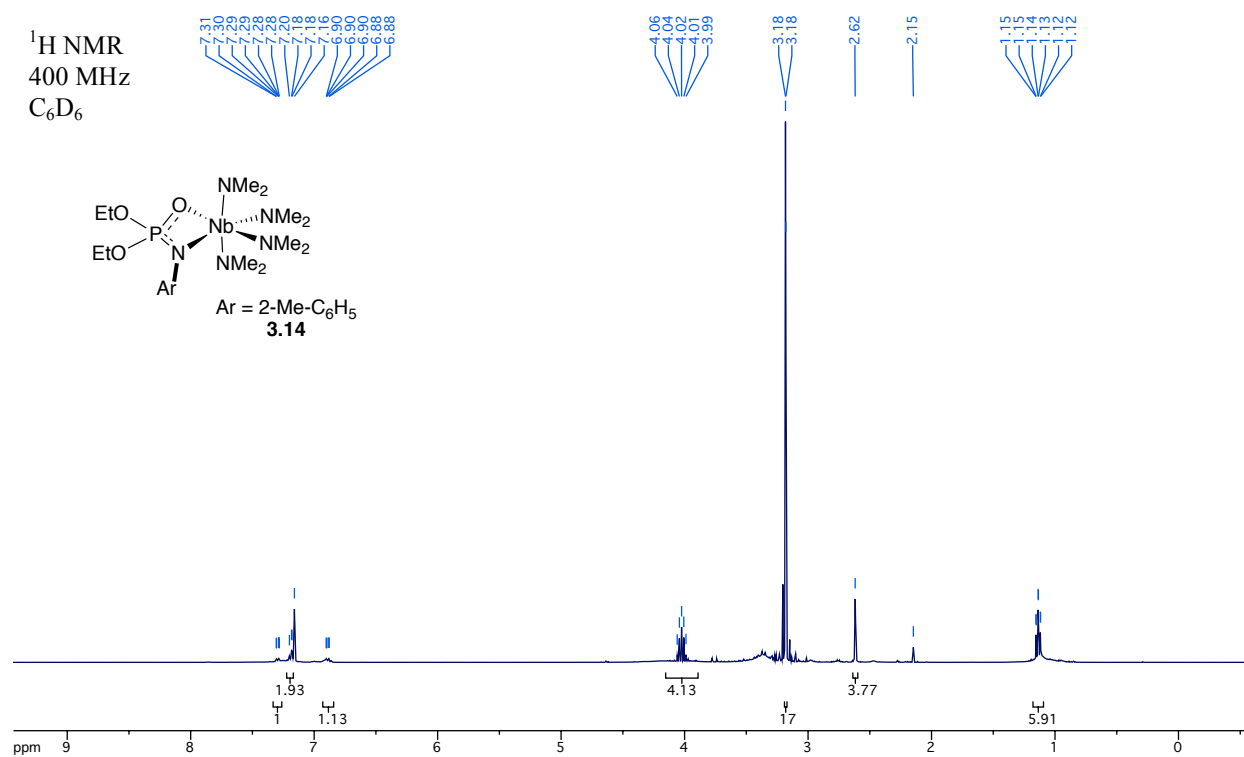
$^2\text{H}$  NMR  
61 MHz  
 $\text{Tol-}d_8$





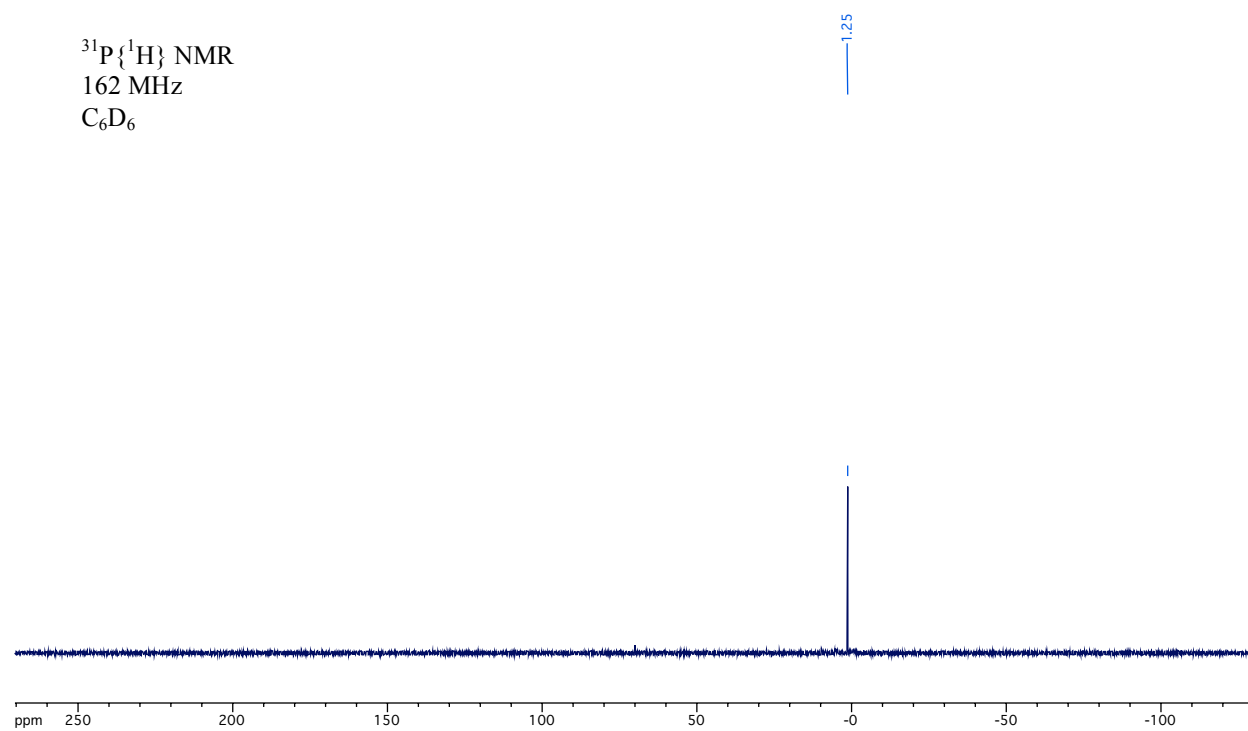
$^{31}\text{P}\{^1\text{H}\}$  NMR  
122 MHz  
 $\text{C}_6\text{D}_6$

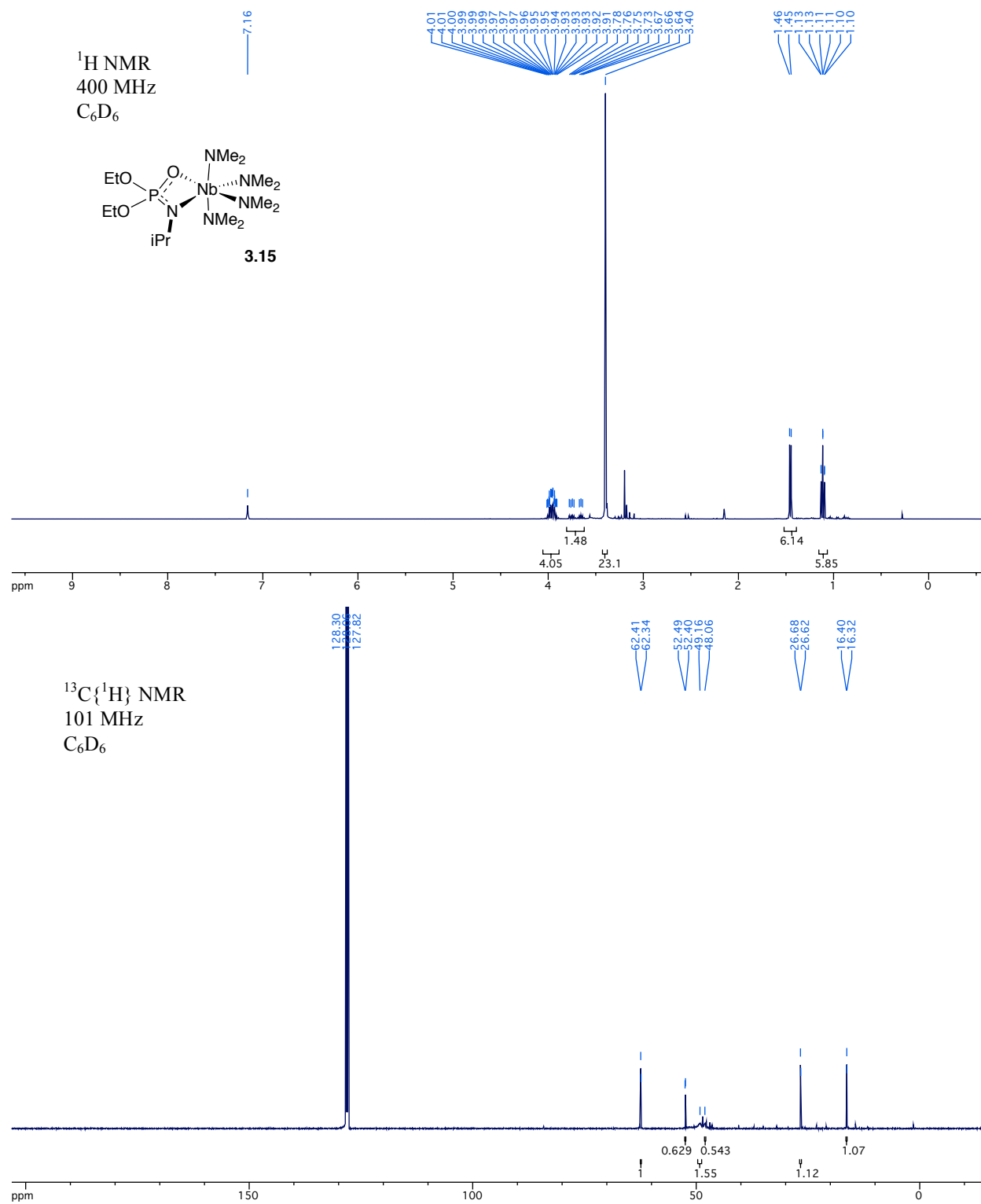




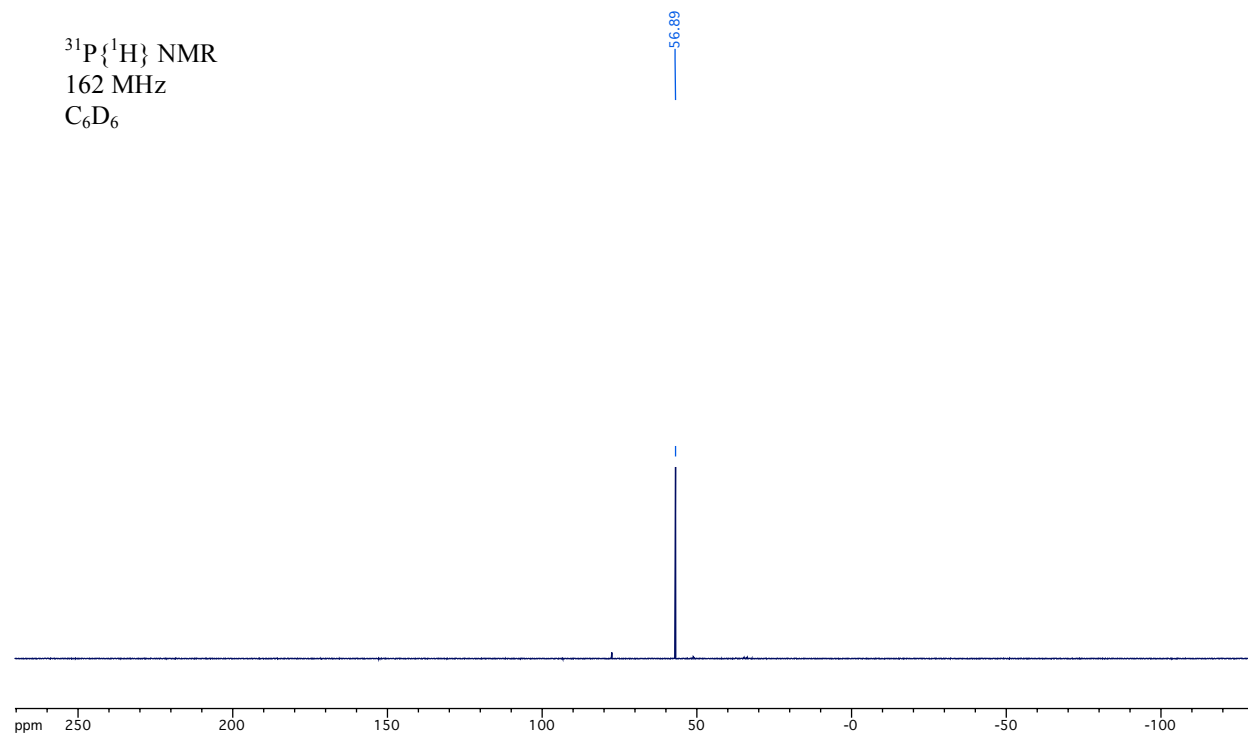


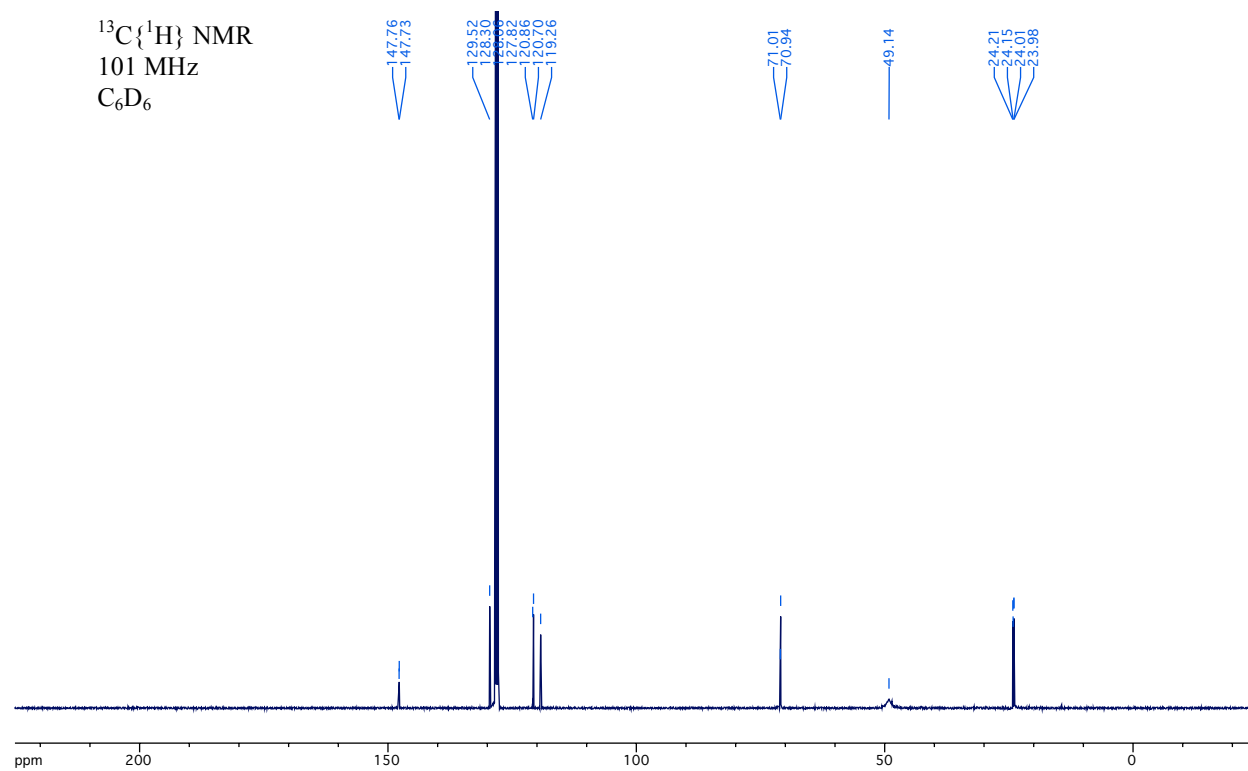
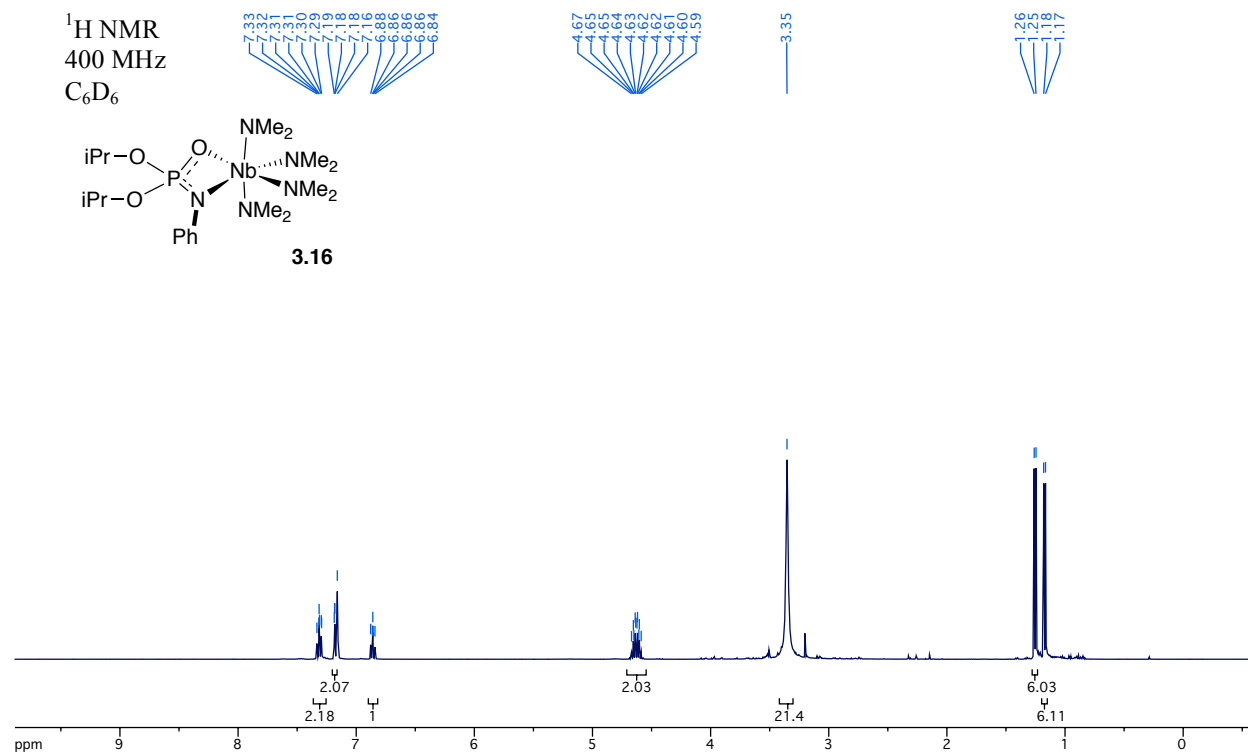
$^{31}\text{P}\{^1\text{H}\}$  NMR  
162 MHz  
 $\text{C}_6\text{D}_6$

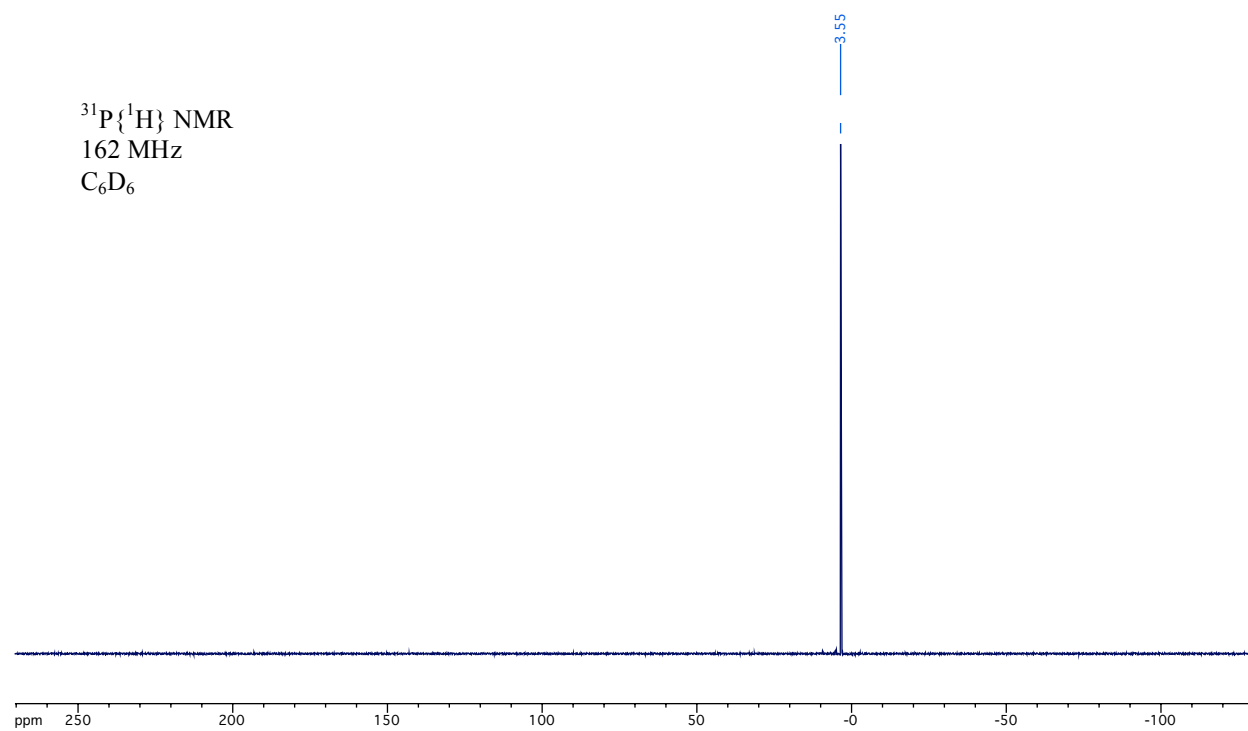


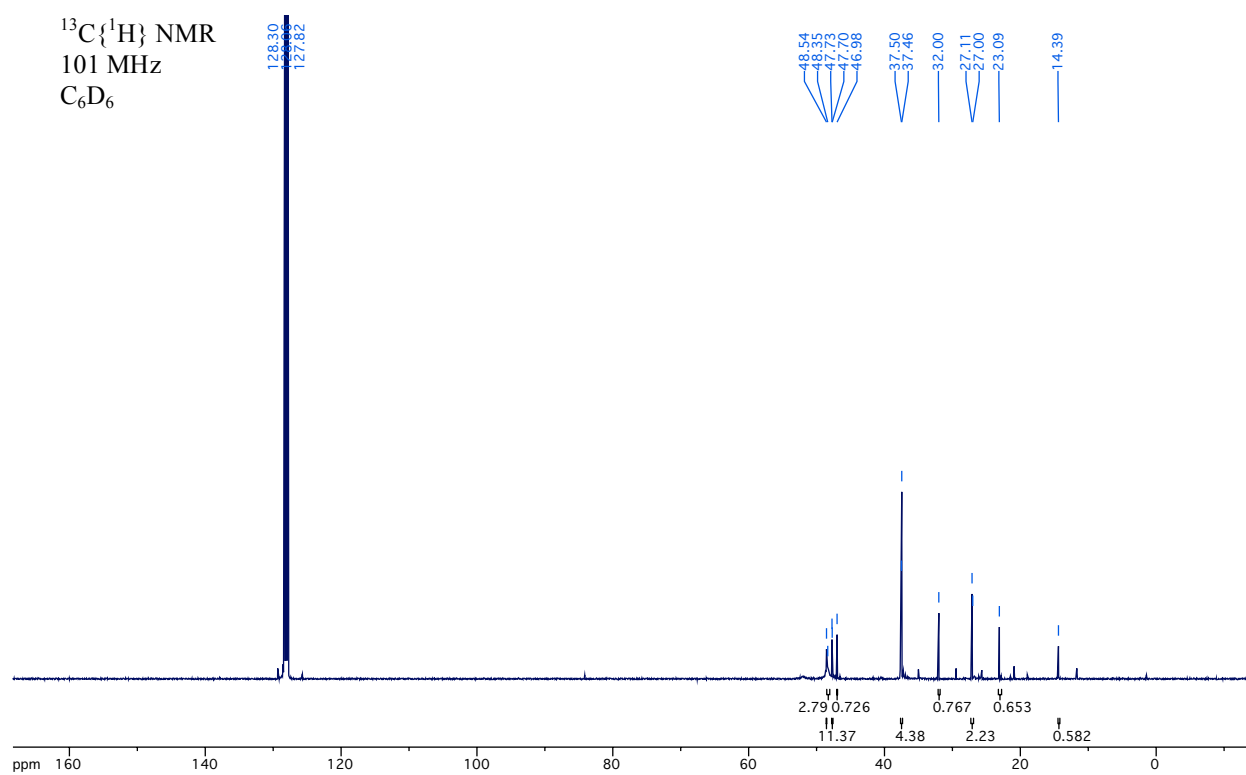
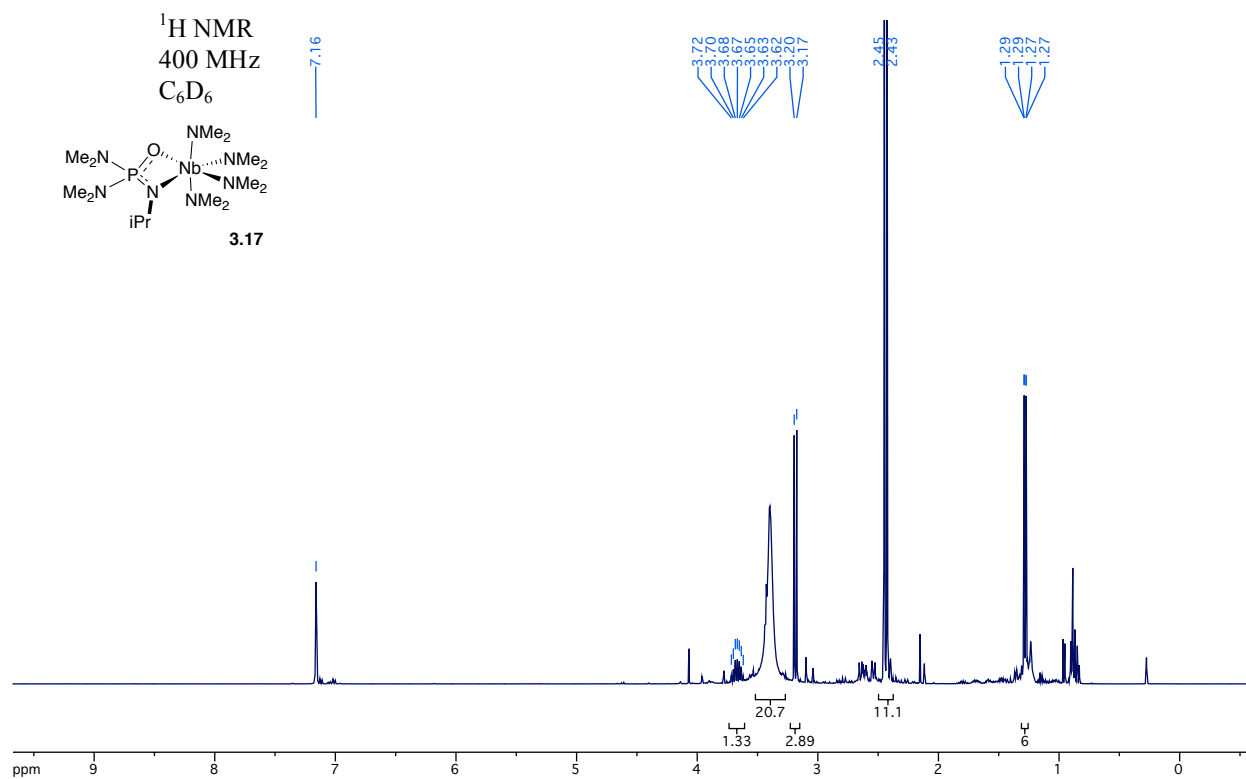


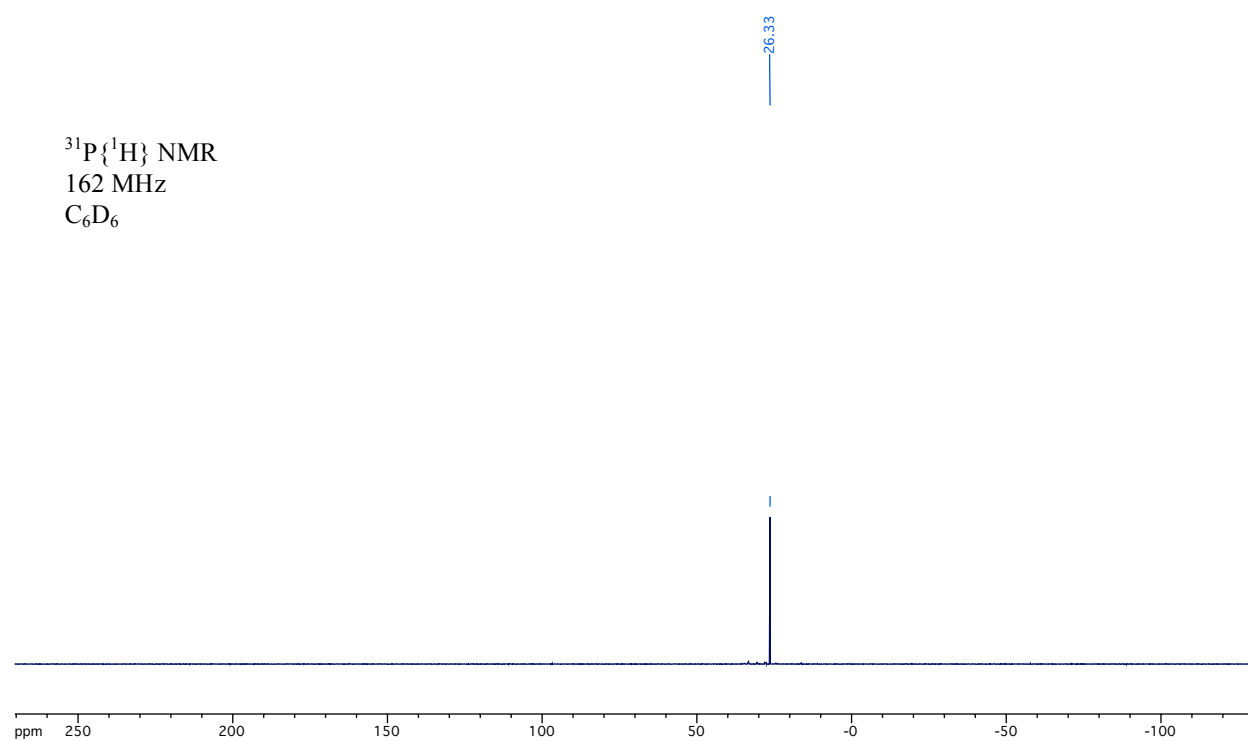
$^{31}\text{P}\{^1\text{H}\}$  NMR  
162 MHz  
 $\text{C}_6\text{D}_6$











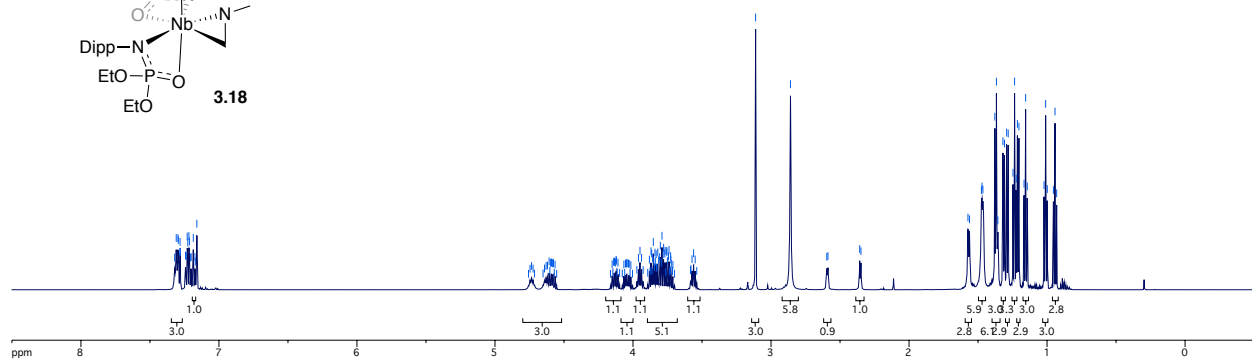
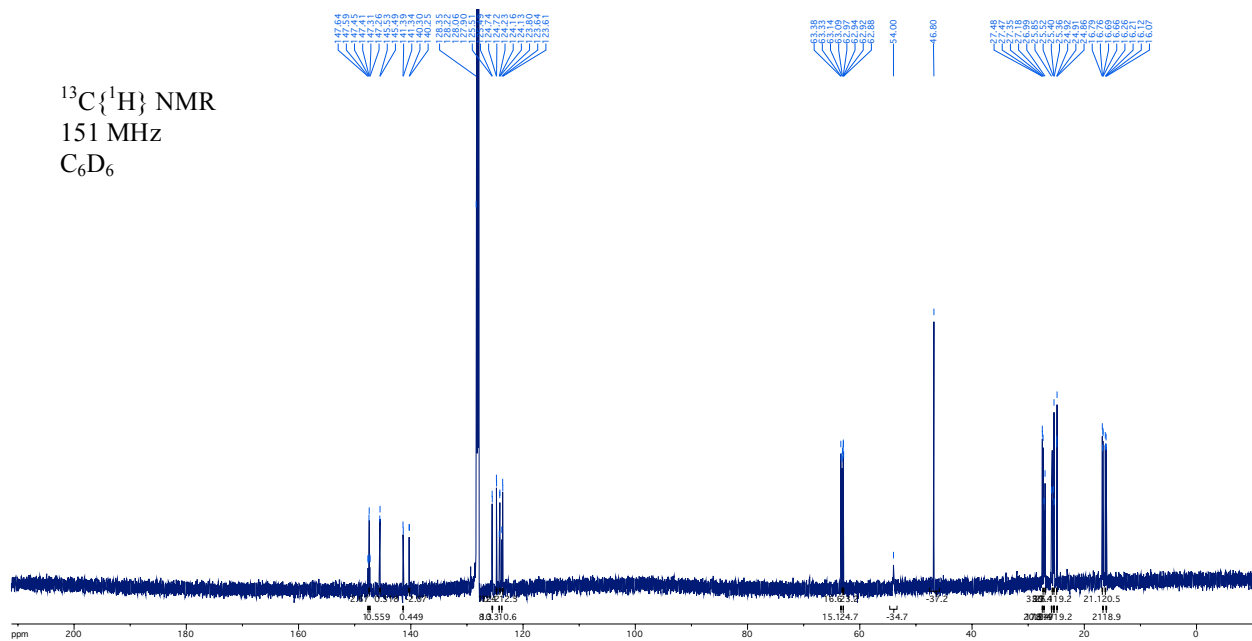
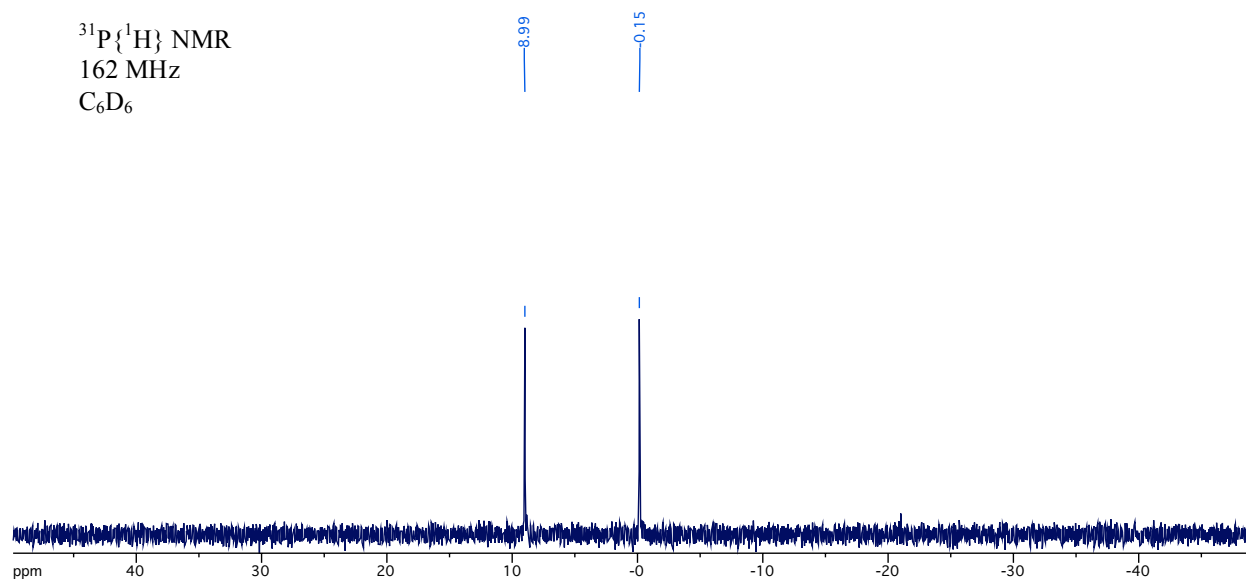


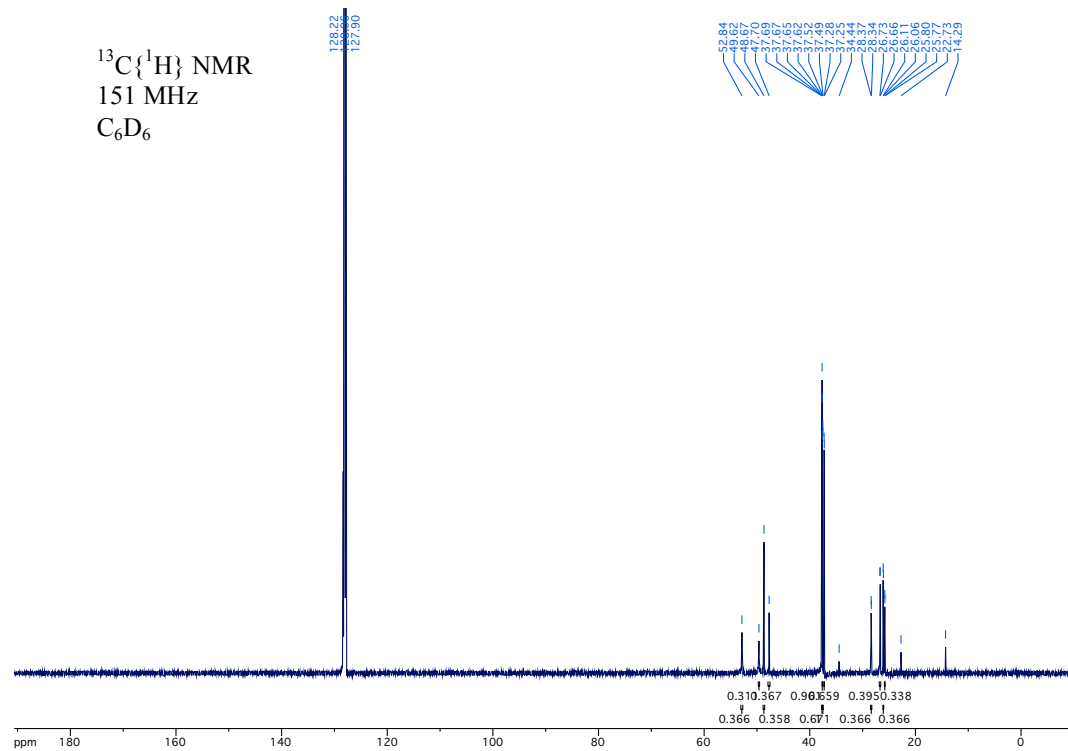
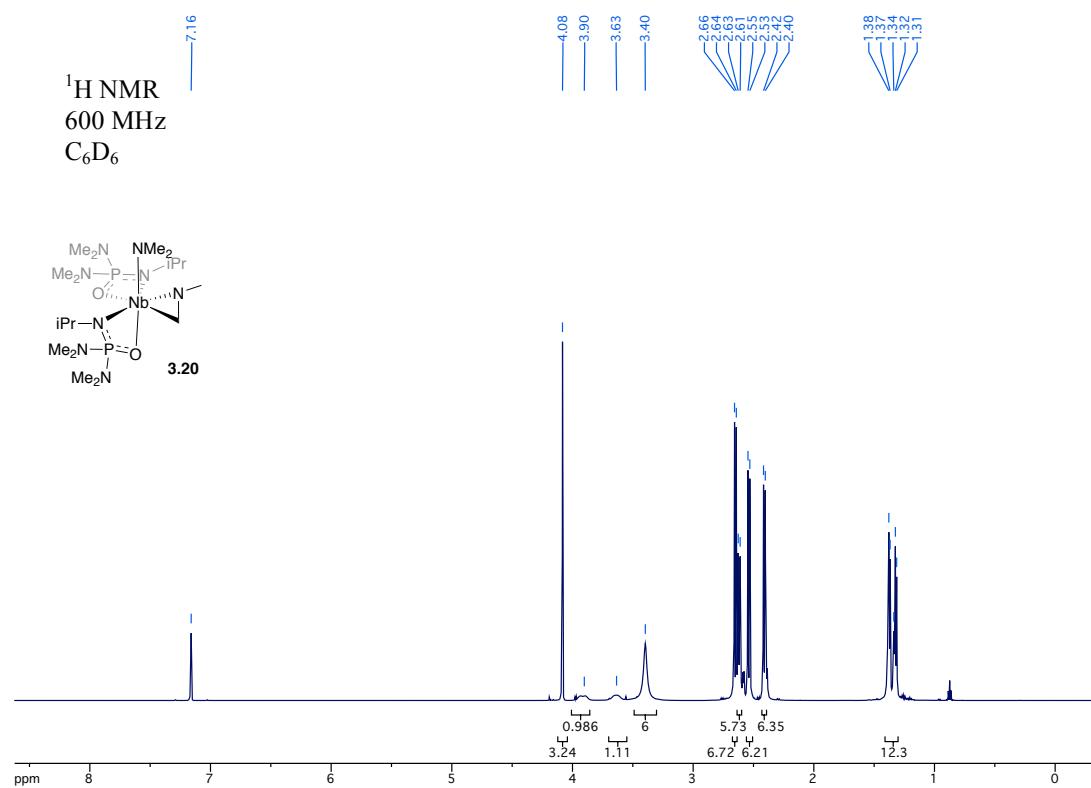
Figure 1 is a schematic diagram of the experimental setup. It shows a top-down view of a rectangular arena. A vertical black line runs through the center of the arena. On the left side of the arena, there are two groups of blue lines representing fish. The top group is labeled "观察组 (观察)" and the bottom group is labeled "实验组 (实验)". On the right side of the arena, there are two groups of blue lines representing fish. The top group is labeled "观察组 (观察)" and the bottom group is labeled "实验组 (实验)". A vertical scale bar on the right side of the arena indicates distances of 4.00 and 6.80 units.



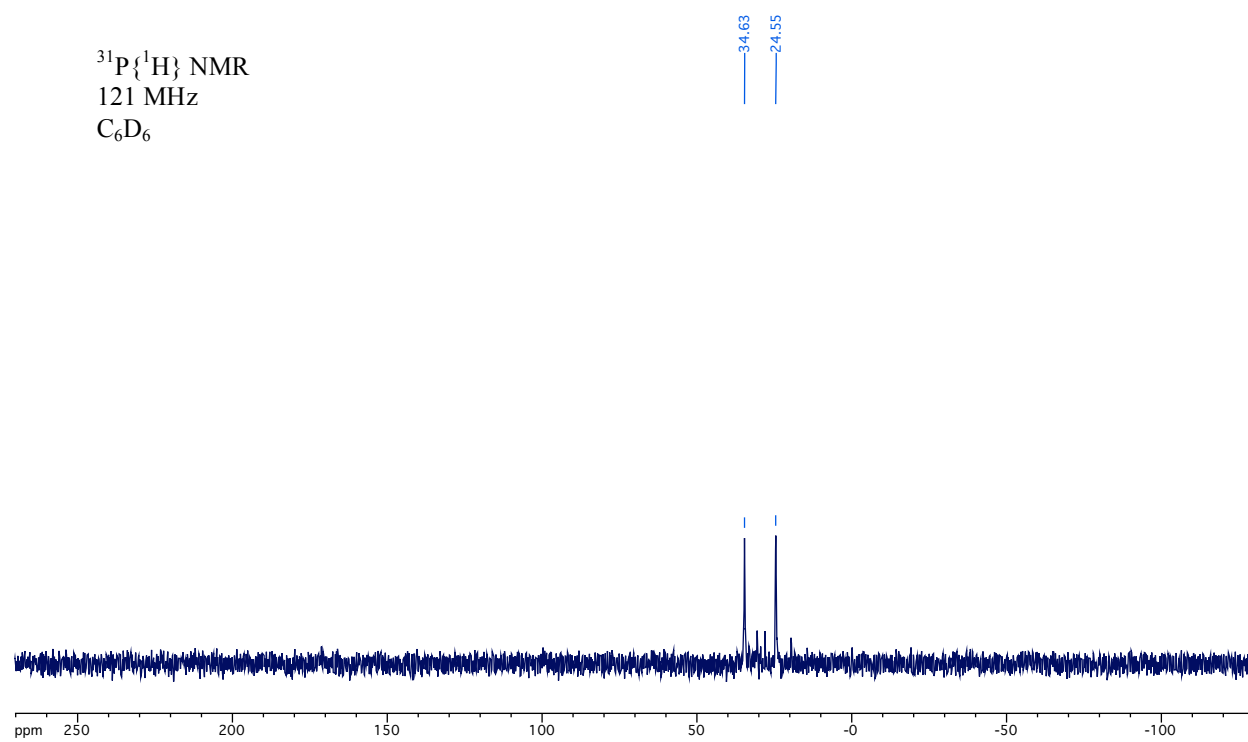


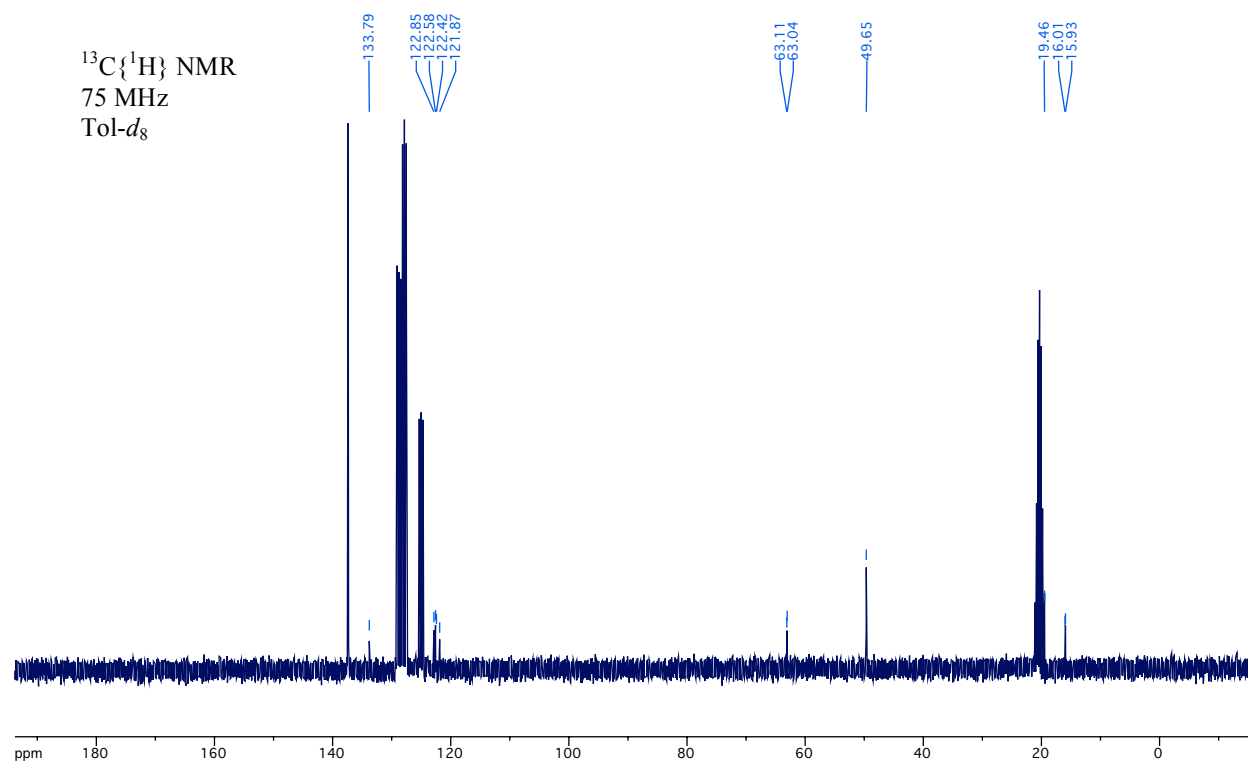
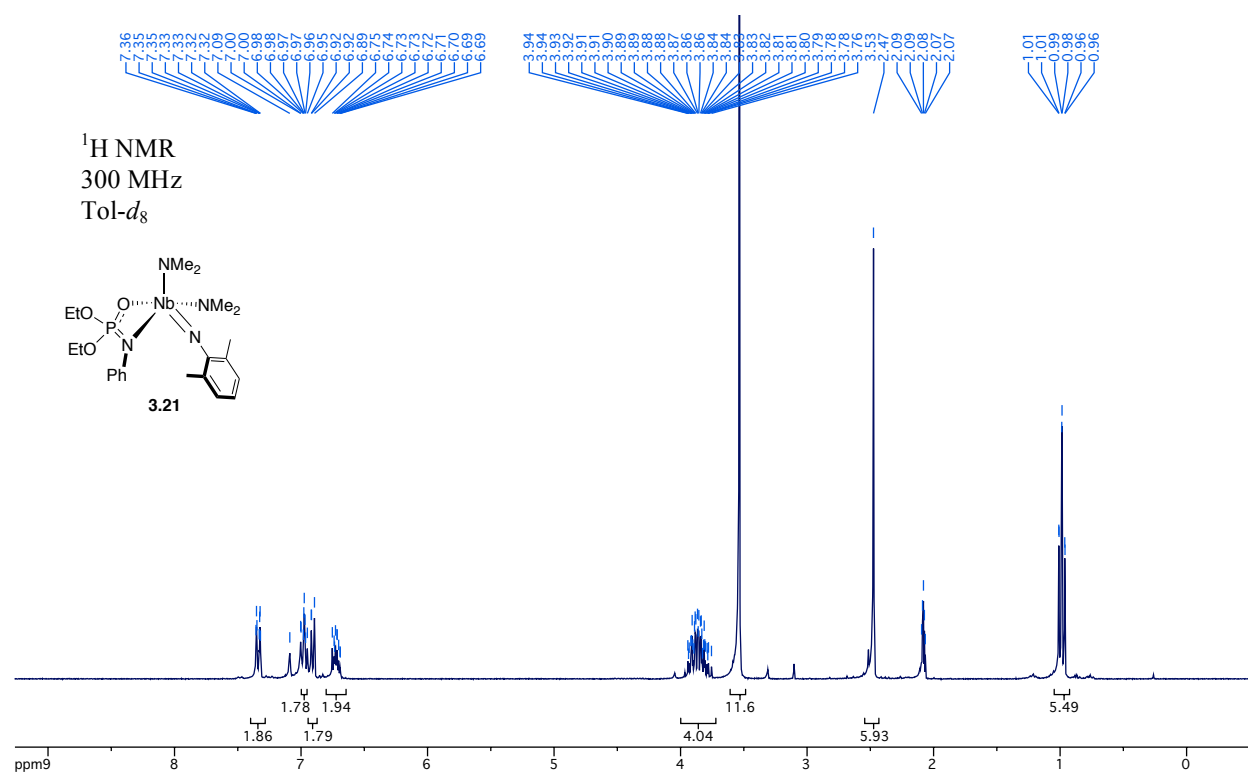
$^{31}\text{P}\{^1\text{H}\}$  NMR  
162 MHz  
 $\text{C}_6\text{D}_6$



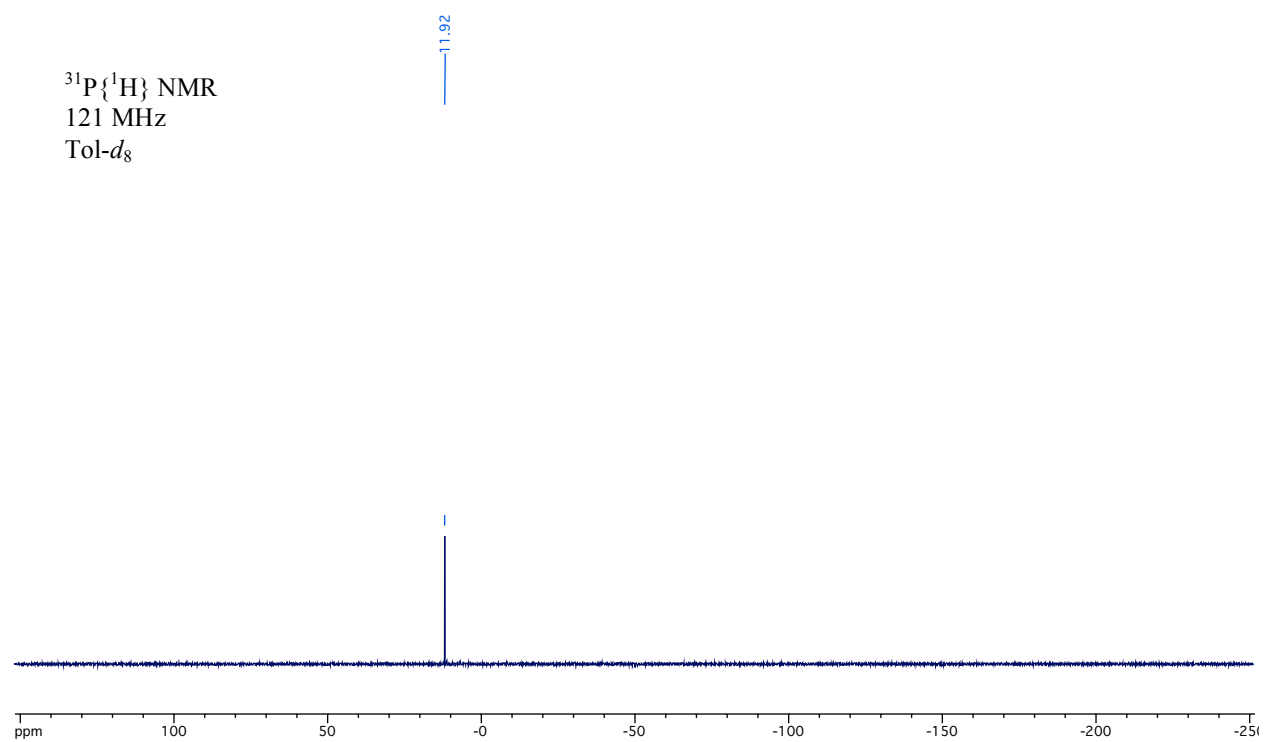


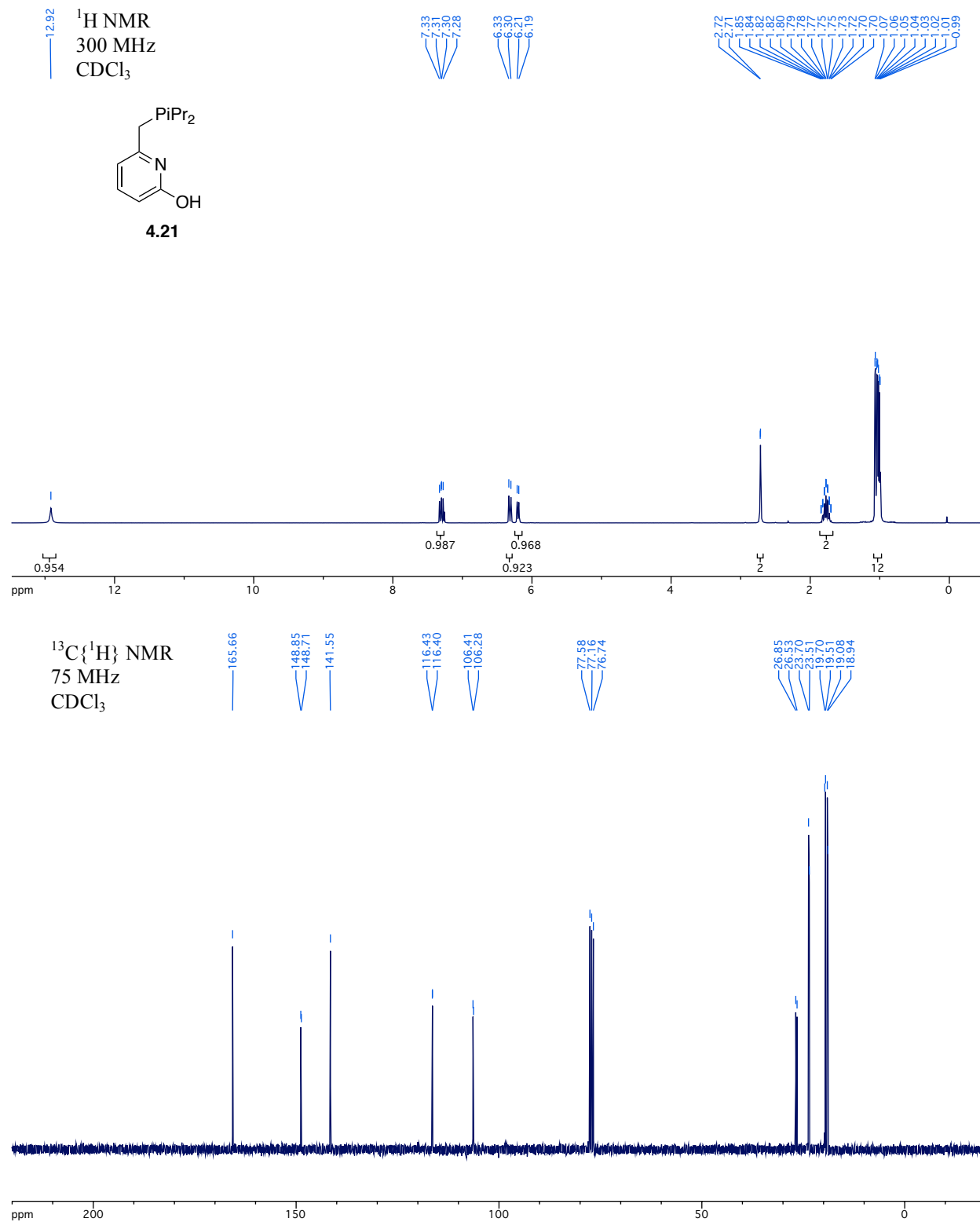
$^{31}\text{P}\{^1\text{H}\}$  NMR  
121 MHz  
 $\text{C}_6\text{D}_6$

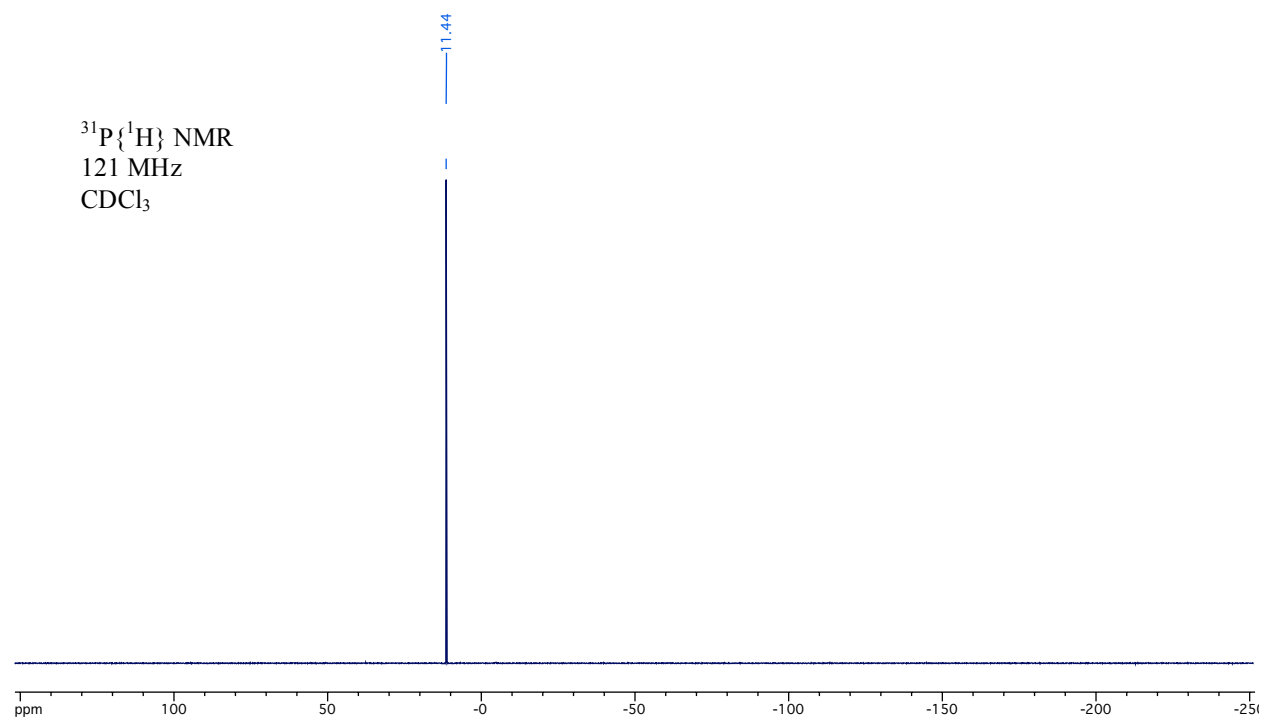


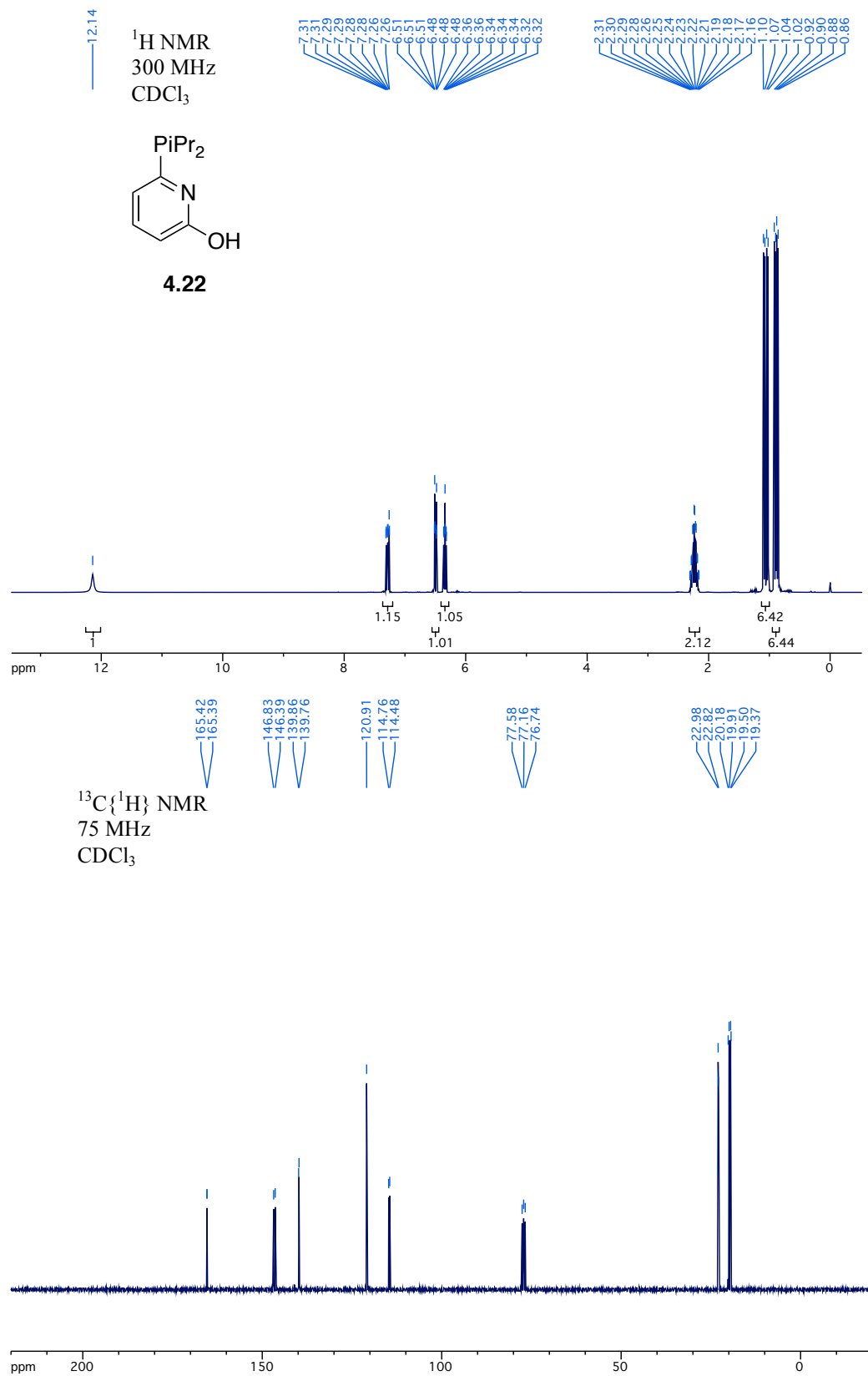


$^{31}\text{P}\{^1\text{H}\}$  NMR  
121 MHz  
Tol- $d_8$

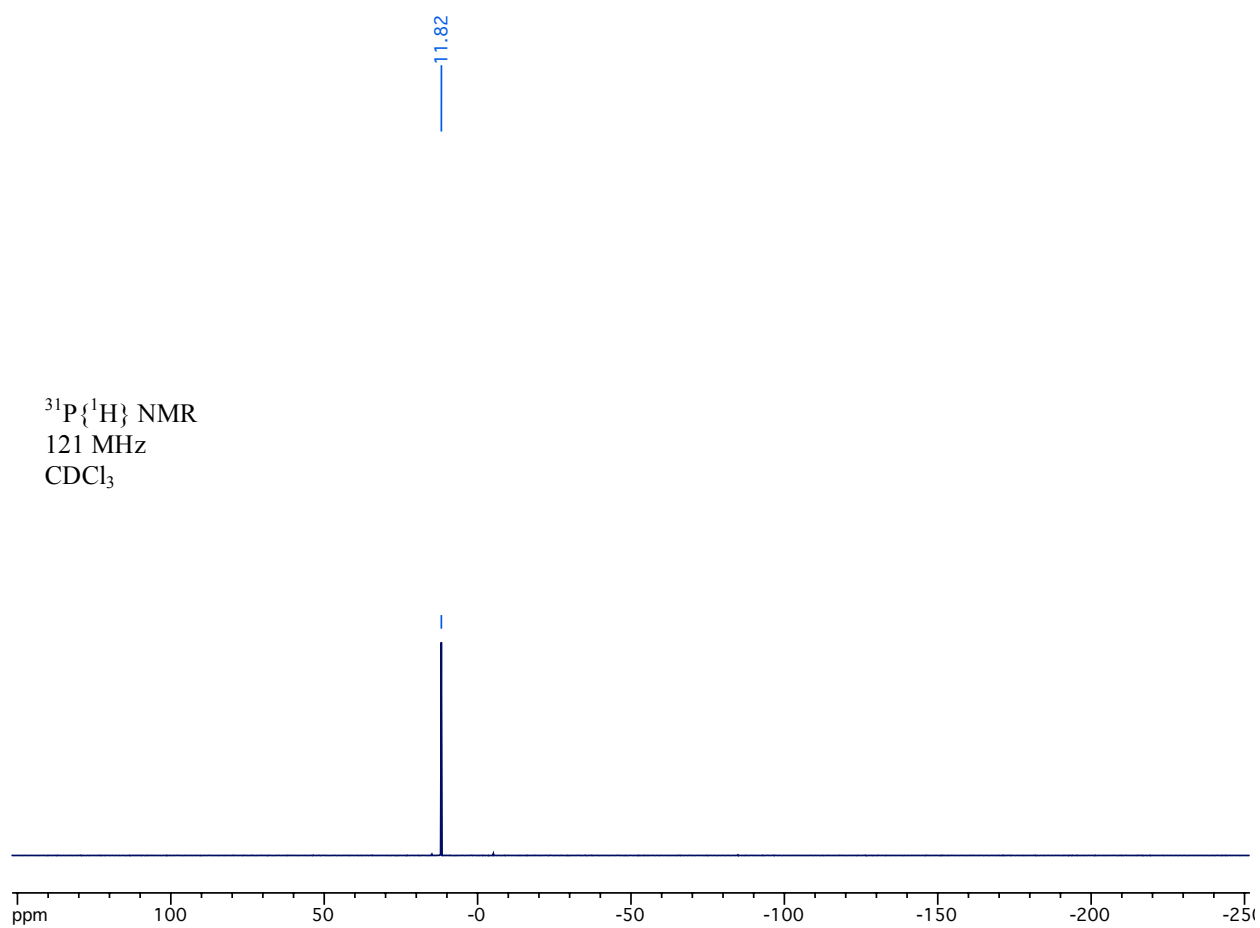


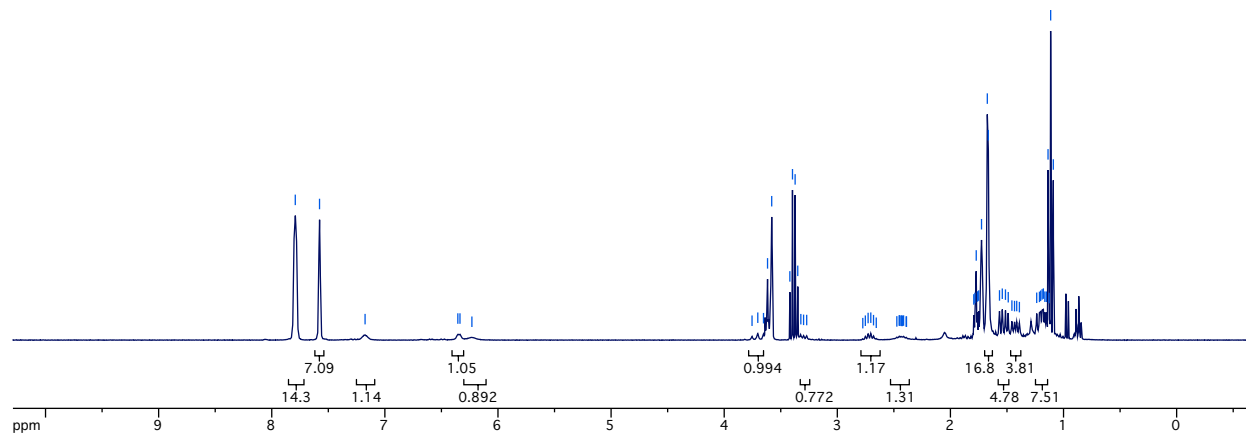




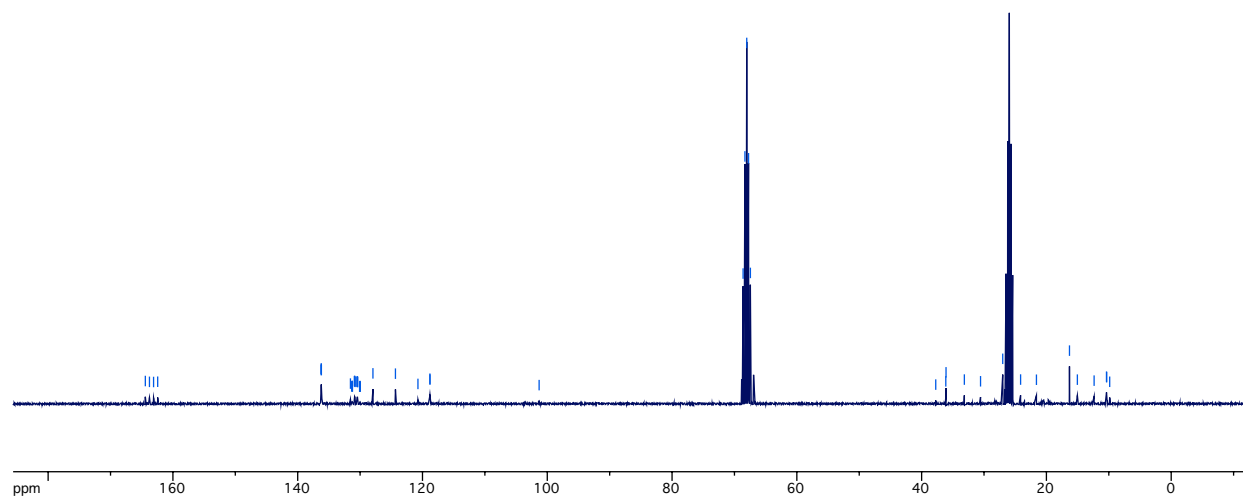




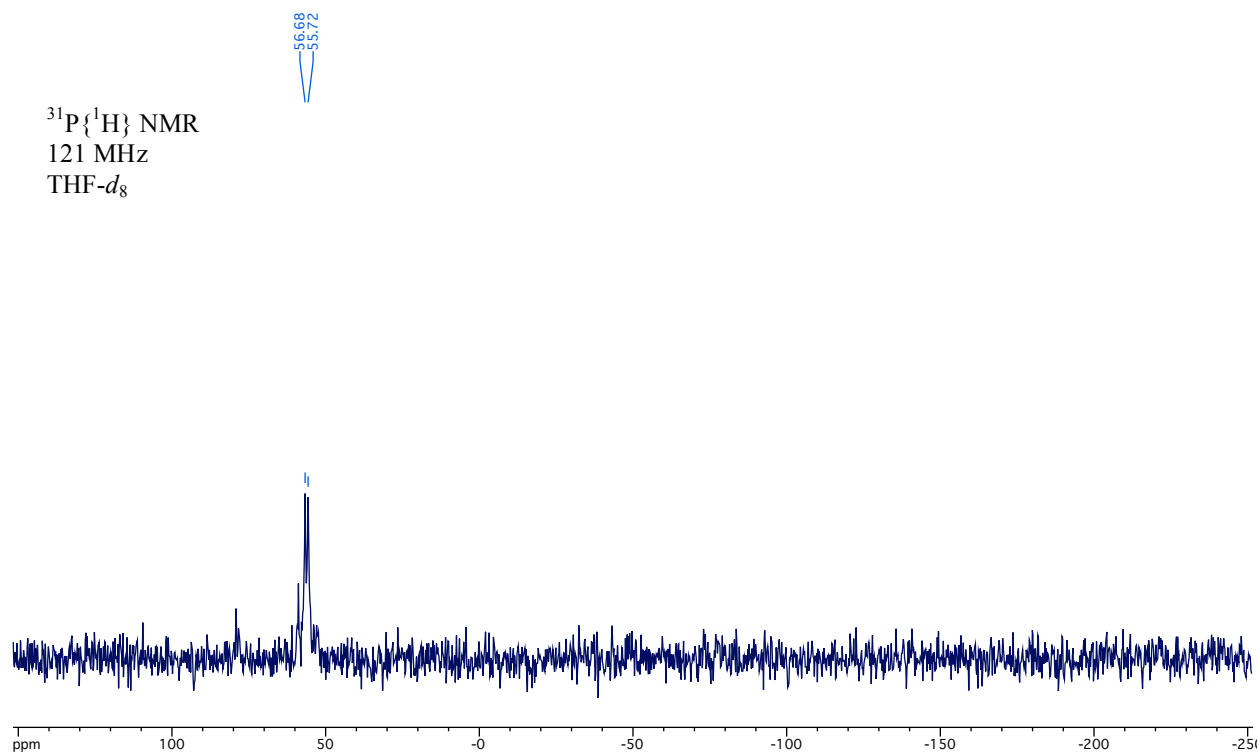




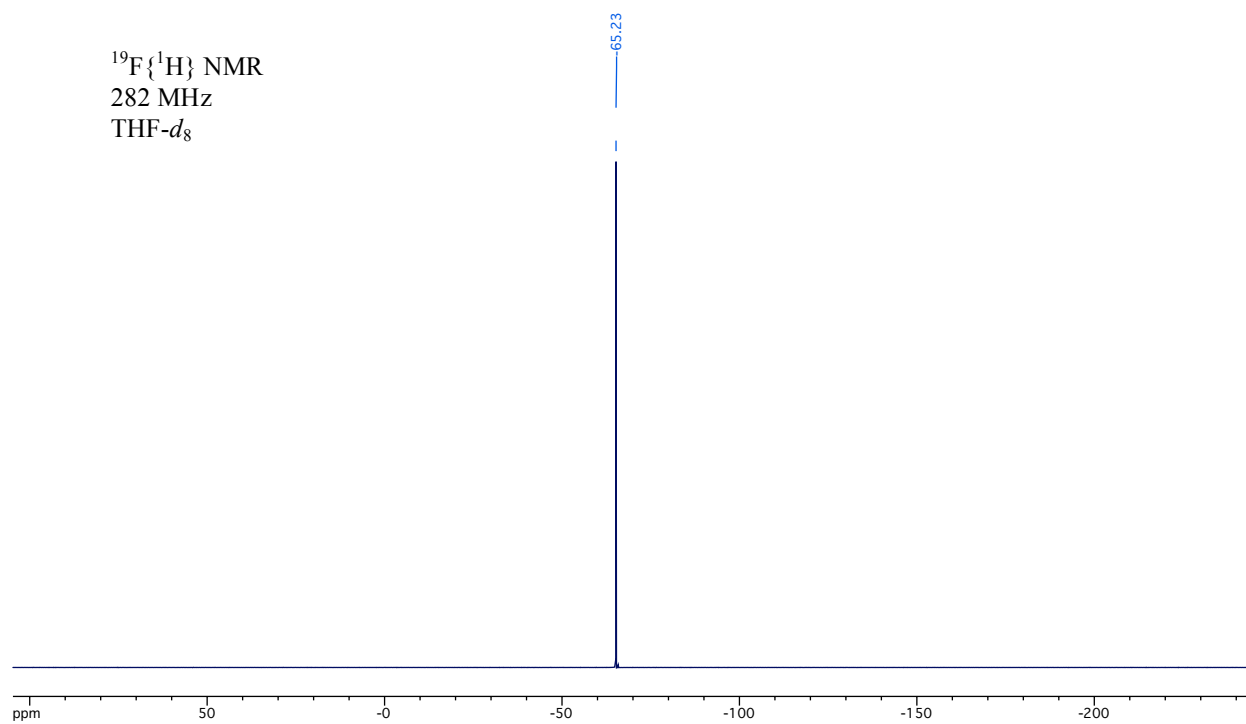
$t$	$\alpha = 0.0$	$\alpha = 0.1$	$\alpha = 0.2$	$\alpha = 0.3$	$\alpha = 0.4$	$\alpha = 0.5$
0	100	100	100	100	100	100
10	90	90	90	90	90	80
20	80	80	80	80	80	60
30	70	70	70	70	70	40
40	60	60	60	60	60	20
50	50	50	50	50	50	10
60	40	40	40	40	40	5
70	30	30	30	30	30	2
80	20	20	20	20	20	1
90	10	10	10	10	10	0.5
100	10	10	10	10	10	0.1

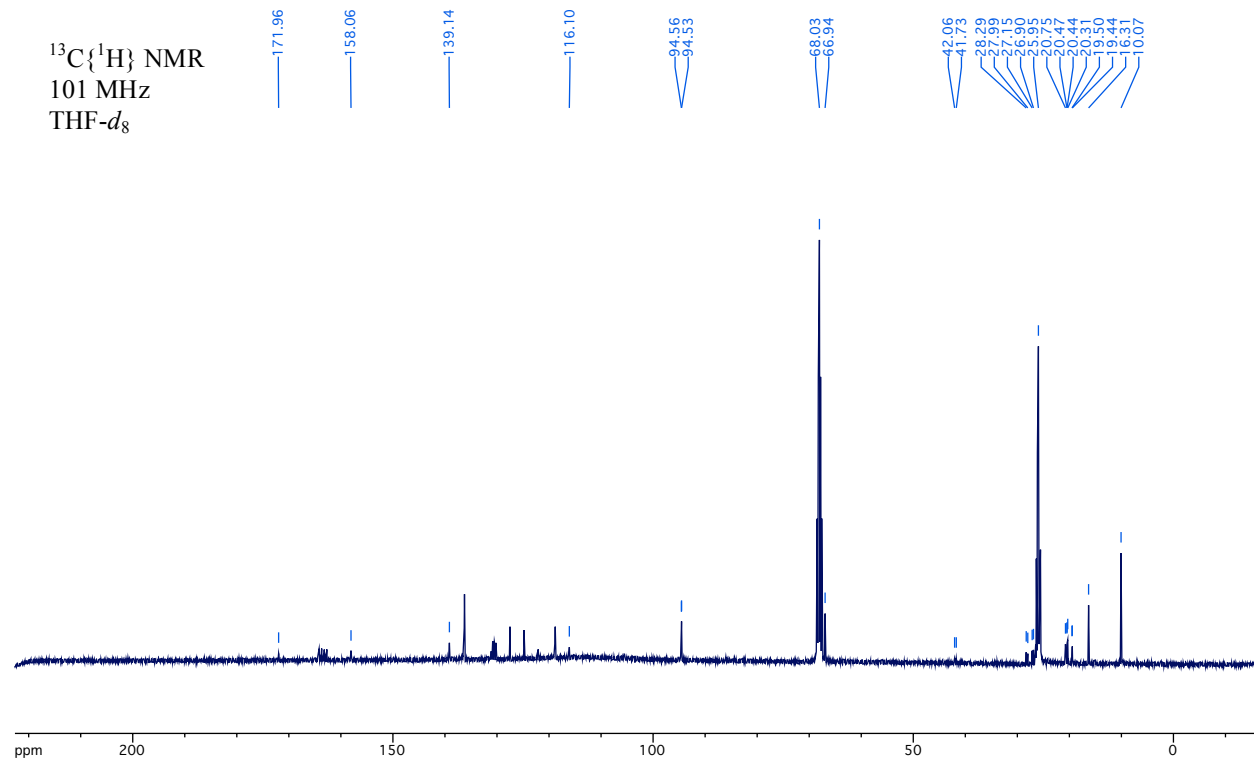
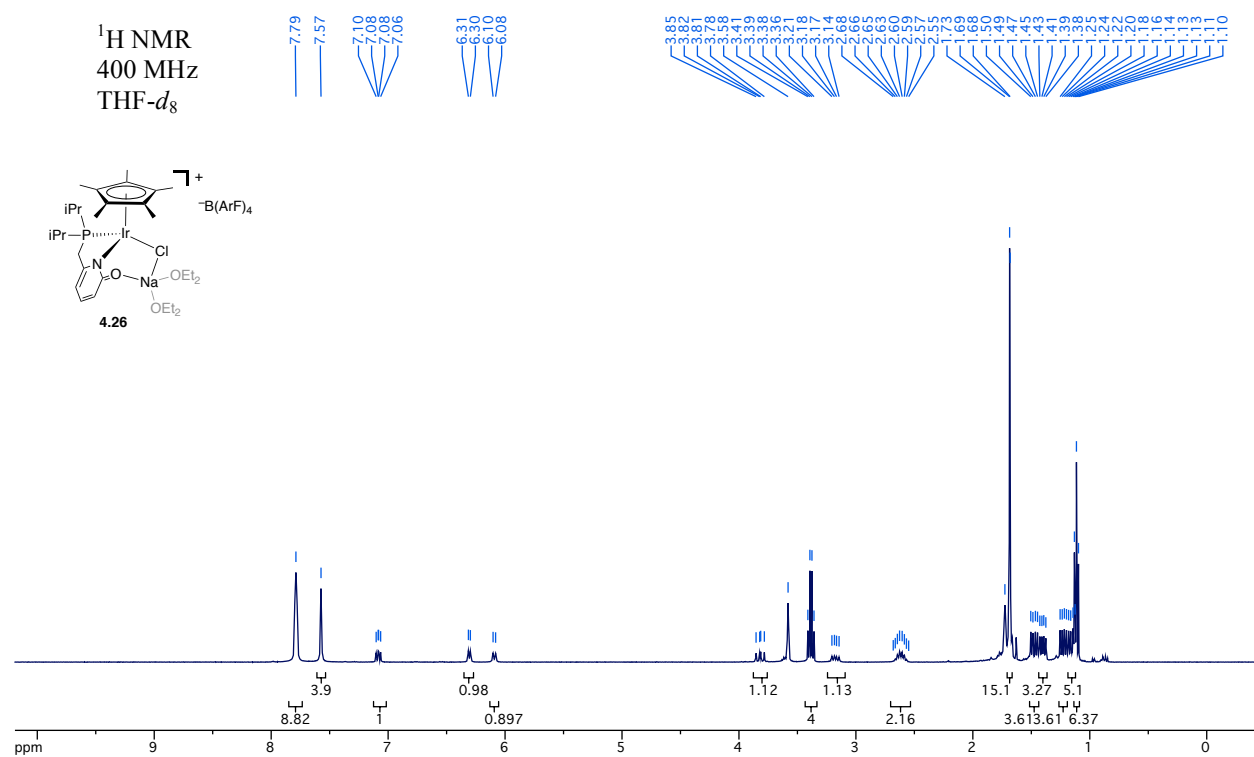


$^{31}\text{P}\{^1\text{H}\}$  NMR  
121 MHz  
THF- $d_8$

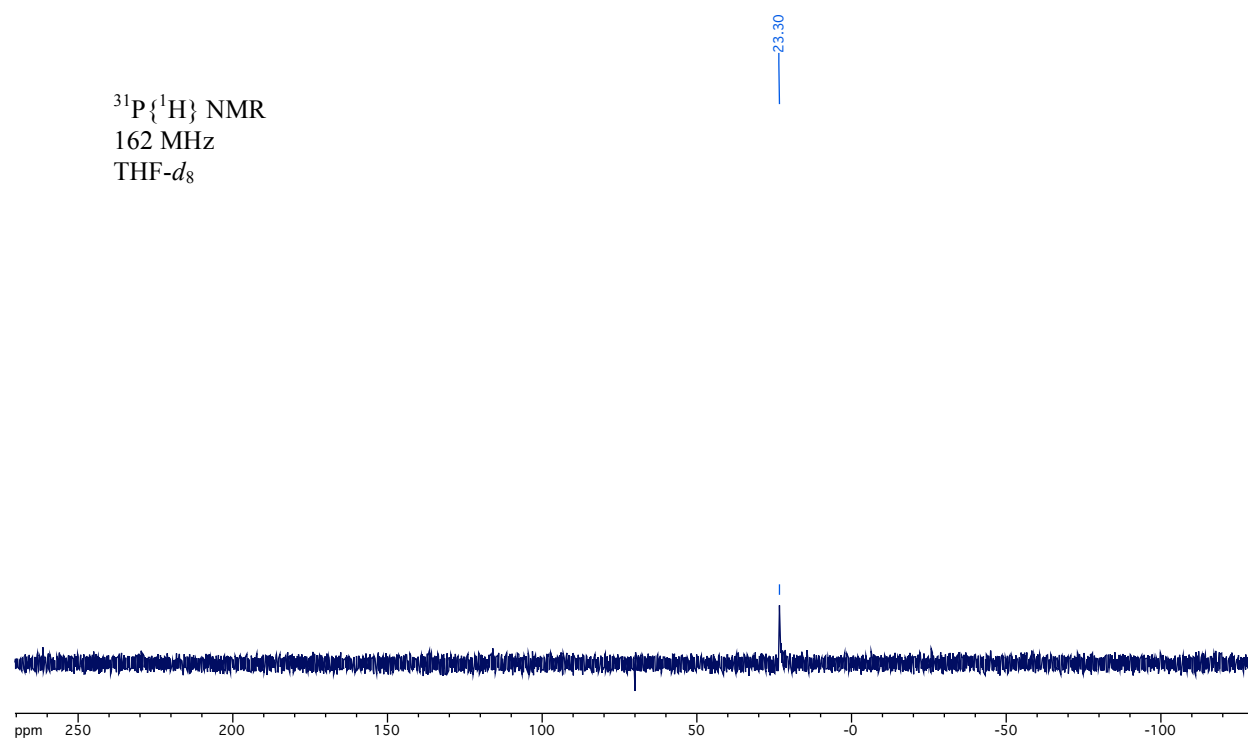


$^{19}\text{F}\{^1\text{H}\}$  NMR  
282 MHz  
THF- $d_8$

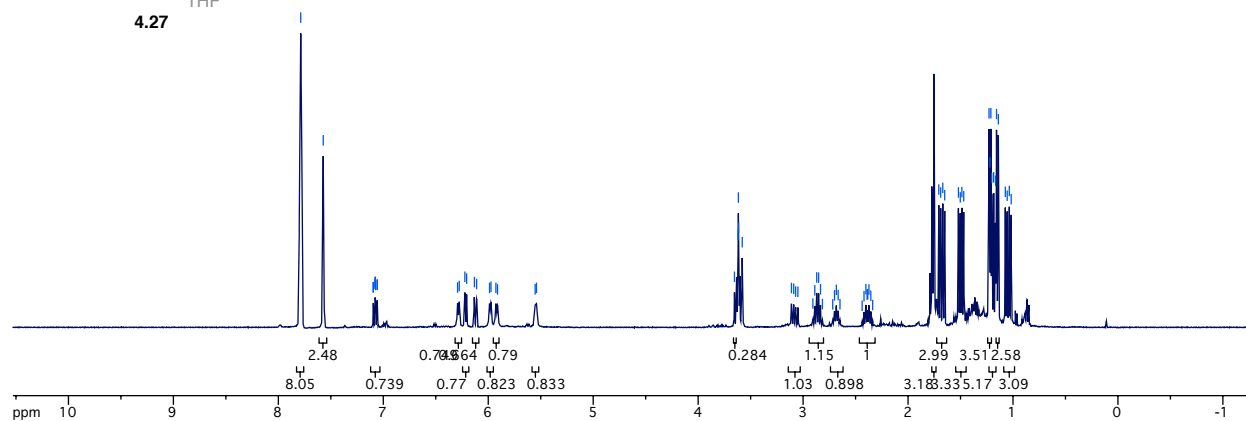




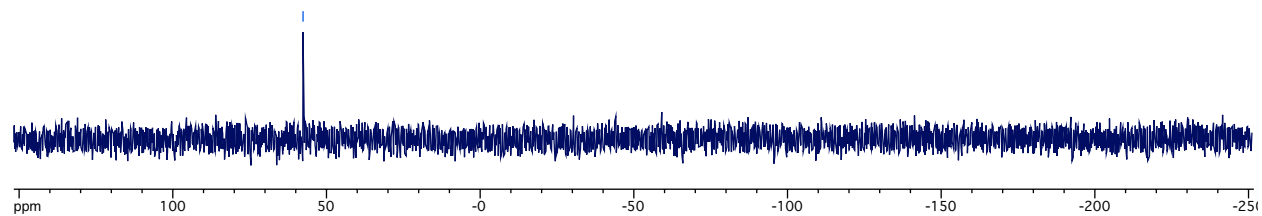
$^{31}\text{P}\{^1\text{H}\}$  NMR  
162 MHz  
THF- $d_8$

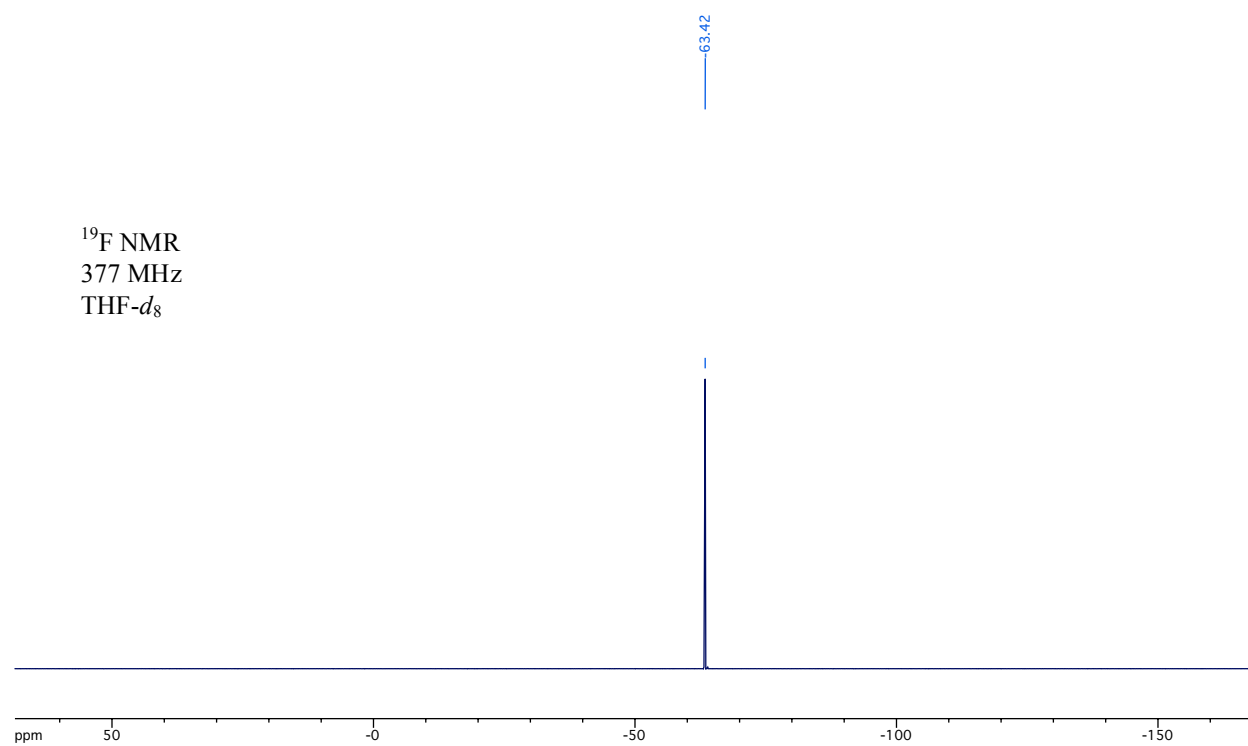


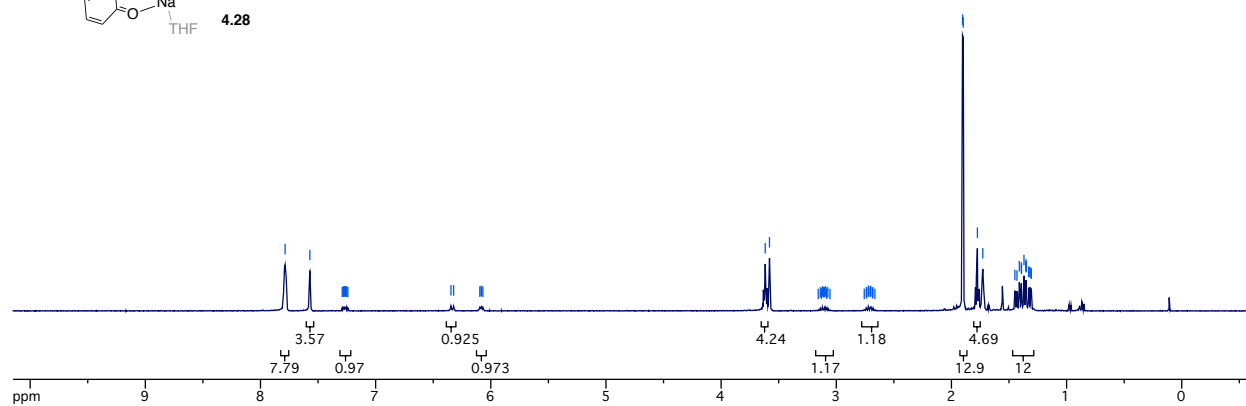
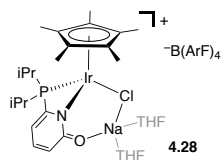
75 74 73 72 71 70 69 68 67 66 65 64 63 62 61 60 59 58 57 56 55 54 53 52 51 50 49 48 47 46 45 44 43 42 41 40 39 38 37 36 35 34 33 32 31 30 29 28 27 26 25 24 23 22 21 20 19 18 17 16 15 14 13 12 11 10 09 08 07 06 05 04



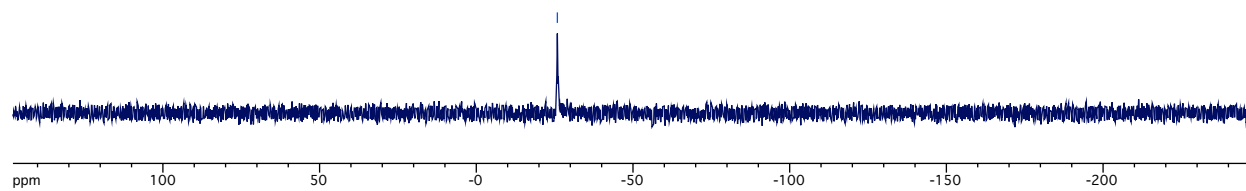
57.62



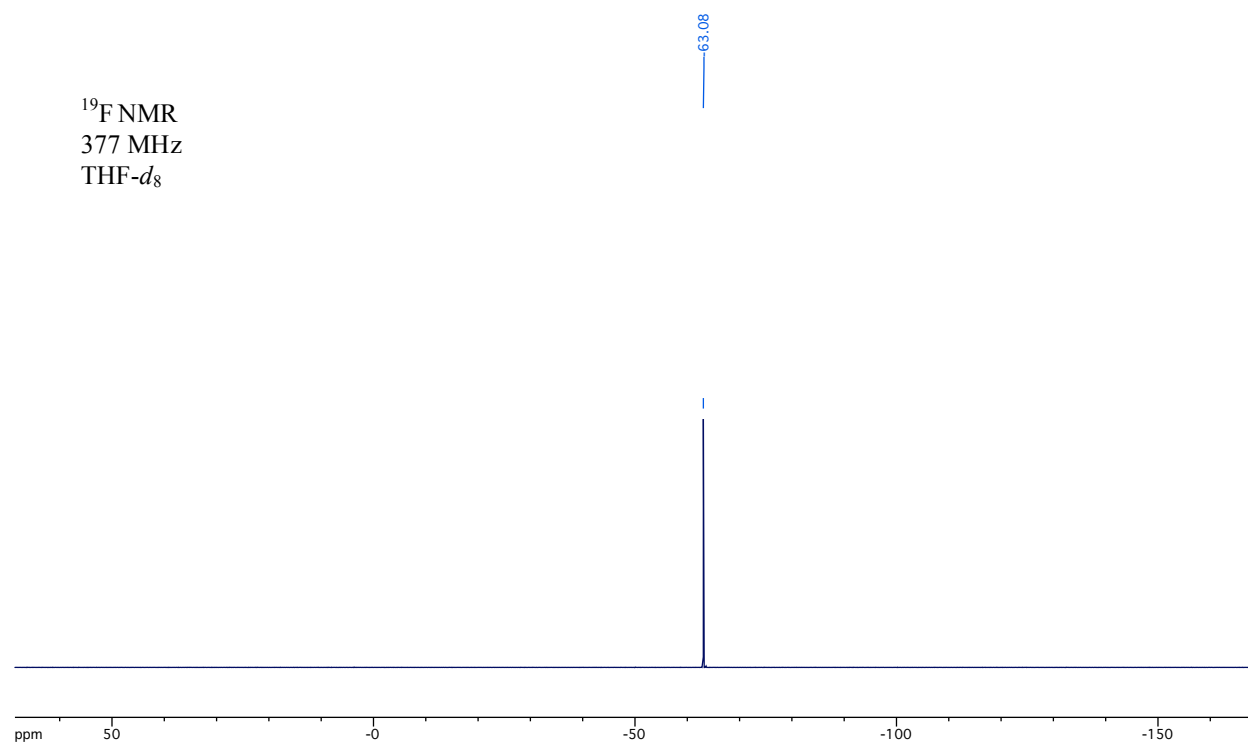


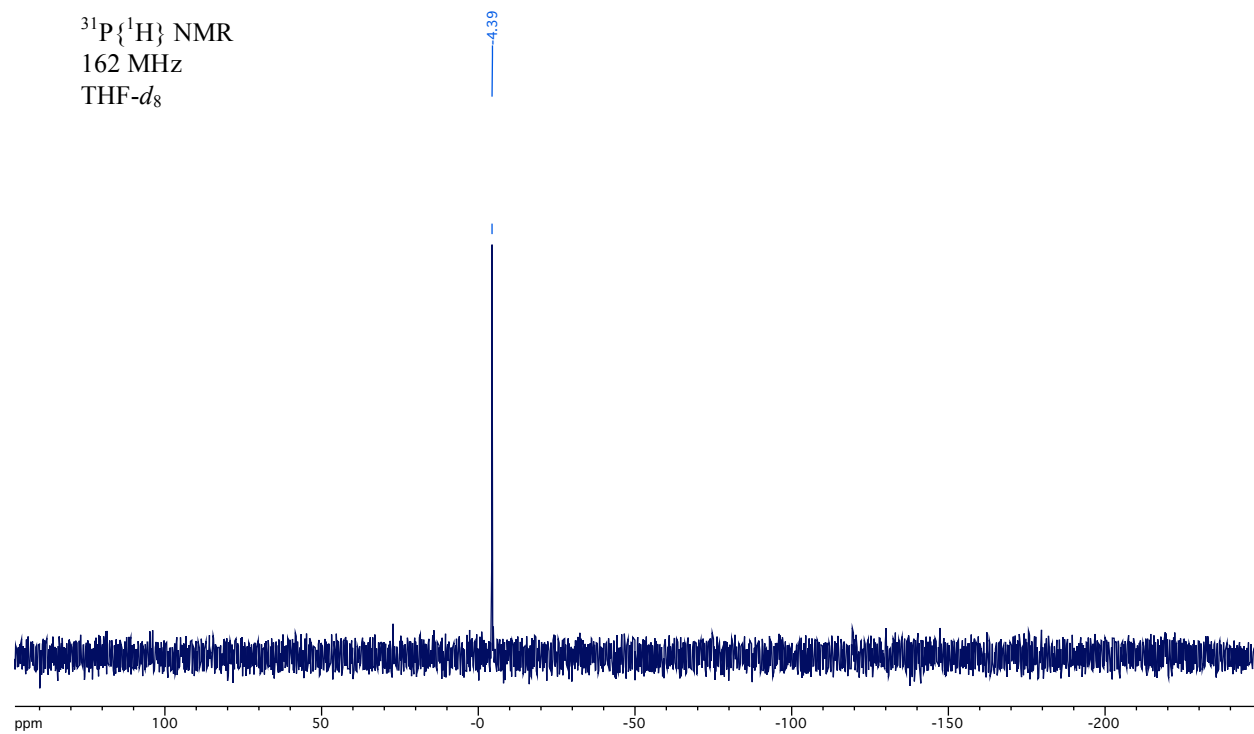
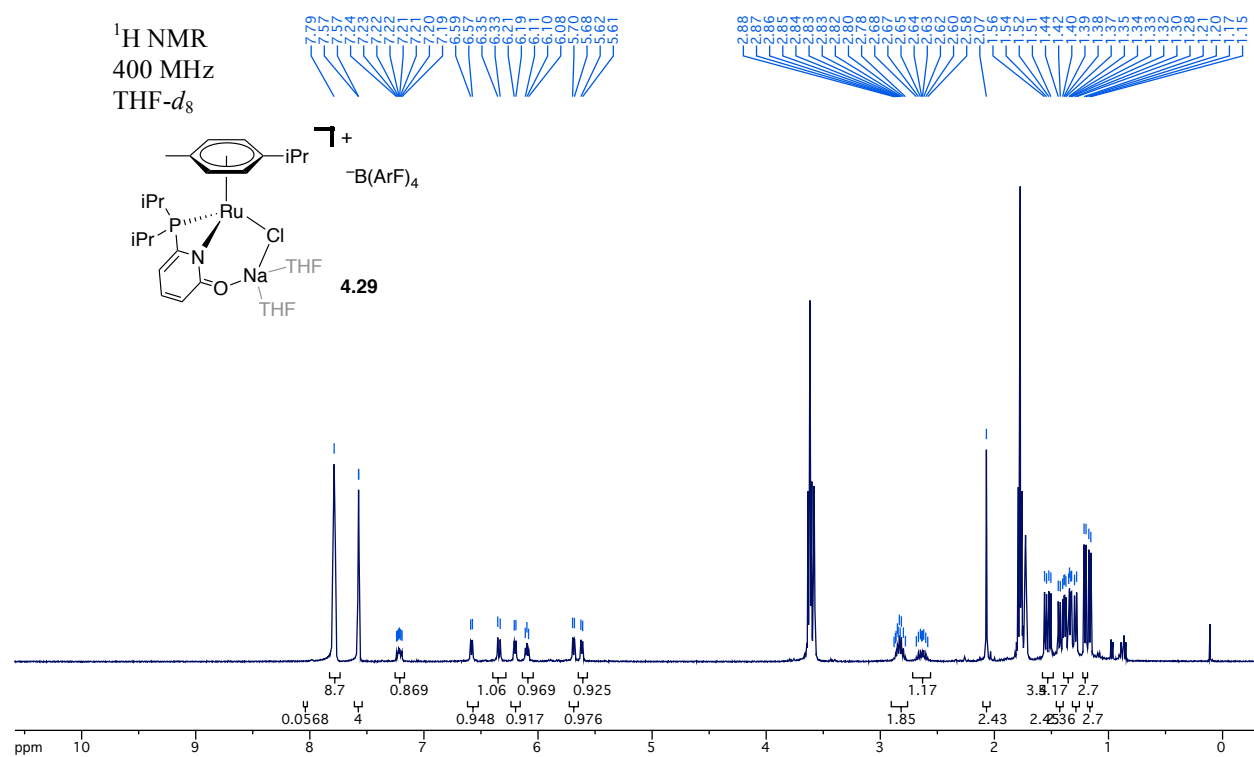


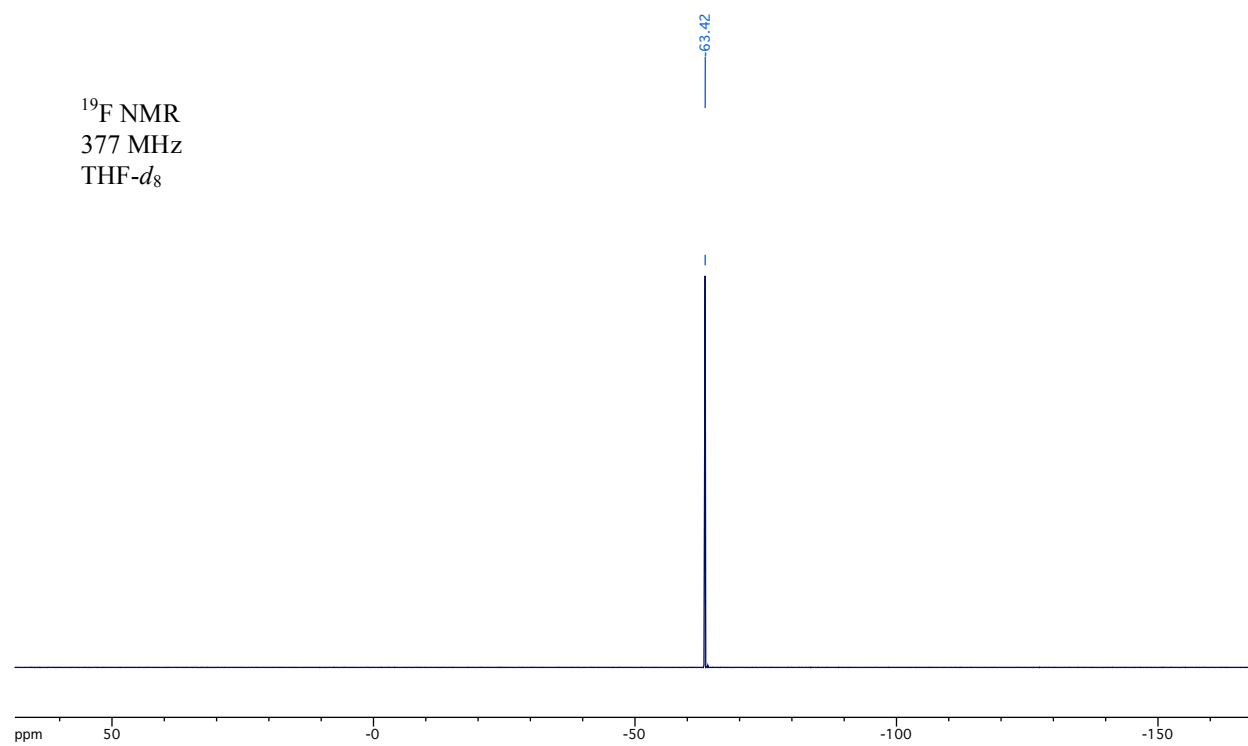
25.87

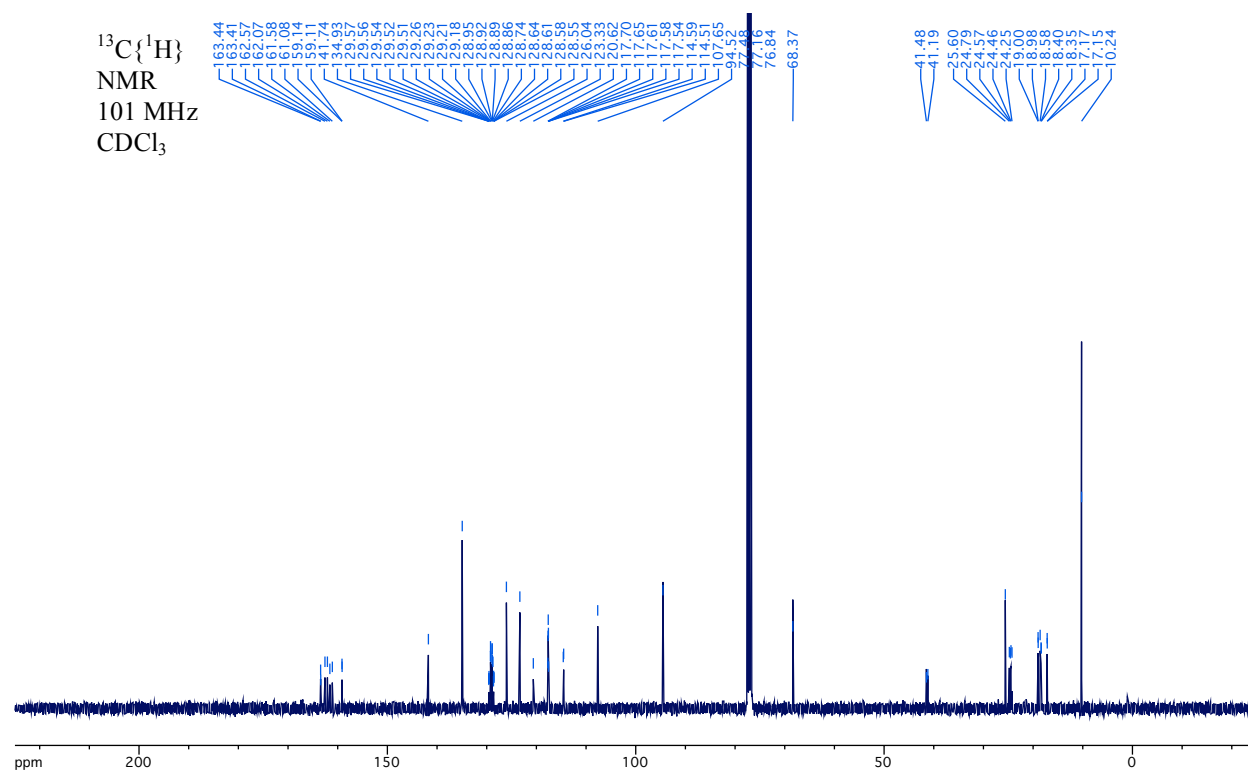
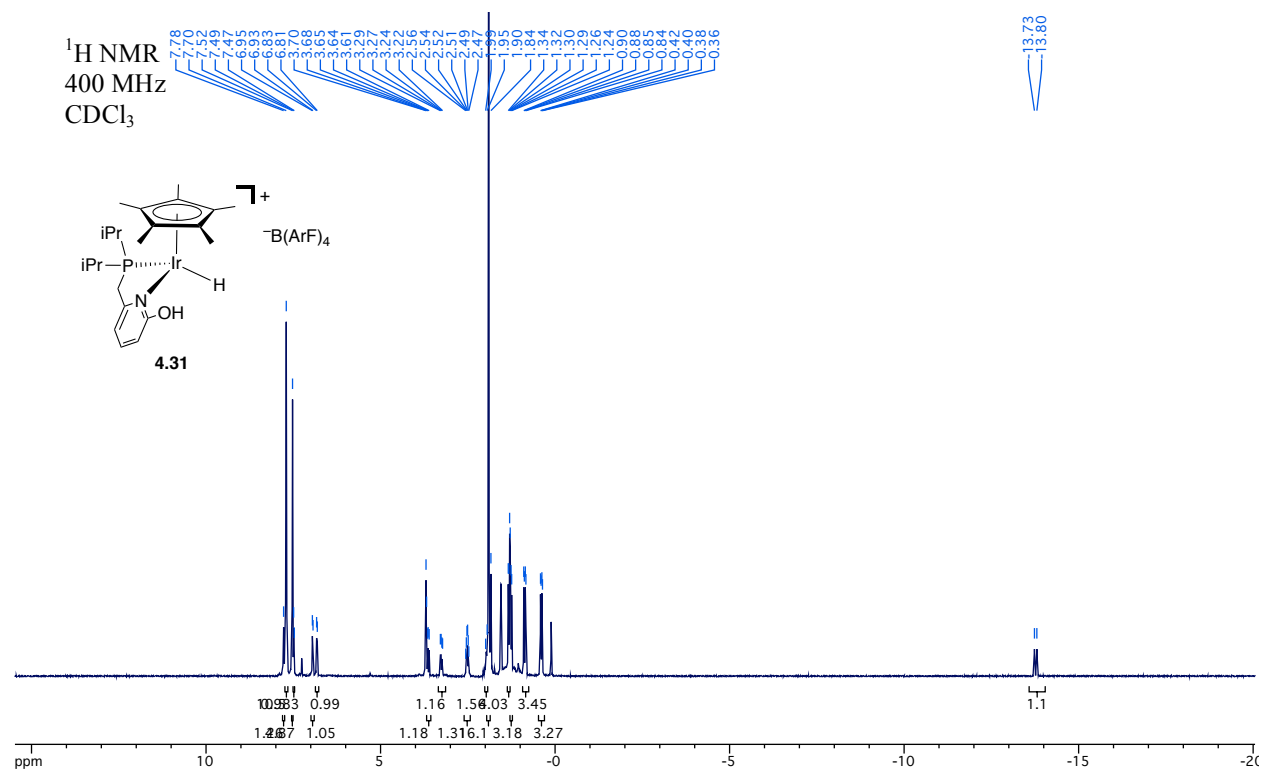




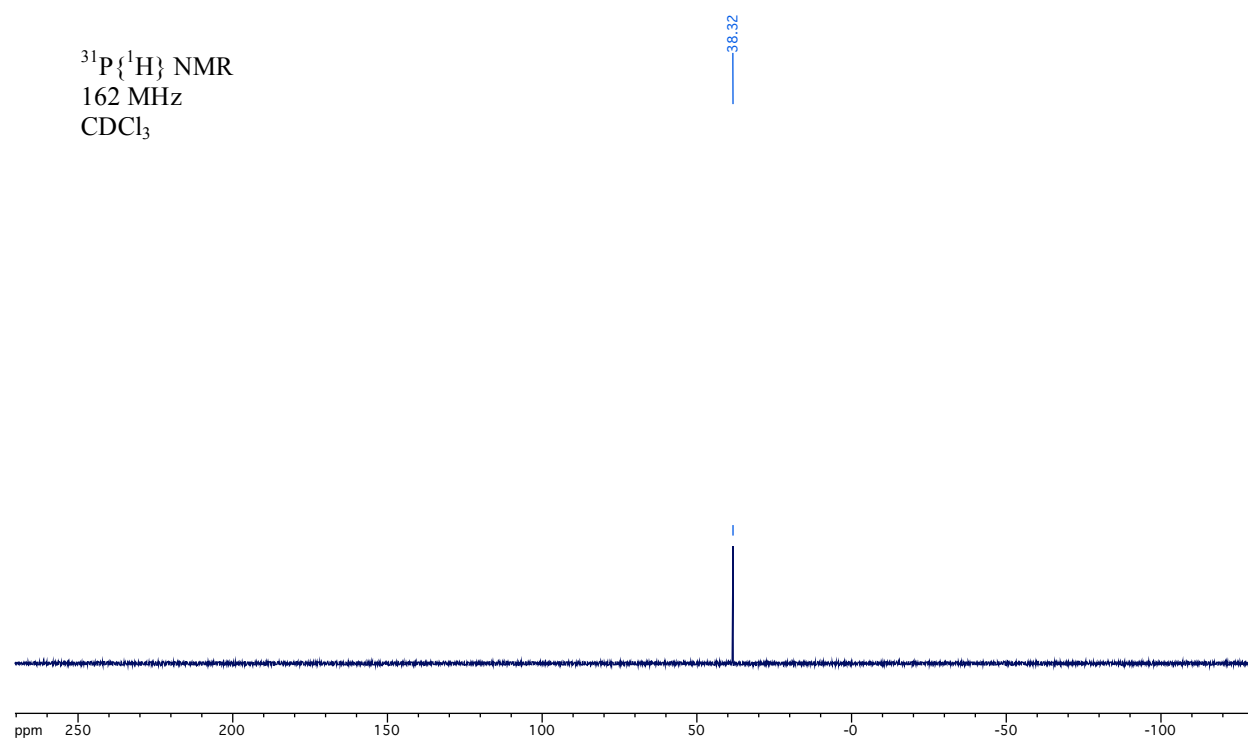


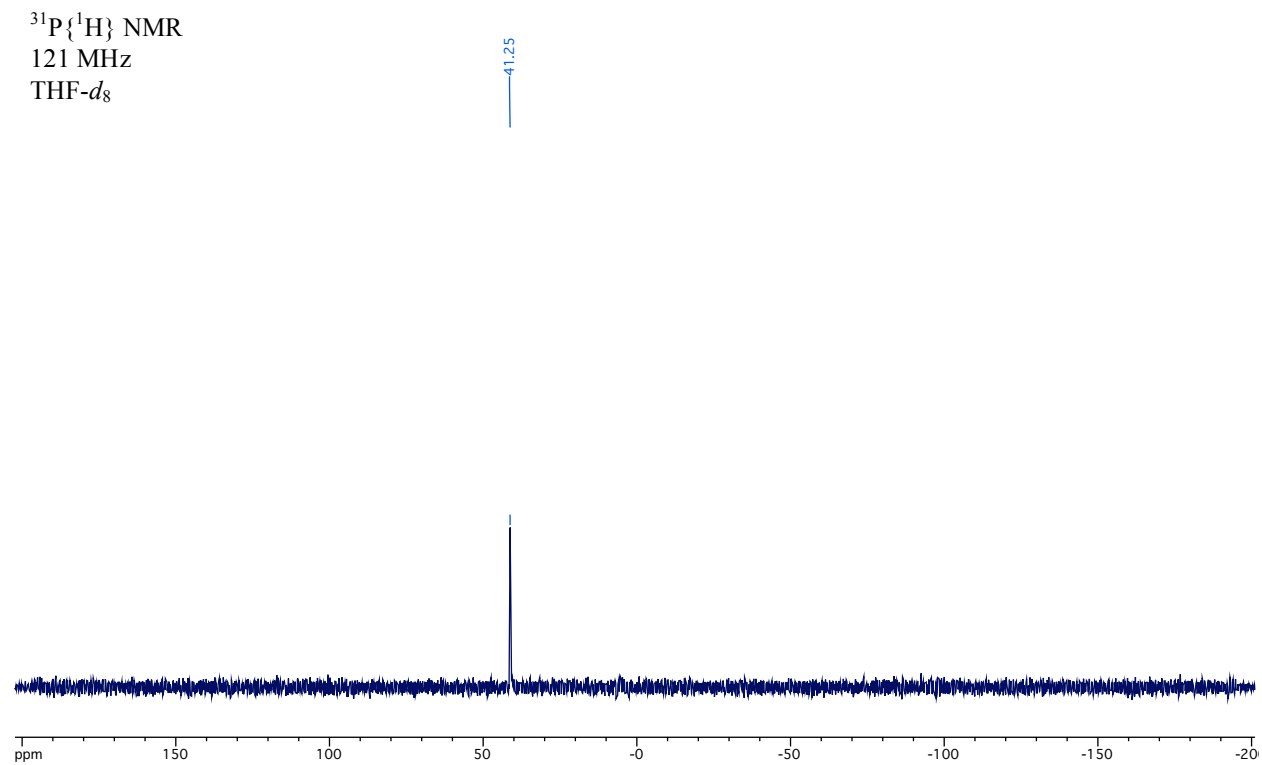
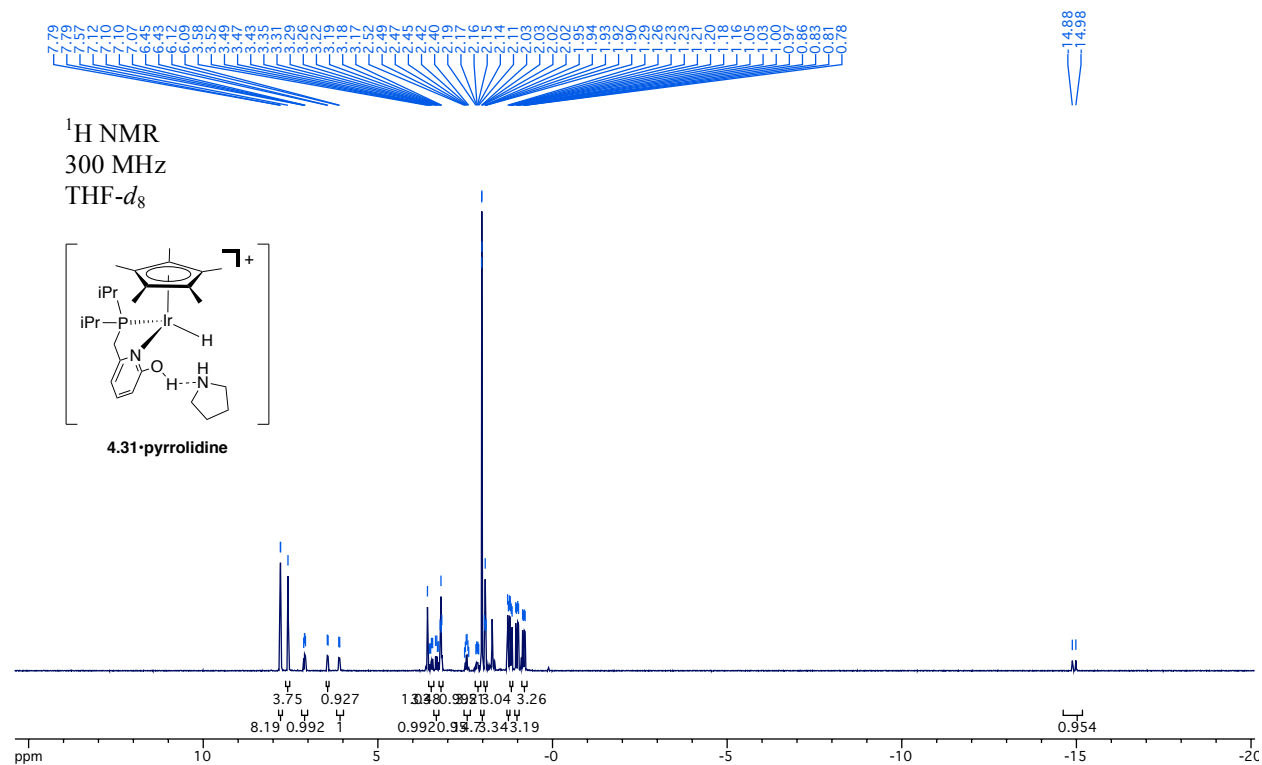


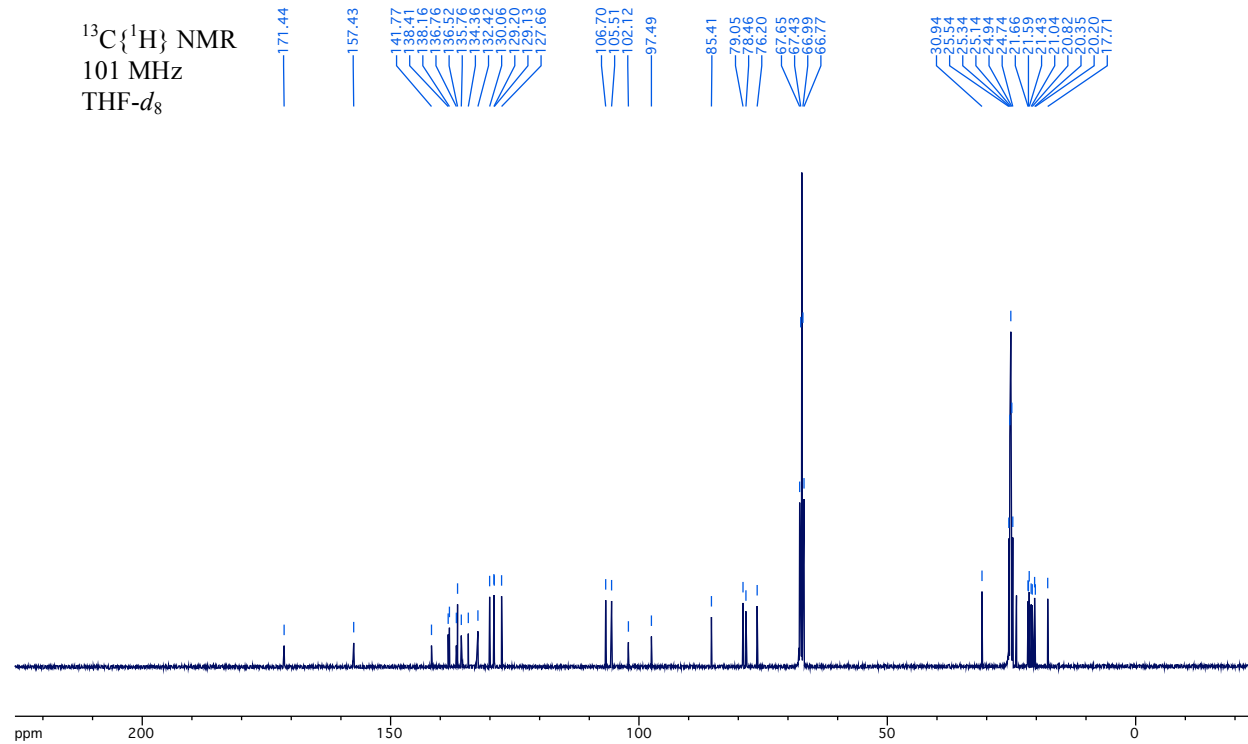
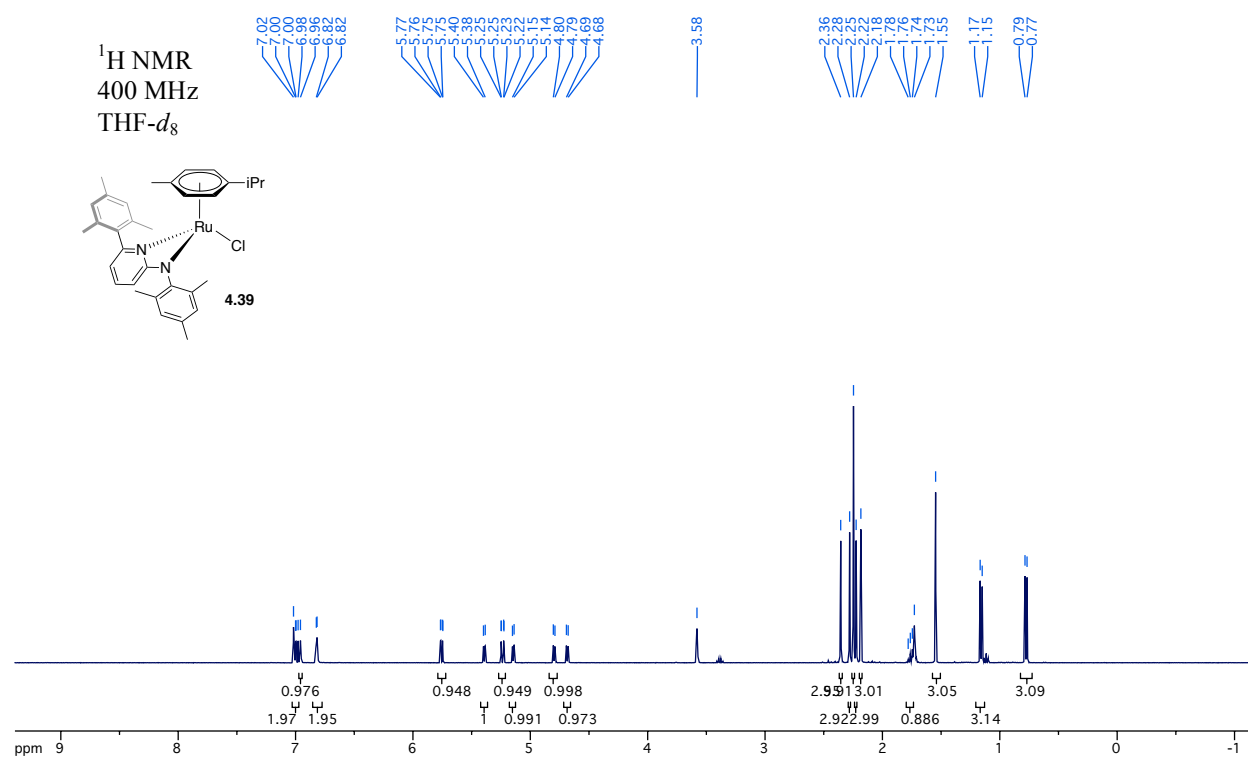


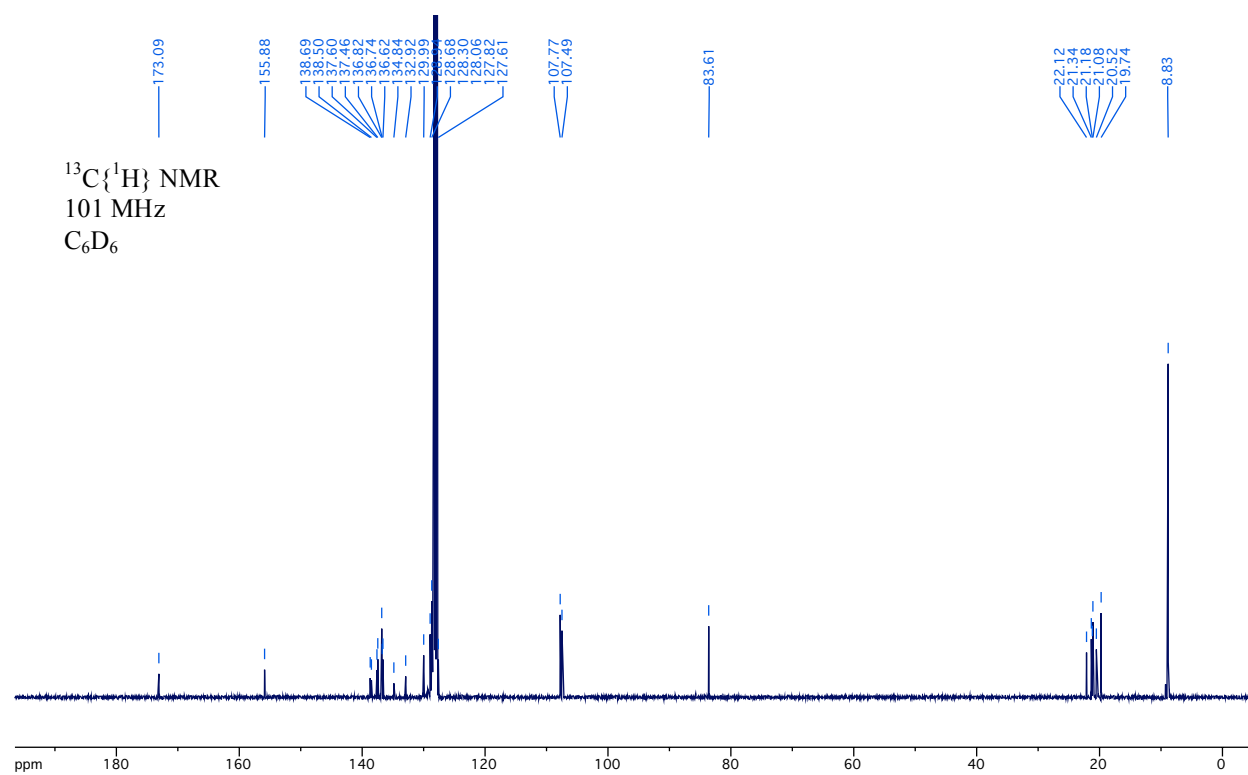
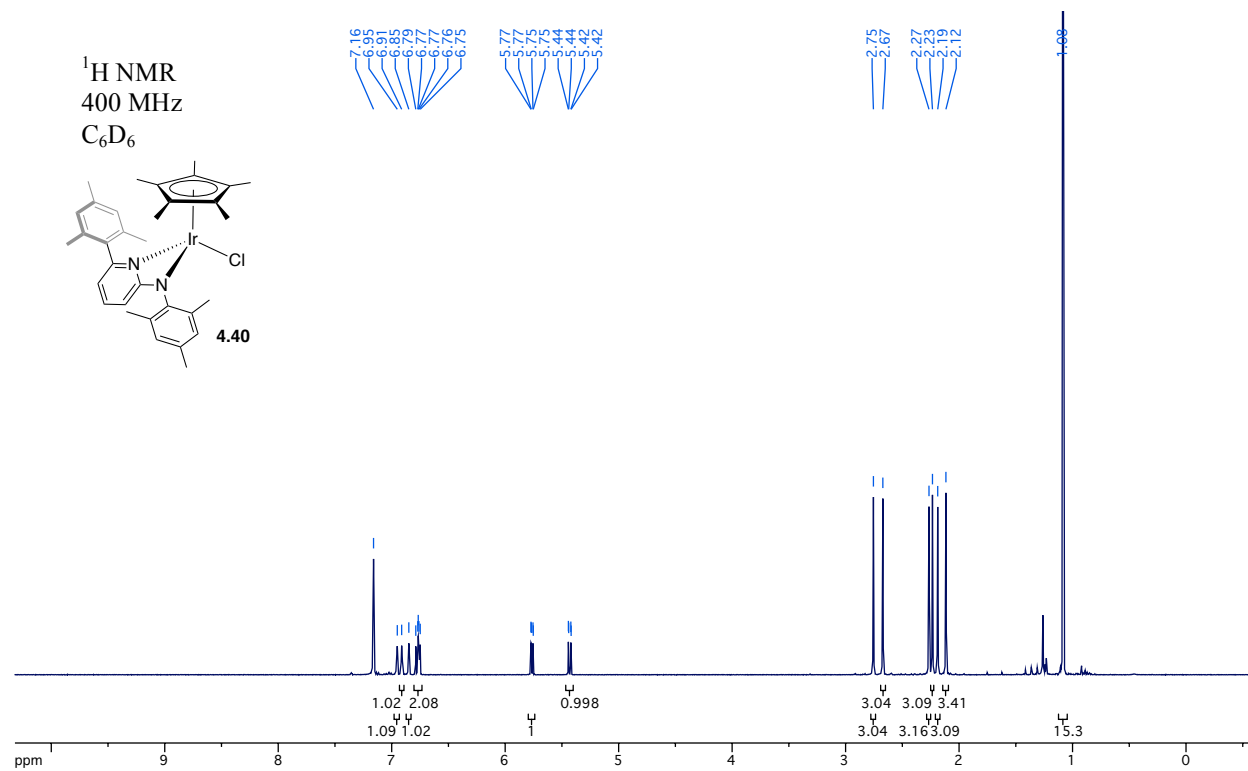


$^{31}\text{P}\{^1\text{H}\}$  NMR  
162 MHz  
 $\text{CDCl}_3$





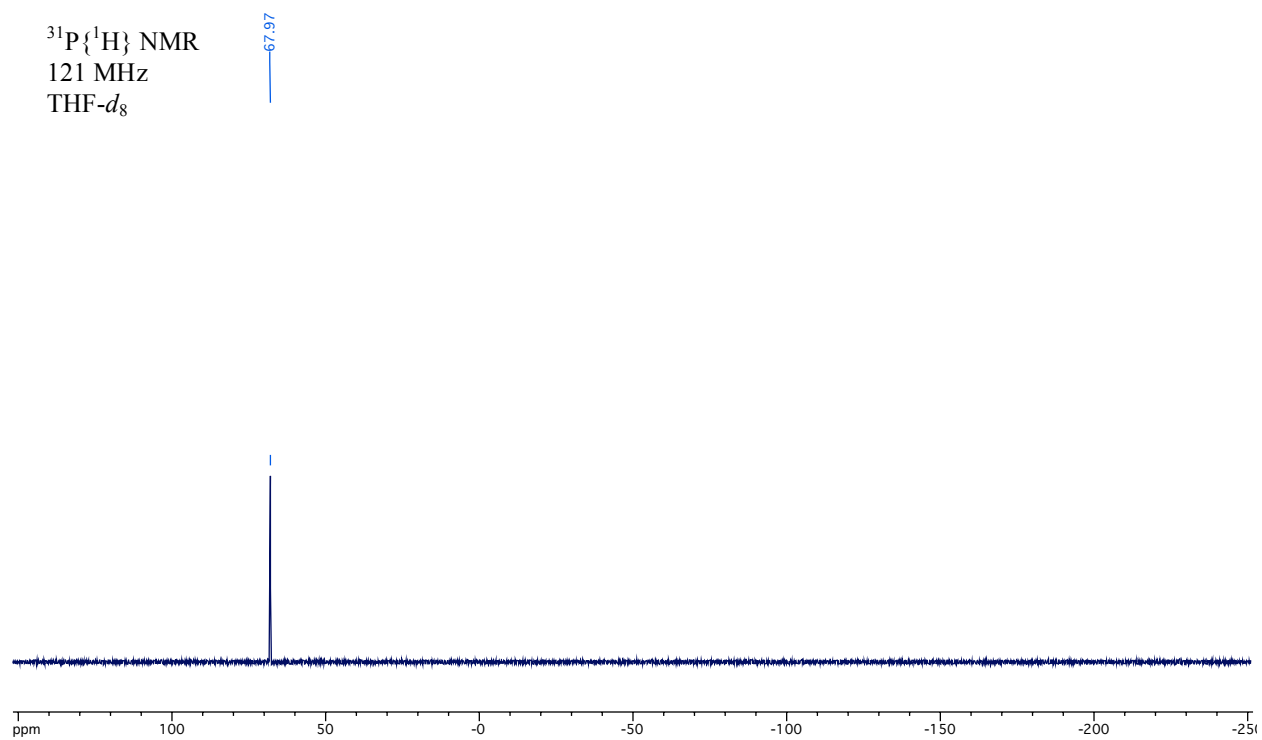


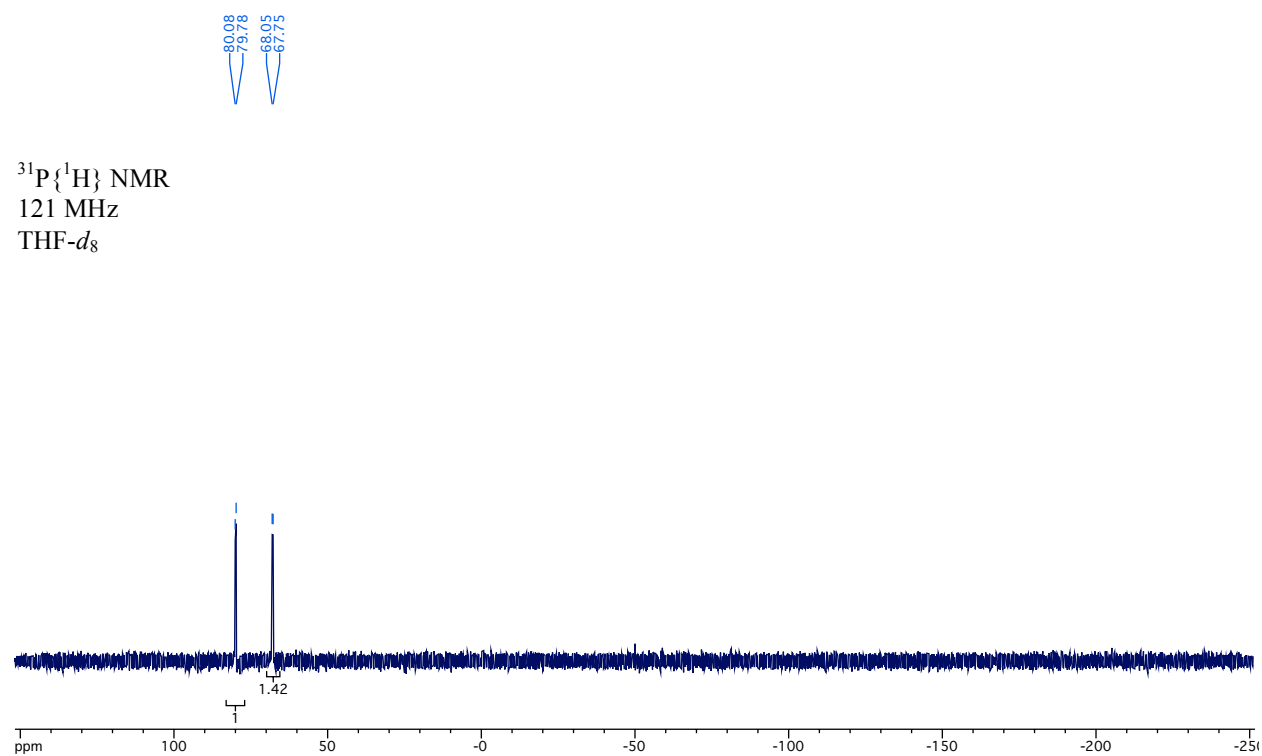
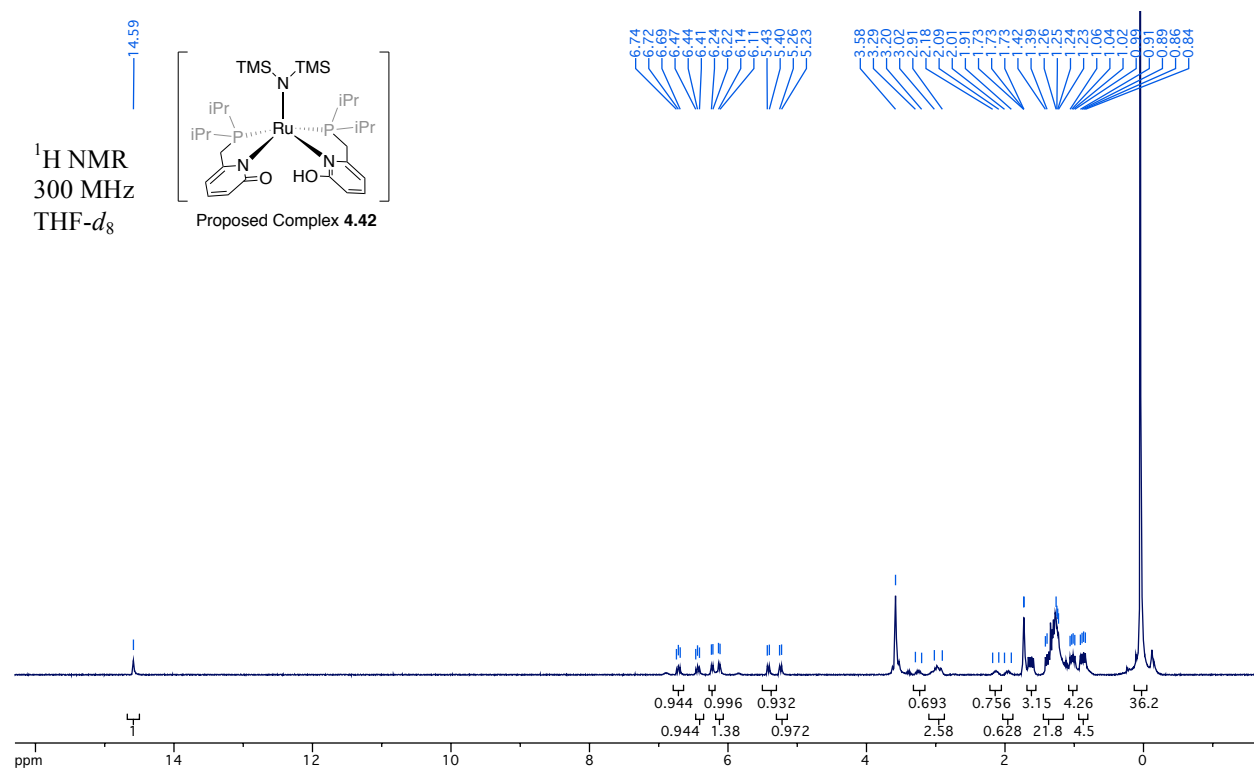




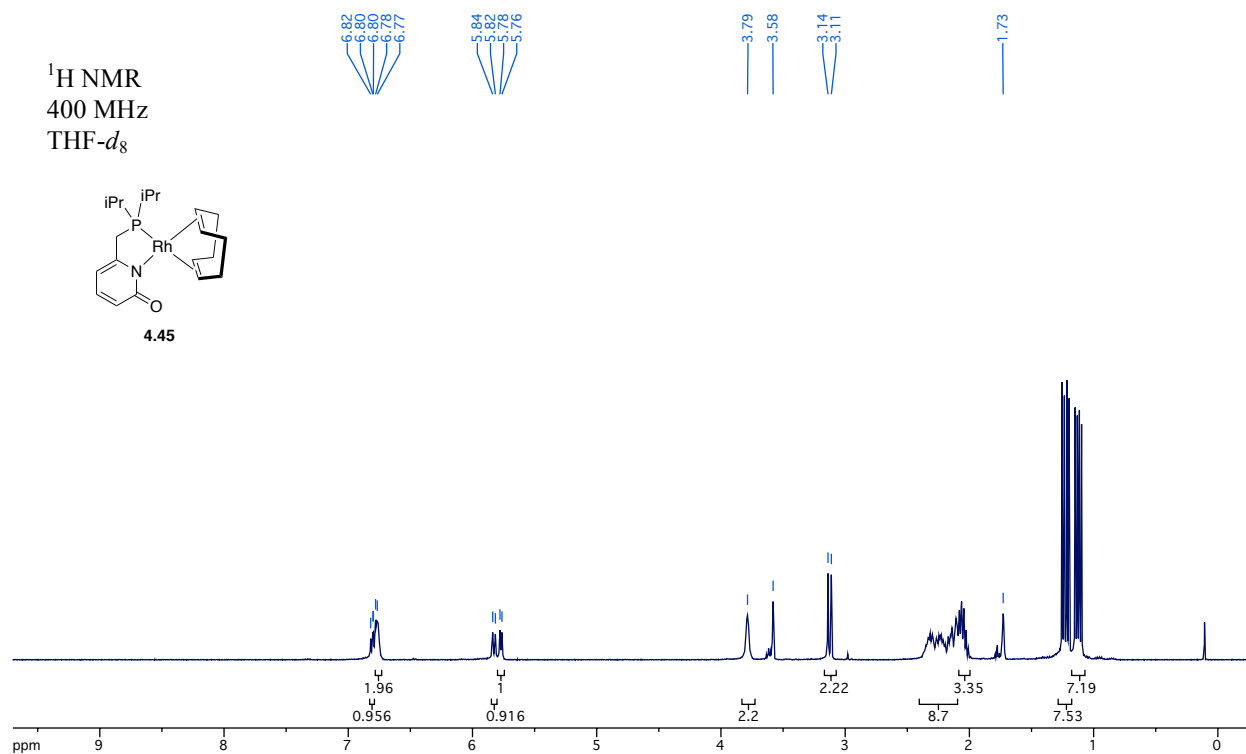
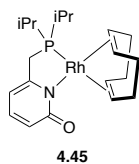


$^{31}\text{P}\{^1\text{H}\}$  NMR  
121 MHz  
THF- $d_8$

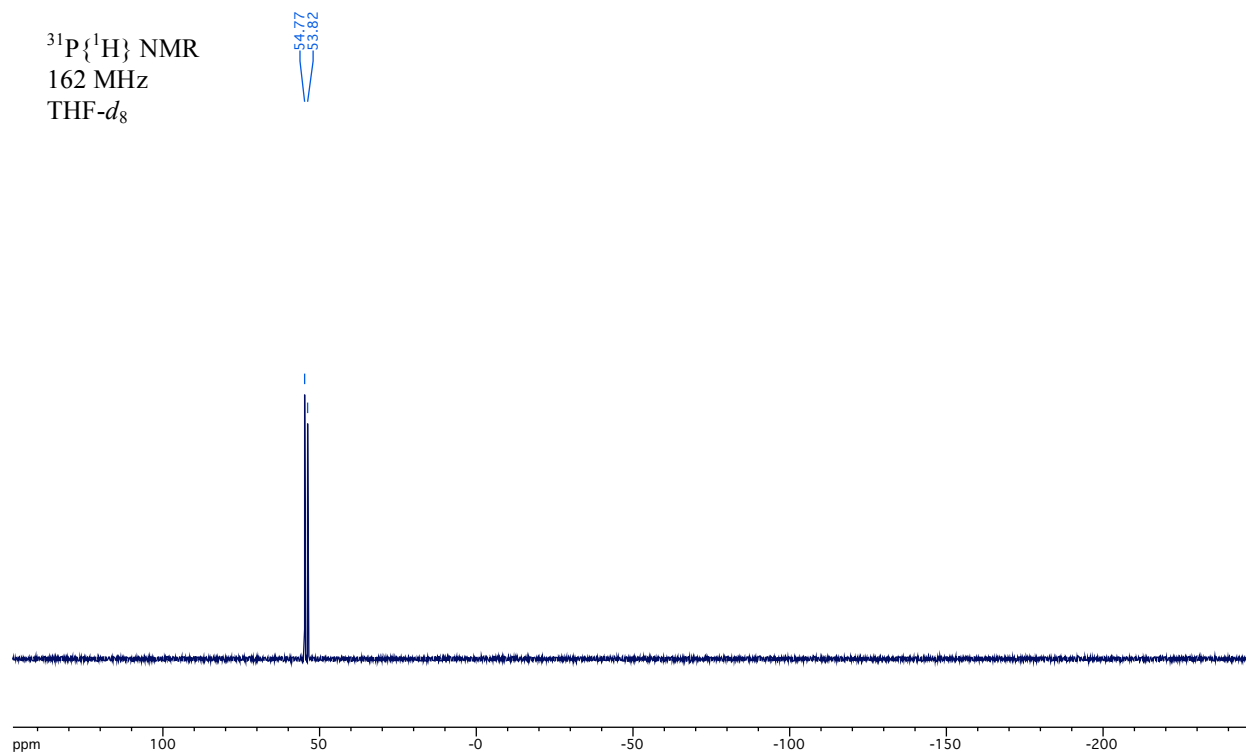




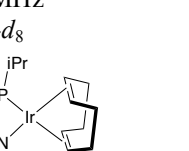
$^1\text{H}$  NMR  
400 MHz  
 $\text{THF-}d_8$




$^{31}\text{P}\{^1\text{H}\}$  NMR  
162 MHz  
 $\text{THF-}d_8$




<sup>1</sup>H NMR  
400 MHz  
THF-*d*<sub>8</sub>

  
**4.46**



$^{31}\text{P}\{^1\text{H}\}$  NMR  
162 MHz  
THF- $d_8$



38.88

ppm

## Appendix B Solid State Molecular Structures and X-ray Data:

Single crystal X-ray structure determinations were performed at the X-ray crystallography lab at the Department of Chemistry, University of British Columbia on either a Bruker X8 APEX or Bruker APEX DUO diffractometer using graphite-monochromated Mo K $\alpha$  radiation ( $\lambda=0.71073$  Å). Collection of data, integration, and absorption correction were performed by Dr. Jacky Yim, Scott Ryken, Damon Gilmour, or Sam Griffin. Unless otherwise noted, data integration was performed using Bruker SAINT (v.8.34A), absorption correction was performed using Bruker SADABS (2014/5), structures were solved using direct methods using SIR2004,<sup>268</sup> and refinement (including modelling of disorder) was performed using SHELXL (2014/7) using the OLEX2 interface.<sup>269-270</sup> ORTEP representations were produced using CCDC's Mercury software.<sup>271</sup>

Compound **2.16**: Crystals were found to be twinned. Both twin domains were integrated using Bruker TWINABS (2012/1), the structure was solved and refined using a dataset consisting of reflections only from the major twin domain.

	<b>2.15</b>	<b>2.16</b>	<b>2.18</b>
formula	C <sub>12</sub> H <sub>24</sub> ClN <sub>4</sub> OTa	C <sub>12</sub> H <sub>21</sub> ClF <sub>3</sub> N <sub>4</sub> OTa	C <sub>17</sub> H <sub>26</sub> ClN <sub>4</sub> OTa
$F_w$	456.75	510.73	518.82
crystal size (mm)	0.25 x 0.19 x 0.17	0.16 x 0.12 x 0.07	0.36 x 0.28 x 0.21
color, habit	yellow, plate	yellow, plate	yellow, prism
crystal system	Monoclinic	Triclinic	orthorhombic

	<b>2.15</b>	<b>2.16</b>	<b>2.18</b>
space group	P2 <sub>1</sub> /c	P-1	Pbca
<i>T</i> (K)	100	100	90
<i>a</i> (Å)	8.6755(12)	7.9749(8)	9.6112(4)
<i>b</i> (Å)	12.7009(19)	8.4714(8)	14.3447(6)
<i>c</i> (Å)	15.100(2)	14.7644(15)	28.6697(12)
$\alpha$ (°)	90	89.788	90
$\beta$ (°)	97.197(3)	86.448	90
$\gamma$ (°)	90	61.895	90
<i>V</i> (Å <sup>3</sup> )	1650.7(4)	877.79(15)	3952.7(3)
<i>Z</i>	4	2	8
$\rho_{\text{calcd}}$ (g cm <sup>-3</sup> )	1.838	1.932	1.744
<i>F</i> (000)	888.0	492.0	2032.0
$\mu$ (MoK $\alpha$ ) (mm <sup>-1</sup> )	6.819	6.447	5.708
$2\theta_{\text{max}}$ (°)	60.084	60.05	60.096
total no. of reflns	20011	5107	30947
no. of unique reflns	4839	5107	5797
<i>R</i> <sub>1</sub> ( <i>F</i> <sup>2</sup> , all data)	0.0152	0.0377	0.0230
<i>wR</i> <sub>2</sub> ( <i>F</i> <sup>2</sup> , all data)	0.0316	0.0556	0.0394
<i>R</i> <sub>I</sub> ( <i>F</i> , <i>I</i> > 2σ( <i>I</i> ))	0.0132	0.0292	0.0194
<i>wR</i> <sub>2</sub> ( <i>F</i> , <i>I</i> > 2σ( <i>I</i> ))	0.0310	0.0551	0.0384

	<b>2.15</b>	<b>2.16</b>	<b>2.18</b>
goodness of fit	1.037	1.069	1.097

**Table B.1** Single crystal X-ray diffraction data for complexes **2.15**, **2.16**, and **2.18**

	<b>3.13</b>	<b>3.18</b>	<b>3.20</b>	<b>3.21</b>
formula	C <sub>18</sub> H <sub>39</sub> N <sub>5</sub> NbO <sub>3</sub> P	C <sub>36</sub> H <sub>65</sub> N <sub>4</sub> NbO <sub>6</sub> P <sub>2</sub>	C <sub>18</sub> H <sub>49</sub> N <sub>8</sub> NbO <sub>2</sub> P <sub>2</sub>	C <sub>22</sub> H <sub>37</sub> N <sub>4</sub> NbO <sub>3</sub> P
$F_w$	497.42	804.77	564.50	529.43
crystal size (mm)	0.41 x 0.23 x 0.22	0.25 x 0.24 x 0.20	0.47 x 0.46 x 0.39	0.37 x 0.37 x 0.24
color, habit	red, plate	yellow, plate	yellow, plate	yellow, prism
crystal system	Monoclinic	Triclinic	monoclinic	monoclinic
space group	P2 <sub>1</sub> /c	P-1	P2 <sub>1</sub> /c	P2 <sub>1</sub> /c
$T$ (K)	90	90	90	90
$a$ (Å)	12.5545(13)	11.3648(10)	9.7447(17)	13.800(2)
$b$ (Å)	12.9294(13)	14.2901(12)	14.759(3)	9.1504(15)
$c$ (Å)	14.2200(14)	15.4990(13)	19.720(4)	20.890(4)
$\alpha$ (Å)	90	94.786(2)	90	90
$\beta$ (Å)	92.210(2)	111.422(2)	100.356(4)	106.875(3)
$\gamma$ (Å)	90	113.251(2)	90	90
$V$ (Å <sup>3</sup> )	2306.5(4)	2075.3(3)	2789.9(9)	2524.3(7)
$Z$	4	2	4	4



	<b>3.13</b>	<b>3.18</b>	<b>3.20</b>	<b>3.21</b>
$\rho_{\text{calcd}}$ (g cm <sup>-3</sup> )	1.432	1.288	1.3438	1.393
$F(000)$	1048.0	856.0	1192.6	1108.0
$\mu$ (MoK $\alpha$ ) (mm <sup>-1</sup> )	0.619	0.412	0.575	0.569
$2\theta_{\text{max}}$ (°)	59.7	61.232	59.94	60.456
total no. of reflns	43833	101321	32074	28595
no. of unique reflns	6564	12472	8065	7422
$R_1$ ( $F^2$ , all data)	0.0230	0.0371	0.0213	0.0366
$wR_2$ ( $F^2$ , all data)	0.0549	0.0911	0.0902	0.0760
$R_I$ ( $F$ , $I >$ $2\sigma(I)$ )	0.0187	0.0295	0.0192	0.0292
$wR_2$ ( $F$ , $I >$ $2\sigma(I)$ )	0.0501	0.0777	0.0845	0.0718
goodness of fit	1.091	1.130	0.797	1.046

**Table B.2** Single crystal X-ray diffraction data for complexes **3.13**, **3.18**, **3.20**, **3.21**

	<b>4.25</b>	<b>4.26</b>	<b>4.41</b>
formula	$\text{C}_{29}\text{H}_{38.5}\text{B}_{0.5}\text{Cl}_{0.5}\text{N}_{0.5}\text{Na}_{0.5}\text{O}_2\text{P}_{0.5}\text{Rh}_{0.5}$	$\text{C}_{31}\text{H}_{32.5}\text{B}_{0.5}\text{Cl}_{0.5}\text{F}_{12}\text{Ir}_{0.5}\text{N}_{0.5}\text{Na}_{0.5}\text{O}_{1.5}\text{P}_{0.5}$	$\text{C}_{24}\text{H}_{40}\text{Cl}_2\text{N}_2\text{O}_2\text{P}_2\text{Ru}$
$F_w$	527.67	810.28	622.49
crystal size (mm)	0.58 x 0.20 x 0.08	0.201 x 0.056 x 0.026	0.213 x 0.187 x 0.158
color, habit	orange, blade	yellow, prism	Brown-red, prism
crystal system	triclinic	triclinic	monoclinic
space group	P-1	P-1	P2 <sub>1</sub> /c
$T$ (K)	100	100	100
$a$ (Å)	11.661(2)	12.2496(12)	10.6280(9)
$b$ (Å)	14.185(3)	15.9609(15)	13.8180(11)
$c$ (Å)	17.002(3)	18.9485(18)	18.6807(16)
$\alpha$ (°)	93.391(4)	114.073(3)	90
$\beta$ (°)	102.357(4)	91.081(2)	91.454(2)
$\gamma$ (°)	96.662(4)	94.196(2)	90
$V$ (Å <sup>3</sup> )	2718.4(9)	3368.4(6)	2742.5(4)
$Z$	4	4	4
$\rho_{\text{calcd}}$ (g cm <sup>-3</sup> )	1.289	1.598	1.508
$F(000)$	1114.0	1618.0	1288.0
$\mu$ (MoK $\alpha$ ) (mm <sup>-1</sup> )	0.446	2.162	0.907
$2\theta_{\text{max}}$ (°)	53.006	54.46	54.294
total no. of reflns	40899	52907	24002

	<b>4.25</b>	<b>4.26</b>	<b>4.41</b>
no. of unique reflns	11190	14939	6051
$R_1 (F^2, \text{all data})$	0.0783	0.0712	0.0655
$wR_2 (F^2, \text{all data})$	0.1767	0.1179	0.1247
$R_1 (F, I > 2\sigma(I))$	0.0561	0.0494	0.0540
$wR_2 (F, I > 2\sigma(I))$	0.1570	0.1096	0.1197
goodness of fit	1.269	1.038	1.110

**Table B.3 Single crystal X-ray diffraction data for complexes 4.25, 4.26, and 4.41**